AN ABSTRACT OF THE THESIS OF

David B. Linton for the degree of Master of Science in Wood Science and Civil Engineering presented March 20, 2012.

Title: Tsunami Loading on Light-Frame Wood Structures

Abstract approved:

Rakesh Gupta   Daniel T. Cox

Since 2004 there have been multiple devastating tsunamis around the globe triggered by large magnitude earthquakes; with the most recent being the Tohoku, Japan tsunami in March 2011. These tsunamis have caused significant loss of life and damage to the coastal communities impacted by these powerful waves. The resulting devastation has raised awareness of the dangers of tsunamis and the Network for Earthquake Engineering Simulation (NEES) housesmash project (NEEShousesmash), was started to investigate several different areas of tsunami inundation. The work presented in the following two manuscripts was performed at the O.H. Hinsdale Wave Lab and Gene D. Knudson Wood Engineering Lab, which are located at Oregon State University. This work represents a small portion of the total NEEShousesmash project, and is focused on improving the knowledge and predictability of tsunami loading and structural performance.

The first manuscript investigates tsunami wave impact on full scale light-frame wood walls, and compares the measured forces to calculated values using the linear momentum equation, previously evaluated by Cross (1967). The results show for each wave height tested a peak transient force followed by a sustained quasi-static force, with a ratio of transient force to quasi-static force of 2.2. The results also show that the linear momentum equation did an acceptable job of predicting the measured transient forces on the walls to within ±10%, and that increased wall flexibility, 2x4 vs. 2x6 dimensional lumber, resulted in lower measured transient forces when subjected to similar tsunami wave heights. These results are important for practical use because the linear momentum equation is a simple equation to use, that only requires a couple of site specific input variables.

The second manuscript is a continuation of the work done in the wave lab for the first manuscript. These experiments provide a starting point for expanding the testing of the structural response and performance of larger scale structures subjected to tsunami wave loads. By simulating tsunami loading in a traditional structures laboratory, the inherent limits of testing structural performance in small scale tsunami laboratory facilities is removed. The results show that a light-frame wood shear wall, built to current standards, is susceptible to premature failures from concentrated impact loads at intermediate heights compared to the design strength at full height. It is also shown that the out-of-plane walls subjected to both elastic and inelastic loads behave like a one way slab with minimal load sharing between adjacent studs. The failures observed during the hydrodynamic wave testing of the nailed connection between the bottom plate and studs was successfully reproduced, and shows that current construction standards are not fully utilizing the available capacity of each stud when subjected to tsunami waves. The reinforcement of this connection with traditional metal brackets would help increase the capacity of the out-of-plane wall to resist tsunami wave loads.

Tsunami Loading on Light-Frame Wood Structures

by
David B. Linton

A THESIS

submitted to

Oregon State University

In partial fulfillment of
the requirements for the
degree of

Master of Science

Presented March 20, 2012
Commencement June 2012

Master of Science thesis of <u>David B. Linton</u> presented on <u>March 20, 2012</u>.

APPROVED:

_____

Co-Major Professor, representing Wood Science

_____

Co-Major Professor, representing Civil Engineering

_____

Head of the Department of Wood Science and Engineering

_____

Head of the School of Civil and Construction Engineering

_____

Dean of the Graduate School

I understand that my thesis will become part of the permanent collection of Oregon State University libraries. My signature below authorizes release of my thesis to any reader upon request.

_____

David B. Linton, Author

ACKNOWLEDGEMENTS

I would like to thank the following people for their support in helping me complete this project. Their continuous guidance, support, and encouragement helped make this endeavor a very fulfilling life achievement.

- Dr. Rakesh Gupta – Professor, Oregon State University
- Dr. Dan Cox – Professor, Oregon State University
- Dr. John van de Lindt – Professor, University of Alabama
- Milo Clauson - Senior Faculty Research Assistant, Oregon State University
- Sangki Park – Ph.D. candidate, University of Alabama
- Toby Polocoser – M.S. candidate, Oregon State University
- Faculty and staff in Civil and Construction Engineering department, OSU
- Faculty and staff in Wood Science and Engineering department, OSU
- NSF grant CMMI-0530759

I would also like to thank my parents; Roger and Louise Linton, for always emphasizing the importance of a good education and helping me get to this point. Last, but not least I am very appreciative and thankful for the continuous support and encouragement of my loving wife, Taliesin Linton.

CONTRIBUTION OF AUTHORS

Dr. Rakesh Gupta, Dr. Dan Cox, and Dr. John van de Lindt were a great source of knowledgeable background for writing these manuscripts and helped edit the text and figures to prepare them for publication. Milo Clauson was of great help in data collection and analysis for both projects.

TABLE OF CONTENTS

LIST OF FIGURES

Manuscript 1: Evaluation of Tsunami Loads on Wood Frame Walls at Full Scale

Manuscript 2: Load Distribution in Light-Frame Wood Buildings under Simulated Tsunami Loads

List of Figures (continued)

LIST OF TABLES

Manuscript 1: Evaluation of Tsunami Loads on Wood Frame Walls at Full Scale

Manuscript 2: Load Distribution in Light-Frame Wood Buildings under Simulated Tsunami Loads

LIST OF APPENDIX FIGURES

List of Appendix Figures (continued)

List of Appendix Figures (continued)

List of Appendix Figures (continued)

LIST OF APPENDIX TABLES

Tsunami Loading on Light-Frame Wood Structures

INTRODUCTION

The recent string of devastating tsunamis around the world, over the past decade has brought the United States' preparedness for a similar event in to question. The coastal towns in the Pacific Northwest are at significant risk for a near field tsunami caused by a subduction zone earthquake similar to the 2011 Tohoku Japan tsunami. The Cascadia Subduction Zone (CSZ) runs off the coast of Washington, Oregon and northern California, and there is a 14% chance that a large magnitude quake will cause a near field tsunami along the CSZ in the next 50 years (Groat, 2005; USGS, 2006). During a near field tsunami the tsunami wave reaches land in 15-30 minutes, which doesn't provide sufficient time for a majority of the population to evacuate.

The current United States' tsunami evacuation procedures are to evacuate everybody from the inundation zone; which is often unrealistic and ignores the possibility of using vertical evacuation. The use of vertical evacuation allows people who do not have sufficient time to evacuate the inundation zone to seek shelter in specially designed tsunami resilient structures. The Federal Emergency Management Agency (FEMA) recently published a design guide for vertical evacuation building, and computer simulations have shown that use of these structures can significantly reduce the loss of life (FEMA, 2008; Yeh et al., 2009). As the results of recent tsunami projects are published, these design guidelines can be improved.

The experiments outlined in this Master's Thesis are part of a large multiyear project, "Housesmash," founded by the Network for Earthquake Simulation (NEES). The NEES Housesmash project is a six part research project investigating mitigating the risk of coastal infrastructure through better understanding of tsunami-structure interaction. This thesis examines work done for task 1 and task 2. Work for task 1 was conducted at Oregon State Universities' O.H. Hinsdale Wave Lab large wave flume (LWF), and consisted of 12 unique sub experiments that looked at tsunami wave impact on light-frame wood walls. The work for task 2 was conducted at Oregon State Universities' Gene D. Knudson Wood Structural Testing Laboratory; where 10 sub experiments were conducted. The experiments in task 2 used similar wood walls as task 1, and further investigated the performance of light-frame wood structure under simulated tsunami loading conditions.

The first manuscript will present the findings from a subset of the experiments conducted during task 1, with specific discussion of wood wall performance under tsunami loading, hydrodynamic force quantification, and evaluation of the linear momentum equation. The second half of this thesis, manuscript 2, will discuss the results from task 2. More specifically, manuscript 2 discusses the elastic and inelastic response of light-frame wood shear walls monotonically loaded at intermediate heights, the elastic stiffness and behavior of an out-of-plane wall in multiple configurations, and replicated failures observed during testing in the LWF as part of task 1.

The information gained from these experiments is useful for advancing both the tsunami research and design communities as more emphasis is placed on tsunami mitigation along the Pacific coast. This information helps designers make informed decisions when designing tsunami resilient structures.

MANUSCRIPT 1:
EVALUATION OF TSUNAMI LOADS ON WOOD FRAME WALLS
AT FULL SCALE

David Linton, Rakesh Gupta, Dan Cox, John van de Lindt, Mary Elizabeth Oshnack, Milo
Clauson

Abstract

The performance of full-scale light-frame wood walls subjected to wave loading was examined using the Large Wave Flume of the Network for Earthquake Engineering (NEES) Tsunami Facility at Oregon State University. The hydrodynamic conditions (water level and bore speed) and structural response (horizontal force, pressure, and deflection) were observed for a range of incident tsunami heights and for several wood wall framing configurations. The walls were tested at the same cross-shore location with a dry bed condition. For each tsunami wave height tested, the force and pressure profiles showed a transient peak force followed by a period of sustained quasi-static force. The ratio of the transient force to quasi-static force was 2.2. These experimental values were compared to the predicted values using the linear momentum equation previously evaluated by Cross (1967), and it was found that the equation predicted the measured forces on the vertical wall within an accuracy of approximately 20% without using a momentum correction coefficient. The experiments also showed that the more flexible 2x4 wall resulted in lower peak forces when compared to the 2x6 walls subjected to similar tsunami heights. However, the 2x6 walls were able to withstand larger waves before failure.

Introduction

The recent earthquake and subsequent tsunami that devastated Japan in March 2011, along with the December 2004 Indian Ocean Tsunami that caused severe damage and loss of life to numerous coastal communities, underscores the need for a better understanding of tsunami-structure interaction. These events along with several recent smaller tsunamis have further reminded the world of the vulnerability of coastal communities during tsunami events. Prior to this disaster little research has focused on tsunami structure-interaction. A majority of the previous knowledge was from field reconnaissance (Lukkunaprasit and Ruangrassamee, 2008), or small scale laboratory experiments (e.g., Cross, 1967; Ramsden, 1996; Lukkunaprasit et al., 2009). Several experiments have been conducted on small scale vertical walls with regular or random waves, however large scale tsunami loading has been limited (Arikawa, 2009). Approximately 95% of buildings in the United States utilize light frame wood construction. For this reason the experiments in this study focus on investigating full-scale wood frame wall performance, force, and pressure data for solitary waves similar to those that occur during a tsunami. This paper presents the methodology and results of a large-scale experimental program for tsunami waves on wooden vertical walls in the Large Wave Flume of the Network for

Earthquake Engineering (NEES) Tsunami Facility at Oregon State University. The purpose of this work was to investigate how a flexible structure performs when subjected to a solitary wave bore, and compare the measured forces with predictive equations from the literature. The specific objectives were:

- To evaluate the linear momentum equation developed for steady flow assumptions, and determine if the force coefficient, C_f, developed by Cross (1967) is necessary.
- To observe the performance of light frame wood walls during a tsunami event.

Numerous studies have been conducted on the generation and propagation of tsunamis across the ocean. However, research on the inundation and subsequent impact of tsunamis on structures is less common. For many years research has been conducted on wave forces on vertical walls, but a majority of these experiments have been conducted at a small scale. Ramsden (1996) focused on the impact of translator waves (bores and dry-bed surges) on a vertical wall at a small scale, rather than breaking waves at a large scale. The measured forces and moments in Ramsden's study should only be used in relation to sliding and overturning, as they are not applicable to punching failures. Also tested at a small scale were several scale model houses. Thusyanthan and Madabhushi (2008) investigated the effects of openings and anchorage on force and pressure for a 1:25 scale model house. Wilson et al. (2009) developed an understanding of the nature of wave loading on a wood-framed scale residential building model for a variety of building configurations and test conditions. Testing was performed on a 1/6th scale two-story wood-framed residential structure. The structure was impacted with waves and tested in both flooded and non-flooded conditions. The measured forces were mainly uplift forces due to wave loading, and resulting overturning moments. The qualitative analysis of the data showed that differences in structural stiffness throughout the structure will cause a different load distribution in the structure, e.g., overhanging eaves above the garage can provide unanticipated loading conditions, water traveling beneath the structure generates predominantly uplift forces and the effect of waves breaking on or near the structure greatly increases the loading. The ratio of force from the windows closed condition to the windows open condition is approximately 2.5:1. Using the results from the 1/6th scale house, van de Lindt et al. (2009b) developed a base shear force relationship to wave height.

Arikawa (2009) used a large-scale hydraulic flume to determine the failure mechanisms due to impulsive tsunami loads on concrete walls. Based on wave speed and profile that study also focused on qualitatively dividing surge front tsunami force into three types: overflow, bore, and breaking. Overflow is defined by a low flood velocity. Bore flow is characterized by quick flow and the inundated tsunami carries out soliton fission. The third type, breaking, is described where the tsunami breaks in front of the structure; often caused when the building is close to the shore or a steep sea bed. Oshnack (2010) utilized the same wave flume and bathymetry discussed in this paper to examine the tsunami load effects from varying the cross shore location of a vertical rigid aluminum wall. Robertson et al. (2011) examined the forces from waves propagating on a flooded reef, using the same flume bathymetry and aluminum wall as Oshnack. The results were then compared to equations, including the work of Cross (1967), and a new equation was developed for use with flooded reef conditions.

Along with the numerous laboratory experiments to study the effects of tsunamis discussed above, there have been many lessons learned from field reconnaissance. The buildings of the 2004 Indian Ocean Tsunami in Thailand were analyzed by: Lukkunaprasit and Ruangrassamee (2008), Ruangrassamee et al. (2006), and Saatcioglu et al. (2006). The hydrodynamic forces from the tsunami were larger than anticipated and exceeded the design wind loads for the coastal buildings. The poor construction and detailing standards also contributed to the substantial structural failures observed during this tsunami.

A Special Issue of the *Journal of Disaster Research* (Volume 4, Number 6, December 2009) contained multiple papers that focused on tsunami loading on structures. Arikawa (2009) performed large-scale experiments in Japan investigating performance of both concrete and wooden walls under impulsive tsunami forces. Arikawa concluded that the walls would break when a 2.5m tsunami force hit the walls. Oshnack et al. (2009) evaluated the effectiveness of seawalls in reducing tsunami forces on an aluminum wall and van de Lindt et al. (2009a) measured lateral force on one-sixth scale residential building typical of North American coastal construction due to tsunami wave bores. Several authors examined tsunami forces on various structures: Arnason et al. (2009), Fujima et al. (2009), and Lukkunaprasit et al. (2009).

For the case of uniform steady flow impinging on a vertical boundary, the force per unit width, F, can be estimated using the conservation of linear momentum (Cross, 1967) as

$$F = \frac{1}{2}\rho g h^2 + \rho h u^2 \qquad (1)$$

where ρ is the fluid density, g is the gravitational constant, h is the water depth of the flow, and u is the depth uniform velocity. For the case of a wedge of water with non-uniform flow, Cross (1967) gives

$$F = \frac{1}{2}\rho g h^2 + C_f \rho h u^2 \qquad (2)$$

where C_f is a force coefficient and can be related to the angle θ made by the leading edge to the dry bed. The force coefficient is small for small angels and varies $1 < C_f < 1.5$ for theta in the range $0 < \theta < 30$ degrees. Comparing to laboratory observation using a small, 6.9 m wide by 0.15 m wide, glass walled flume, Cross (1967) found that Eq 1 adequately predicted the force for surges with surface slopes less than 10 to 15 degrees, and gave some indication that the force coefficient in Eq 2 should be used to predict the sharp peak resulting from splash back of water after the initial impact. An objective of this work is to use large-scale tests to evaluate whether Eq 1 holds for the case of an unsteady bore impinging on a wall or whether a correction coefficient, C_f, is needed.

For clarity, since both the maximum force and the quasi-steady force are related to the hydrodynamic conditions for a tsunami bore impinging on a fixed object, the term "transient force" is used to describe the peak force during the initial bore-structure interaction, and "quasi-static force" is used to describe the quasi-static force as the bore is reflected from the structure.

Experimental Setup

Wave Flume Bathymetry

The experiments were conducted at the NEES Tsunami Facility in the Large Wave Flume (LWF) at the O.H. Hinsdale Wave Research Laboratory at Oregon State University. The flume was 104 m long, 3.66 m wide and 4.57 m deep. The flume was equipped with a piston type wavemaker with a 4 m stroke and maximum speed of 4 m/s, with the capacity of generating repeatable solitary waves. The LWF bathymetry consisted of a 29 m flat section in front of the

wavemaker, followed by a 1:12 slope impermeable beach for 26 m, with the rest of the flume consisting of a flat section on a 2.36 m high false floor. This section will be referred to as the "reef" to be consistent with other experiments conducted at the O. H. Hinsdale Wave Research Laboratory (e.g., Robertson et al., 2011). The LWF bathymetry is shown in Fig. 1.1, including the test specimen in relation to the wavemaker.

Flume Instrumentation

The LWF was instrumented (Fig. 1.1) with ten wire resistance wave gages (WG) and four ultrasonic wave gages (USWG) along the flume to measure variations in the instantaneous water surface level as the wave moved inland. These gauges were calibrated at the start of the experiment and when the flume was drained and refilled. WG 1 to 10 were placed at x-positions of 17.64 m, 28.60 m, 35.91 m, 40.58 m, 42.42 m, 44.25 m, 46.09 m, 48.23 m, 50.37 m, and 54.41 m respective to the wavemaker in the zeroed position. USWG 1 was co-located with WG 4 (40.58 m), and this enabled the calibration of the other surface piercing gages. USWG 2 and 3 were located at x-positions 54.35 m and 58.07 m respectively. A fourth USWG was located on the moveable bridge at x-position 21.50 m. The wavemaker was instrumented with sensors to track the wavemaker x-position and water level on the wavemaker board. The LWF was also equipped with four acoustic-Doppler velocimeters (ADV) to collect wave particle velocities at (x, y, z) positions, meters, of: ADV 1 (43.33, -1.10, 1.67), ADV 2 (47.01, -1.08, 1.95), ADV 3 (54.24, -1.28, 2.45), and ADV 4 (57.89, -1.33, 2.45). The locations for these wave profile and velocity instruments can be found in Fig. 1.1. The velocity from ADV 4, 0.09 m above reef, and wave height from USWG 3 were used in calculating Eq 1, because they were co-located closest to the structure. WG 2 was used to measure the offshore tsunami wave height, H_2.

Specimens and Configurations

The test specimens used in these experiments were flexible wood walls commonly found in residential and light commercial construction. During the transverse wood wall (TW) experiments three different specimens, see Table 1.1, were used. The first specimen used was "Specimen 1", a 2x6 (38 mm x 140 mm) wall sheathed with 13 mm (0.5 inch) 5-ply Structural 1 plywood. Two replicates (1A,B) of Specimen 1 were built and tested. The wall was 3.58 m (11.75 ft) long and 2.44 m (8 ft) high having a stud spacing of 40.6 cm (16 inches) on center. The second wall, "Specimen 2," was the same dimension as Specimen 1, but was made with 2x4 (38

mm x 88 mm) dimension lumber instead of 2x6. Two replicates (2A,B) of specimen 2 were built and tested. The last specimen was "Specimen 3," which was a similar 2x6 wall as Specimen 1, but had a stud spacing of 61 cm (24 inches) instead of 40.6 cm. Only one specimen 3 (3A) was built and tested.

All the walls utilized a nailing pattern of 10.2 cm on center on edges and 30.5 cm on center in the field, with 8d common nails (63.5 mm long x 2.87 mm dia.). Each wall was constructed with Douglas-fir, kiln dry, #2 and better studs, and utilized double end studs.

During the eight different TW tests, see Table 1.2, three different anchorage and load cell configurations were utilized. Only the first four experiments are analyzed in this paper, because they have similar configurations and allow for comparison to Eq 1. For experiments "TransverseWoodWall_1" (TW 1), "TransverseWoodWall_2" (TW 2), "TransverseWoodWall_3" (TW 3), the wall was only anchored to the four horizontal load cells. Fig. 1.2 shows a picture of the wall and load cells, and Fig. 1.3 shows a schematic of the wall with instrumentation. For the "TransverseWoodWall_4" (TW 4) experiment the bottom sill was anchored to the flume floor with six anchor bolts (1.59 cm dia.) at distances of 0.41 m, 1.11 m, and 1.68 m from the center of the wall. The individual specimen information can be found in Table 1.1 and a summary of each experiment configuration and specimen used are shown in Table 1.2.

Wall Instrumentation

The walls were equipped with uni-axial donut shaped load cells with a capacity of ±89 kN (±20 kip). The TWs were equipped with four load cells, one at each corner of the wall (Fig. 1.2). They were mounted between a metal bracket bolted to the flume wall and a plate attached to the wall. This configuration measured the horizontal forces imposed on the wall during the tsunami event, and allowed for comparing the predicted forces from Eq 1 to the measured forces. Three pressure transducers were also installed on each wall at varying heights. The pressure transducers were mounted to aluminum plates, which were then placed into small holes in each wall. The walls were also equipped with two linear variable differential transformers (LVDT) at the middle of the wall to measure the deflection of the wall at critical locations. The LVDTs were placed at heights of 0.04 m (bottom plate) and 2.18 m (top plate) from the bottom of the wall.

When the wall was anchored, TW 4, the bottom LVDT was moved up to, 1.22 m, the mid height of the wall. Fig. 1.2 shows a picture of a TW 1 with all the instrumentation. Fig. 1.3 shows the location of each instrument for a typical TW experiment, and Table 1.3 summarizes the load cell and LVDT locations.

Experimental Procedure

Data Acquisition and Processing

Hydrodynamic data (free surface displacement and velocity) were collected at a sampling rate of 50 Hz. Force, pressure, and displacement data were collected with a sampling rate of 1000 Hz. The experiment names and trial numbers correspond to those in the experimental notebook supported under the Network for Earthquake Engineering Simulation (NEES) program of the National Science Foundation. Data from this project can be found on the NEEShub at http://nees.org/.

Experimental Process

As indicated in Fig. 1.1, the experiments were performed with a dry reef. When the wavemaker was in the zero position the water level was set at 2.38 m. The wavemaker was then retracted, causing a decrease in the still water depth to 2.29 m, referred to as D_o. This gives a depth below the reef of -0.07 m, referred to as D_R. Idealized solitary waves were used to model a tsunami caused by the forward motion of the wavemaker paddle. Because of the finite volume of the flume, this produced a still water level approximately +0.03 above the reef at the end of each run. For each experiment the wall configuration were tested at an x-position of 61.23 m from the wavemaker. During the eight different TW tests a total of 60 trials were run with a range of wave heights between 0.09 m and 1.04 m. The number of trials, wave heights, specimens used, load cell configuration, and failures are outlined in Table 1.2 for each individual experiment.

Unprocessed Data

Fig. 1.4 shows a portion of the raw data from TW 1 Trial01 tests with $H_2 = 0.29$ m as an example of the hydrodynamic forcing conditions and the structural response. Fig 6a shows the free surface time series measured at WG 2 at the toe of the slope (Fig 1) and is used to estimate the offshore tsunami height, H_2. Fig 6b shows the free surface profile of the bore over the reef measured by the third ultrasonic wave gage (USWG3) located 3.6 m seaward of the wall and is

used for h in Eq 1. Fig 6c shows the velocity measured by the fourth ADV (A4) co-located with USWG3 and used to provide u. Severe signal dropout occurred in the ADV record during the passing of the leading edge due to air entrainment. Thus, it was necessary to extrapolate the signal back to arrival of the bore indicated by USWG3. Independent video measurements show that this is a reasonable approximation and that the maximum velocity occurs at the leading edge for this type of flow (Rueben et al., 2011). Use of the extrapolated velocity increased the predicted forces in Eq 1 by an average of 18%. Fig. 1.4d shows the measured and extrapolated momentum flux per unit width, hu^2. Fig. 1.4e shows the pressure measured on the wall. Fig. 1.4f shows the measured total force found by summing the four the load cells. The transient force (circle) is highlighted as the maximum force in the figure and occurs after the initial impact and is related to the collapse of the water column after impact. The quasi-static force is estimated as the mean of the total force measured for a period of 1.0 s, starting 0.5 s after the peak transient force was observed and is indicated by a horizontal line. During this time, the bore has reflected from the wall is propagating back over the reef at a speed slower than the incident bore. It is important to note that no impulsive forces (defined as a sudden sharp rise in force of short duration during the initial interaction of the bore with the wall) were observed in these tests. Fig. 1.4g shows the deflection of the structure measured by LVDTs along the centerline of the specimen measured at the top plate ($D1$, $z = 2.36$ m) and bottom plate ($D2$, $z = 0.4$ m). These deflection measurements are used to assess the relative performance under transient and quasi-static load of the different wall assemblies described earlier.

Results and Discussions

Observed Maximum Transient Force and Quasi-static Force

Fig. 1.5 shows the measured maximum transient force and average quasi-static forces defined in Fig. 1.4f as a function of the offshore tsunami height H_2 measured at the toe of the slope. It is apparent that both the transient and quasi-static forces increase with offshore tsunami height. The variation in the transient force can be considered linear, although it does not pass through the origin, possibly due to the inertial effects of accelerating the wall at impact. The variation in the quasi-static force is also linear overall, except possibly for the larger observed wave heights ($H_2 > 0.55$ cm) where there is larger scatter in the data, shown by the large error bars for these points. In any case, it is of interest to compare the relative magnitudes of transient

force to quasi-static force as shown in Fig. 1.6. For this case, the relationship appears to be linear (R^2 = 0.938) with transient force being larger than the quasi-static force by a factor 2.2 overall.

Comparison with Cross (1967)

The predicted forces from Eq 1 were compared to the measured transient forces. For this comparison, the predicted force per unit width F was multiplied by the breadth of the wall, 3.66 m. The maximum momentum flux per unit mass, hu^2, was estimated using the extrapolated velocity, and the flow depth, h, from USWG3. The hydrostatic pressure term in Eq 1 was calculated using the flow depth corresponding to the maximum momentum flux.

Fig. 1.7 shows the measured transient force from TW 1, TW 2, and TW 3. These three experiments were chosen because they were unanchored along the bottom sill, so the force from the wave was measured by the four load cells. Trials with small tsunami wave heights (H_2~0.1 m) were excluded because of the poor quality of the ADV data due to air entrainment. As can be seen in Fig. 1.7, Eq 1 gives reasonable predictions of the peak transient force within an accuracy of about 20%. The force coefficient, C_f, was calculated using Eq 2, and the average was found to be C_f = 0.96 for this data set. Therefore, from a practical standpoint it is not necessary to include C_f to obtain reasonable estimates of the transient forces for engineering design. It is noted that although Cross (1967) expresses C_f as a function of the angle of the leading edge, such detailed information about the flow would likely be unavailable for engineering design.

Wall Performance

Fig. 1.8 compares the pressure (8a) and total force (8b) measured on three walls (TW 1, TW 2, and TW 3) with different framing configurations with the same incident tsunami conditions (H_2 = 0.29 m). The pressure was taken as the average of P2 and P3 located z = 20 cm from the bottom of the wall. For the wall construction, TW 1 and TW 2 had the same stud spacing (40.6 cm, or 16 inch on center) and TW 3 had a larger stud spacing (61.0 cm or 24 inch on center). TW 1 and TW 3 used the same dimensional lumber for the studs (2 x 6 studs), and TW 2 used smaller studs (2 x 4). All three used the same sheathing (1/2 inch plywood) and bottom sill (2 x 6). Therefore, it can be said that TW 1 was the stiffest of the three chosen for comparison, and other two were less stiff because they used smaller studs (TW 2) or greater stud spacing (TW 3). Fig. 1.8a shows that the pressure exerted by the tsunami on the wall were

similar, indicating that each wall was subjected to a similar wave loading, with peak pressures at about 4 kPa. The peak transient force responses were similar for TW 1 and TW 3 indicating that the stud spacing had little effect on the measured peak forces (Fig. 1.8b). However, the measured forces on TW 2 were measurably lower by about 25% because the smaller studs led to a greater deformation of the wall assembly thereby lowering the peak force. This reduction in load is only evident during transient force, before stabilizing to a similar quasi-static force as the other two walls. The same trends were observed for the range of wave heights tests for these three wall configurations, with an average transient force reduction in TW 2 of about 18%. This is a significant reduction in the forces that would be subsequently transferred to the rest of the structural systems when part of a building.

This reduction in transient force could be in direct relation to the flexibility of each wall. Fig. 1.9 shows the maximum deflection at $z = 2.36$ m, the top plate (9a), and $z = 0.04$ m, the bottom plate (9b), along the centerline of the wall as a function of the offshore tsunami height. The overall deflection of both the top and bottom plates are larger for TW 2 (square symbols). The increased flexibility of the 2x4 wall shown by higher deflections compared to the stiffer 2x6 walls, allows for dampening of the initial impact of the wave. This in turn reduces the transient forces on the wall. It should be noted that although the 2x4 wall was shown to reduce the transient force, the wall failed at a smaller wave height ($H_2 = 0.65$ m) than the similar 2x6 wall, because the 2x4 walls flexural capacity was lower. Although the forces on the overall system were reduced by the 2x4 wall, due to lower strength capacity, 2x6 construction should be used in tsunami zones.

The three transverse walls analyzed above show a good trend between wall flexibility and transient forces on each wall. However these walls were unanchored along the bottom plate, which is an uncommon scenario in standard building construction. Thus it is important to look at the effects of anchoring the wall in a similar fashion to common building construction, i.e. a slab on grade or stem wall foundation. Fig. 1.10 shows the maximum transient force vs. tsunami wave height for experiments TW 1 (Unanchored) and TW 4 (Anchored), which utilized identical specimens (1A,B). This shows the transient force on the anchored wall is significantly less; this is to be expected as the anchors absorb a large proportion of the load into the foundation (flume floor). This data indicates that the transient force is approximately half for the anchored wall.

Also, the measured deflection for the anchored condition is greatly reduced in comparison to the unanchored TW 1 setup. The unanchored wall also failed at a smaller wave height, while the anchored wall was not tested to failure because the physical limitations of the facility had been reached. Fig. 1.11 shows the complete failure of the bottom plate during Trial 16 of the unanchored wall test, TW 1, with a measured offshore wave height $H_2 = 0.87$ m. This failure was observed as the impact of the wave exceeded the bending capacity of the bottom sill plate (2x6 dimensional lumber, nominal capacity 1700 N-m). When the bottom plate was anchored to the flume floor during TW 4, this bending failure was no longer seen.

Summary and Conclusions

In this study a series of idealized, large-scale two-dimensional tsunami wave tests were performed on light frame wood walls used in typical coastal construction. The following can be concluded based on the work presented in this paper:

1. Transient forces were generated by the impact of the bore on a wall shortly after the initial impact. This was followed by a quasi-static force after the bore reflected from the structure. No impulsive forces were observed for these tests.
2. The ratio of the peak transient force to mean quasi-static force was 2.2 overall.
3. Eq 1 from Cross (1967) gives a good estimate of the measured peak transient force within about 20% uncertainty, and it was not necessary to include the momentum correction coefficient, C_f, in Eq 2.
4. The standard of construction can affect the peak transient force experienced by the wall by approximately 20% for the three types of construction considered here. Because the wave force is unaffected, the reduction in the peak transient force would either be transferred to other parts of the system or would contribute to permanent deformation of the wall and ultimately failure.
5. The quasi-static forces were similar for the three different wall specimens.
6. The deflection of the wall was greatly reduced when the bottom sill was anchored, as expected, and the anchor bolts absorbed half of the load when compared to the same wall in an unanchored configuration.
7. The controlling failure of the unanchored walls was bending of the bottom plate.

This study represents a significant step towards understanding the complex nature of wave-structure interaction, and the performance of light-frame wood construction often used in residential and light commercial buildings. By better understanding the failure modes of a wood wall during a tsunami event, building designs can be improved to better protect life safety and mitigate costly damage. Further research is necessary to investigate the effects of openings, three-dimensional flow, and plan irregularities on stress and load concentrations within a more complex structural system.

Acknowledgements
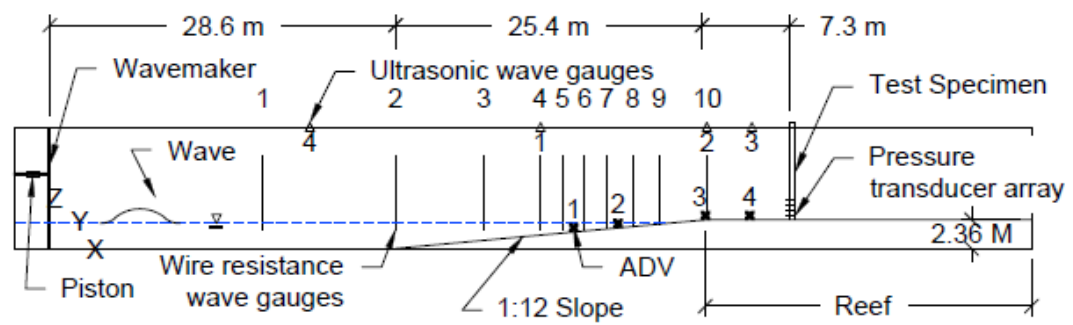
Fig. 1.

Fig. 1.1: Elevation view of wave flume with transverse wall setup
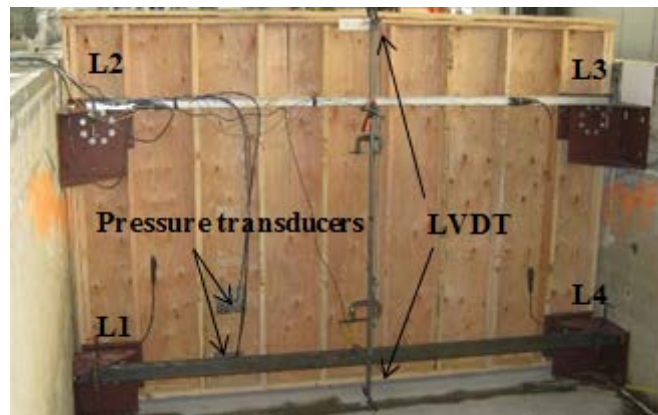
Fig. 1.2: Transverse wall instrumentation picture
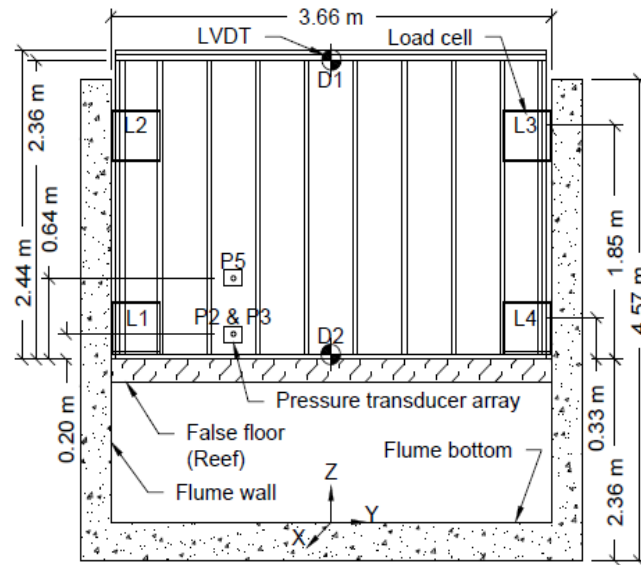
Fig. 1.3: Typical transverse wall setup with instrumentation
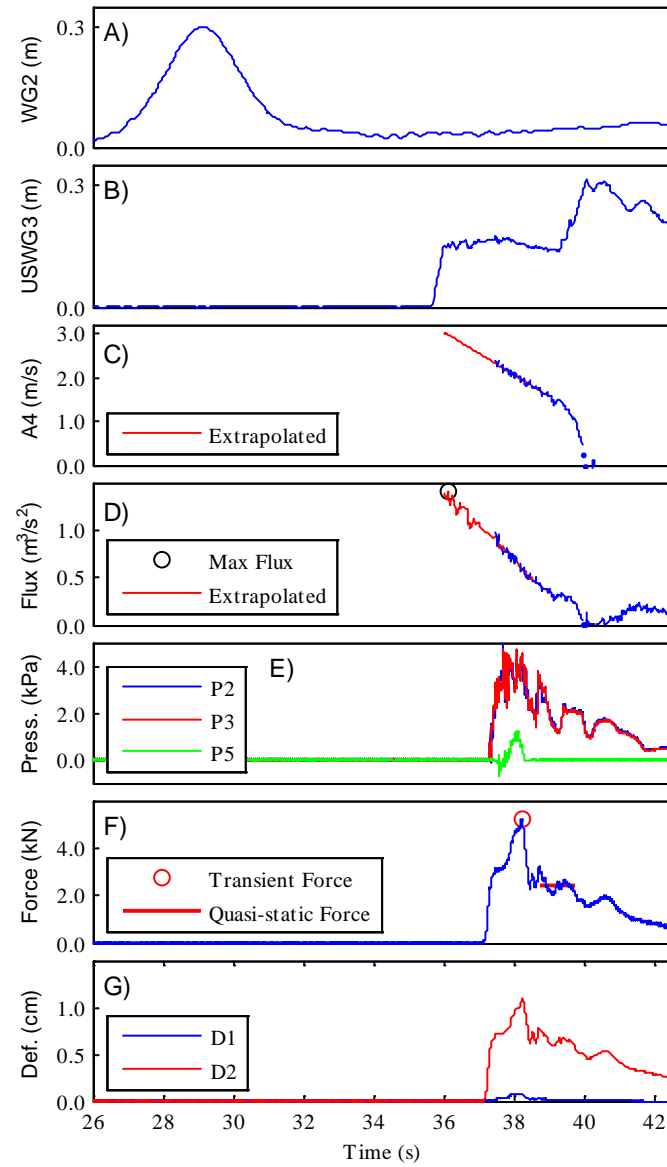
Fig. 1.4: Example raw data time history

(a) offshore wave height at WG 2; (b) onshore wave height at USWG 3; (c) velocity at ADV 4; (d) momentum flux at USWG 3 and ADV 4; (e) pressures; (f) total force, transient force, and quasi-static force; (g) deflection
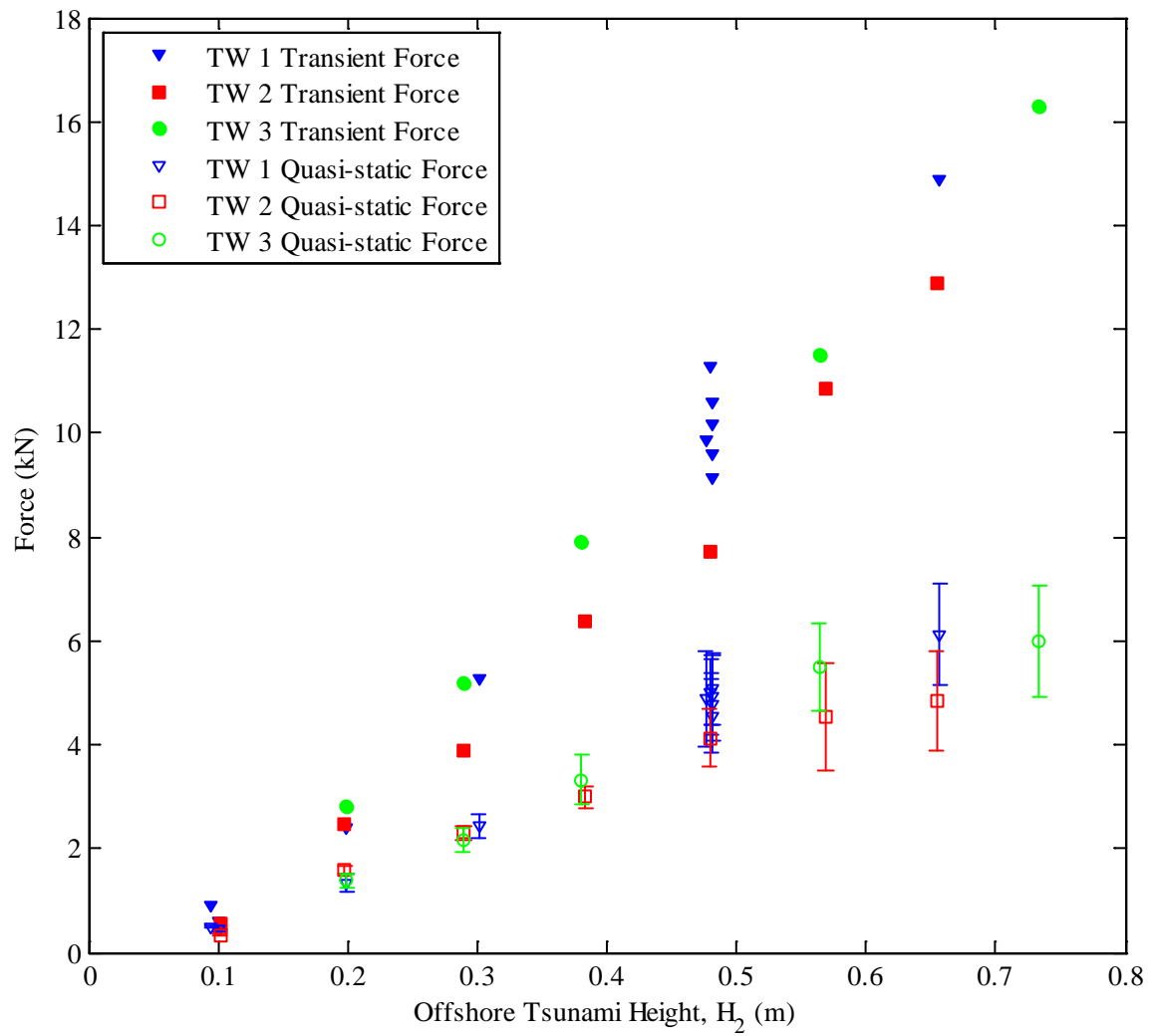
Fig. 1.5: Transient and quasi-static force comparison for TW1, 2, and 3
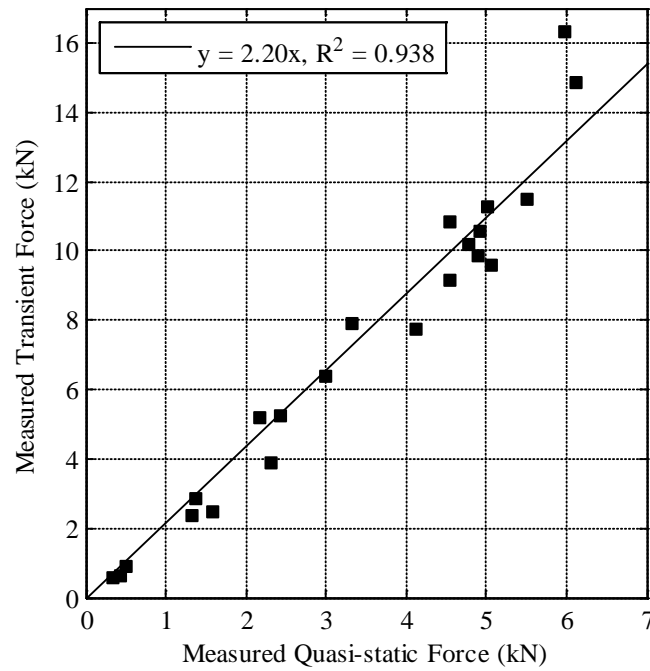
Fig. 1.6: Measured transient force versus measure quasi-static force
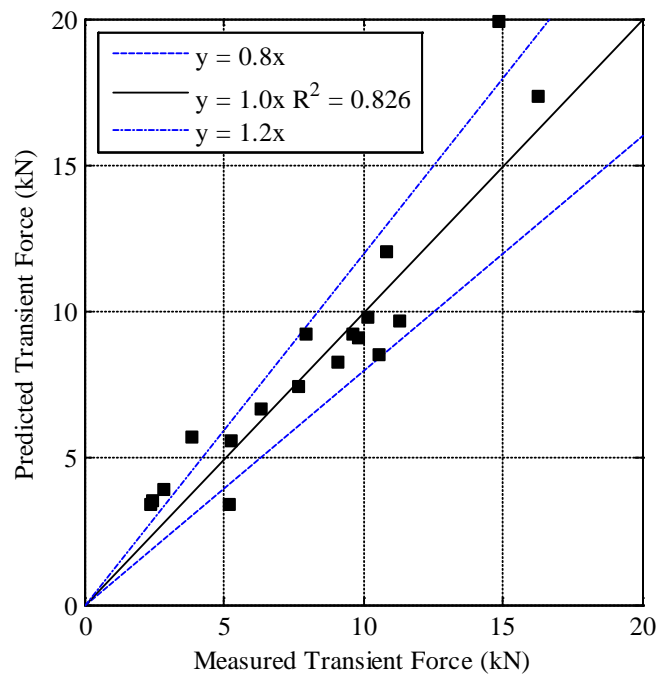
Fig. 1.7: Predicted (Cross 1967) versus measure transient force
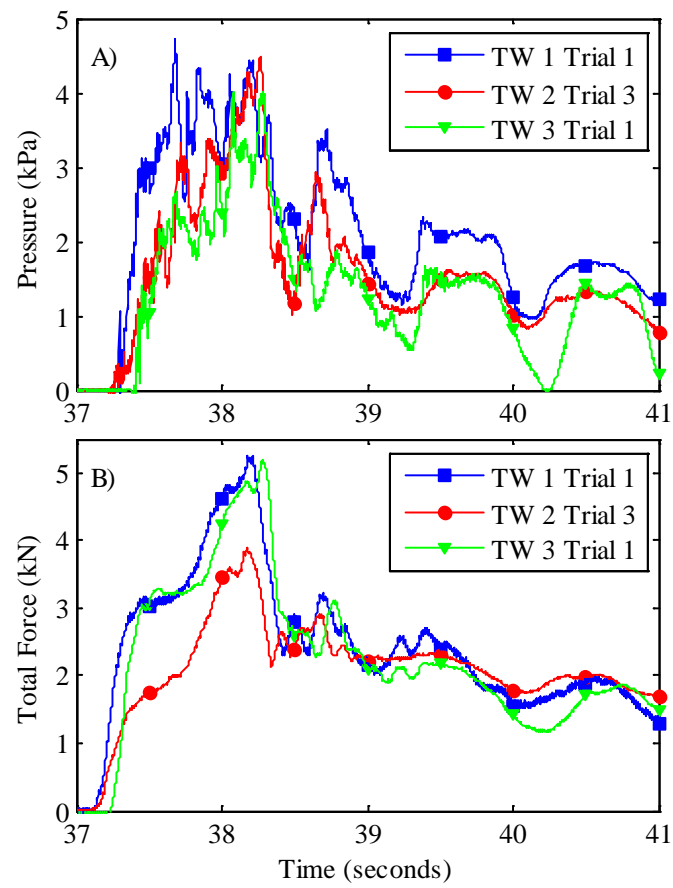
Fig. 1.8: Pressure (a) and total force (b) comparisons for TW 1-3 (H_2 = 0.29 m)
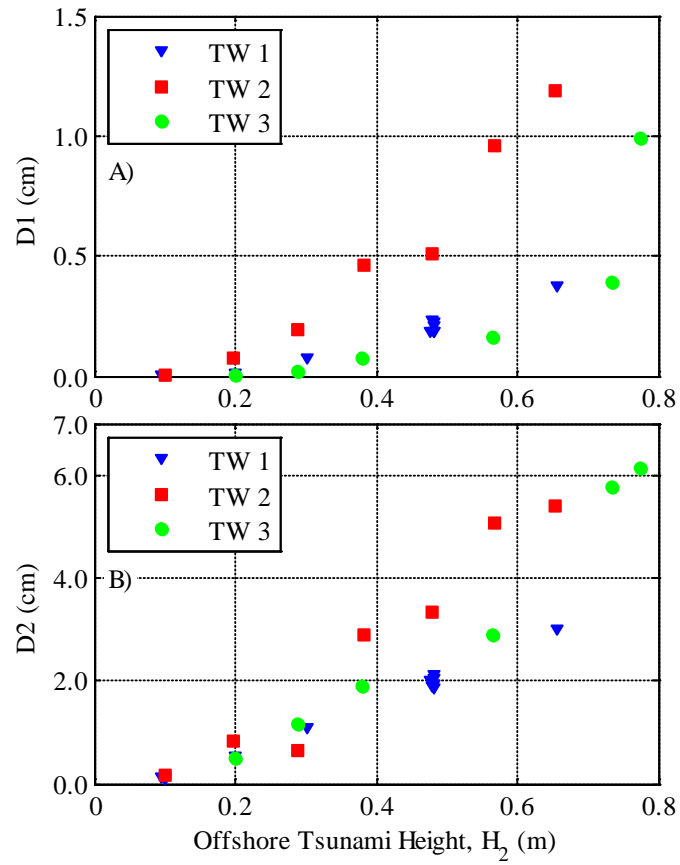
Fig. 1.9: Deflection D1 (a) and D2 (b) comparison for TW 1, 2, and 3
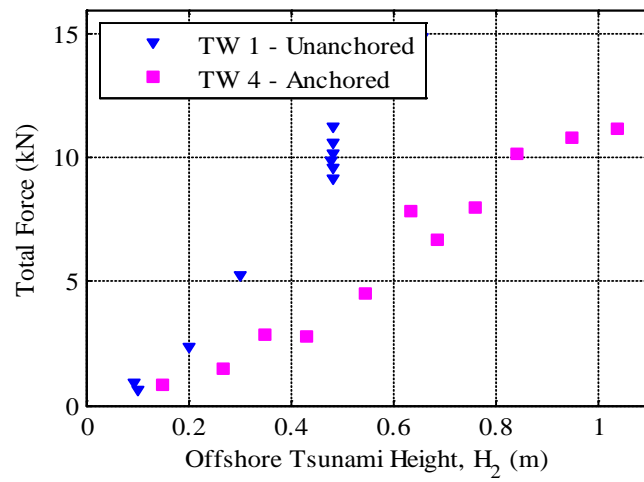
Fig. 1.10: Transient force comparison for TW1 and 4

Fig. 1.11: Failed bottom plate of TW 1 (Unanchored, Specimen 1A)

Table 1.1: Specimen Information

Specimens -	Spacing (cm)	Lumber Size	Length (m)
Specimen 1A,B	40.6	2x6	2.67
Specimen 2A,B	40.6	2x4	2.67
Specimen 3A	61.0	2x6	2.67

Table 1.2: Experiment Summary

Experiment	Trials	Wave Heights H_2 (m)	Specimen	Anchored	Load Cells	Failure
TW 1	12	0.10-0.87	1A	No	4	Yes
TW 2	7	0.10-0.65	2A	No	4	No
TW 3	6	0.20-0.78	3A	No	4	Yes
TW 4	11	0.15-1.04	1B	Yes	4	No
TW 5	11	0.14-0.93	1B	Yes	2 top	No
TW 6	4	0.25-0.68	2B	Yes	4	No
TW 7	4	0.26-0.71	2B	Yes	2 top	No
TW 8	5	0.09-0.48	2B	No	4	Yes

Table 1.3: Load Cell and LVDT locations

Experiment	Instrument	X	Y	Z
-	-	(m)	(m)	(m)
Load Cell (L)				
Transverse Walls[A]	L1[B]	61.44	-1.65	0.33
	L2	61.44	-1.65	1.85
	L3	61.44	1.65	1.85
	L4[B]	61.44	1.65	0.33
Linear Variable Differential Transformer (D)				
TW 1 – 3 & TW 8	D1	61.44	0	2.36
(unanchored)	D2	61.44	0	0.04
TW 4 – 7	D1	61.44	0	2.36
(anchored)	D2	61.44	0	1.22

x-location is measured from zeroed wavemaker

y-location is measured from center of flume

z-location is from base of test specimen

[A] Trials 1-6 for initial experiment TransverseWoodWall: L1 and L2 were switched locations

[B] Load cells 1 and 4 removed for experiments TransverseWoodWall_5 and TransverseWoodWall_7

References

Arikawa, T. (2009). "Structural Behavior Under Impulsive Tsunami Loading." *Journal of Disaster Research*, 4 (6), 377-381.

Arnason, H., 2005, *Interactions Between an Incident Bore and a Free-Standing Coastal Structure*, Ph.D. dissertation, University of Washington, Seattle, Washington.

Arnason, H., Petroff, C. and Yeh, H. (2009). "Tsunami Bore Impingement onto a Vertical Column." *Journal of Disaster Research*, 4 (6), 391-403.

Cross, R. (1967). "Tsunami Surge Forces." *Journal of the Waterways and Harbors Division*, Am. Soc. of Civil Engineers, 201-231.

Fujima, K., Achmad, F. and Shigihara, Y. (2009). "Estimation of Tsunami Force Acting on Rectangular Structures." *Journal of Disaster Research*, 4 (6), 404-409.

Lukkunaprasit, P. and Ruangrassamee, A. (2008). "Building damage in Thailand in the 2004 Indian Ocean tsunami and clues for tsunami-resistant design." *The IES Journal Part A: Civil & Structural Engineering*, 1 (1), 17-30.

Lukkunaprasit, P., Thanasisathit, N. and Yeh, H. (2009). "Experimental Verification of FEMA P646 Tsunami Loading." *Journal of Disaster Research*, 4 (6), 410-418.

Oshnack, M. E. (2010). "Analysis of Wave Forces on Prototype Walls under Tsunami Loading." M.S. Thesis. Corvallis, OR: Oregon State University.

Oshnack, M. E., Aguiniga, F., Cox, D., Gupta, R., & van de Lindt, J. (2009). "Effectiveness of Small Onshore Seawall in Reducing Forces Induced by Tsunami Bore: Large Scale Experimental Study." *Journal of Disaster Research*, 4 (6), 382-390.

Ramsden, J. (1996). "Forces on a Vertical Wall Due to Long Waves, Bores, and Dry-Bed Surges." *Journal of Waterway, Port, Coastal, and Ocean Engineering*, 122 (No. 3), 134-141.

Robertson, I. N., Riggs, R. H., and Mohamed, A. (2011). "Experimental Results of Tsunami Bore Forces on Structures." *Proceeding of the 30th International Conference of Ocean,* Off shore *and Arctic Engineering*. Rotterdam: ASME.

Ruangrassamee, A., Yanagisawa, H., Foytong, P., Lukkunaprasit, P., Koshimura, S. and Imamura, F. (2006). "Investigation of Tsunami-Induced Damage and Fragility of Buildings in Thailand after the December 2004 Indian Ocean Tsunami." *Earthquake Spectra*, 22 (S3), S377-S401.

Rueben, M., Cox, D.T., Holman, R., and Stanley, J. (2011) "Optical Measurements of Tsunami Inundation and Debris Movement using a Large-Scale Wave Basin" *Coastal Engineering.* (in preparation).

Saatcioglu, M., Ghobarah, A. and Nistor, I. (2006). "Performance of Structures in Thailand during the December 2004 Great Sumatra Earthquake and Indian Ocean Tsunami." *Earthquake Spectra*, 22 (S3), S355-S375.

Thusyanthan, N. and Madabhushi, S. (2008). "Tsunami Wave Loading on Coastal Houses: a Model Approach." *New Civil Engineering International*, 161, 27-31.

van de Lindt, J. W., Gupta, R., Garcia, R. and Wilson, J. (2009a). "Tsunami bore forces on a compliant residential building model." *Engineering Structures*, 31, 2534-2539.

van de Lindt, J., Gupta, R., Cox, D. T. and Wilson, J. (2009b). "Wave Impact Study on a Residential Building." *Journal of Disaster Research*, 4(6):419-426.

Wilson, J., Gupta, R., van de Lindt, J. Clauson, M. and Garcia, R. (2009) "Behavior of a one-sixth scale wood-framed residential structure under wave loading." *J. of Performance of Constructed Facilities*, 23(5):336-345.

MANUSCRIPT 2:
LOAD DISTRIBUTION IN LIGHT-FRAME WOOD BUILDINGS UNDER SIMULATED TSUNAMI LOADS

David Linton, Rakesh Gupta, Dan Cox, John van de Lindt

Abstract

The goal of this project was to better understand the contribution of individual elements to the performance of typical light-frame wood structures under simulated tsunami loading. A secondary goal was to replicate failures in a structural test facility that were observed during laboratory experiments on wood walls at the NEES Tsunami Facility at Oregon State University. The elastic and inelastic response of shear walls, out-of-plane walls, and a full light-frame wood structural system subjected to varying lateral loads (simulated tsunami loads) were observed using Digital Image Correlation (DIC). DIC provided a non-contact, three-dimensional measurement system that returned displacement measured at multiple areas of interest on the wall surface. Overall, these experiments show that the elastic stiffness and ultimate capacity at intermediate heights of a shear wall are significantly less compared to the stiffness and capacity at full height. The ultimate lateral capacity of the shear wall was reduced when tested in a full structural system with no additional lateral bracing. The results also indicate that the out-of-plane wall behaves like a one way slab with limited contribution from adjacent studs in carrying load. The stud to bottom plate connection failures observed during the wave tank tests were successfully reproduced, and indicated that the nailed connection needs to be reinforced to utilize the available capacity of the individual framing members.

Introduction

A series of several devastating tsunamis over the past decade has highlighted the need to develop a better understanding of these natural disasters, and how communities can better prepare for the next tsunami. With most tsunamis originating from a subduction zone earthquake the coastal communities of the Pacific Northwest are in a tsunami hazard zone. The Cascadia Subduction Zone (CSZ) runs along the Pacific coast from Northern California to Vancouver Island, and there is a 14% chance in the next 50 years that a near field tsunami will occur along the CSZ (Groat, 2005). The CSZ is the same fault type as the recent large earthquakes in Japan and Chile, and is expected to produce a major magnitude 9.0 earthquake; which highlights the need for proper preparedness for these high risk communities. With the vast majority of buildings in the United States being wood structures there is a need to better understand the performance of these structures during a tsunami event along the Pacific coast.

With the inherent limitations of testing full scale structures the majority of previous knowledge has come from field data reconnaissance (Lukkunaprasit and Ruangrassamee, 2008) or small scale laboratory experiments (van de Lindt et al., 2009). Testing full scale structures is generally limited to transverse walls in wave flumes (Linton et al., 2012, Arikawa, 2009). Due to the difficulty in testing full scale structures under tsunami loading this study focuses on simulating tsunami loading in a typical structural engineering laboratory on a full scale wood structure. This paper presents the methods and results of full scale testing of individual light frame wood walls and a typical wood structural system in the Gene D. Knudson Wood Engineering Laboratory at Oregon State University. The purpose of this research was to further investigate how a typical light frame wood structure performs under simulated tsunami loads. Specific objectives for this study were to simulate tsunami loads and to: 1) evaluate the elastic stiffness of individual structural components of a light frame wood structure, 2) investigate the contribution of each component to the performance of a full structural system, and 3) reproduce failure modes observed during hydrodynamic laboratory testing (Linton et al. 2012) in the tsunami testing facility at Oregon State University.

With wood shear walls being the primary lateral force resisting system in most light-frame wood structures, they are the light frame wood structural component that has received the most research focus. The majority of shear wall tests have been conducted under the ASTM E564 standard (ASTM, 2000), where an individual shear wall is loaded through the top plate of the wall. This testing procedure is used to evaluate the static load capacity and deflection of wood frame walls to be used in a lateral force resisting system. Additionally, wood shear walls are often tested using cyclic loading protocols to further capture the response observed during seismic events, i.e. the 1994 Northridge Earthquake. There have been numerous investigations, e.g., (Salenikovich and Dolan, 2003, Toothman et al., 2003, Seaders, 2009), into the contribution of fasteners, wall sheathing, hold downs, and various aspect ratios on wall capacity and stiffness. Sinha and Gupta (2009) evaluated the load and strain distributions in shear walls sheathed with both oriented strand board (OSB) and gypsum wall board (GWB) and only OSB on one side. The observed strains showed load was concentrated around the fasteners on the panel edges and the strains in the field of the panel were below the detectable limit of the data acquisition system. The behavior of the load distribution in the fasteners is important for better understanding the load path of lateral loads through the shear wall. Due to the load path observed during seismic loading

the effect of lateral loads applied at intermediate heights on a shear wall has been less important. This capacity at intermediate heights is of much greater importance during a tsunami event because of potentially large lateral loads from debris impact.

The out-of-plane performance of wood structures is also important to resist tsunami loading, and is therefore a significant portion of this project. The majority of previous work related to out-of-plane loading on wood walls is focused on wind design. Polensek and Gromala (1984) used computer software to simulate strength and stiffness distributions of a typical wood frame wall, and concluded that they could sustain wind loads in excess of a 100 year event. Rosowsky et al. (2005) and Bulleit et al. (2005) investigated the strength and reliability of wood walls subject to combined axial and transverse loads. The effect of combined loads is often overlooked when determining capacities for individual wall elements. The work of Rosowsky et al. and Bulleit et al. addressed this by correlating a simple beam-spring model with available test data. Winkel and Smith (2010) also researched the effect of combined in-plane and out-of-plane loading on wood walls and observed a capacity decrease of 25 to 40% when compared to only in-plane loading. The connections of the studs to the base plate strongly influenced the overall capacity of the wall when subjected to combined loading.

The testing of full structural systems is limited due to the difficulty of testing at full scale, essentially limiting full building analysis to finite element modeling. Martin (2010) used SAP2000 to model the load path of hurricane loads on a wood structure. Van de Lindt et al. (2010) tested a full scale six story wood frame apartment building on the world's largest shake table in Miki, Japan. The results were used to help validate the performance-based seismic design parameters developed in the NEESWood project.

With tsunami research being primarily limited to scale experiments, the investigation into detailed structural response has been limited and tsunami research has primarily focused on quantifying tsunami forces (Ramsden, 1996). The main source for structural performance knowledge has come from field reconnaissance (Lukkunaprasit and Ruangrassamee, 2008). Wilson et al. (2009) investigated wave loading on a 1/6th scale two-story wood-framed residential building utilizing several building configurations and test conditions. Uplift forces were measured from wave impact in both flooded and non-flooded conditions. From this a

qualitative analysis showed that differences in structural stiffness of components can cause different load distributions in the structure. Garcia (2008) used the same $1/6^{th}$ scale model as Wilson et al. (2009) to calibrate a nonlinear computer model (Pei and van de Lindt, 2007), which was then used to calculate the internal building forces based on the measured displacements from the wave tank tests. Arikawa (2009) tested both concrete and wood walls in a wave flume, and concluded that a 2.5 m off shore tsunami would cause the wood walls to fail. Linton et al. (2012) tested full-scale wood walls in a large wave flume, and observed both wall, performance and measured wave impact forces. The results showed that the linear momentum equation for steady flow assumptions did a good job of predicting the tsunami wave forces. Linton et al. also observed that increased wall flexibility resulted in lower transient forces, but didn't affect the quasi-static forces measured on the wall.

Materials and Methods

Specimens

All test specimens were designed in accordance with the prescribed sections of the 2008 Oregon Residential Specialty Code (ICC, 2008), and were constructed using No. 2 and better grade 38 x 140 mm (2 x 6 nominal size) kiln dried Douglas-fir dimension lumber. Specimen 1 was a 2.44 x 2.44 m shear wall with double top plates and double end studs at one end as shown in Fig. 2.1. Specimen 2, out-of-plane (OOP) wall, was the same size as specimen 1, but had two end studs (one flat) as shown in Fig. 2.2. Specimen 1 had a single stud at one end of the wall, that when combined with the two stud corner of specimen 2 is a typical three stud corner used in residential construction (ICC, 2008). This was used to more accurately represent current building practices.

For both wall specimens 1 and 2 the vertical studs were spaced at 0.40 m on center (o.c.), and were vertically sheathed with two 1.22 x 2.44 m x 11.1 mm 24/16 APA rated OSB panels. The double end studs and double top plates were face nailed at 610 mm o.c. with two 10d (3.3 x 75 mm) framing nails. Specimen 3 is a 2.44 x 2.44 m diaphragm with joists spaced at 0.61 m and sheathed with two 1.22 x 2.44 m x 18.3 mm sized for spacing sturd-I-floor APA rated tongue and groove plywood. All stud and joists were end nailed with three 16d (3.3 x 82.6 mm) nails per connection. Sheathing panels were connected to the framing using 8d (2.9 x 60 mm) nails spaced 0.15 m o.c. along the panel edges and 0.31 m o.c. in the field. All framing nails were full round

head, strip cartridge, and smooth shank nails that were driven using a pneumatic nail gun. Table 2.1 outlines the details for each specimen, a total of seven shear walls, three OOP walls, and one diaphragm were used.

Test Setup

There were two primary test setups used during these experiments. Setup 1 consisted of a single shear wall (Specimen 1, Table 2.1) bolted to a steel floor beam (foundation) as shown in Fig. 2.3. An additional steel beam (lateral restraint) was connected to the top plates with two 12.7 mm A307 bolts and was laterally braced to the strong wall. Setup 1 was used for the "Shear Wall" tests (SW1-5, Table 2.2). Setup 2A-C (Table 2.2) used two shear walls, an OOP wall (Specimen 2, Table 2.1), and a diaphragm (Specimen 3, Table 2.1) configured in a full structural system shown in Fig. 2.4 and Fig. 2.5. For setup 2 the diaphragm was connected to the top plates of the shear walls using Simpson H1 brackets at each joist, and Simpson HGA10KT brackets in-between each joist connected to the rim board. The HGA10KT brackets were used instead of toe nails to make it easy to change out specimens. Three different variations of setup 2 were used during testing. In all three variations the shear wall and diaphragm were connected together as discussed above. In the first variation, setup 2A, the OOP wall was isolated from the system by two load cells as shown in Fig. 2.4. The top corners of the OOP wall were attached to an 8.9 kN (2 kip) load cell at the top corner of each shear wall. Setup 2A was laterally restrained to the strong wall because the OOP wall didn't provide lateral support. For the second variation, setup 2B, the OOP wall was connected to the SW, but the diaphragm was not connected to the top plate of the OOP wall. Setup 2C was the same as setup 2B; however, the diaphragm was connected to the top plate of the OOP wall using three evenly spaced HGA10KT brackets. Fig. 2.4 shows setup 2C with the SW, OOP wall, and diaphragm all connected into a full system. The OOP wall was connected to a steel floor beam (foundation) using two 12.7 mm A307 bolts spaced at 1.83 m. Neither setup 2B nor 2C were laterally restrained.

These setups were used to show the individual influence of each component in a full structural system as each subsequent setup has more complicated boundary conditions. Setup 1 allowed for analysis of the individual shear wall, setup 2A isolated the OOP wall, setup 2B added in the SW and OOP wall corner boundary condition, and finally setup 2C included all three components working as a system.

All specimens were loaded using a 44.5 kN (10 kip) hydraulic actuator attached to the strong wall and supported by a ratchet strap. The hydraulic actuator had a 0.15 m total stroke, and was controlled by an MTS 406 servo controller. Attached to the hydraulic actuator was a 111.2 kN (25 kip) load cell.

Experimental Process

Individual shear walls (setup 1) were loaded in-plane at eight locations that correspond to increments of 0.31 m (1 ft) along the height of the wall, see Fig. 2.3. Elastic stiffness tests were performed where a single point load was applied at a rate of 2.54 mm/min (0.1 in/min) until a force of approximately 1.78 kN (400 lbf) was reached. Following the elastic tests a series of monotonic failure tests were performed on the shear walls at 0.61 m (2 ft) height increments. The failure tests were performed at a rate of 7.62 mm/min (0.3 in/min) to help maintain acceptable data acquisition and analysis. SW1 and SW5 are identical experiments, it was necessary to repeat the failure test due to improper setup of the load cell during SW1.

Following the SW tests a series of elastic stiffness experiments, "OOP1" (setup 2A), "OOP2" (setup 2B), and "OOP3" (setup 2C), using the same loading protocol were performed on the structural system of setup 2. For each of the OOP experiments the OOP wall was loaded with a point load normal to the surface, and was repeated at twenty different locations shown in Fig. 2.5. The twenty load locations were as follows: the edge of the wall (grid A) at the same eight heights from the SW experiments; and three interior studs (grids B-D) at height increments of 0.61 m (2 ft) on each stud. All heights are measured from the bottom of the wall. Note that the load location for each trial is labeled with the alphabetical grid and height, i.e. B4 or A7. The targets are labeled in Fig. 2.5. Table 2.2 outlines the setup, specimens used, number of trials, and load locations for experiment.

After the OOP tests two different failure tests, "FAIL1" and "FAIL2", were performed on the complete structural system (setup 2C). FAIL1 consisted of a horizontal distributed load applied across the middle three studs (grids C, D, E), normal to the OOP wall at 0.61 m (2 ft) above the base of the wall. A steel HSS section, shown in Fig. 2.6, was attached to the hydraulic actuator to simulate a distributed load. FAIL2 was a point load applied at the corner of the

diaphragm (A8), and is similar to the monotonic shear wall tests discussed above. Both tests were performed at a rate of 7.62 mm/min (0.3 in/min).

Data Acquisition

Data was collected using an optical measurement system, VicSnap, which used two cameras setup on a tripod to capture a time series of photos. The cameras were externally triggered and connected to a computer where images were saved and data from the load cells and hydraulic actuator displacement were recorded. The images were then analyzed using digital image correlation (DIC) proprietary software, Vic 3D (Correlated Solutions Inc., 2010), where a small subset of pixels were mathematically correlated with the base image (zero load) to get the 3D deflection data for each target. The data was then exported and processed in Excel and Matlab. Targets were used to provide an easily identifiable high contrast pixel area within the desired image area to measure the deflection of specific locations on the wall as shown in Fig. 2.5.

Digital image correlation has been used primarily for small scale stress and strain measurements (Choi et al., 1991), but have more recently been used for large scale experiments (Sinha and Gupta, 2009). Sinha and Gupta (2009) used a similar DIC setup to measure strain distribution in full scale wood walls, and successfully showed that the use of DIC on large scale specimens can provide accurate measurements. The use of DIC was advantageous for the scope of this project because it allows for accurate tracking of multiple areas of interest on the walls that would otherwise need to be individually instrumented.

Results and Discussion

Shear Wall Performance

The individual shear walls tested in setup 1 were loaded with low level forces to remain elastic, and were then loaded to failure. Setup 1 was used to allow comparison to typical monotonic shear wall tests. Fig. 2.7 is an example load vs. deflection plot from the elastic load test, SW5 Trial05, where the load was applied at grid H5. The results from the elastic tests are shown in Fig. 2.8, which shows the average stiffness along the height of the shear wall. The average stiffness was calculated from the load vs. local deflection plots when the load was applied at a specific height. From Fig. 2.8 one can see that the shear wall has significantly more

stiffness when load is applied to the top plate than anywhere else along the height of the wall. This result would be expected because the load path for load at grid 8 (full height) vs. grids 1-7 (intermediate heights) is different. The load at grid 8 is transferred through the top plates into the nails (approximately 30) around the top edges of both OSB panels, before being transferred through shear in the panel to the perimeter studs and bottom plate. In the case of loads at grids 1-7 the stud is loaded in bending with the sheathing nails acting as spring elements. In this case the majority of force is concentrated into only a few nails nearest the load. Also contributing to the total deflection is the rotation of the stud. With OSB sheathing only on one side an unbalanced loading condition exists where there are only nails resisting the applied load on one side of the studs, causing torsion in the stud. The combination of stud rotation and fewer nails sharing load results in lower stiffness values along the height of the wall.

A similar trend discussed above from the elastic tests is continued with the failure tests at grids 2 (0.61 m, 2 ft), 4 (1.22 m, 4 ft), 6 (1.83 m, 6 ft), and 8 (2.44 m, 8 ft). Fig. 2.9 shows the load vs. deflection curves for the failure tests from SW2 (grid 2), SW3 (grid 6), SW4 (grid 4), and SW5 (grid 8). The data from SW1 was not plotted because the load cell was improperly setup and maxed out before the wall failed. Similar to the elastic stiffness results from Fig. 2.8 the intermediate grids (2-6) show significantly lower capacities compared to grid 8. The sudden drop in load for SW3 was a result of the top plate splitting at the stud end nail farthest from the OSB sheathing. Due to the stud rotating this particular nail was highly stressed and caused the top plate to split, shown in Fig. 2.10.

The results from Fig. 2.8 and Fig. 2.9 are important when engineers start to consider debris impact loads during a tsunami event. Unlike a typical concrete or masonry shear wall, the wall has different load path characteristics and performs much different when intermediate points on the wall are loaded compared to the loading at the top which is considered for typical seismic design. The overall structural system could be sufficient to withstand the wave impact, but insufficient for local concentrated loads. The addition of blocking between studs at these locations could help transfer the load into the sheathing and subsequently increase the available capacity.

The inclusion of setup 2C in this testing provided a unique opportunity to compare the performance of an individual shear wall with a full structural system when loaded with a point load at the diaphragm level. Fig. 2.11 shows the load vs. deflection curves from failure experiments SW5 (setup 1) and FAIL2 (setup 2C). Due to different DIC camera positions for these two setups the displacements *u, v*, and *w* from the global directions *x, y*, and *z* don't correspond, so the results were transferred to a similar set of displacement coordinates $\delta 1, \delta 2$ and $\delta 3$. These coordinates are shown in Fig. 2.3 for SW5 and Fig. 2.5 for FAIL2. The three load vs. deflection curves in Fig. 2.11A correspond to the horizontal ($\delta 1$) and vertical ($\delta 2$) in-plane displacement and out-of-plane ($\delta 3$) displacement for an individual shear wall (setup 1) loaded at grid 8 (SW5 Trial 09). Fig. 2.11B shows the same load vs. deflection curves for a full structural system (FSS) (setup 2) loaded at grid A8 (FAIL2). The structural behavior of the FSS compared to the individual shear wall was similar, but because the FSS was semi-laterally braced by the out-of-plane wall the FSS had much larger out-of-plane displacements. The FSS had about three times the amount of out-of-plane deflection ($\delta 3$); whereas the individual shear wall was fully laterally restrained and had very little out-of-plane deflection. Due to this decreased lateral stability, the FSS only carried about 90% of the ultimate load compared to the individual shear wall. It was also observed that the FSS had less vertical uplift ($\delta 2$), which is most likely also attributed to the increase in out-of-plane deflection.

Out-of-Plane Wall

The contribution of individual structural elements (shear wall, out-of-plane wall, and diaphragm) were investigated using experiments OOP1 (setup 2A), OOP2 (setup 2B), and OOP3 (setup 2C). Similar to the shear wall experiments the elastic stiffness was measured at twenty locations on the OOP wall. Fig. 2.12 shows the stiffness for vertical grids B-D, which correspond to the wall studs shown in Fig. 2.5, and also includes the calculated stiffness for each location using an idealized simply supported beam model. The vertical axis corresponds to the horizontal grids 2-8. Fig. 2.13 shows the local out-of-plane deflections from OOP3 Trial09, where the wall was loaded at D2 with 1.71 kN.

The results from Fig. 2.12 indicate that there doesn't appear to be any significant interaction between adjacent studs or at the wall corner. The measured stiffnesses in Fig. 2.12 compare well to a simplified beam deflection model leading to the conclusion that the OOP wall

stiffness is directly related to the stiffness of each individual stud and therefore the wall can be idealized as a one way slab with the load going through each individual stud into the top or bottom plate like a simply supported beam and then into the shear wall. This is also shown with all three grids having similar stiffness profiles, further lending to the observation that there is no additional stiffness gained from the OSB sheathing and adjacent studs. The stiffness values for OOP3 are very similar to the values for both OOP1 and OOP2, which shows that at the low forces used during these experiments the diaphragm had little or no contribution to the stiffness. This is most likely because the stiffness of the double top plate is much greater than the flat bending stiffness of the 2x6 rim board, resulting in the top plate carrying the entire load at the low forces used during these experiments. Another contributing factor could be the small amount of slop in the connections between the diaphragm and top plate.

The results from an individual trial, OOP3 Trial09, shown in Fig. 2.13 also supports the conclusion that there is very limited contribution from adjacent studs when out-of-plane load is applied on the wall. When the load was applied at D2, we get the largest deflections at D2, with decreasing local deflections along the height of grid D. The other three adjacent studs have minimal deflections, which can likely be attributed to deflection of the top plate and some inherent looseness in the anchor bolt connection to the foundation.

These results are important for engineers, because it validates the common assumptions that out-of-plane walls can be treated as a simply supported beam element. This assumption makes the analysis of out-of-plane walls quick and easy. When looking at the effects of concentrated loads it is unrealistic to distribute loads over an area larger than the contact area because there is no significant load sharing between adjacent studs.

Simulated Failures

The failures of the out-of-plane wall stud to bottom plate connection that were observed during laboratory experiments in the Large Wave Flume at Oregon State University (Linton, 2012) were reproduced during two trials of the FAIL1 experiment. Fig. 2.14 shows the failures from Trial01 (Fig. 2.14A) and Trial02 (Fig. 2.14B). During each trial the same connection failure observed during the wave tank tests was successfully reproduced in the FAIL1 experiment. The loads vs. deflection results from both trials are shown in Fig. 2.15. The deflection is the average

from grids C2, D2, and E2. The small drop in load at approximately 20 mm of deflection for Trial01 was from the stud splitting at the connection as shown in Fig. 2.14A. The observed failures are important because it shows that a tsunami induced force can be simulated. It also shows that to improve the out-of-plane performance of light-frame wood structures during a tsunami event the stud to bottom plate connection needs to be strengthened. This connection could be easily improved with the addition of a simple metal bracket, with many different options available that are common in wood construction. With this connection properly secured the load path would be complete between the studs and bottom plate, thus allowing for more efficient use of the available capacity of the full structural system.

Summary and Conclusions

This study focused on the performance of full scale individual elements of light-frame wood construction, as well as a full structural system. Under a series of both elastic and inelastic load cases the elastic stiffness and ultimate load capacities were observed and the following conclusions can be drawn:

1. Both the elastic stiffness and ultimate load capacity were much greater at the full height of the shear wall compared to the other three intermediate heights.

2. The monotonic capacity of the shear wall when included in a full structural system was less than the capacity of an individual shear wall with a laterally braced, because of the reduced lateral stiffness of the structure.

3. The elastic stiffness and local deflections observed during the "OOP" experiments show that the out-of-plane wall behaves like a one way plate with very limited interaction between adjacent studs.

4. At the low force levels in these experiments it was also shown that the diaphragm provided negligible increase in the out-of-plane wall stiffness, most likely due to the inherent slop in the diaphragm to wall connections.

5. The structural failures observed during the hydrodynamic laboratory experiments at the tsunami testing facility at Oregon State University (Linton, 2012) were successfully reproduced. To better improve the performance of light-frame wood structures during a tsunami event it is necessary to increase the shear capacity of the nailed connection of the studs to the bottom plate along the out-of-plane wall.

The results and observations from this study provide important information towards improving the design of light-frame wood structures to better protect the lives of occupants and reduce structural damage during a tsunami event. The successfully simulation of failures observed during hydrodynamic testing also provides an avenue to expand tsunami simulation testing in a structural laboratory, helping to expand the available resources for researching structural performance during a tsunami. Further research is necessary to better understand the complex nature of tsunami-structure interaction.

Acknowledgements
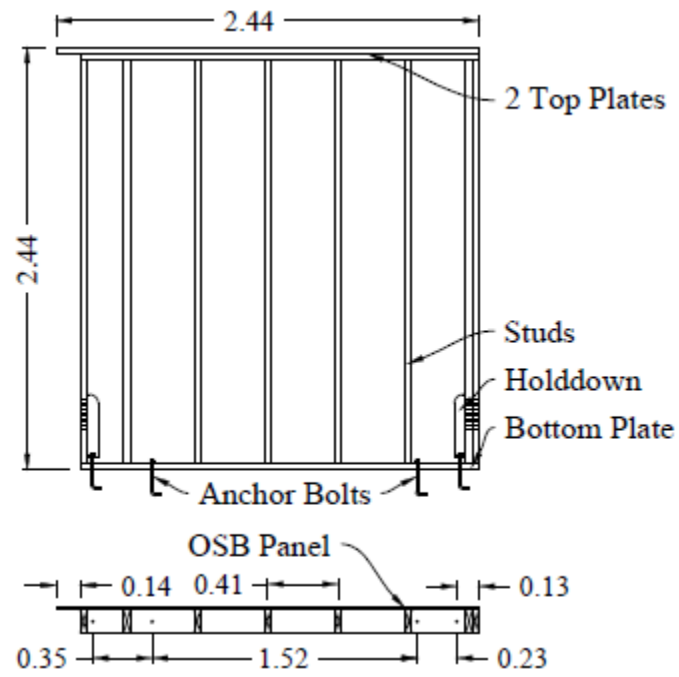
Fig. 2.1: Shear wall (specimen 1) schematic (dimensions in meters)
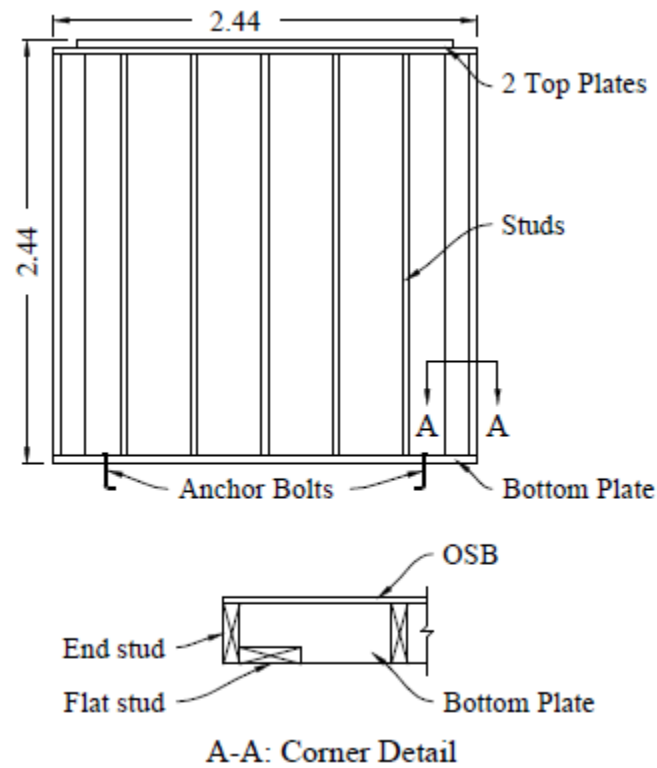
Fig. 2.2: Out-of-plane wall (specimen 2) schematic (dimensions in meters)
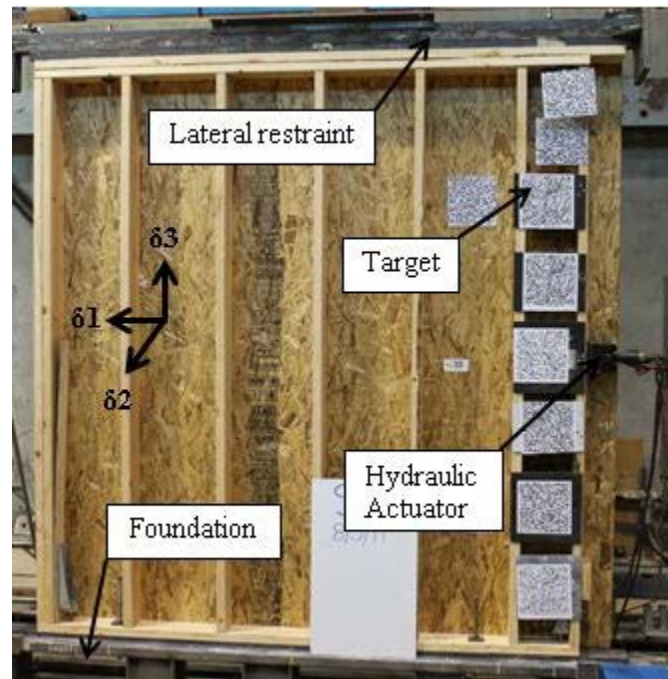
Fig. 2.3: Setup 1 setup (shear wall)
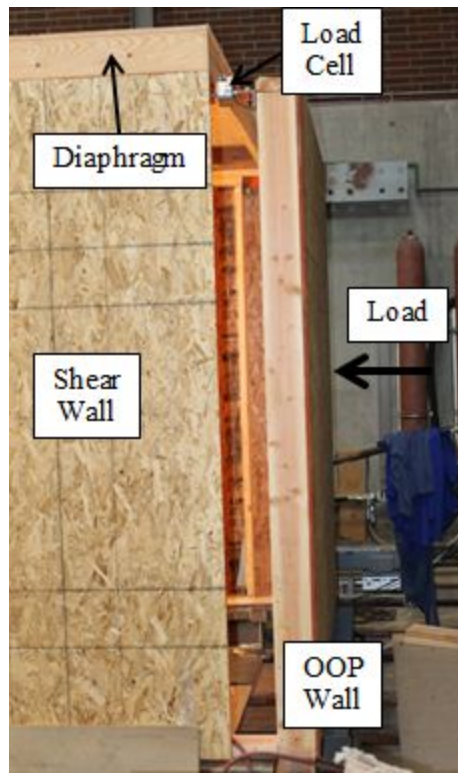
Fig. 2.4: Setup 2A (OOP1)

Fig. 2.5: Test setup 2C with grid and targets
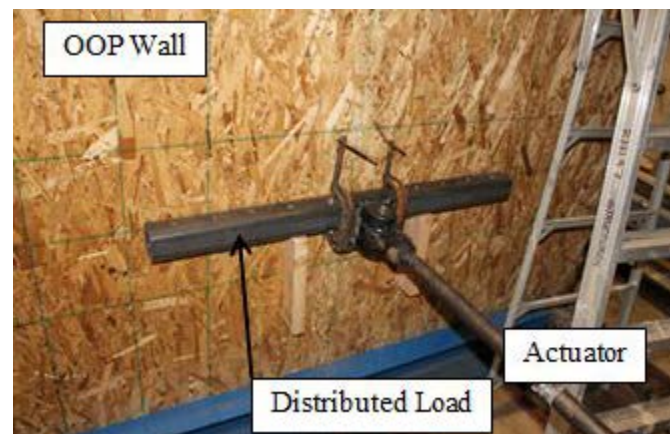
Fig. 2.6: FAIL1 loading setup
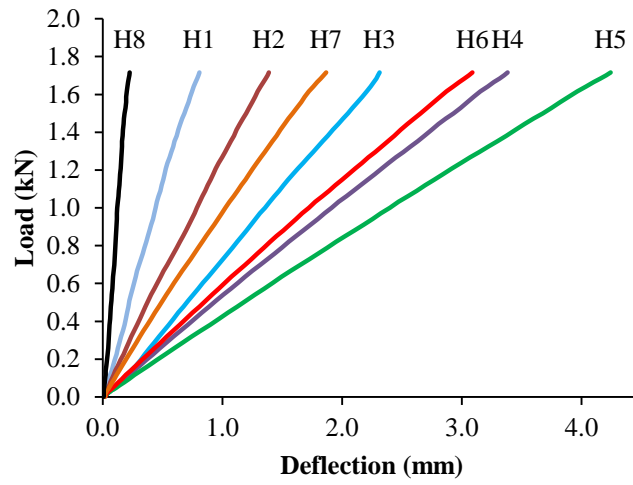
Fig. 2.7: Example data (SW5_Trial05, loaded at H5)
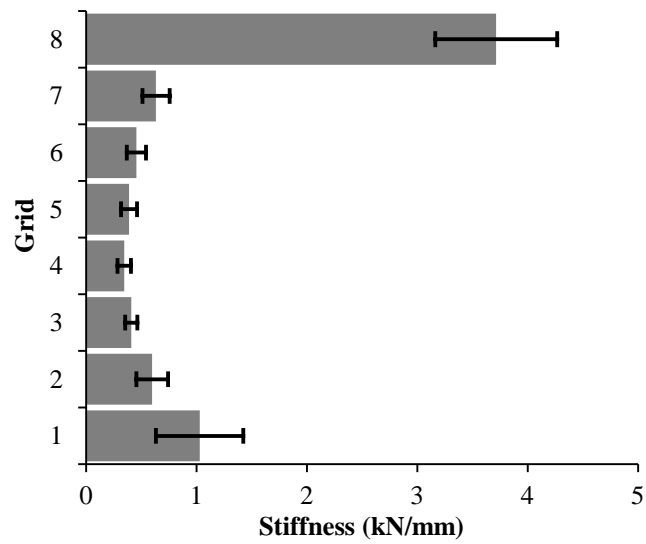
Fig. 2.8: Shear wall stiffness along wall height
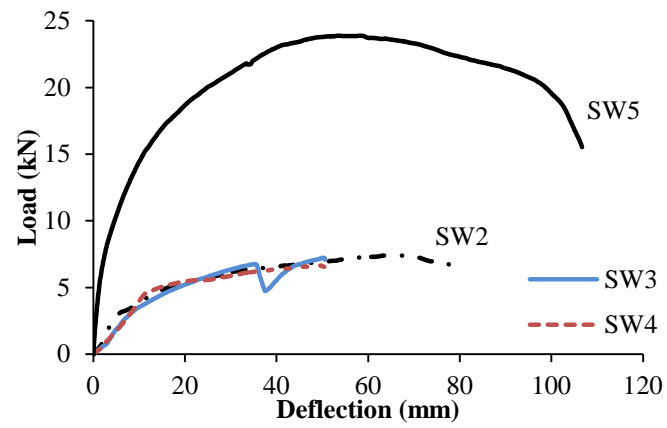
Fig. 2.9: Shear wall load vs. deflection curves

Fig. 2.10: Top plate splitting at stud connection
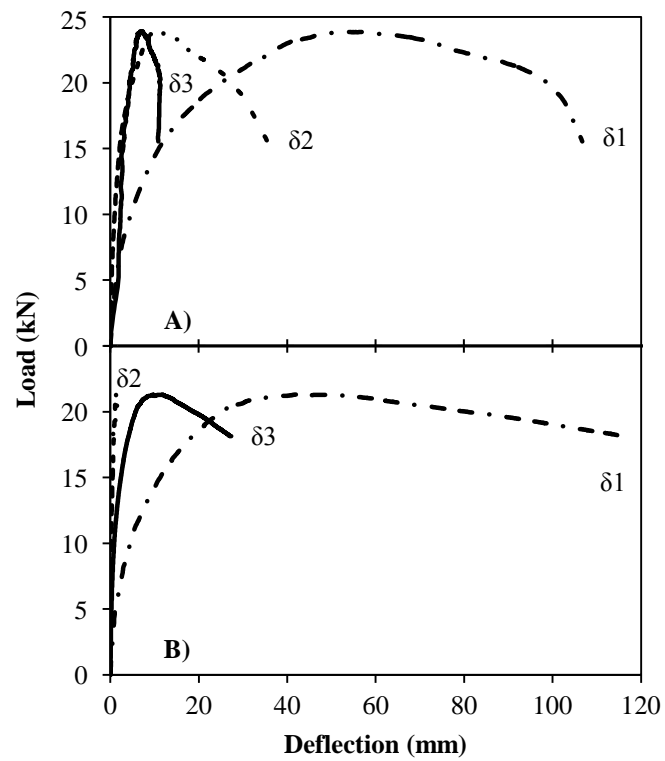
Fig. 2.11: Load vs. deflection curve at shear wall corner for A) setup 1 and B) setup 2C
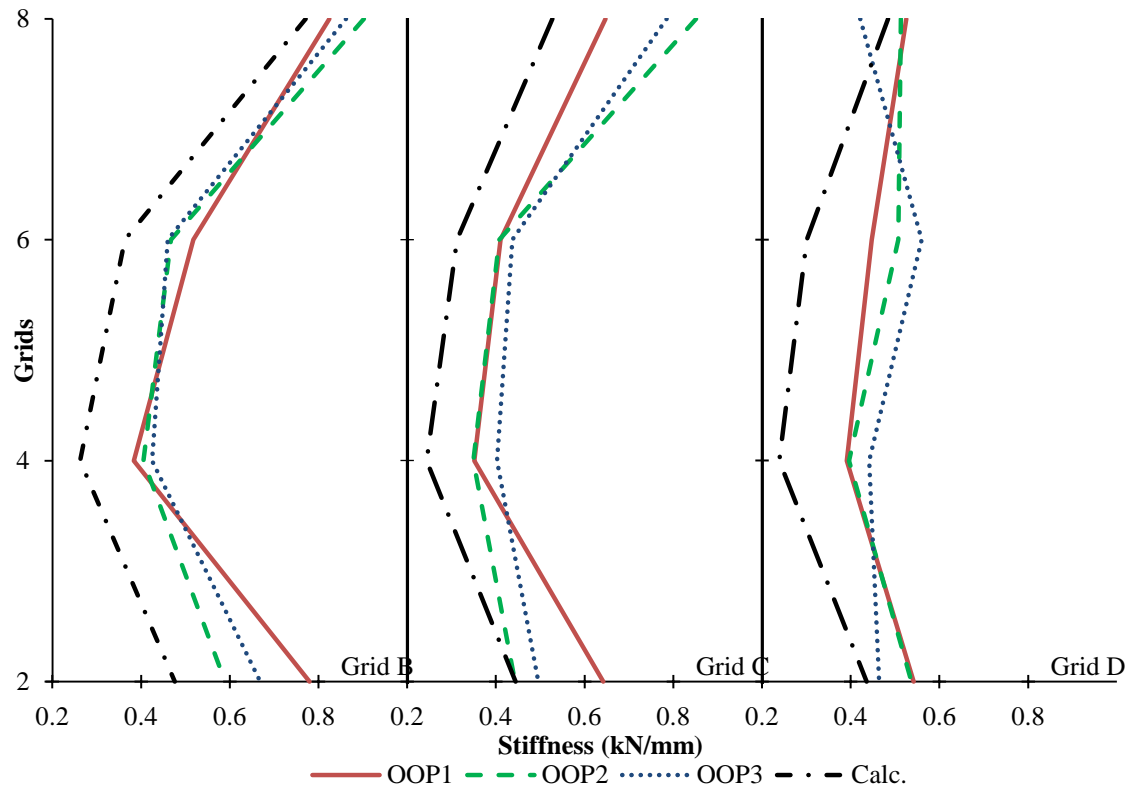
Fig. 2.12: Out-of-plane stiffness for experiments OOP1, OOP2, OOP3
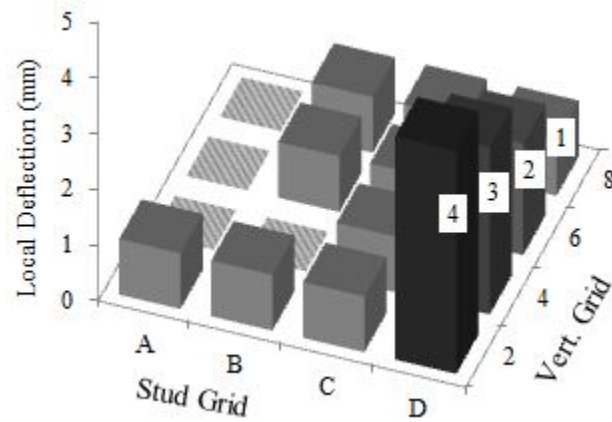
Fig. 2.13: Local deflections for experiment OOP3 Trial09 (setup 2C) with load applied at D2

Fig. 2.14: FAIL1 failures: A) Trial 01 stud splitting, B) Trial 02 stud to bottom plate connection failure
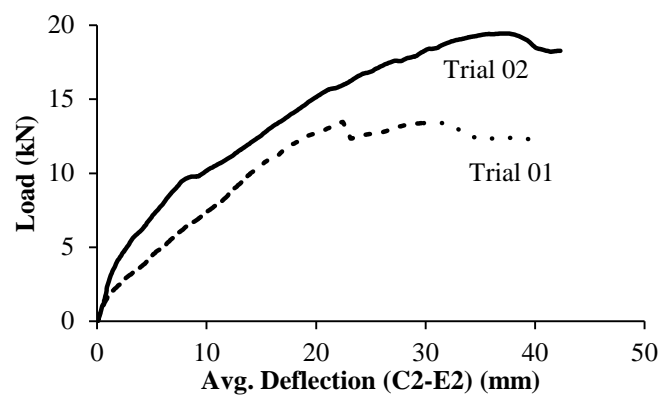
Fig. 2.15: Load vs. average deflection plot for FAIL1 experiment

Table 2.1: Specimen Information

Specimen	I.D.	Spacing	Sheathing
-	-	(mm)	-
Specimen 1A,B,C,D,E,F,G	Shear Wall	406	11.1 mm OSB
Specimen 2A,B,C	OOP Wall	406	11.1 mm OSB
Specimen 3A	Diaphragm	610	18.3 mm Plywood

Table 2.2: Experiment details

Test Setup	Test Name	Specimens Used	Trials	Test Description	Fail Test
1	SW1	1A	13	load at 1-8 ft and failure test @ 8'	Y
"	SW2	1B	9	load at 1-8 ft and failure test @ 2'	Y
"	SW3	1C	9	load at 1-8 ft and failure test @ 6'	Y
"	SW4	1D	9	load at 1-8 ft and failure test @ 4'	Y
"	SW5	1E	9	load at 1-8 ft and failure test @ 8'	Y
2A	OOP1	1F,1G,2A,3A	23	load at 20 grid points	N
2B	OOP2	1F,1G,2A,3A	20	load at 20 grid points	N
2C	OOP3	1F,1G,2A,3A	21	load at 20 grid points	N
2C	FAIL1	1F,1G,2A,3A and 1F,1G,2B,3A	2	load across C to D at 2ft	Y
2C	FAIL2	1F,1G,2C,3A	1	load at A8	Y

References

Arikawa, T. (2009). "Structural Behavior Under Impulsive Tsunami Loading." *Journal of Disaster Research*, 4 (6), 377-381.

ASTM. (2000). "Standard method of static load test for shear resistance of framed walls for buildings." *ASTM E 564-00*, West Conshohocken, Pa.

Bulleit, W.M., Pang, W.C., Rosowsky, D.V. (2005). "Modeling Wood Walls Subjected to Combined Transverse and Axial Loads." *Journal of Structural Engineering*, 131(5): 781-793.

Choi, D., Thorpe, J., Hanna, R. (1991). "Image analysis to measure strain in wood and paper." *Wood Science and Technology*, 25(4): 251-262.

Correlated Solutions Inc. (2010). *Vic 3D user's manual*, West Columbia, S.C.

Garcia, R.A. (2008). Wave and Surge Loading on Light-Frame Wood Structures." MS thesis. Colorado State University, Fort Collins, Colorado.

Groat, C.G. (2005). Statement of C.G. Groat, Director US Geological Survey, US Department of the Interior, Before the Committee of Science, US House of Representatives, January 26.

International Code Council (ICC). (2008). *2008 Oregon Residential Specialty Code*, Country Club Hills, IL.

Linton, D. (2012). "Tsunami Loading on Light-Frame Wood Structures." MS thesis. Oregon State University, Corvallis, Oregon.

Linton, D., Gupta, R., Cox, D., van de Lindt, J., Oshnack, M.E., Clauson, M. (2012). "Evaluation of Tsunami Loads on Wood Frame Walls at Full Scale." *Journal of Structural Engineering,* (in preparation).

Lukkunaprasit, P. and Ruangrassamee, A. (2008). "Building damage in Thailand in the 2004 Indian Ocean tsunami and clues for tsunami-resistant design." *The IES Journal Part A: Civil & Structural Engineering*, 1(1): 17-30.

Martin, K. (2010). "Evaluation of System Effects and Structural Load Paths in a Wood-Framed Structure" MS thesis. Oregon State University, Corvallis, Oregon.

Pei, S. and van de Lindt, J.W. (2007) *SAPWood user's manual*, Fort Collins, CO: Colorado State University.

Polensek, A. and Gromala, D. (1984). "Probability Distributions for Wood Walls in Bending." *Journal of Structural Engineering*, 110(3): 619-636.

Ramsden, J. (1996). "Forces on a Vertical Wall Due to Long Waves, Bores, and Dry-Bed Surges." *Journal of Waterway, Port, Coastal, and Ocean Engineering*, 122 (No. 3), 134-141.

Rosowsky, D., Yu, G., Bulliet, W. (2005). "Reliability of Light-Frame Wall Systems Subject to Combined Axial and Transverse Loads." *Journal of Structural Engineering,* 131(9): 1444-1455.

Salenikovich, A.J., Dolan, J.D. (2003). "The racking performance of shear walls with various aspect ratios. Part I. Monotonic tests of fully anchored walls." *Forest Products Journal*, 53(10): 65-73.

Seaders, P., Miller, T.H., Gupta, R. (2009). "Performance of partially and fully anchored wood-frame shear walls under earthquake loads." *Forest Products Journal*, 59(5): 42-52.

Sinha, S. and Gupta, R. (2009). "Strain Distribution in OSB and GWB in Wood-Frame Shear Walls." *Journal of Structural Engineering*, 135(6): 666-675.

Toothman, A.J. (2003). "Monotonic and cyclic performance of light-frame shear walls with various sheathing materials." MS thesis. Virginia Polytechnic Institute and State University, Blacksburg, Virginia.

van de Lindt, J., Gupta, R., Cox, D. T., Wilson, J. (2009). "Wave Impact Study on a Residential Building." *Journal of Disaster Research*, 4(6):419-426.

van de Lindt, J., Pei, S., Pryor, S., Shimizu, H., Isoda, H. (2010). "Experimental Seismic Response of a Full-Scale Six-Story Light-Frame Wood Building." *Journal of Structural Engineering,* 136(10): 1262-1272.

Wilson, J., Gupta, R., van de Lindt, J., Clauson, M., Garcia, R. (2009). "Behavior of a One-Sixth Scale Wood-Framed Residential Structure under Wave Loading." *Journal of Performance of Constructed Facilities*, 23(5): 336-345.

Winkel, M. and Smith, I. (2010). "Structural Behavior of Wood Light-Frame Wall Subjected to In-Plane and Out-of-Plane Forces." *Journal of Structural Engineering,* 136(7): 826-836.

CONCLUSION

Covered in this thesis is work conducted as part of the NEES Housesmash project, where the performance of light-frame wood structures subjected to tsunami loads was investigated. A series of large-scale experiments were performed in the Large Wave Flume at Oregon State University's O.H. Hinsdale Wave Research Laboratory and Gene D. Knudson Wood Engineering Laboratory.

During the transverse wall experiments, three different light-frame wood wall types were tested at the same cross-shore location over a range of wave heights. For these experiments it was found that there was a ratio of 2.2 between the peak transient force and quasi-static force (Fig. 1.6 – manuscript 1). It was also found that the wall type, i.e., 2x6 vs 2x4 framing lumber can affect the peak transient force measured on the wall by approximately 20% (Fig. 1.5 – manuscript 1). The quasi-static forces were similar for all three wall types. The estimated forces using the linear momentum equation from Cross (1967) were comparable ($\pm 20\%$) to the measured transient forces (Fig. 1.7 – manuscript 1). The momentum correction coefficient, C_f, was unnecessary to include.

Also observed during the transverse wall experiments in the Large Wave Flume, was the performance of the wood walls. When the walls were anchored to the flume floor the wall deflections were greatly reduced, and the anchor bolts subsequently absorbed half of the load in comparison to the same unanchored wall. The controlling failure of the unanchored walls, independent of lumber size, was bending of the bottom plate.

The wood wall tests performed in the Gene D. Knudson Wood Engineering Laboratory were a continuation on the investigation of wood structures performance during tsunami loading. During these experiments both individual 2x6 wood walls and full structural system (FSS) were subjected to simulated tsunami loads and the elastic and inelastic structural response were observed. From the shear wall experiments the elastic stiffness and ultimate load capacity at the full wall height (2.44 m) was much greater compared to the intermediate heights (0.61 m, 1.22 m, 1.83 m). The monotonic ultimate load capacity of the individual shear wall was also greater when compared to the capacity of the FSS. The out-of-plane experiments showed that the out-of-plane wall performed like a simple one way slab with negligible interaction between adjacent studs. It

was also observed that the diaphragm provided minimal increase in the out-of-plane wall stiffness when subjected to elastic forces.

Another important part of manuscript 1 were the failures of the stud to bottom plate connection first observed during the wall testing in the large wave flume (Fig. A.4).This failure mode was successfully reproduced twice during the FSS failure tests in the structures lab (Fig. 2.1 – manuscript 2). This observation shows that this connection needs to be improved if a larger out-of-plane wall capacity is desired during the design process, and also that it is possible to simulate tsunami loading conditions in a typical structural engineering laboratory.

The information presented in this thesis, along with the findings of the NEES Housesmash project, provide an excellent opportunity to advance the current state of practice for tsunami mitigation and design. This information can be used towards improving the design manuals and building codes that currently address tsunami design, helping to improve the safety and preparedness of the coastal communities along the Pacific coast.

BIBLIOGRAPHY

The following sources are referenced in the introduction or conclusion. Sources used in each individual manuscript are referenced in the manuscripts.

Cross, R. (1967). "Tsunami Surge Forces." *Journal of the Waterways and Harbors Division*, Am. Soc. of Civil Engineers, 201-231.

Federal Emergency Management Agency (FEMA). (2008). "Guidelines for Design of Structures for Vertical Evacuation from Tsunamis (FEMA P646)." Federal Emergency Management Agency.

Groat, C.G. (2005). Statement of C.G. Groat, Director US Geological Survey, US Department of the Interior, Before the Committee of Science, US House of Representatives, January 26.

USGS Tsunami Pilot Study Working Group. (2006). "Seaside, Oregon Tsunami Pilot Study-Modernization of FEMA Flood Hazard Maps." Open-File Report 2006-1234. United States Department of the Interior, US Geological Survey.

Yeh, H., Fiez, T., Karon, J. (2009). "A Comprehensive Tsunami simulator for Long Beach Peninsula Phase-1: Framework Development." Final Report to Washington State Military Department July 2009. State of Washington.

APPENDICES

List of Appendix Figures (continued)

List of Appendix Figures (continued)

List of Appendix Figures (continued)

List of Appendix Figures (continued)

LIST OF APPENDIX TABLES

Appendix A

The following information is provided for support of Manuscript 1: "Evaluation of Tsunami Loads on Wood Frame Walls at Full Scale." Also included in Appendix A is information on the shear wall experiments that were performed in conjunction with the transverse wall experiments discussed in Manuscript 1.

Table A.1: Test matrix (ShearWall_1 thru ShearWall_4)

Experiment	Trials	Wave Heights H_2 (m)	Water Depth to Reef (m)	SW Specimens	TW Specimens	Failure
ShearWall_1	4	0.41-0.69	0.44	4A,4B	5A	Yes
ShearWall_2	10	0.19-0.98	-0.07	4A,4B	1C	No
ShearWall_3	3	0.21-0.41	0.44	4A,4B	1C	Yes
ShearWall_4	13	0.30-1.24	-0.07	6B,6C	1D	Yes

Table A.2: Shear wall specimen information

Specimens -	Spacing (cm)	Lumber Size	Length (m)	Sheathing -
Specimen 1C,1D	40.6	2x6	3.66	Plywood
Specimen 4A,B	40.6	2x6	2.44	OSB
Specimen 5A	40.6	2x4	2.44	Plywood
Specimen 6A,6B	40.6	2x6	2.44	Plywood

Table A.3: TransverseWoodWall experiment pressure transducer locations

Experiment	Instrument	X	Y	Z
-	**-**	**(m)**	**(m)**	**(m)**
Pressure Transducer (P)				
TransverseWoodWall	2	61.23	-0.86	0.20
	3	61.23	-0.83	0.20
	5	61.23	-0.84	0.64
TransverseWoodWall_2	2	61.23	-0.86	0.20
	3	61.23	-0.83	0.20
	5	61.23	-0.84	0.64
TransverseWoodWall_3	2	61.23	-0.86	0.20
	3	61.23	-0.83	0.20
	5	61.23	-0.84	0.64
TransverseWoodWall_4	2	61.23	-0.86	0.15
	3	61.23	-0.83	0.24
	5	61.23	-0.84	0.69
TransverseWoodWall_5	2	61.23	-0.86	0.20
	3	61.23	-0.83	0.20
	5	61.23	-0.84	0.64
TransverseWoodWall_6	2	61.23	-0.86	0.71
	3	61.23	-0.83	0.24
	5	61.23	-0.84	0.72
TransverseWoodWall_7	2	61.23	-0.86	0.71
	3	61.23	-0.83	0.24
	5	61.23	-0.84	0.72
TransverseWoodWall_8	2	61.23	-0.86	0.71
	3	61.23	-0.83	0.24
	5	61.23	-0.84	0.72

x-location is measured from zeroed wavemaker
y-location is measured from center of flume
z-location is from base of test specimen
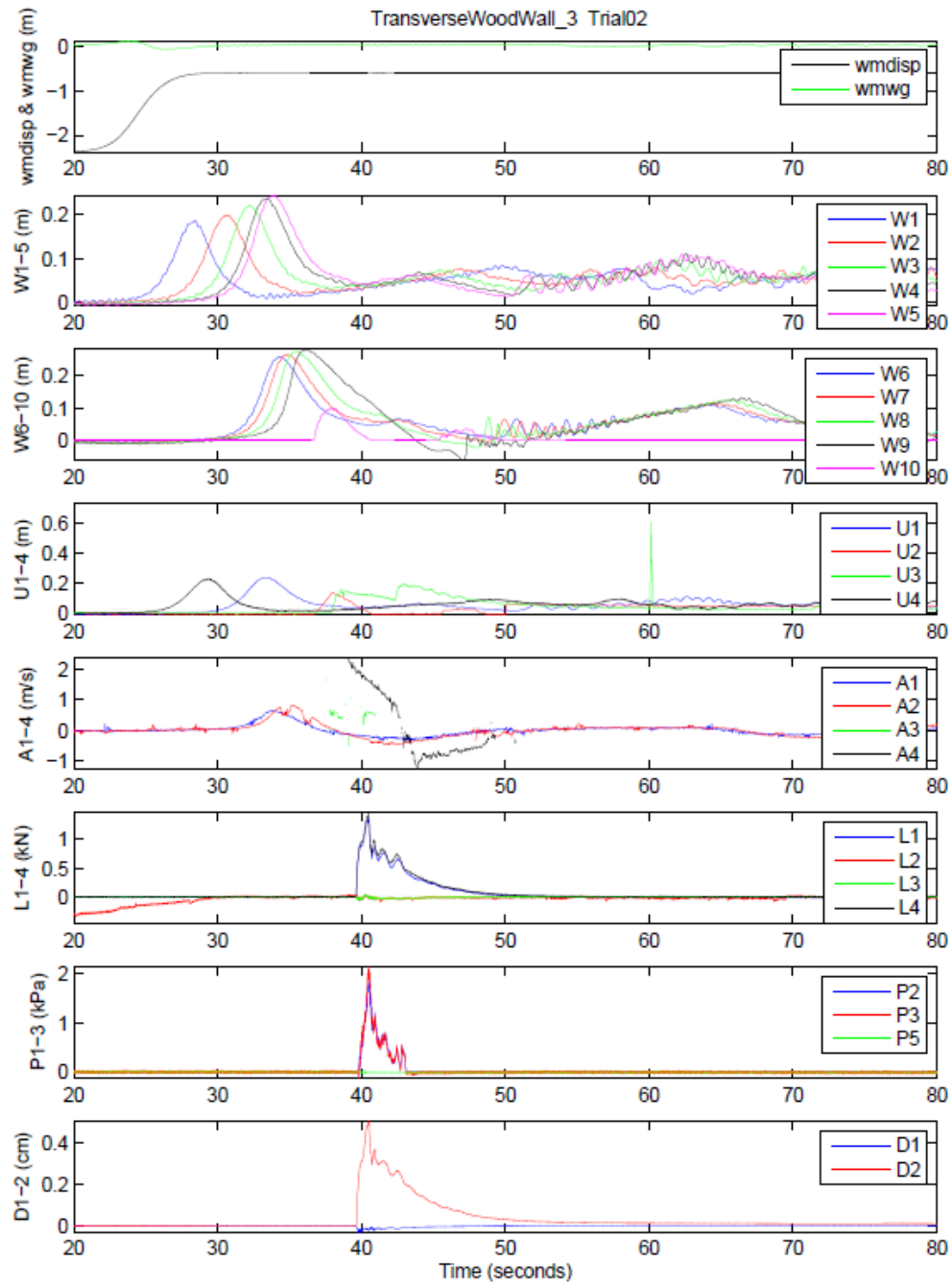
Fig. A.1: Example "Quicklook" for transverse wall experiments

These "quicklooks" were made for each trial and are available on the wave lab network at:
wrl/2009/NEEShousesmash/docs/linton/programs/Quicklook

Fig. A.2: ShearWall_1 setup with 8 ft. transverse wall

Fig. A.3: Shear wall load cell setup

Fig. A.4: Stud to bottom plate connection failure of transverse wall

Fig. A.5: Punching failure of transverse wall

Appendix B

The following information is provided to support Manuscript 2: "Load Distribution in Light-Frame Wood Buildings under Simulated Tsunami Loads."

Table B.1: Test matrix (SW1, SW2, SW3, SW4, SW5)

Experiment	Trial	Location	Test	Experiment	Trial	Location	Test
SW1	1	H1	Elastic	SW4	1	H8	Elastic
	2	H2	Elastic		2	H7	Elastic
	3-6	H3	Elastic		3	H6	Elastic
	7	H4	Elastic		4	H5	Elastic
	8	H5	Elastic		5	H4	Elastic
	9	H6	Elastic		6	H3	Elastic
	10	H7	Elastic		7	H2	Elastic
	11	H8	Elastic		8	H1	Elastic
	12	H8	Inelastic		9	H4	Failure
	13	H8	Failure	SW5	1	H1	Elastic
SW2	1	H8	Failure		2	H2	Elastic
	2	H7	Elastic		3	H3	Elastic
	3	H6	Elastic		4	H4	Elastic
	4	H5	Elastic		5	H5	Elastic
	5	H4	Elastic		6	H6	Elastic
	6	H3	Elastic		7	H7	Elastic
	7	H2	Elastic		8	H8	Elastic
	8	H1	Elastic		9	H8	Failure
	9	H2	Failure				
SW3	1	H1	Failure				
	2	H2	Elastic				
	3	H3	Elastic				
	4	H4	Elastic				
	5	H5	Elastic				
	6	H6	Elastic				
	7	H7	Elastic				
	8	H8	Elastic				
	9	H6	Failure				

Table B.2: Test matrix (OOP1, OOP2, OOP3)

OOP1		OOP2		OOP3	
Trial	**Location**	**Trial**	**Location**	**Trial**	**Location**
1	A1	1	B2	1	A1
2	A1	2	B4	2	A2
3	A1	3	B6	3	A3
4	A2	4	B8	4	A4
5	A3	5	C8	5	A5
6	A4	6	C6	6	A6
7	A5	7	C4	7	A7
8	A6	8	C2	8	A8
9	A7	9	D2	9	D2
10	A8	10	D4	10	D4
11	D2	11	D6	11	D6
12	D4	12	D8	12	D8
13	D6	13	A8	13	C2
14	D8	14	A7	14	C2
15	C2	15	A6	15	C4
16	C4	16	A5	16	C6
17	C6	17	A4	17	C8
18	C6	18	A3	18	B8
19	C8	19	A2	19	B6
20	B8	20	A1	20	B4
21	B6			21	B2
22	B4				
23	B2				

Table B.3: Test matrix (FAIL1, FAIL2)

Experiment	Trial	Location	Test
FAIL1	1	C2-E2	Failure
	2	C2-E2	Failure
FAIL2	1	A8	Failure
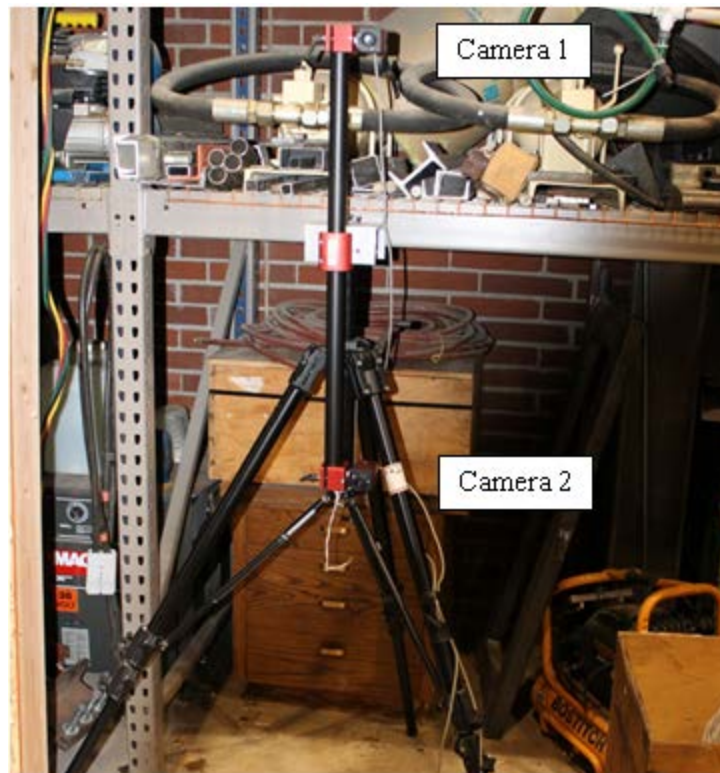
Fig. B.1: DIC camera setup
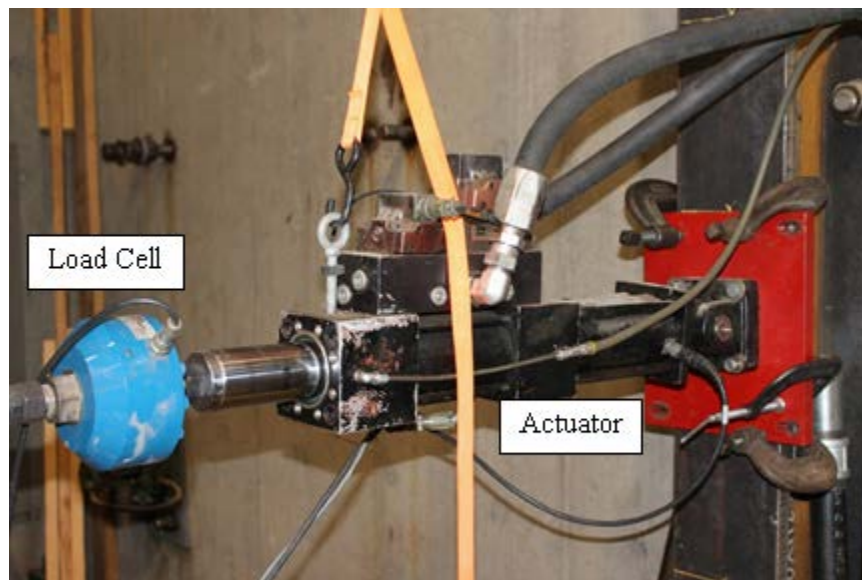
Fig. B.2: Hydraulic actuator and load cell

Fig. B.3: Load cell setup for OOP1 experiments
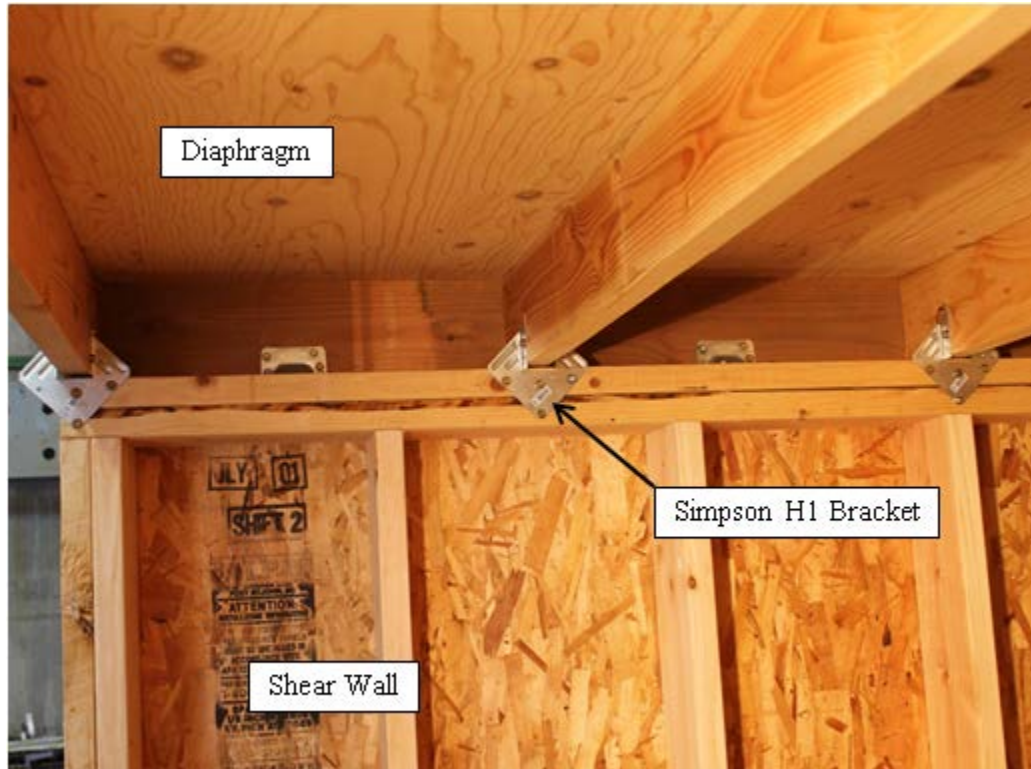
Fig. B.4: Diaphragm to shear wall connection
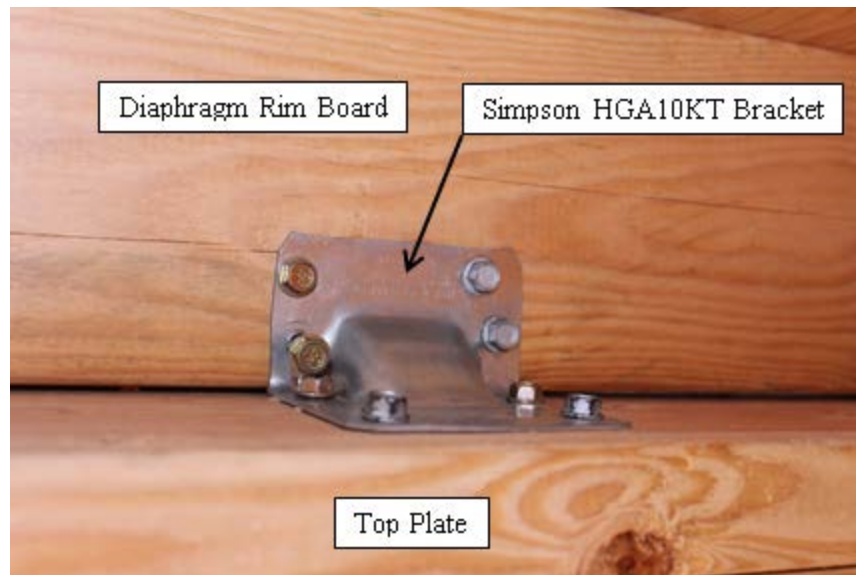
Fig. B.5: Diaphragm connection
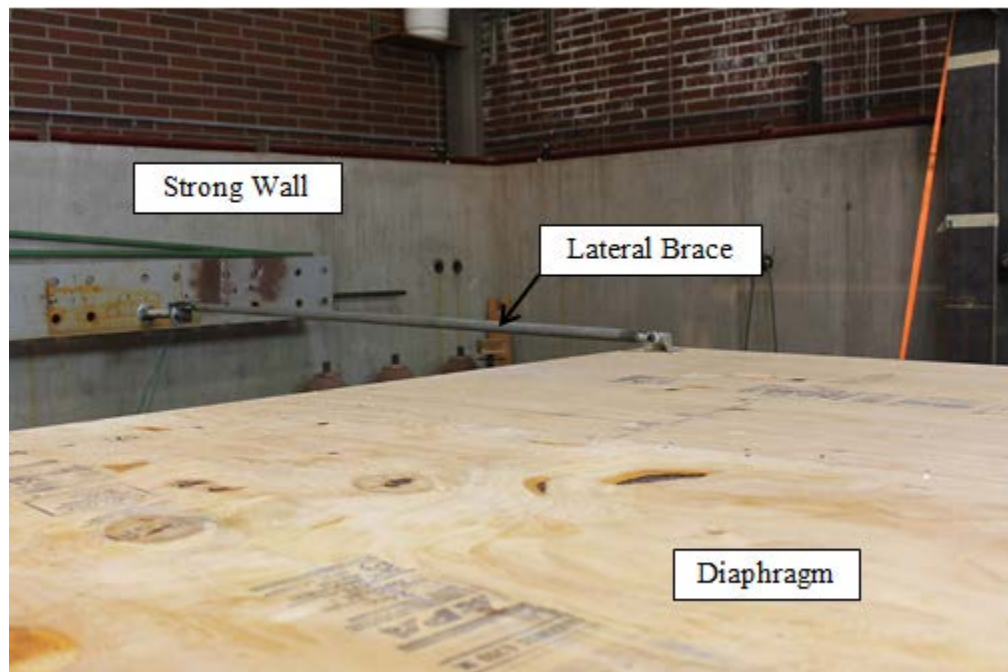
Fig. B.6: Lateral restraint attached to diaphragm for OOP1 experiment

Fig. B.7: SW2 Trial09 deflected shape

Fig. B.8: SW3 Trial09 top plate splitting at nailed connection

Fig. B.9: SW4 Trial09 top plate splitting at nailed connection
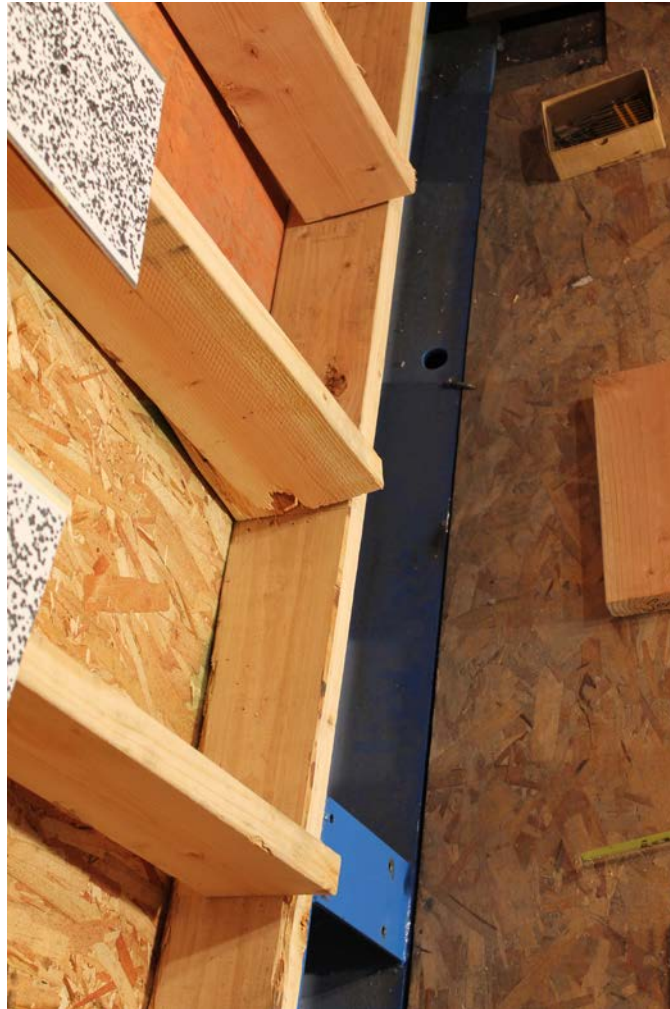
Fig. B.10: FAIL1 Trial01 failed connection of stud to bottom plate

Fig. B.11: Racking of OSB sheathing on shear wall during FAIL2 experiment

Fig. B.12: Out-of-plane deflection of NE corner during FAIL2 experiment

Appendix C

The following information discusses the Digital Image Correlation techniques used for Manuscript 2: "Load Distribution in Light-Frame Wood Buildings under Simulated Tsunami Loads."

Digital Image Correlation (DIC) is a full field, non-contact measurement technique for both displacements and strains. Two cameras are mounted at an angle to each other to capture stereoscopic images, which are processed using a software program called Vic3D (Correlated Solutions Inc.) to get three-dimensional displacement data for a particular area of interest.

To verify that the values measured by the DIC were reasonable and accurate the displacement values from the DIC output were compared to the displacement sensor on the hydraulic actuator. Fig. C.1 shows an example load vs. displacement curve for both the cylinder and DIC. This shows that even at the small displacements measured during the elastic tests the DIC provides an accurate measurement system. Prior to each test a series of zero displacement images were taken to check the accuracy and calibration of the DIC. The average absolute error observed was 0.07 mm.
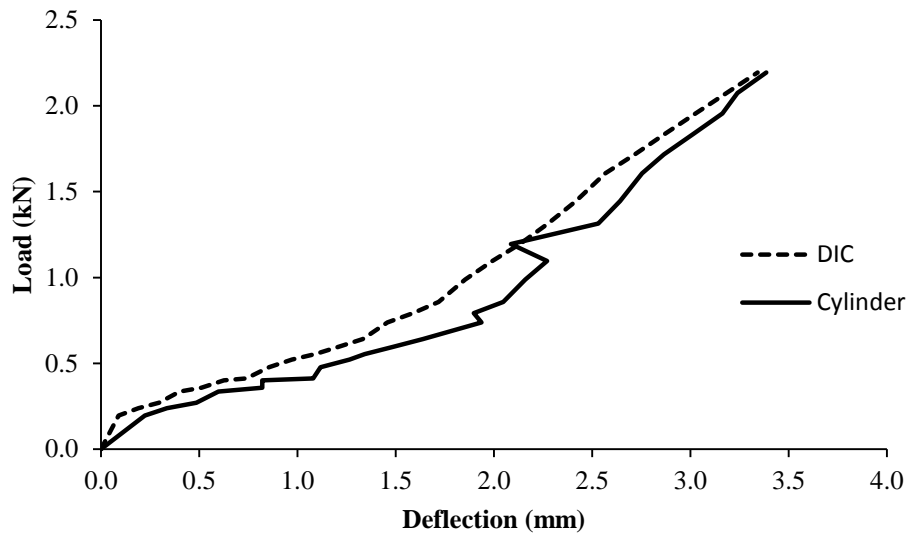
Fig. C.1: DIC vs. Cylinder deflection comparison

Appendix D

The following load vs. deflection curves are provided to support Manuscript 2: "Load Distribution in Light-Frame Wood Buildings under Simulated Tsunami Loads."
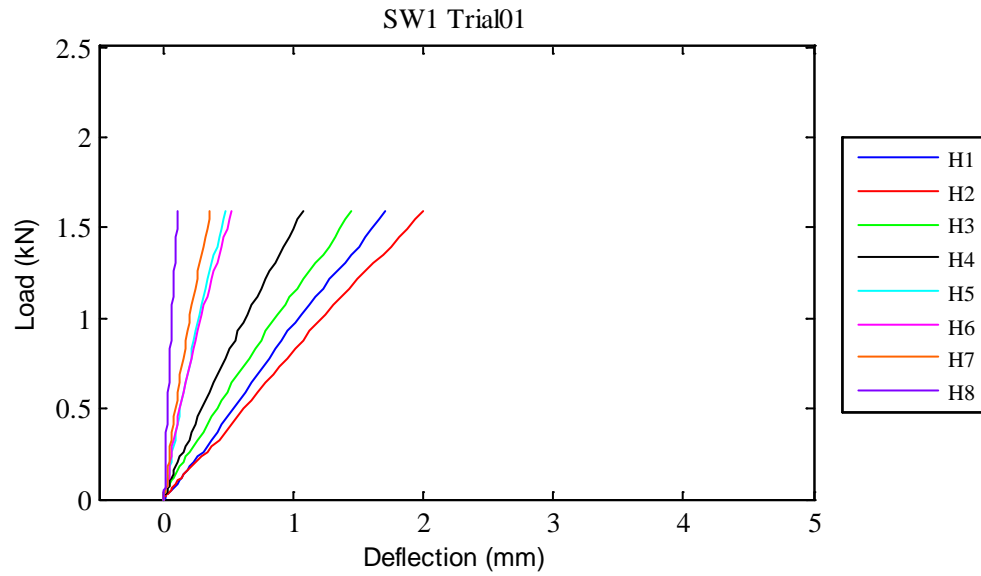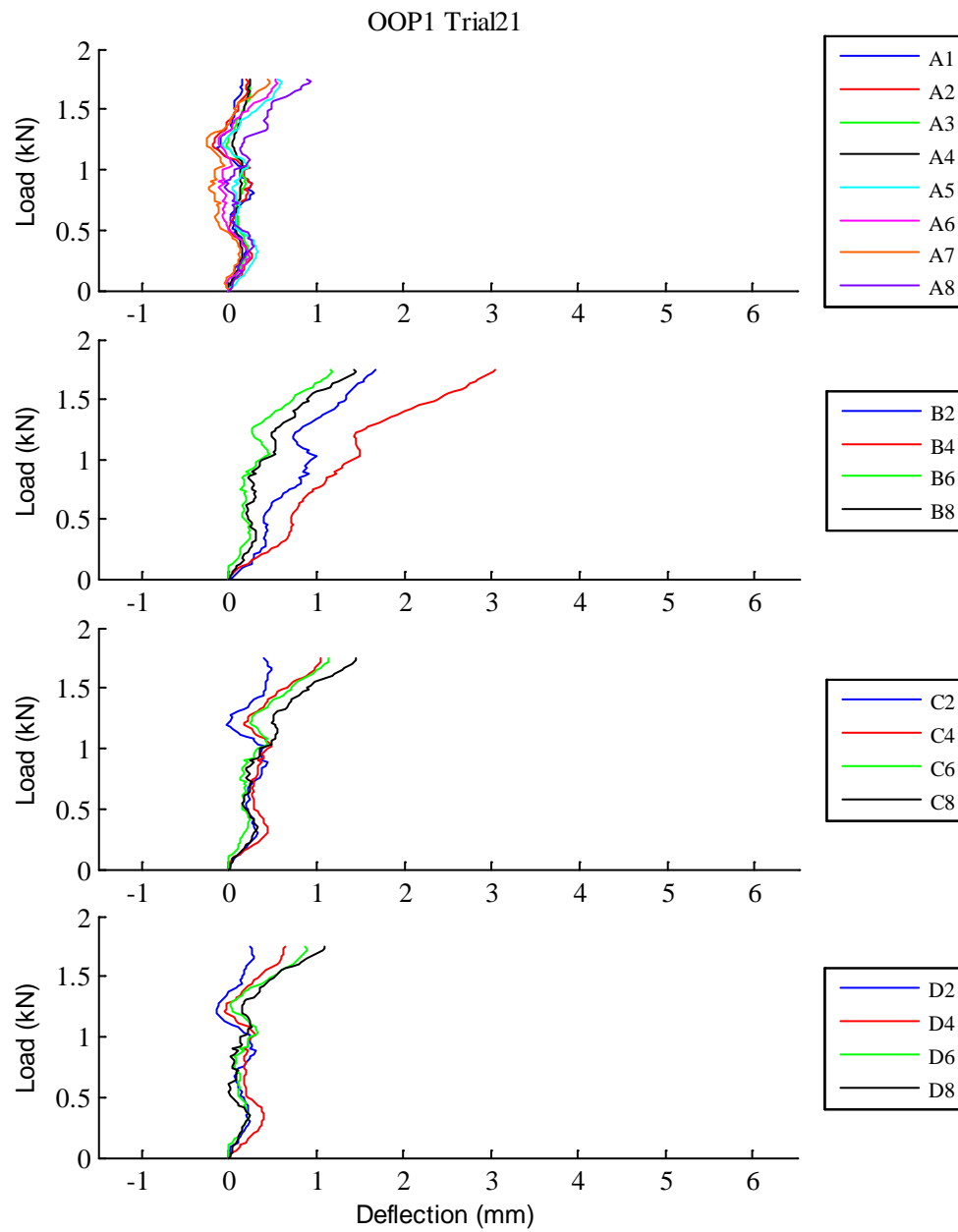

Fig. D.1: SW1 Trial01 load vs. deflection curves
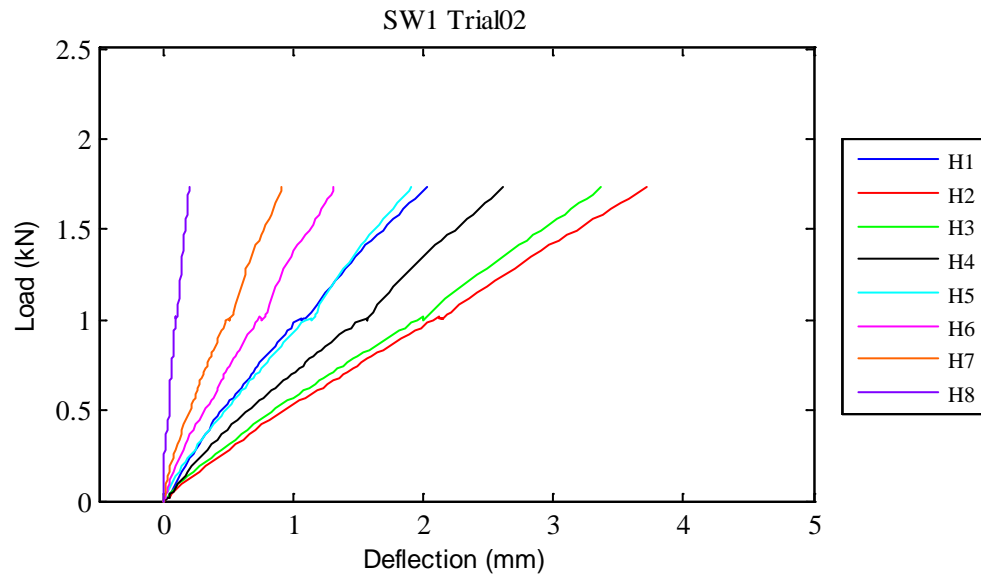
Fig. D.2: SW1 Trial02 load vs. deflection curves
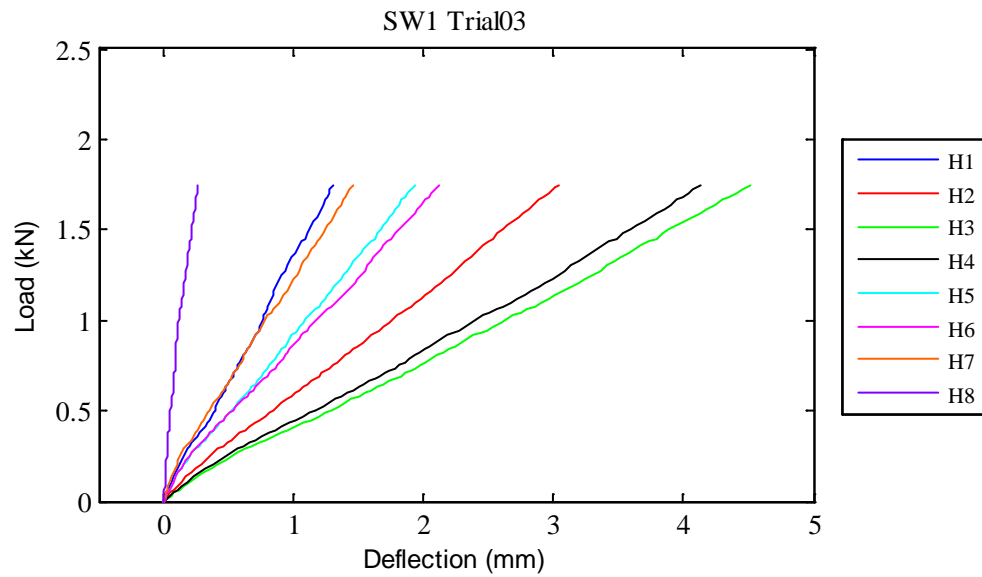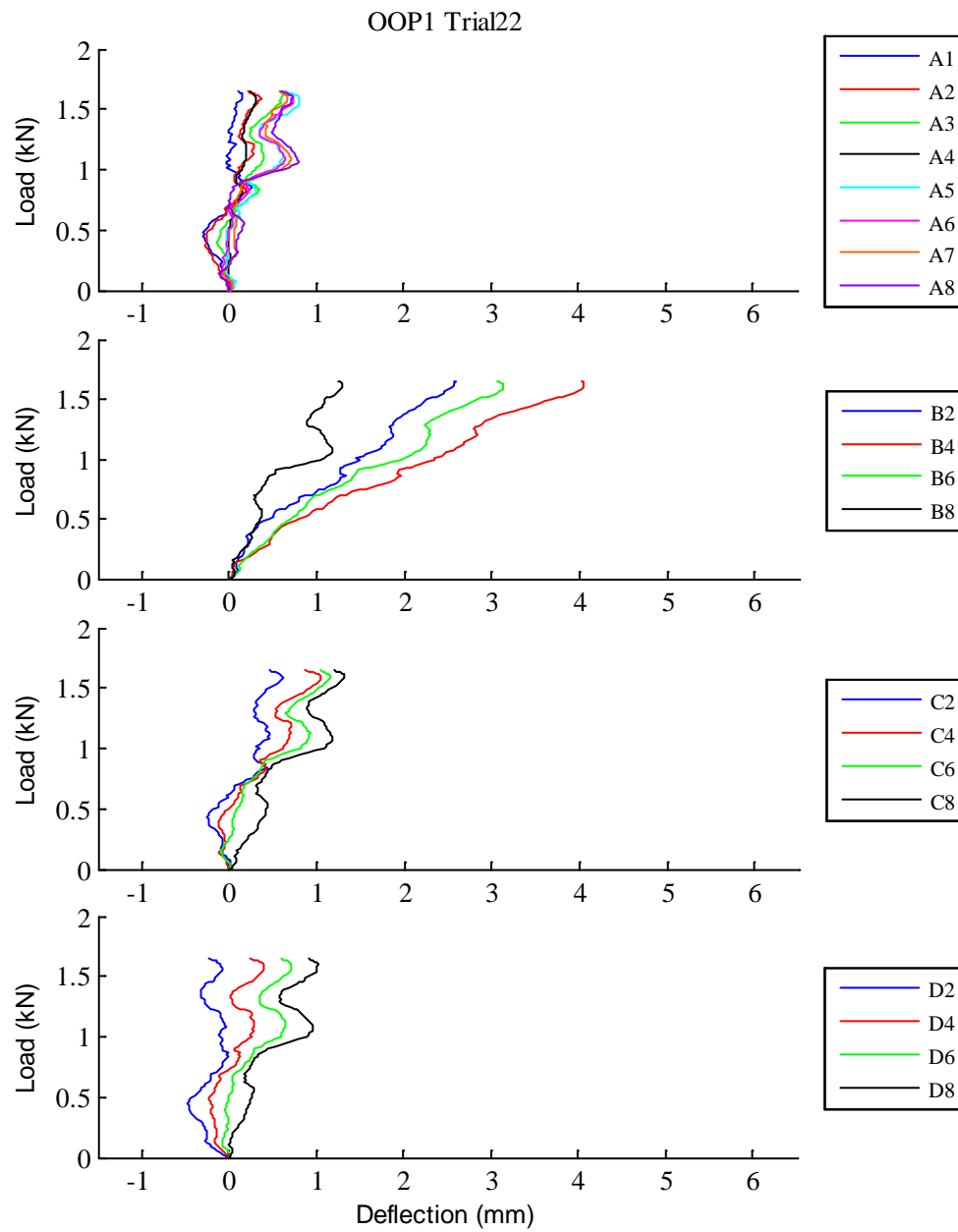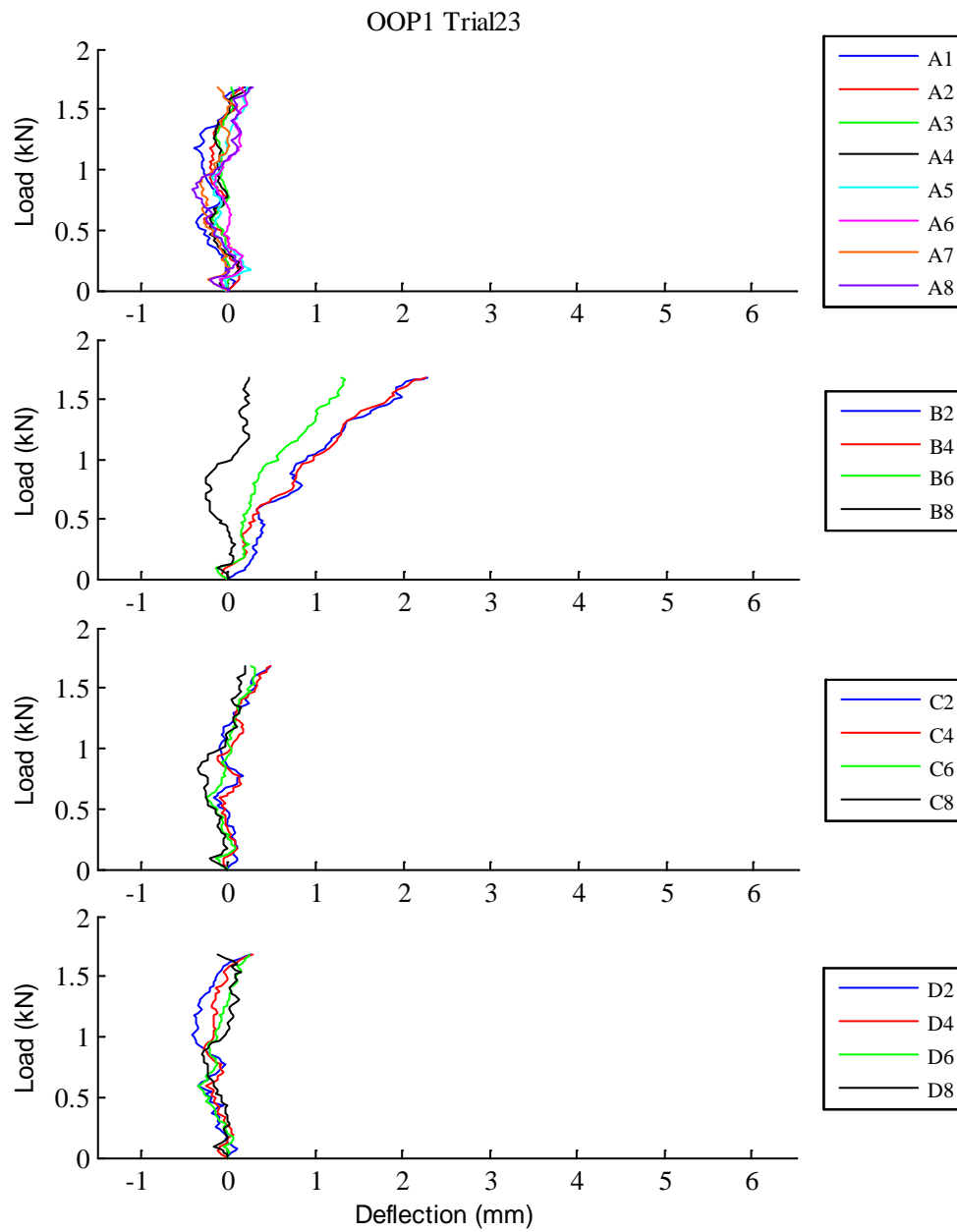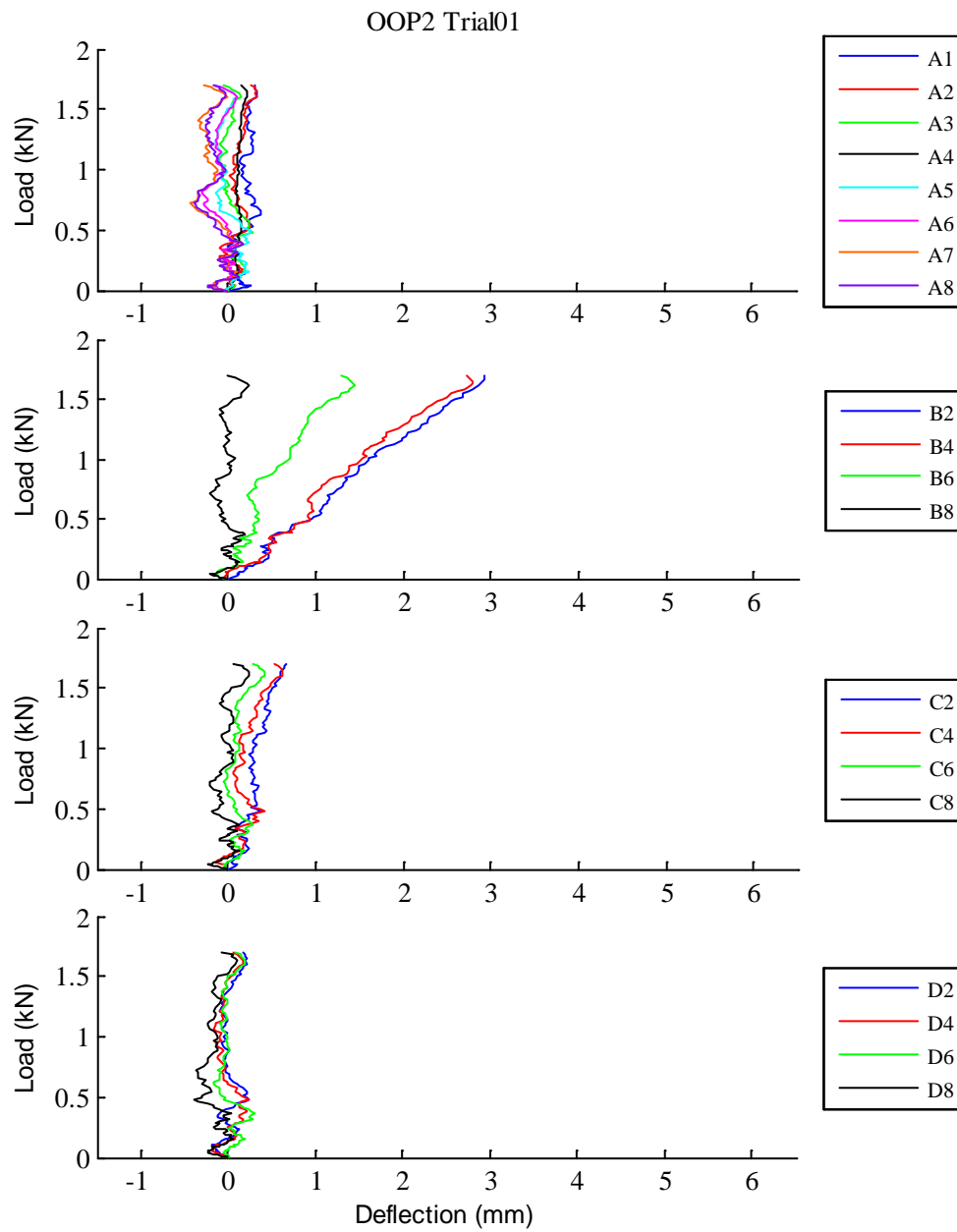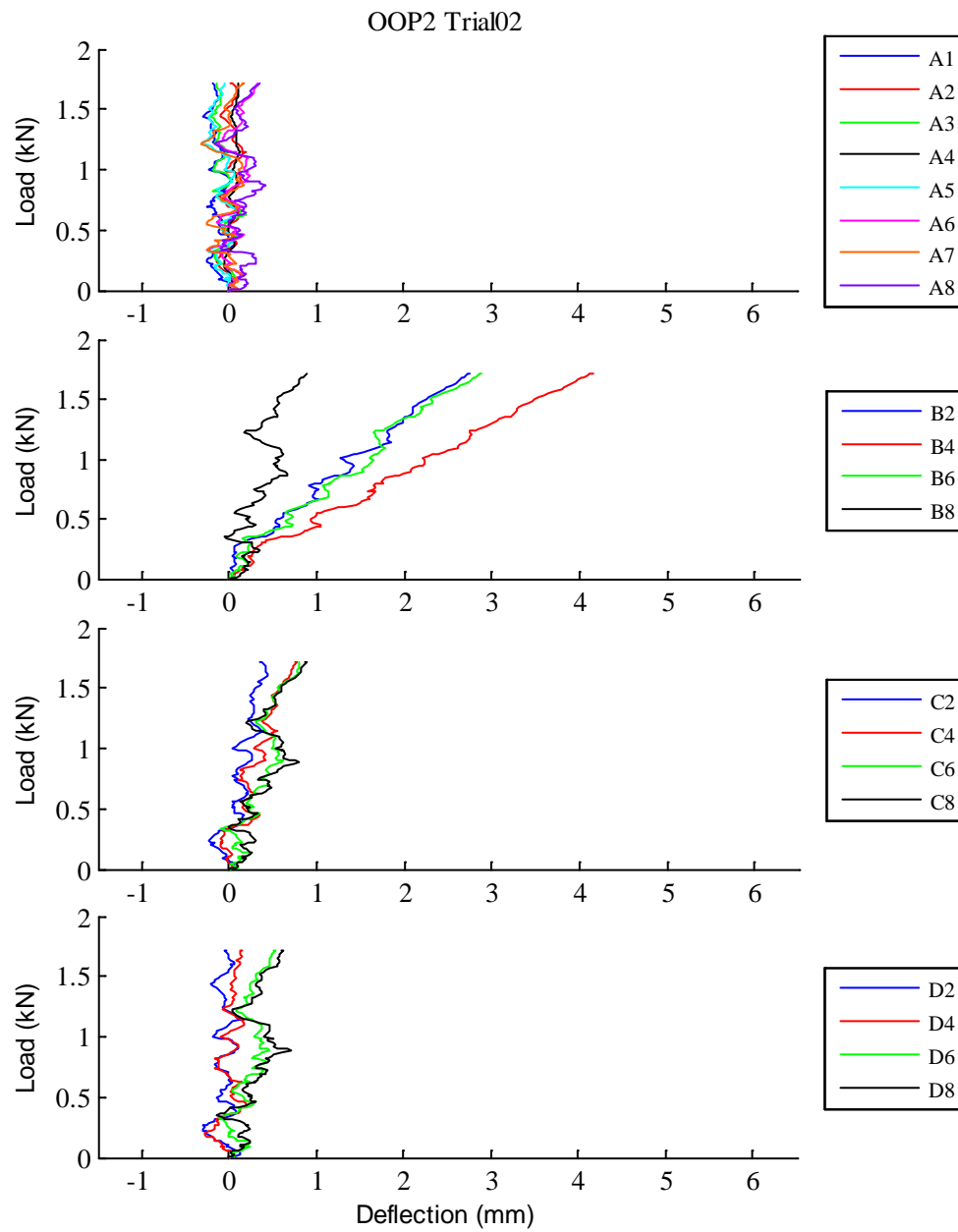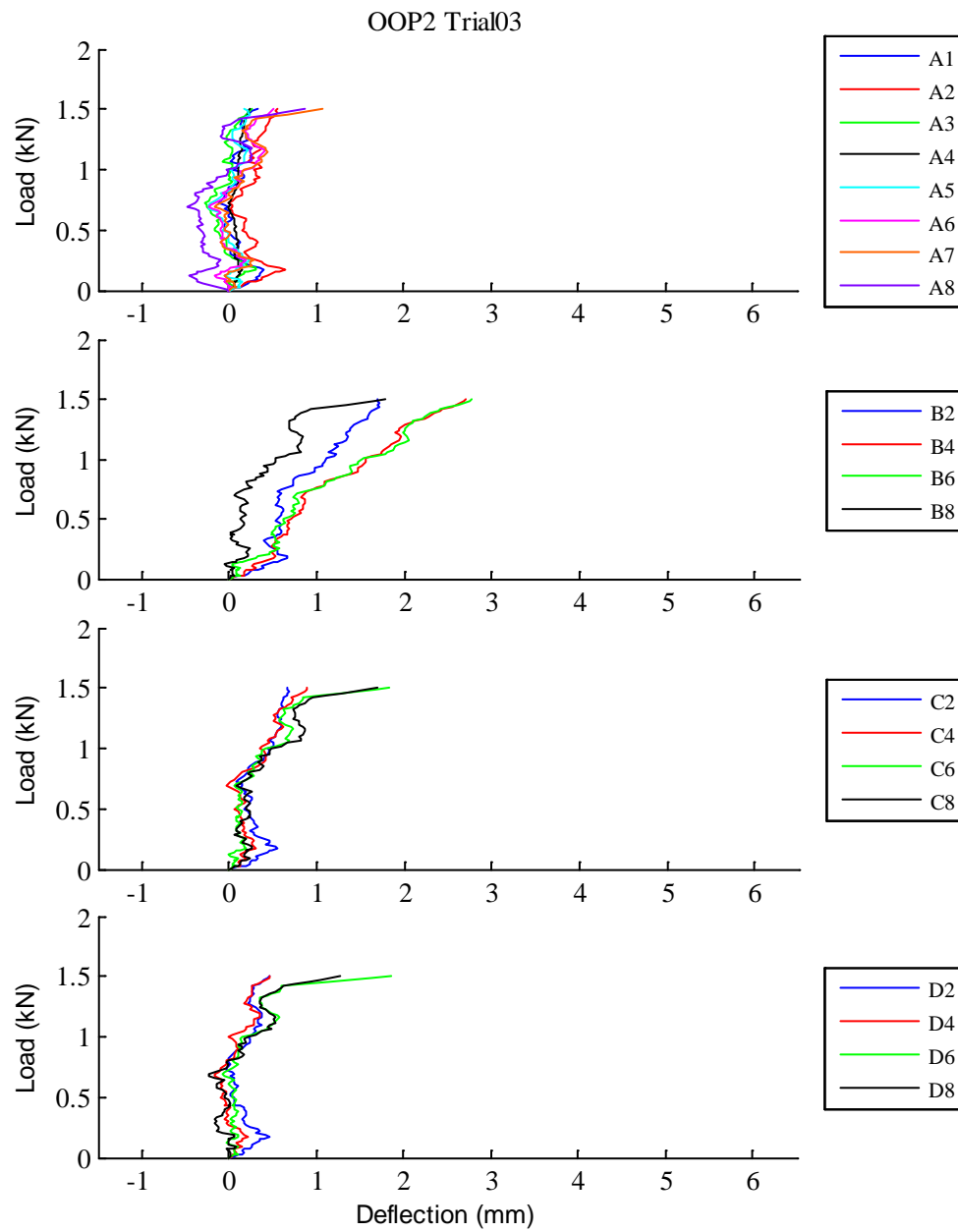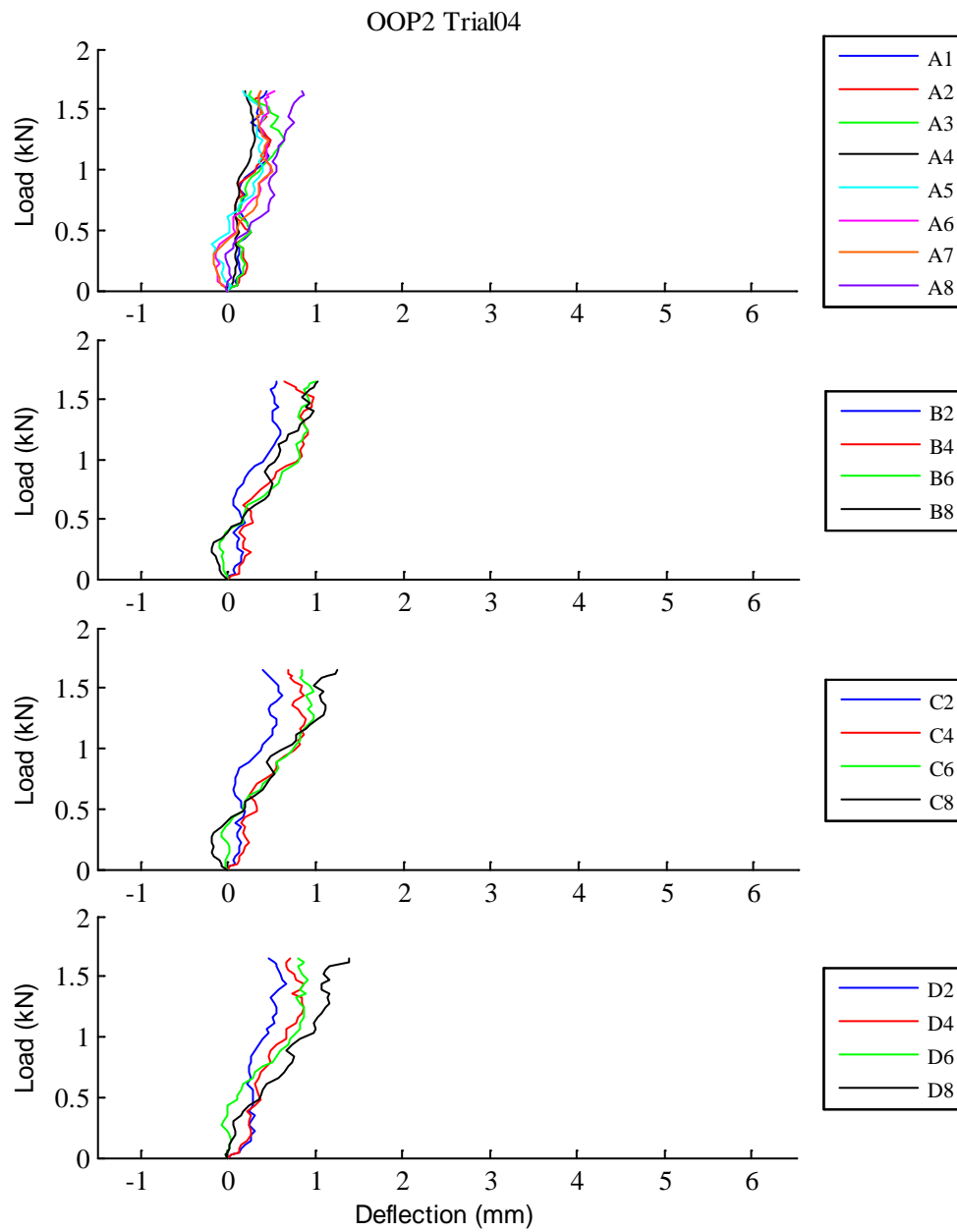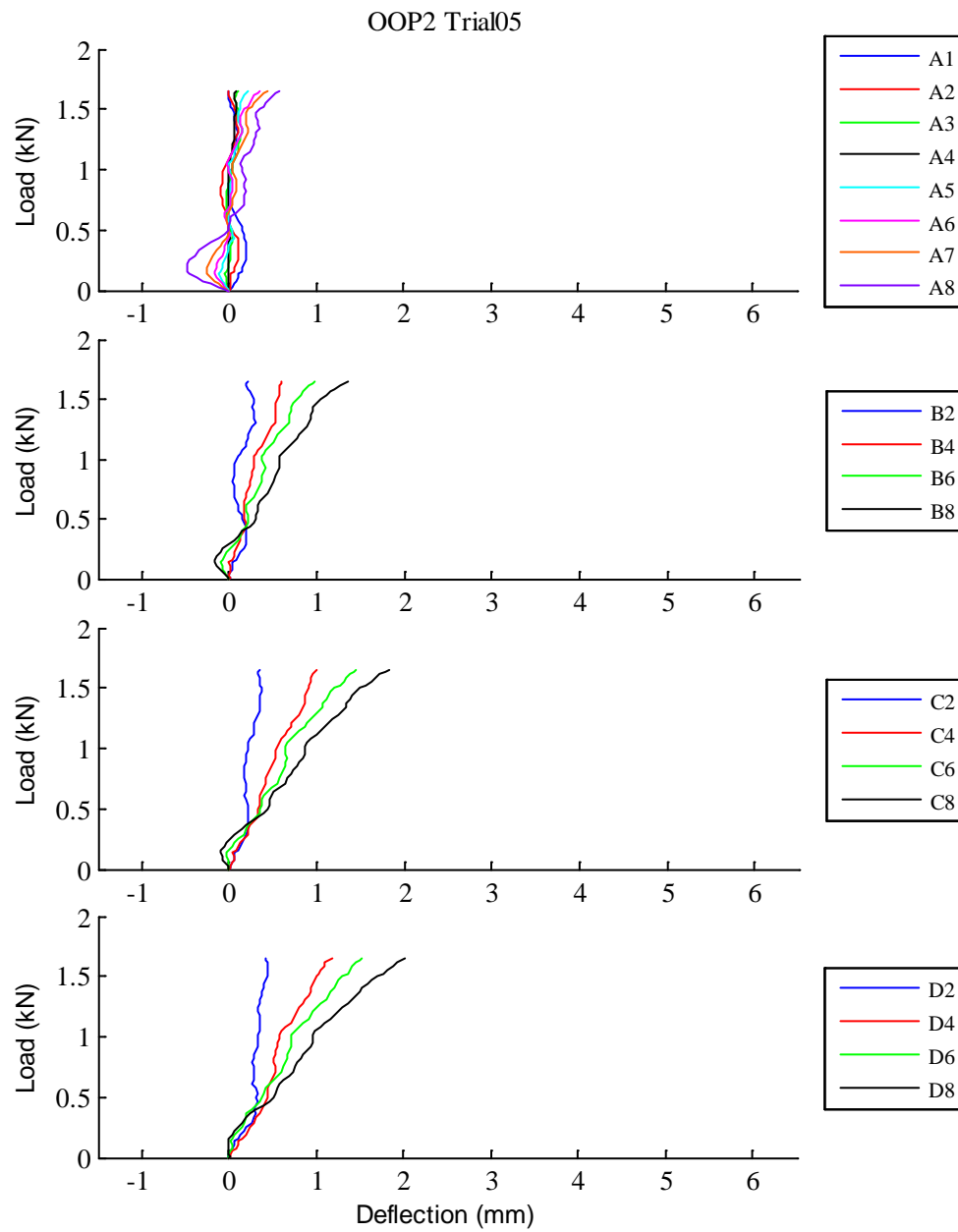
Fig. D.3: SW1 Trial03 load vs. deflection curves
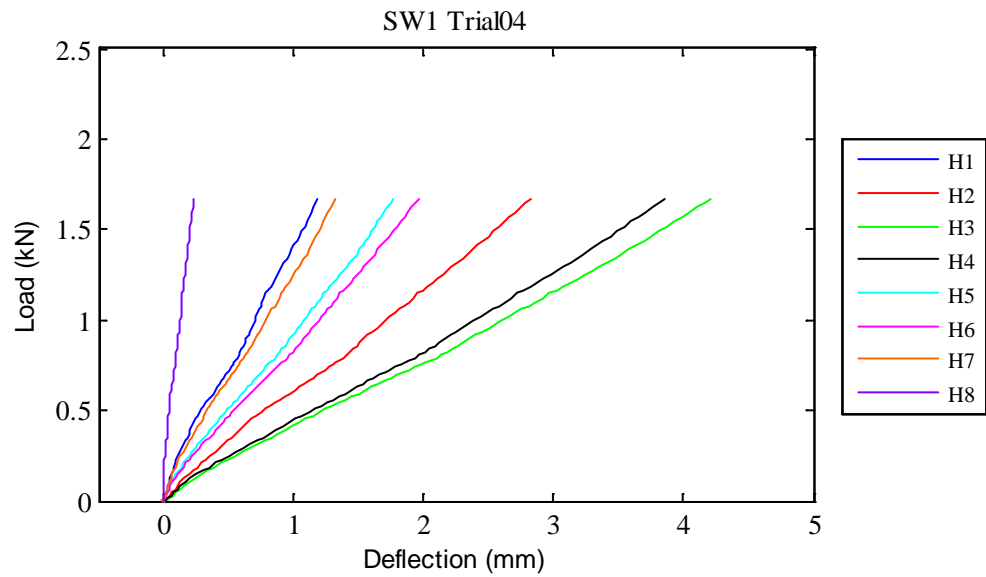
Fig. D.4: SW1 Trial04 load vs. deflection curves
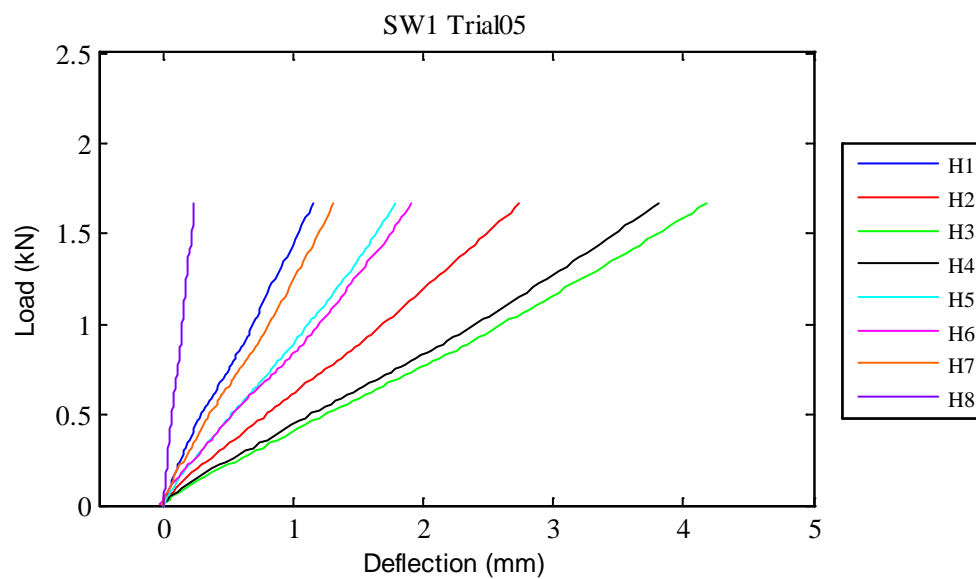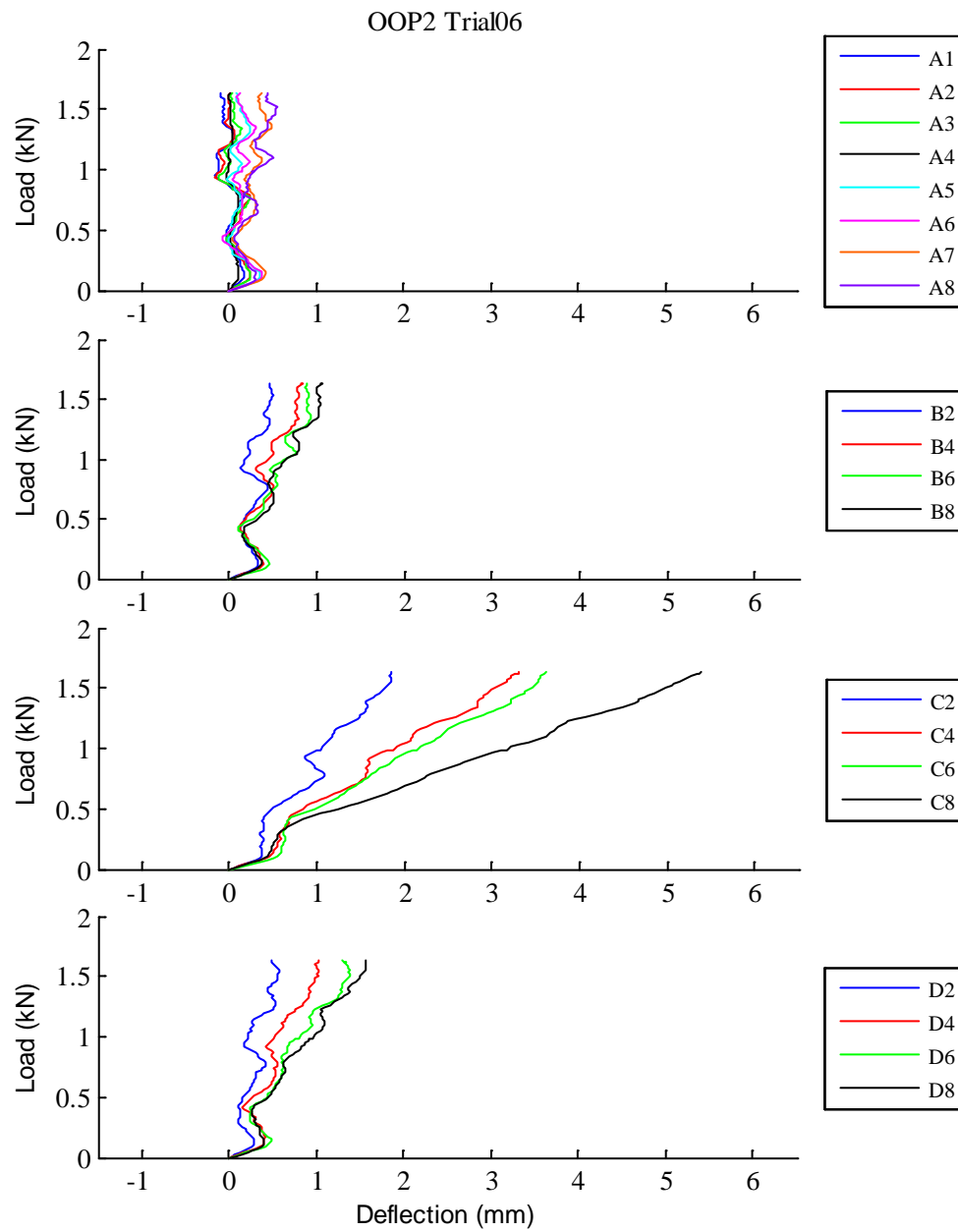
Fig. D.5: SW1 Trial05 load vs. deflection curves
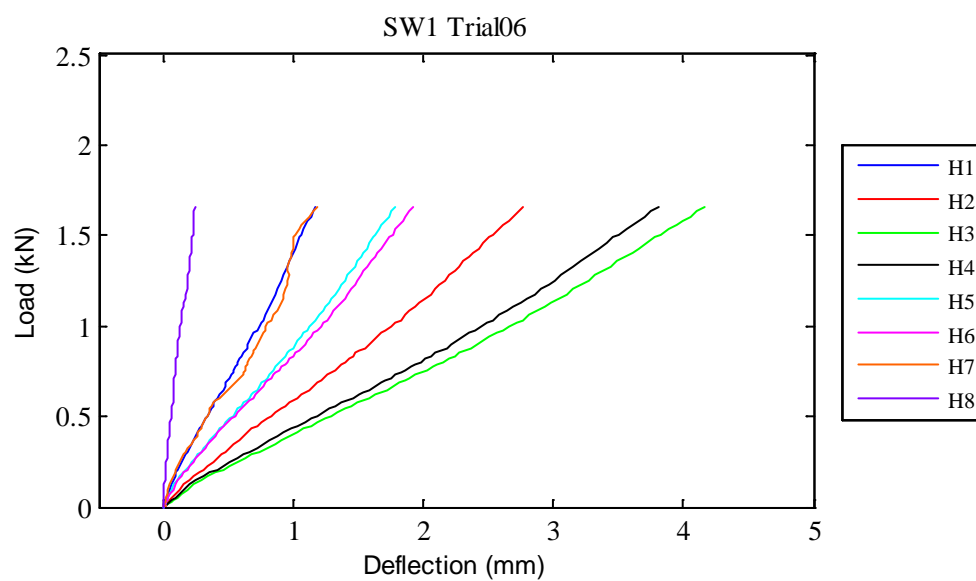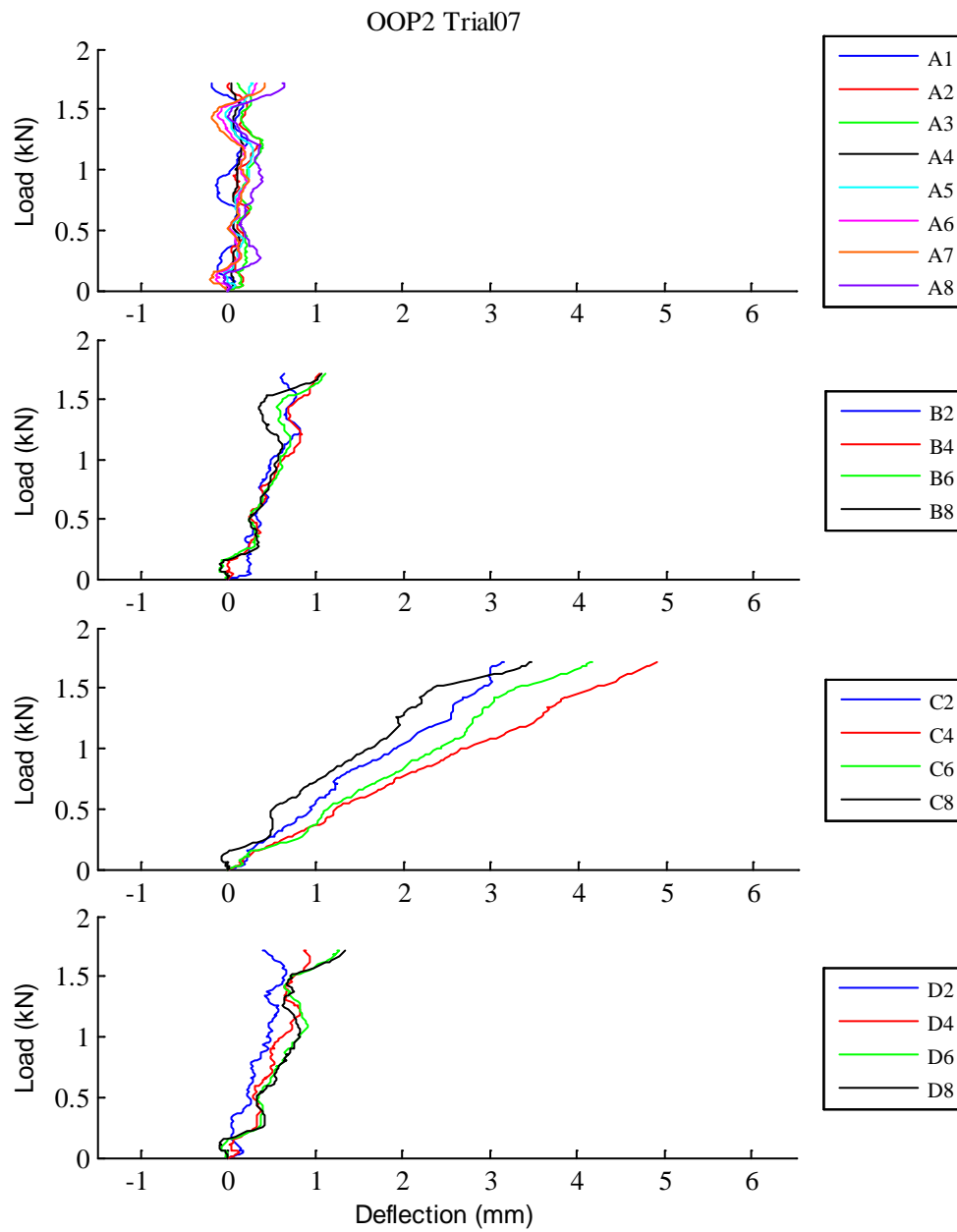

Fig. D.6: SW1 Trial06 load vs. deflection curves
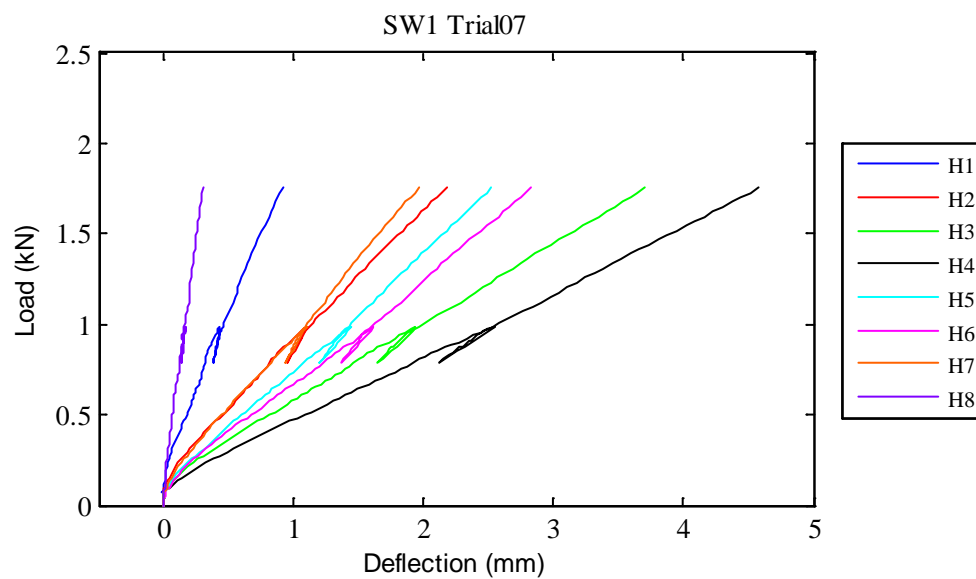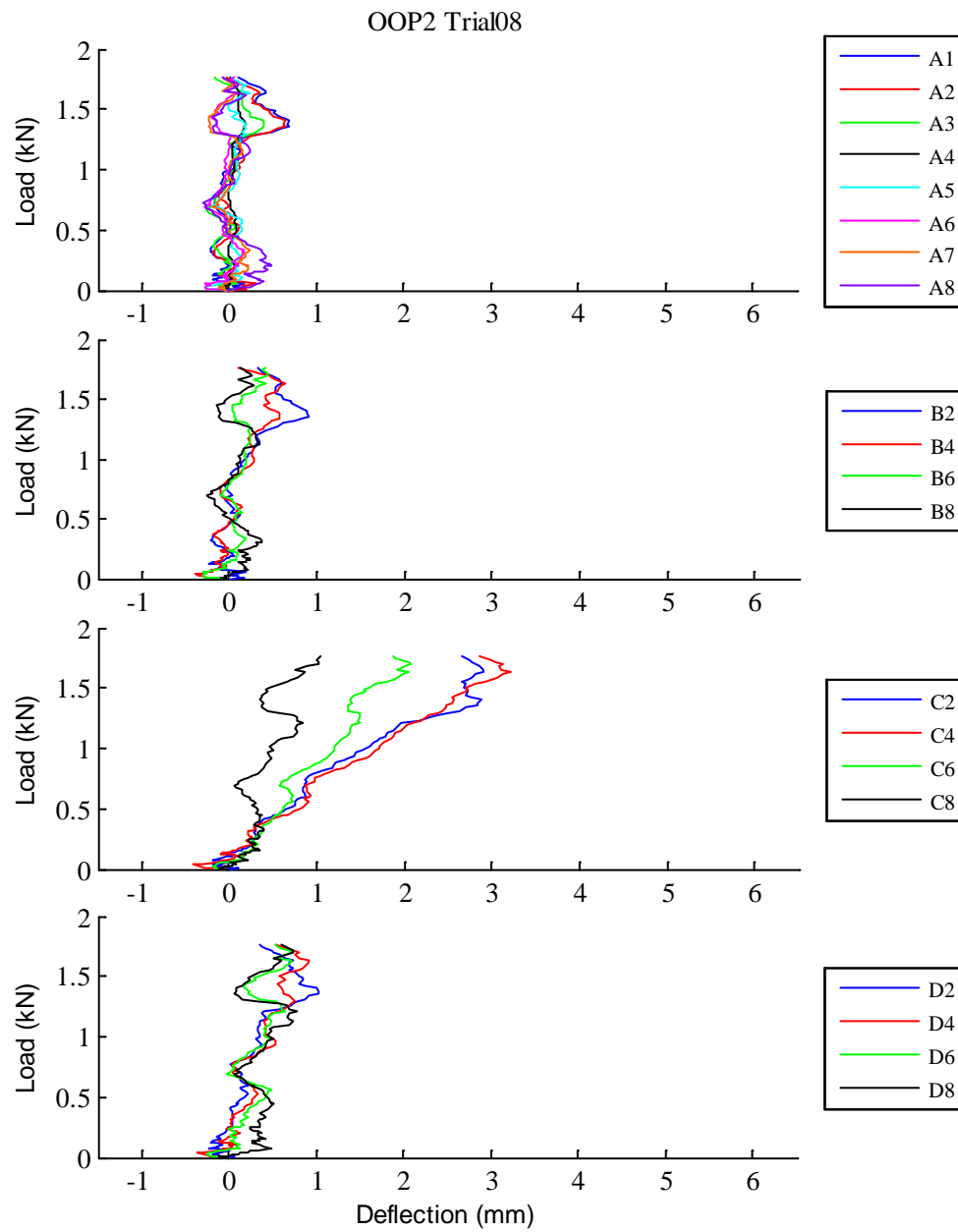
Fig. D.7: SW1 Trial07 load vs. deflection curves
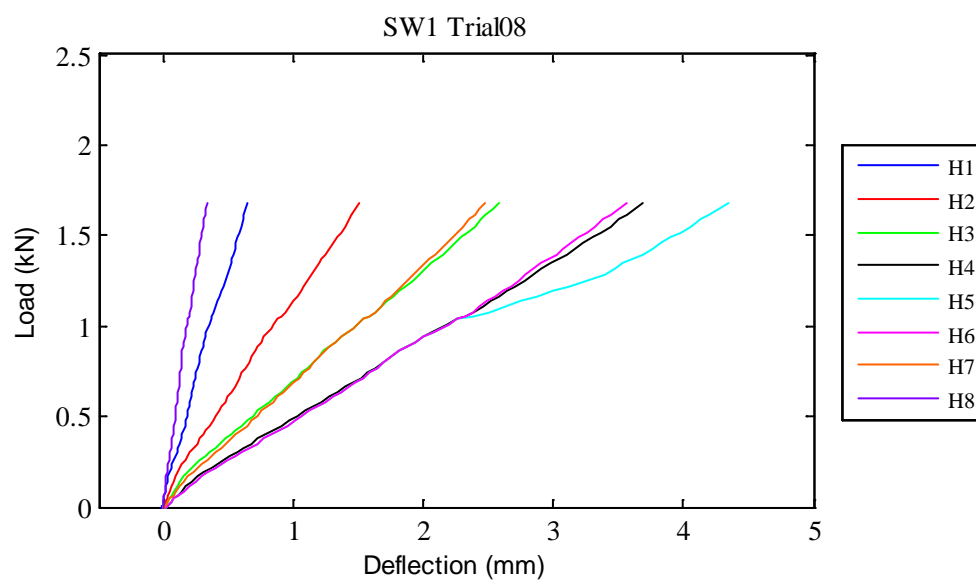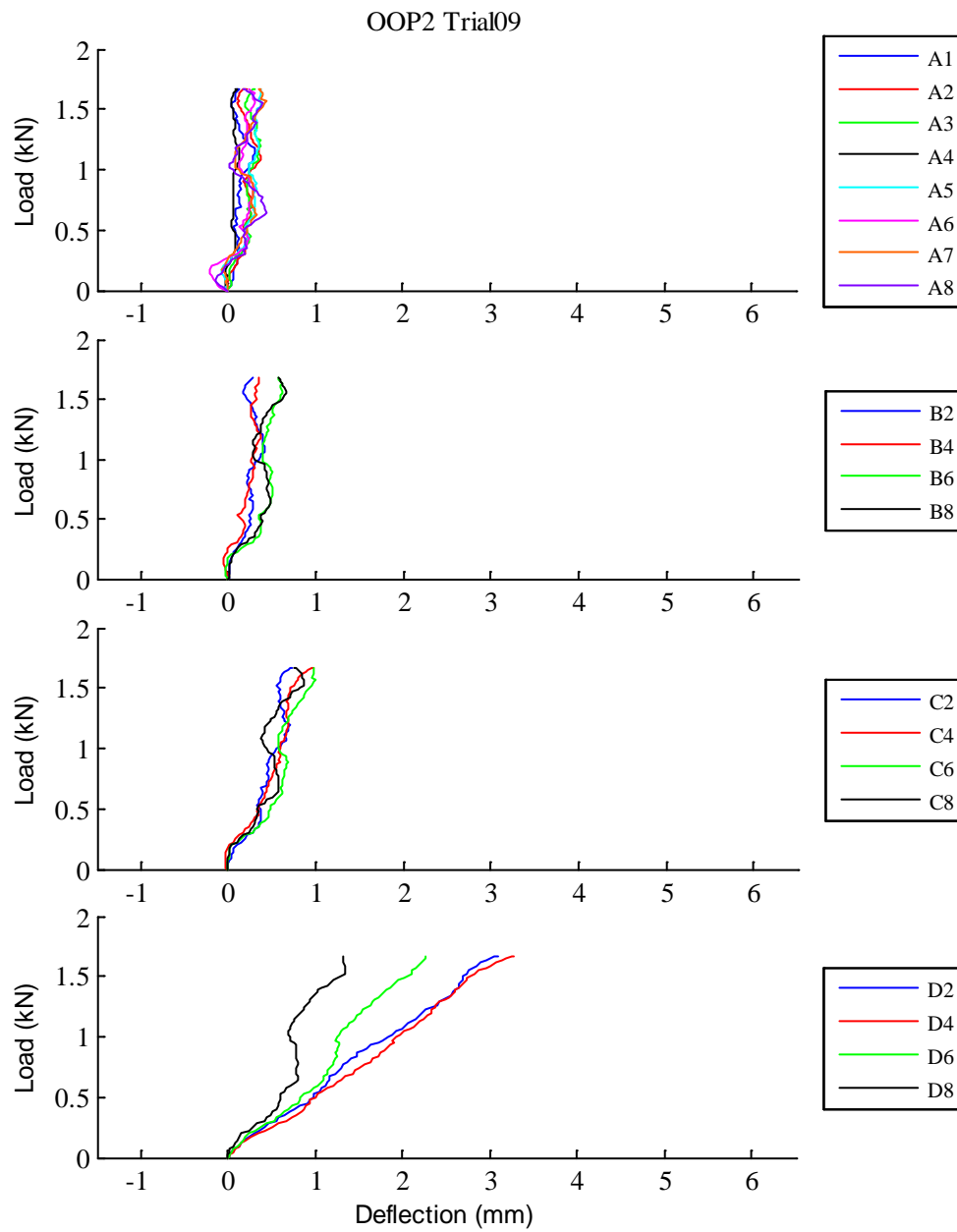

Fig. D.8: SW1 Trial08 load vs. deflection curves
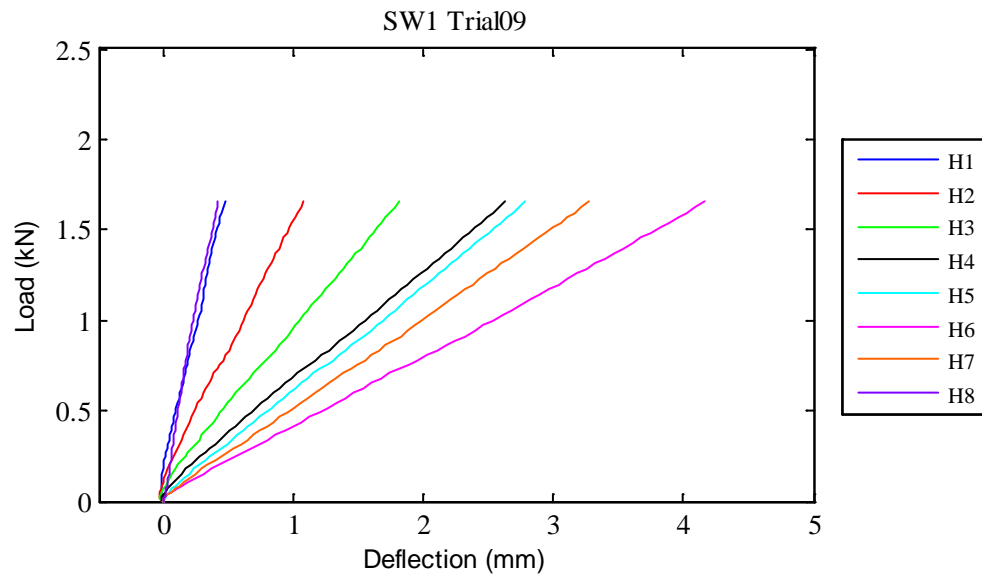
Fig. D.9: SW1 Trial09 load vs. deflection curves
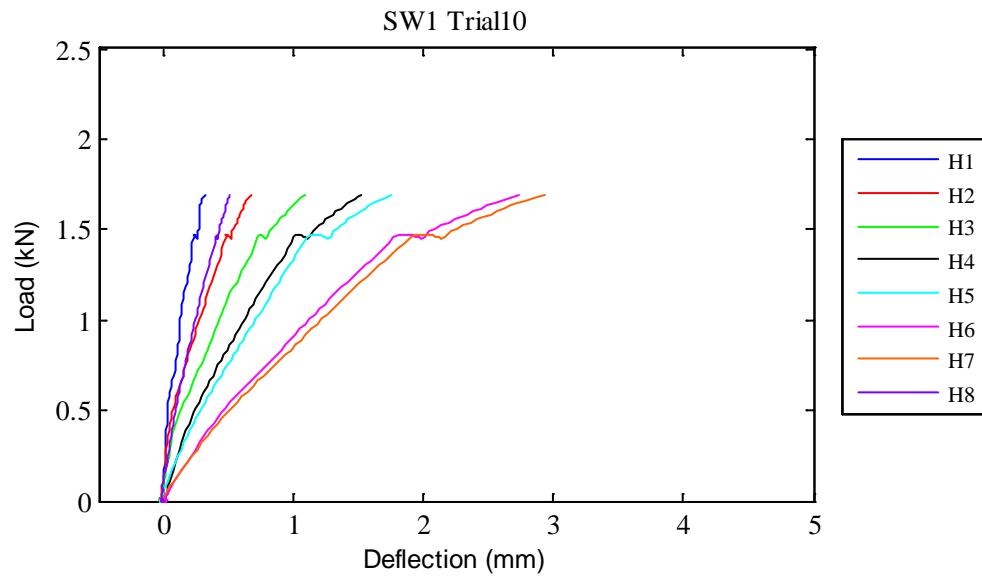
Fig. D.10: SW1 Trial10 load vs. deflection curves
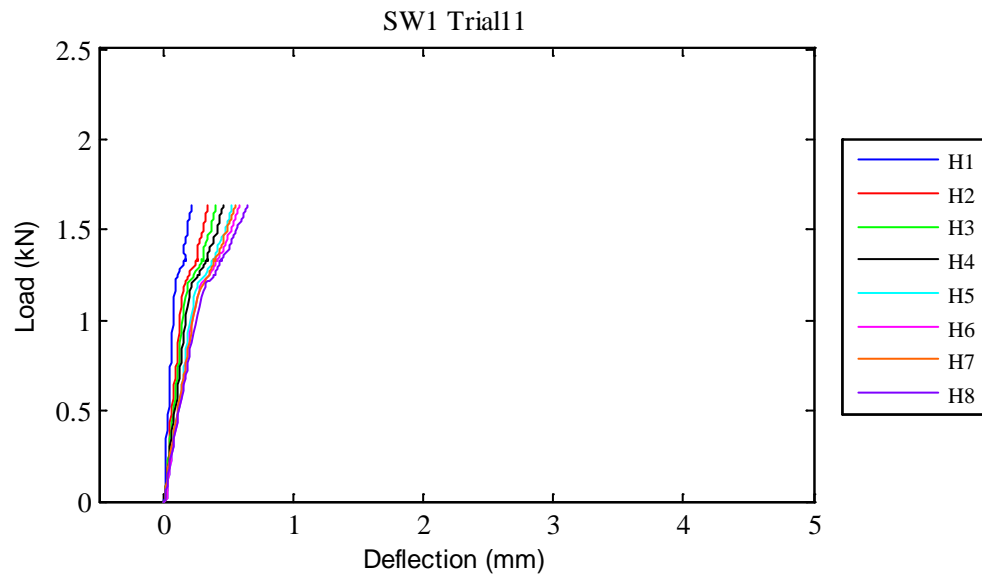
Fig. D.11: SW1 Trial11 load vs. deflection curves
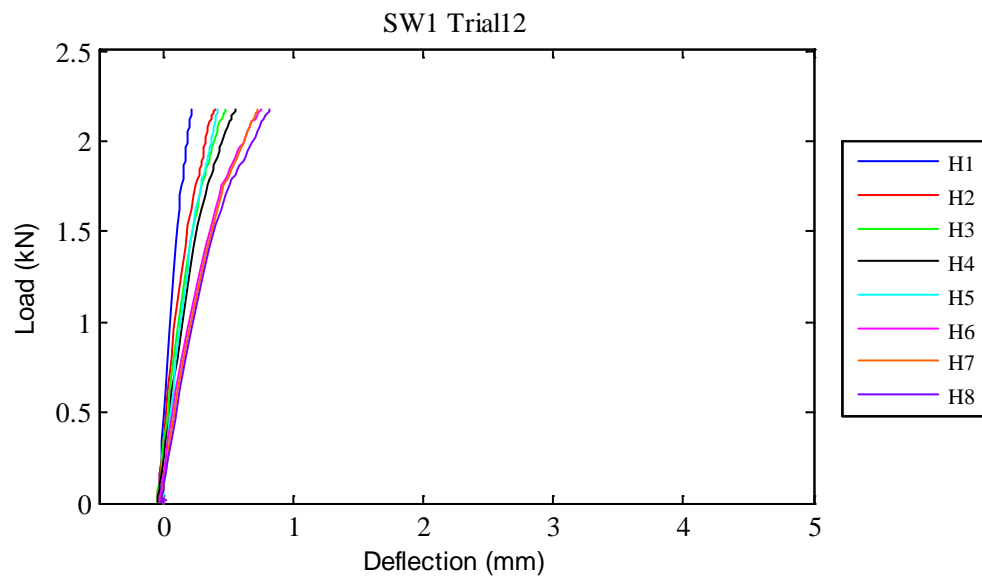
Fig. D.12: SW1 Trial12 load vs. deflection curves
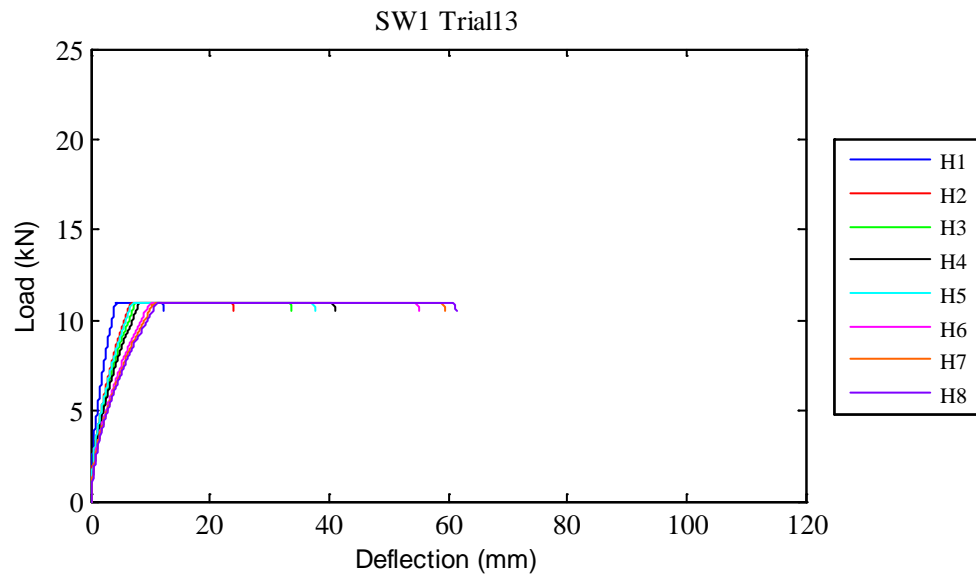
Fig. D.13: SW1 Trial13 load vs. deflection curves
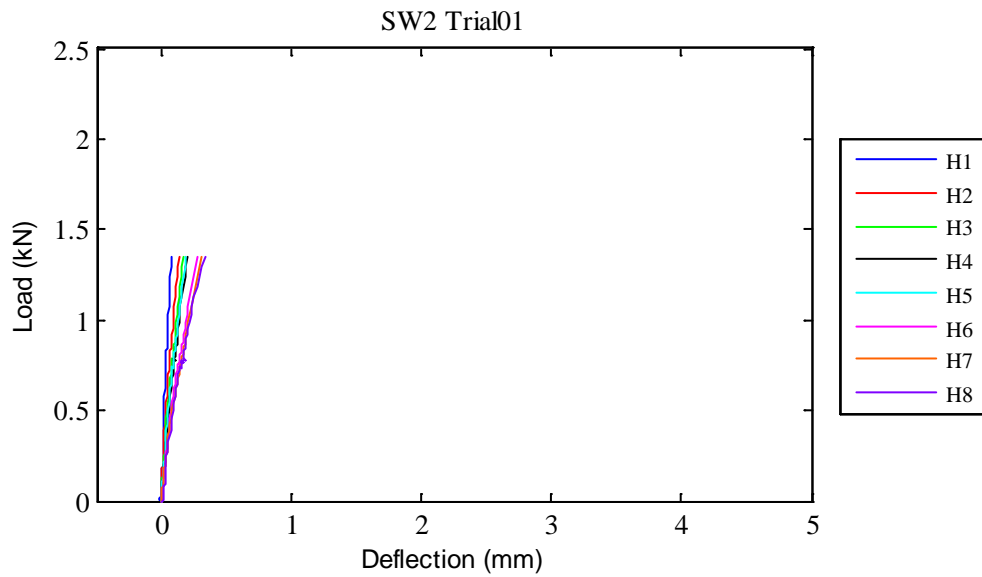
Fig. D.14: SW2 Trial01 load vs. deflection curves
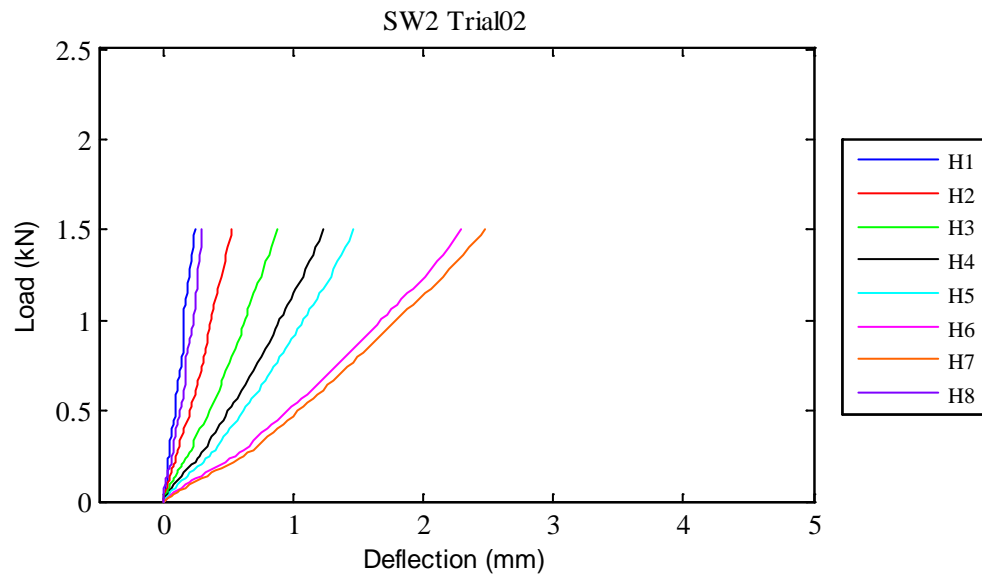
Fig. D.15: SW2 Trial02 load vs. deflection curves
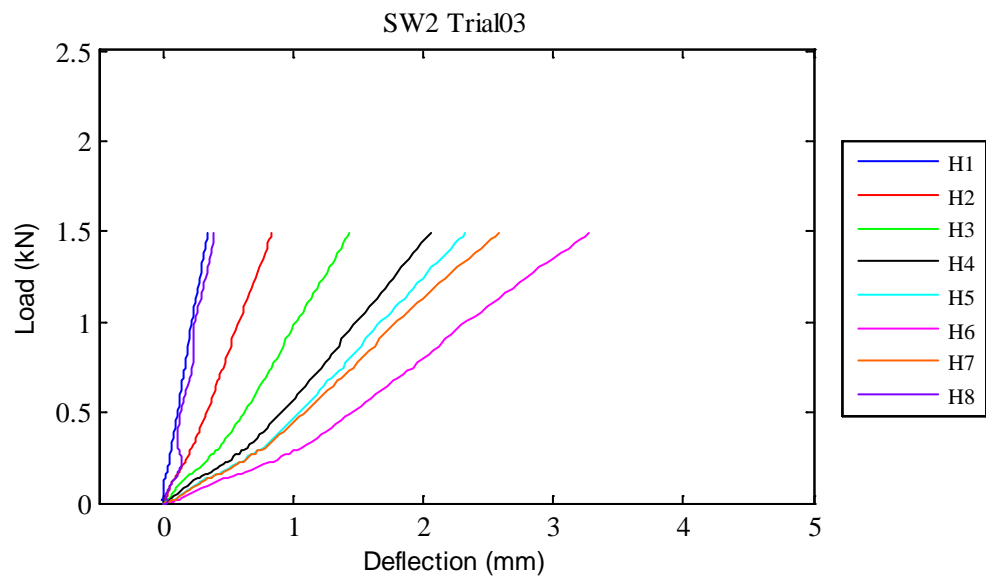
Fig. D.16: SW2 Trial03 load vs. deflection curves
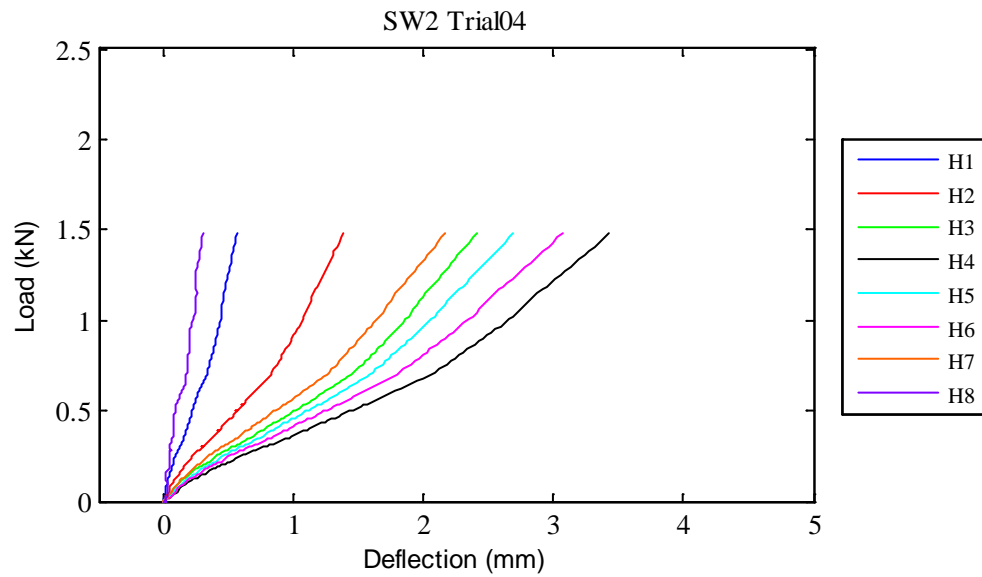
Fig. D.17: SW2 Trial04 load vs. deflection curves
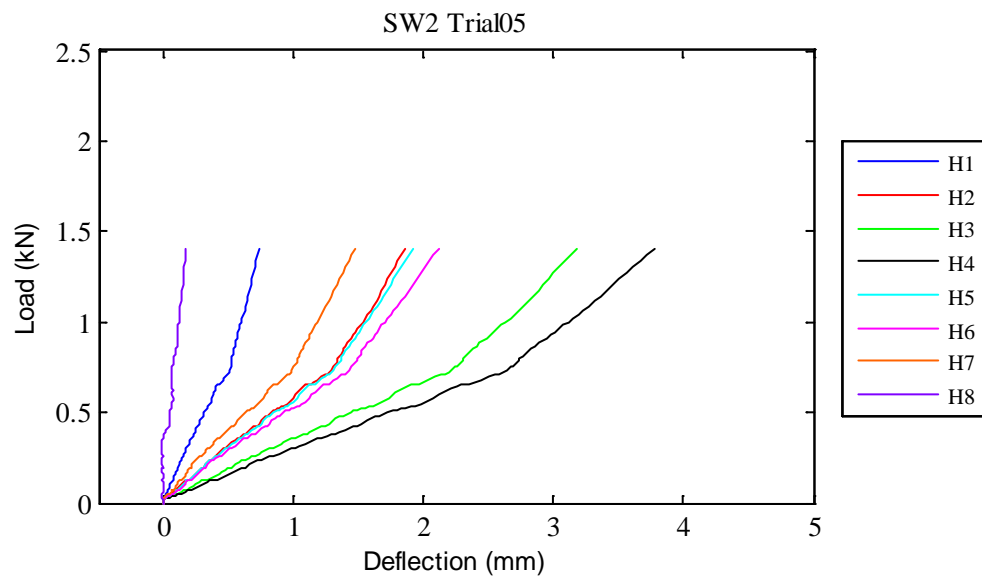
Fig. D.18: SW2 Trial05 load vs. deflection curves
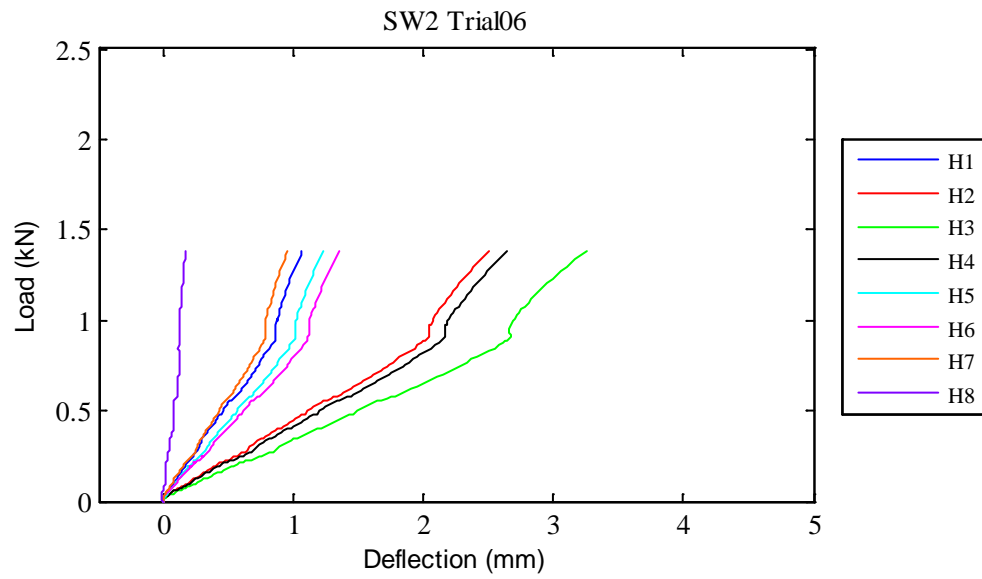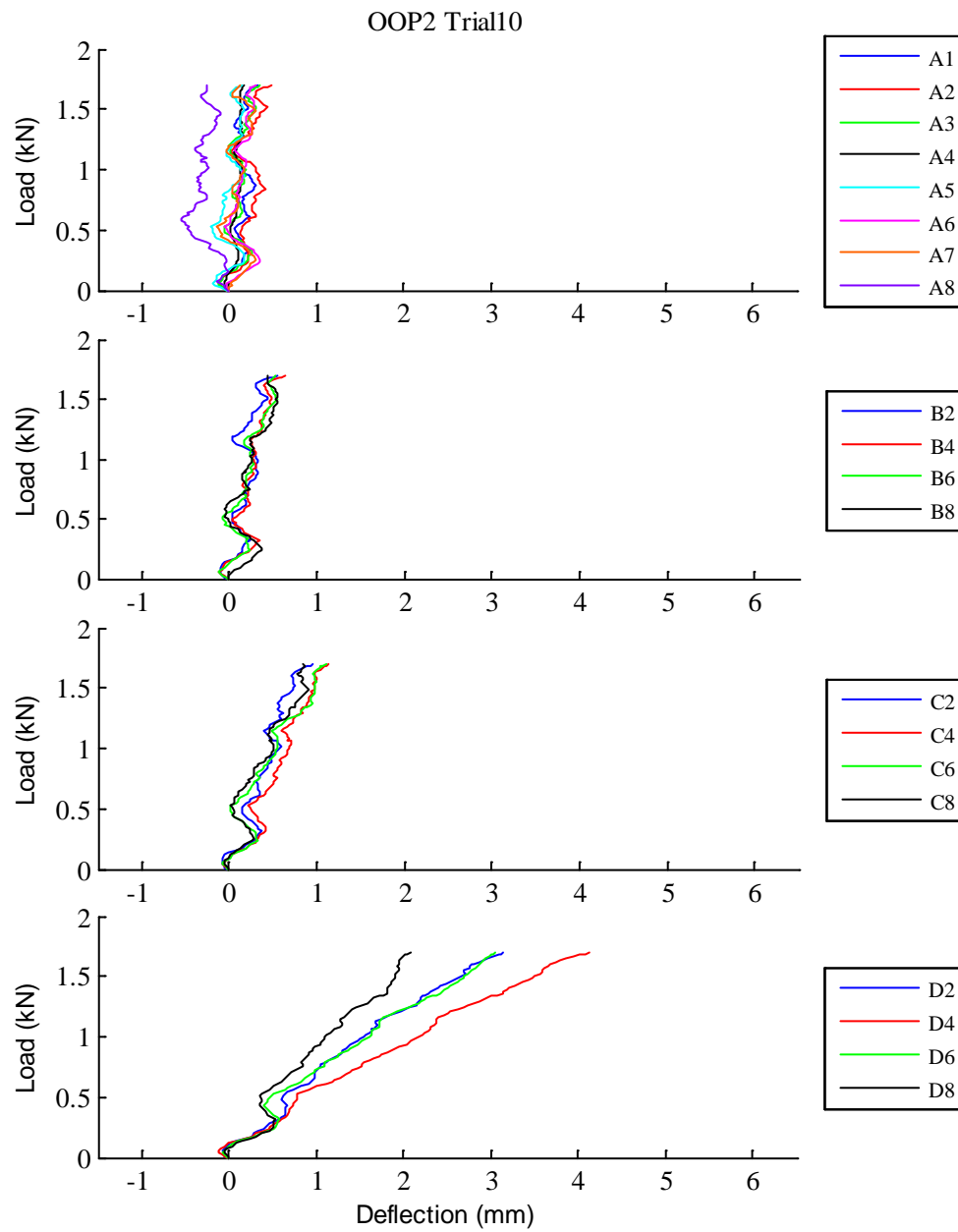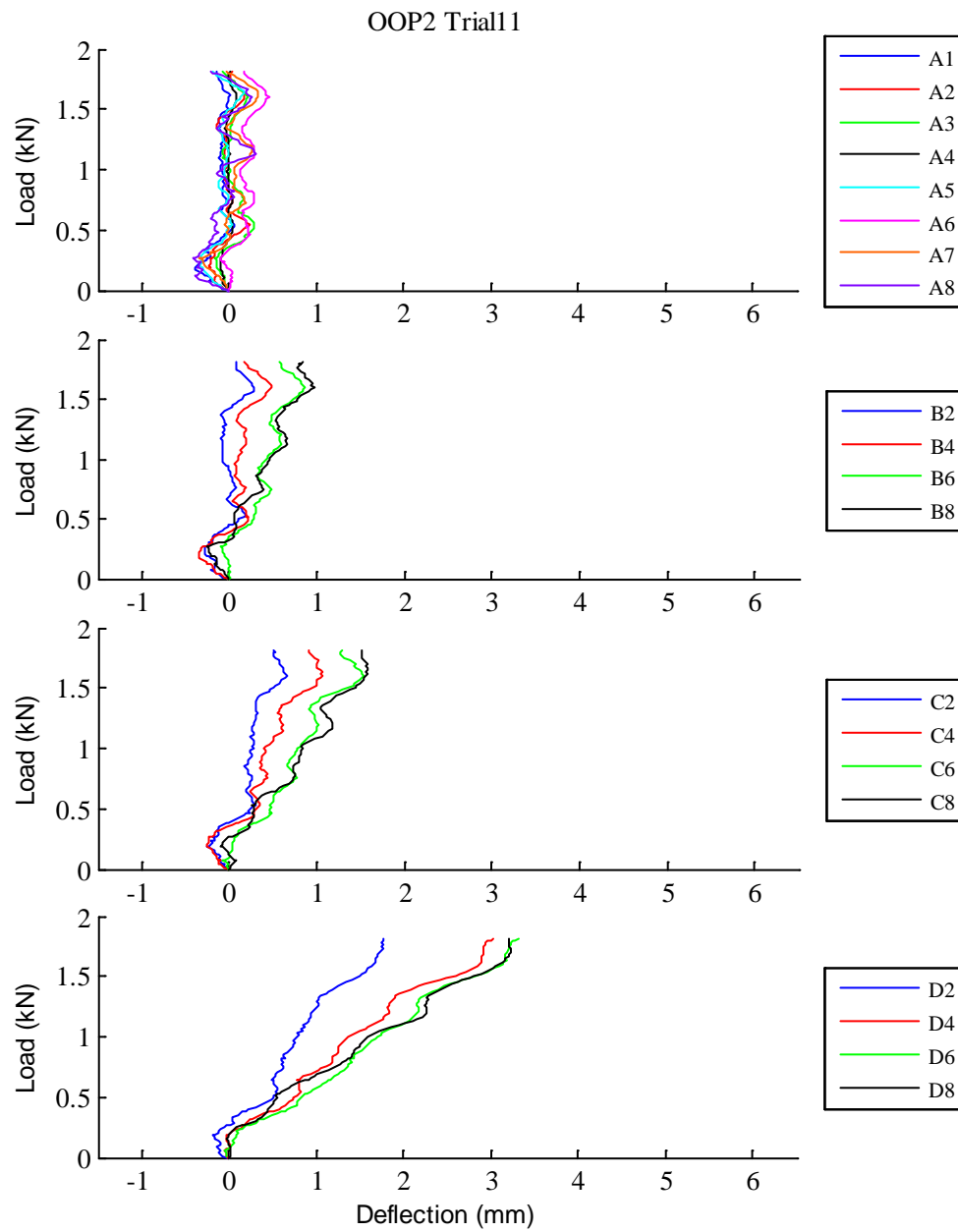
Fig. D.19: SW2 Trial06 load vs. deflection curves
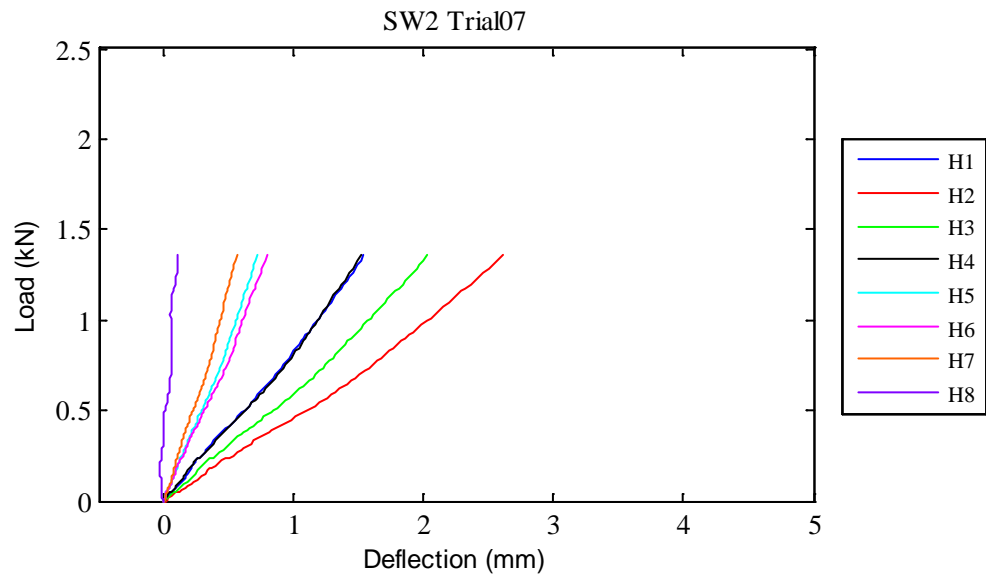
Fig. D.20: SW2 Trial07 load vs. deflection curves
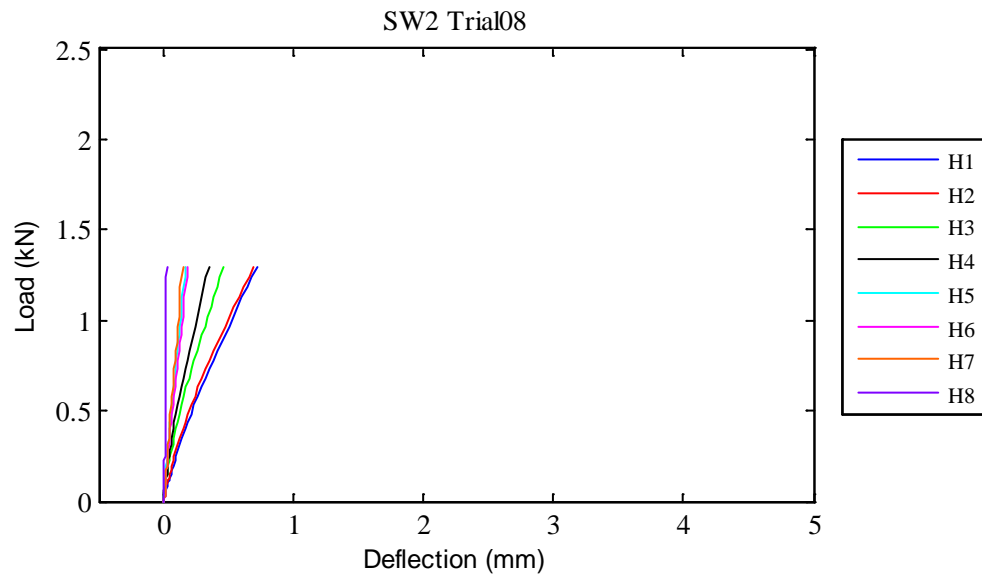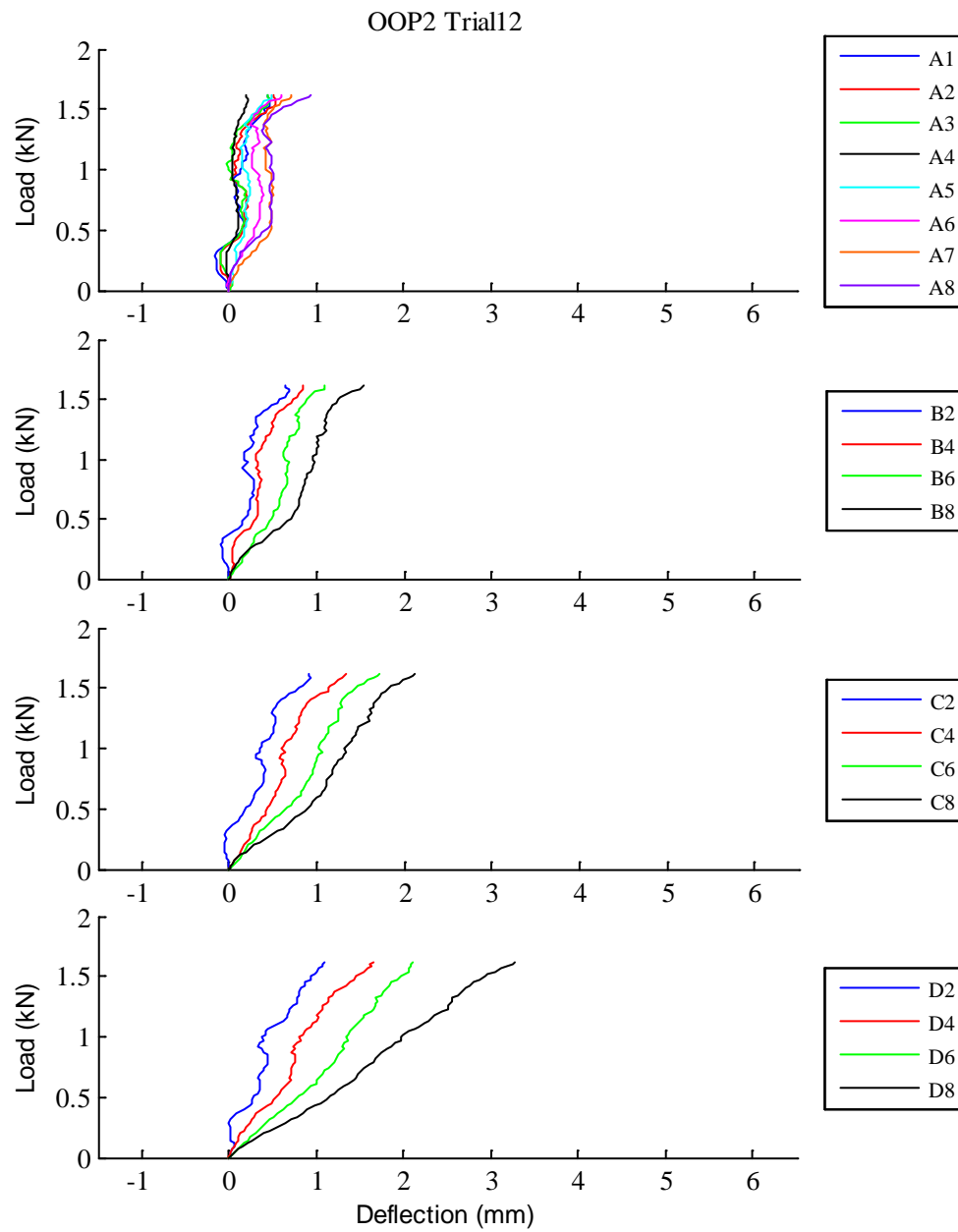
Fig. D.21: SW2 Trial08 load vs. deflection curves
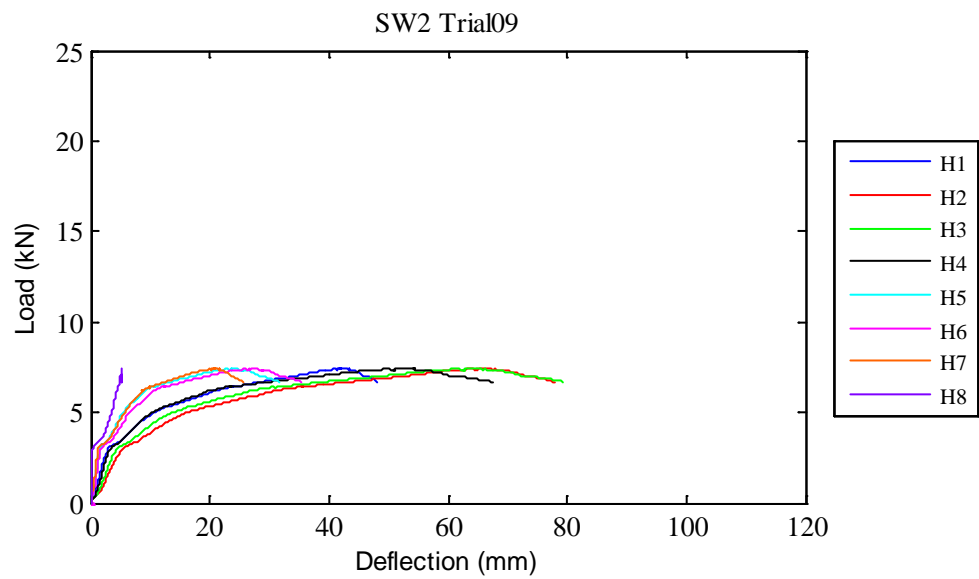
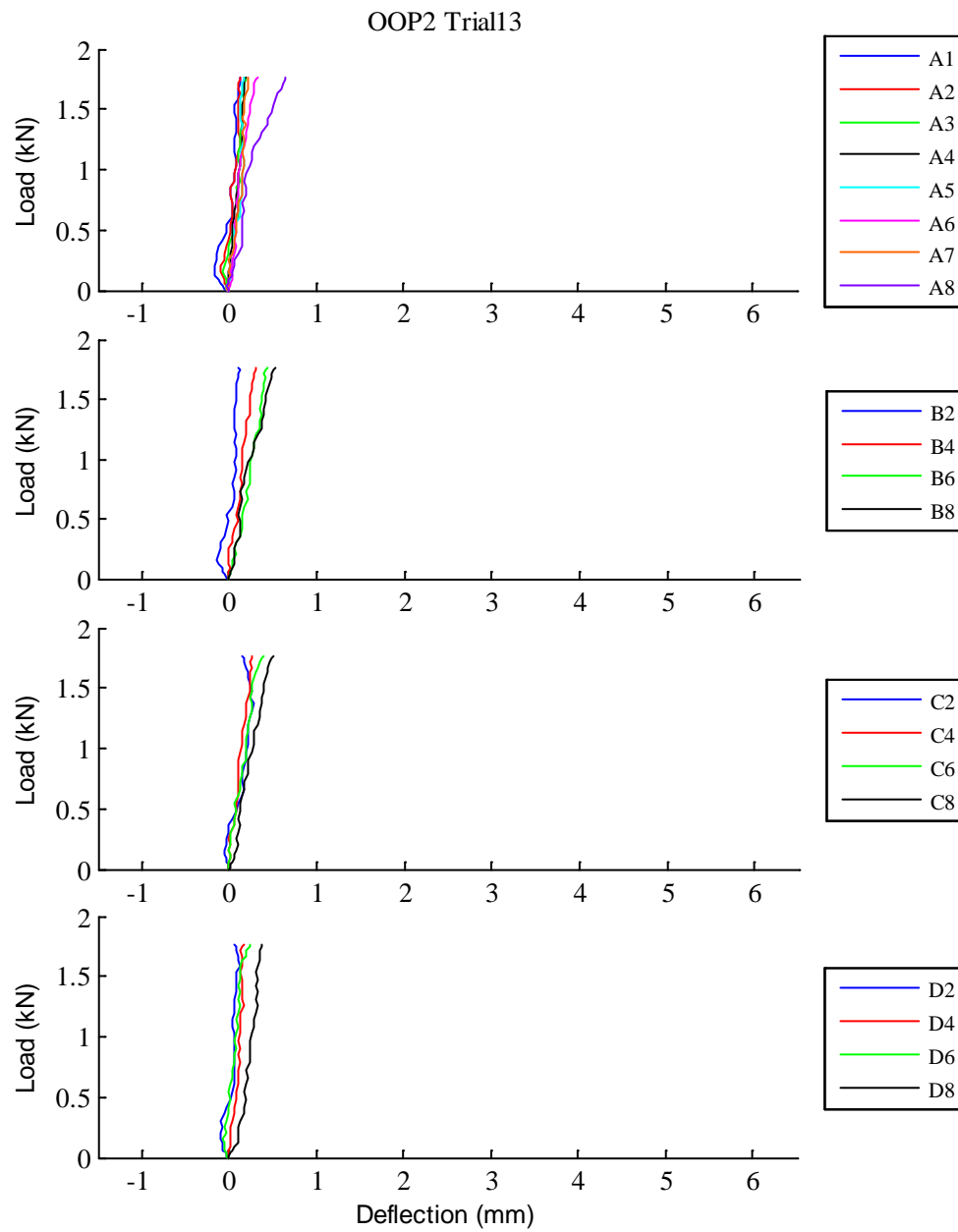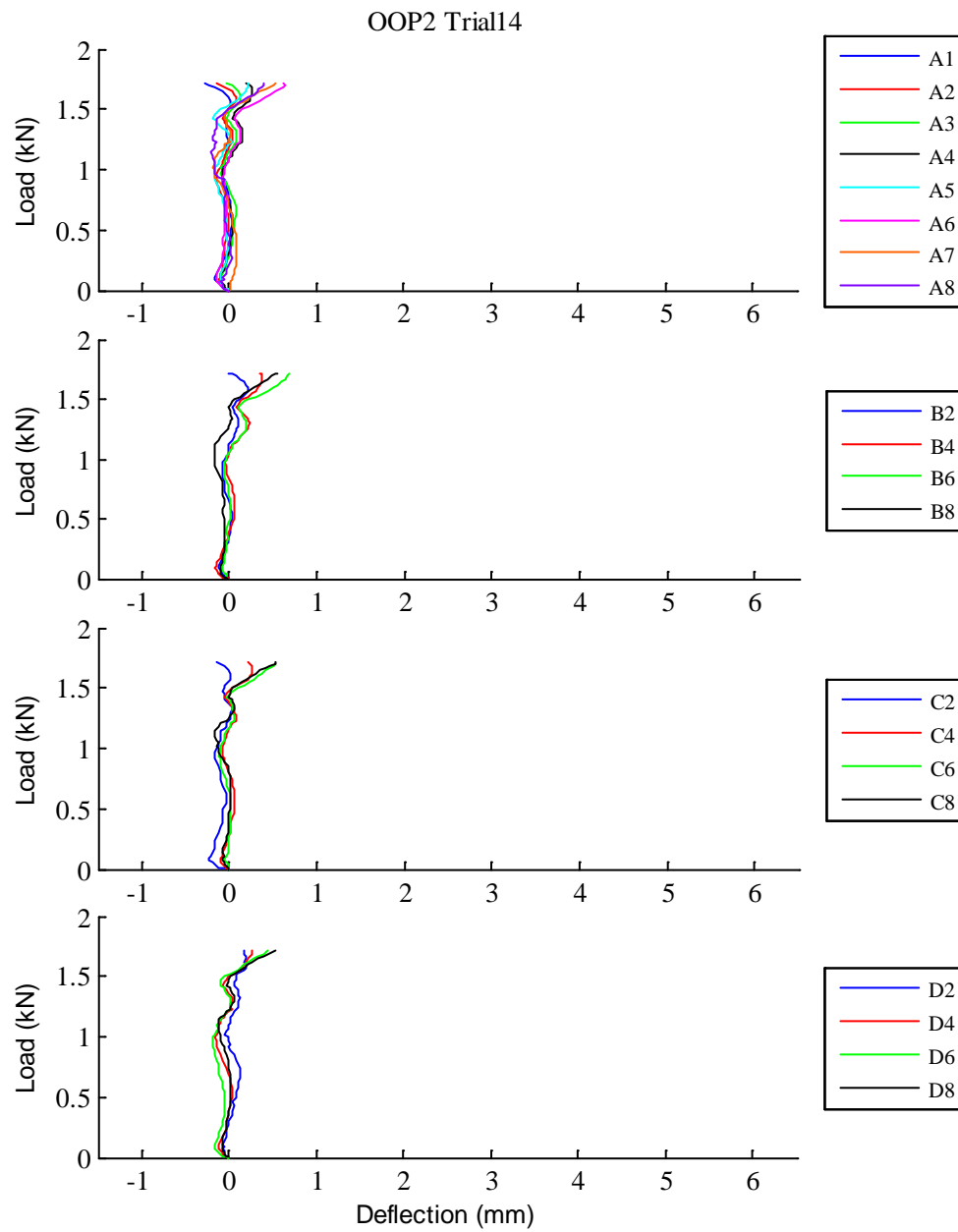

Fig. D.22: SW2 Trial09 load vs. deflection curves
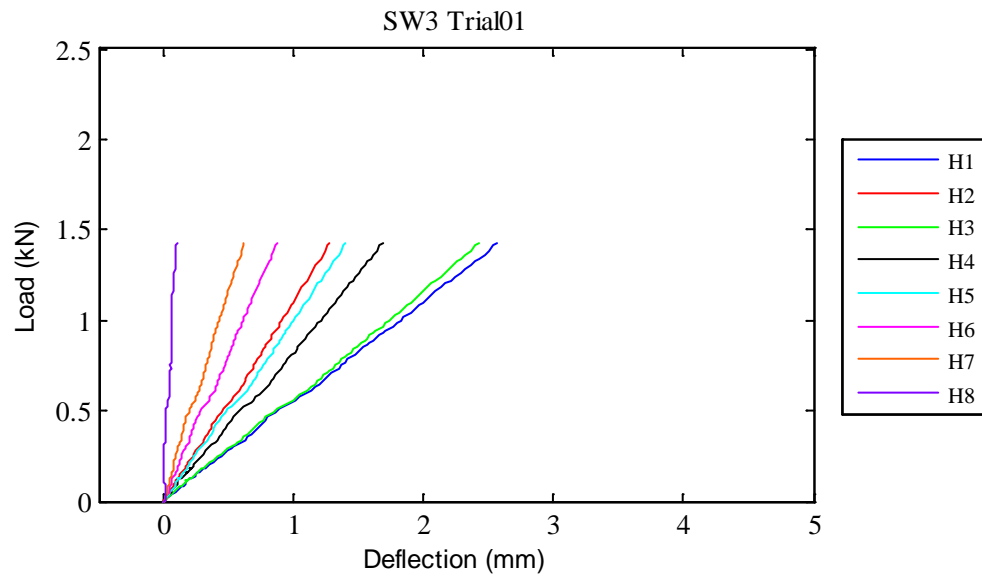
Fig. D.23: SW3 Trial01 load vs. deflection curves
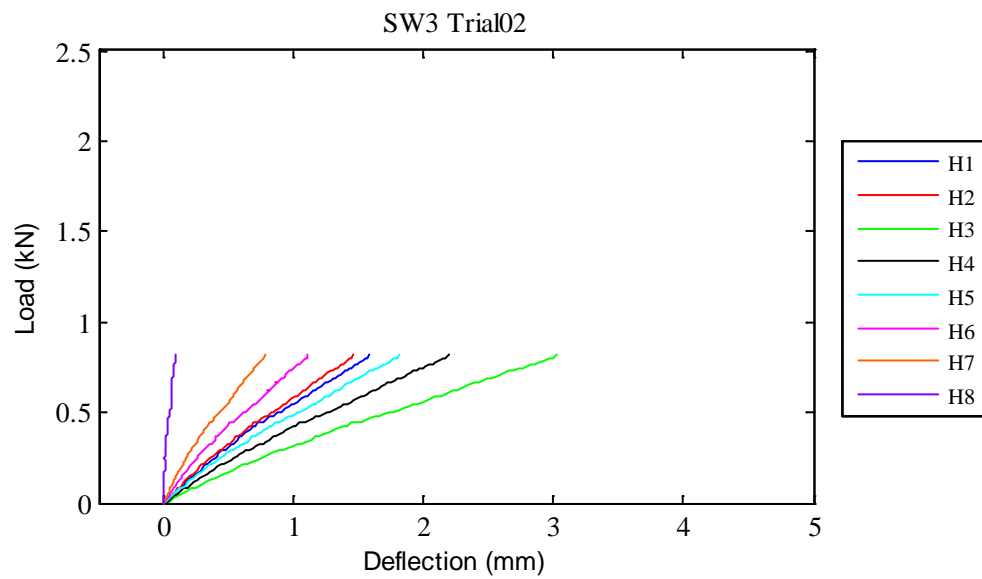
Fig. D.24: SW3 Trial02 load vs. deflection curves
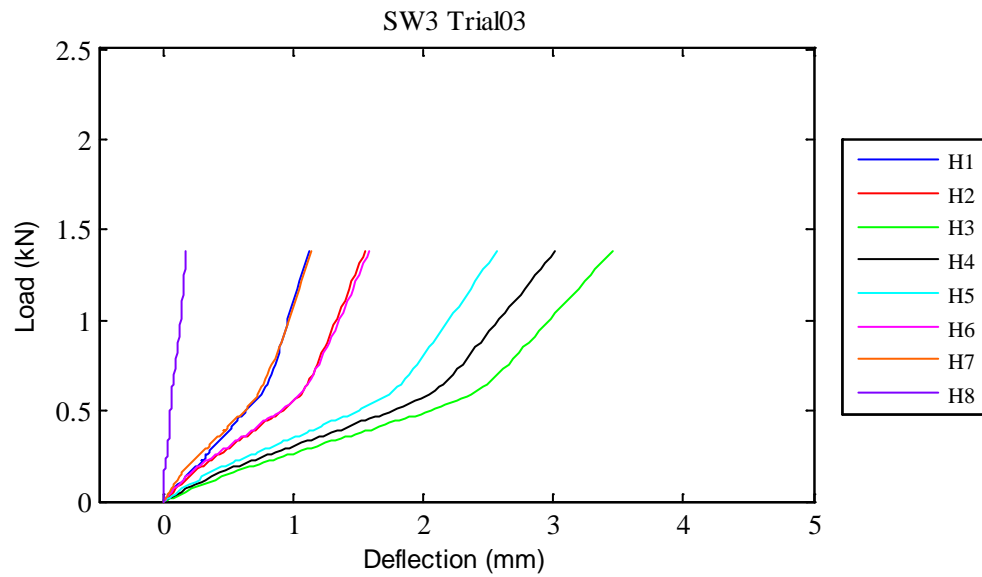
Fig. D.25: SW3 Trial03 load vs. deflection curves
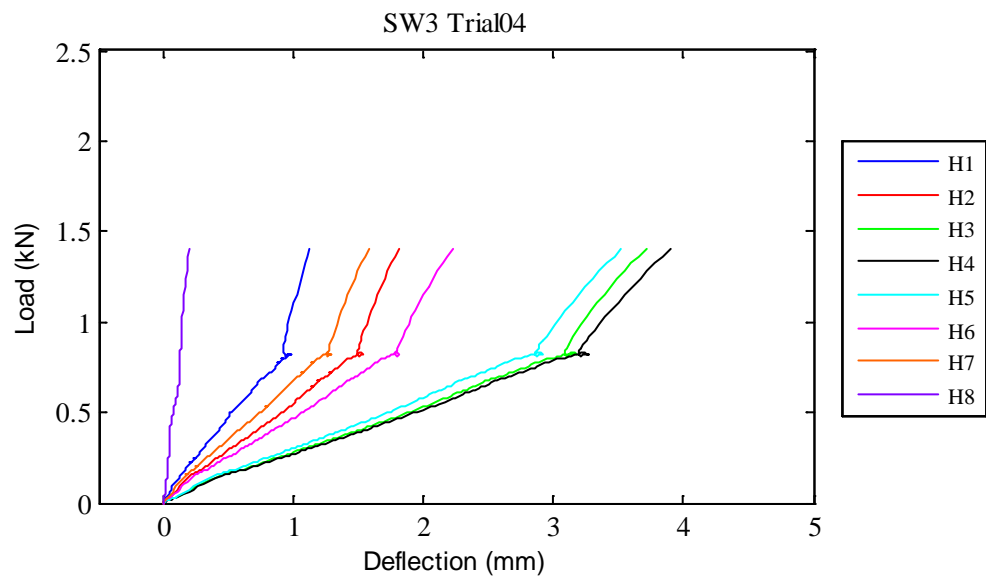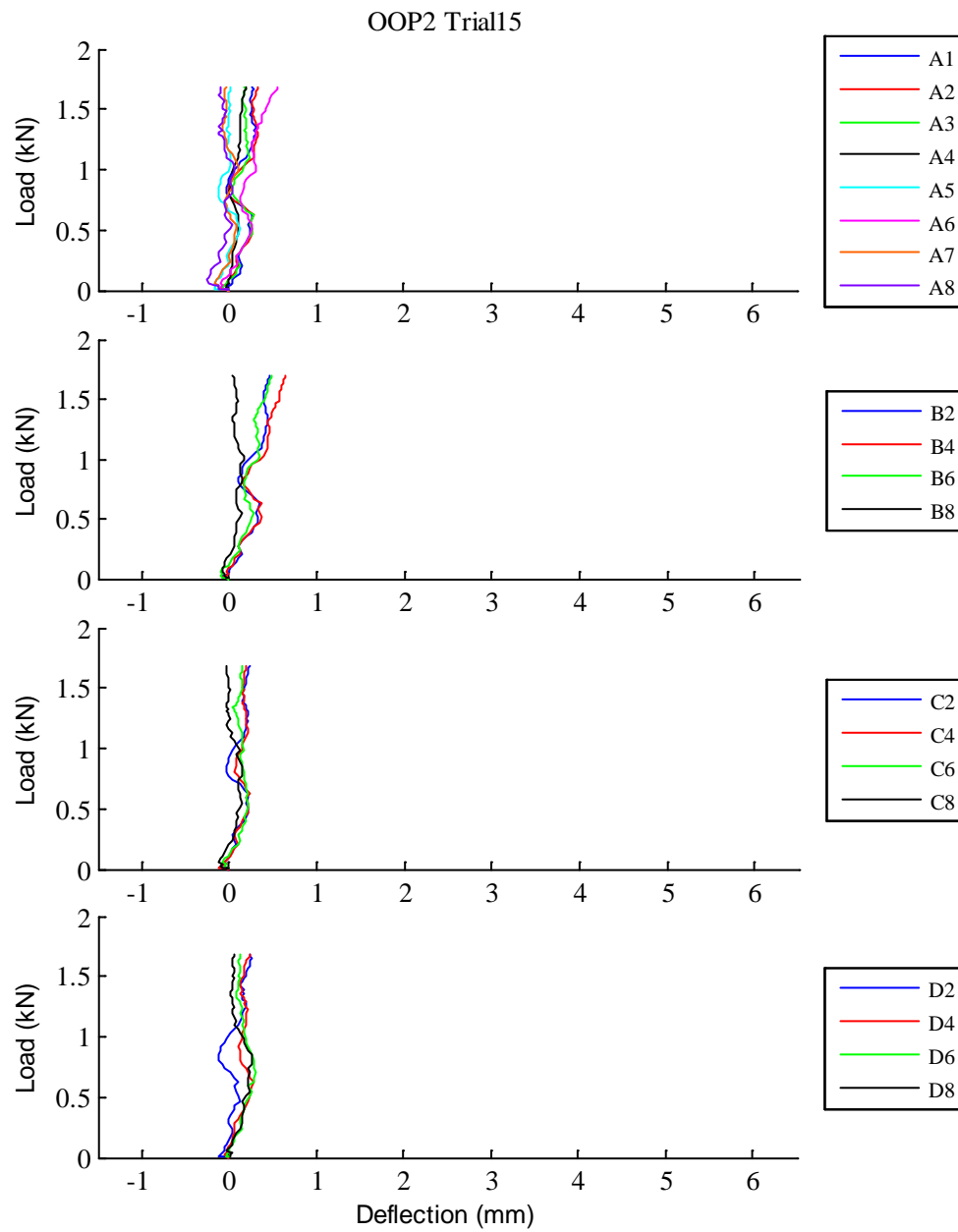

Fig. D.26: SW3 Trial04 load vs. deflection curves
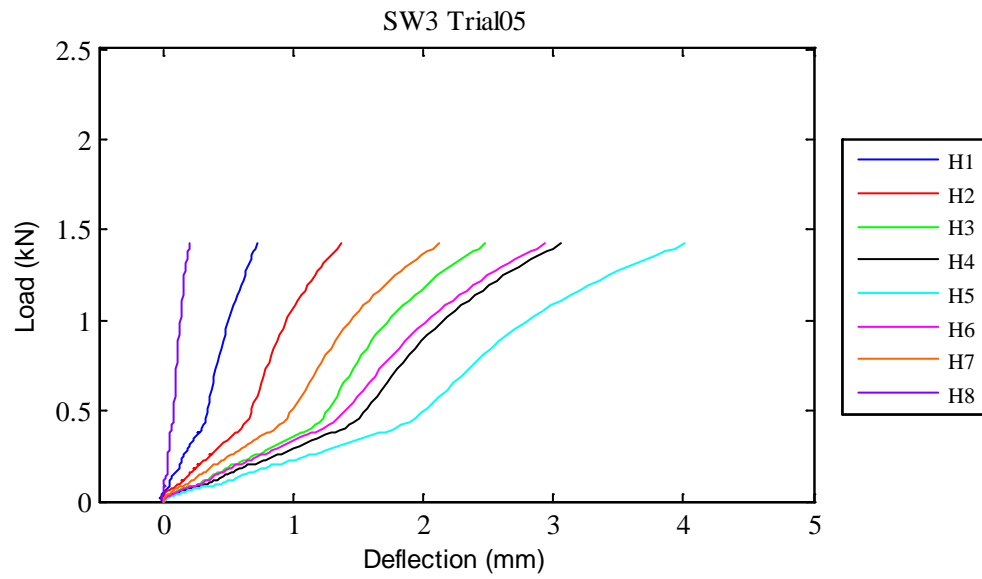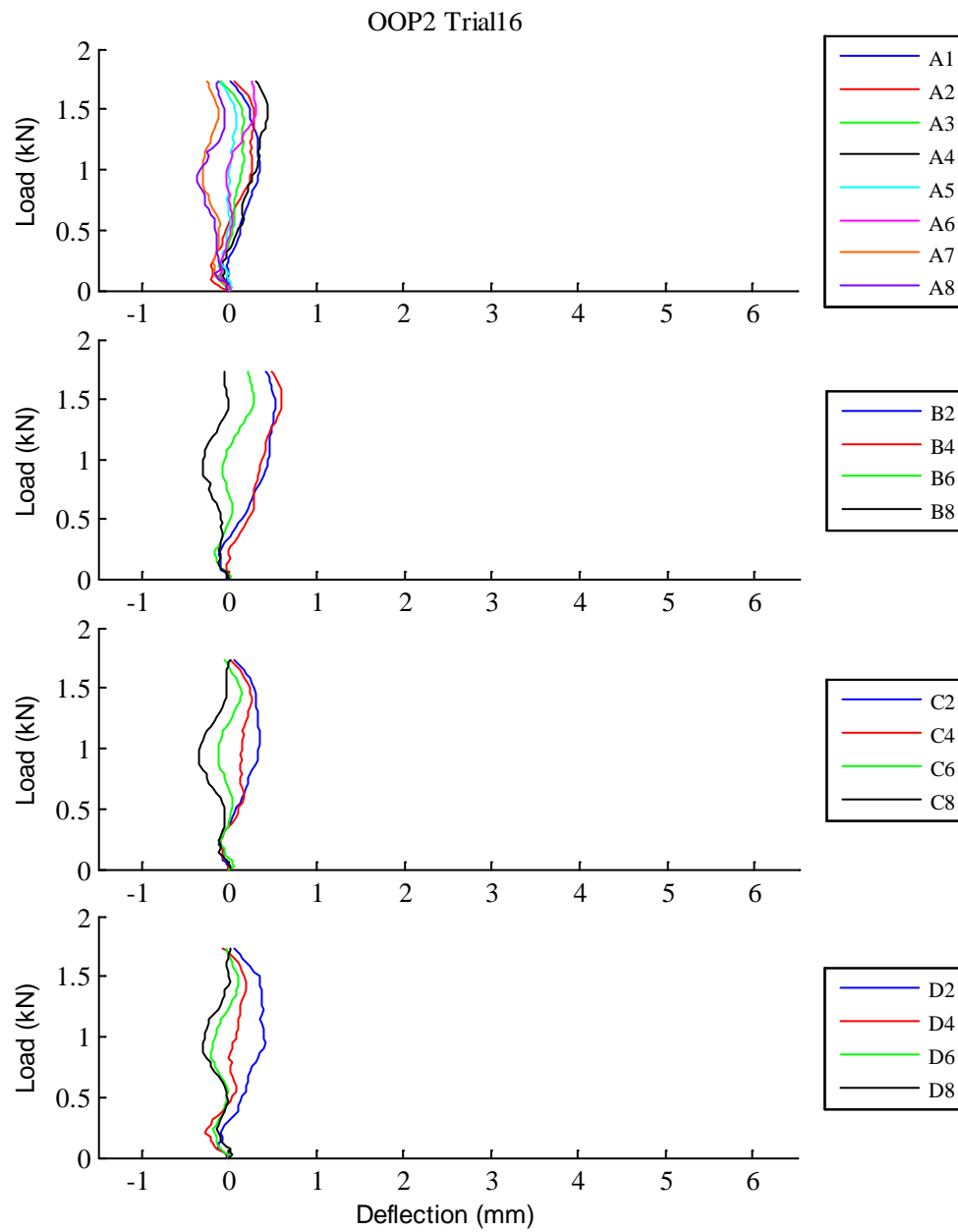
Fig. D.27: SW3 Trial05 load vs. deflection curves
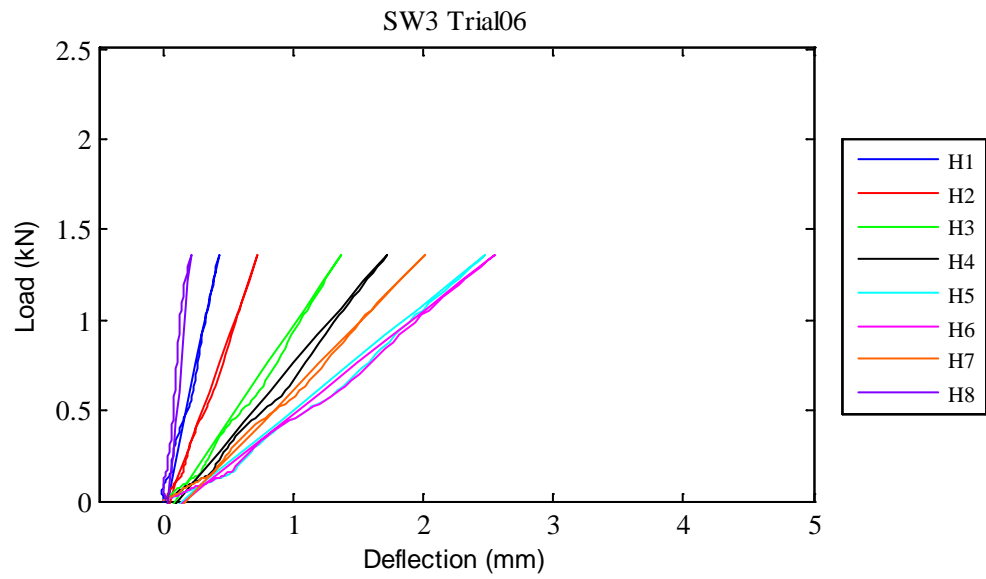
Fig. D.28: SW3 Trial06 load vs. deflection curves
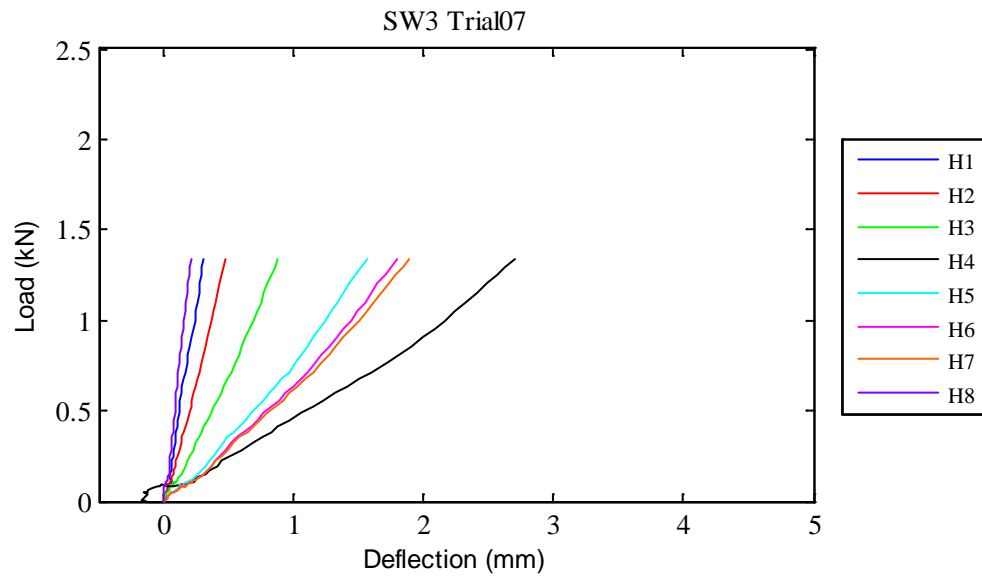
Fig. D.29: SW3 Trial07 load vs. deflection curves
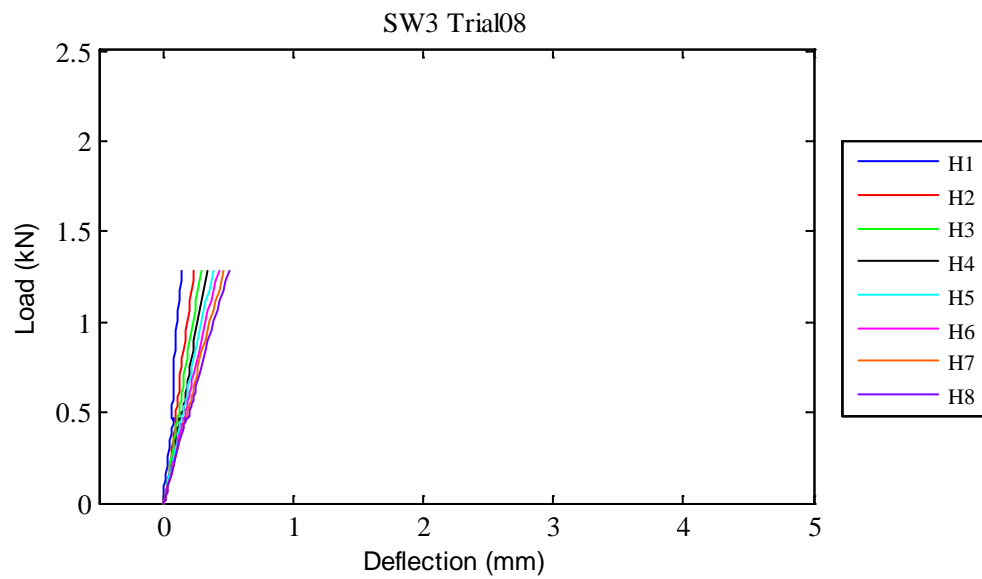
Fig. D.30: SW3 Trial08 load vs. deflection curves
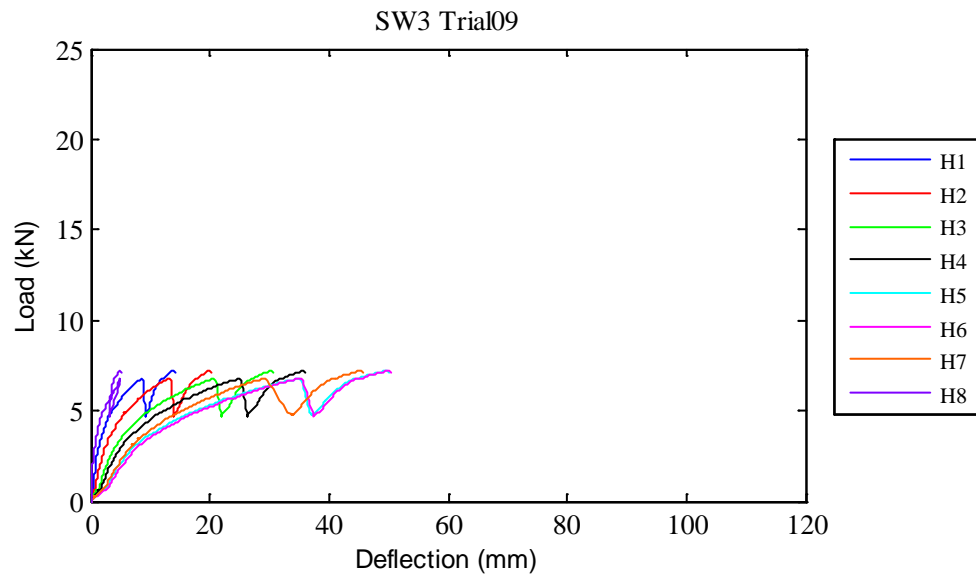
Fig. D.31: SW3 Trial09 load vs. deflection curves
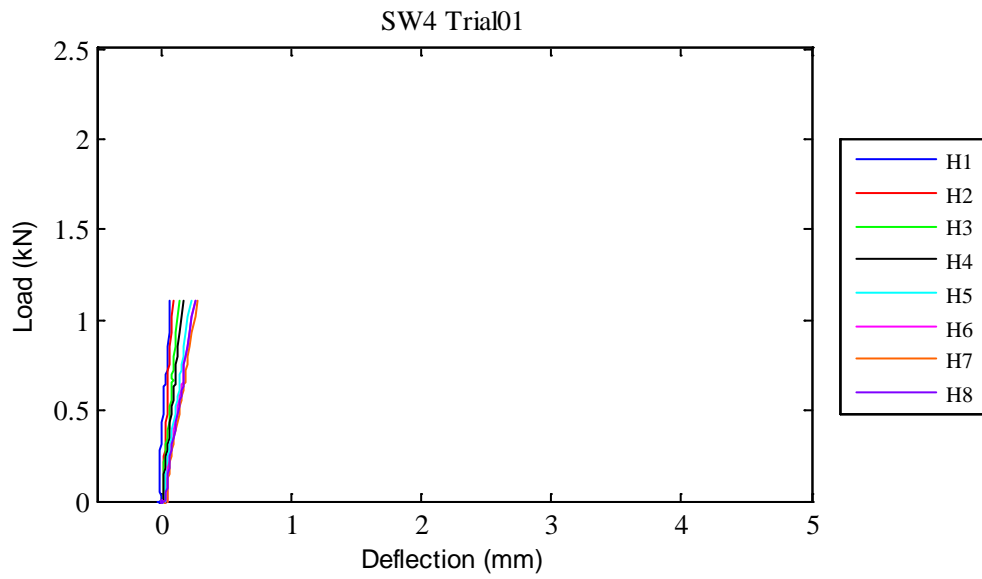
Fig. D.32: SW4 Trial01 load vs. deflection curves
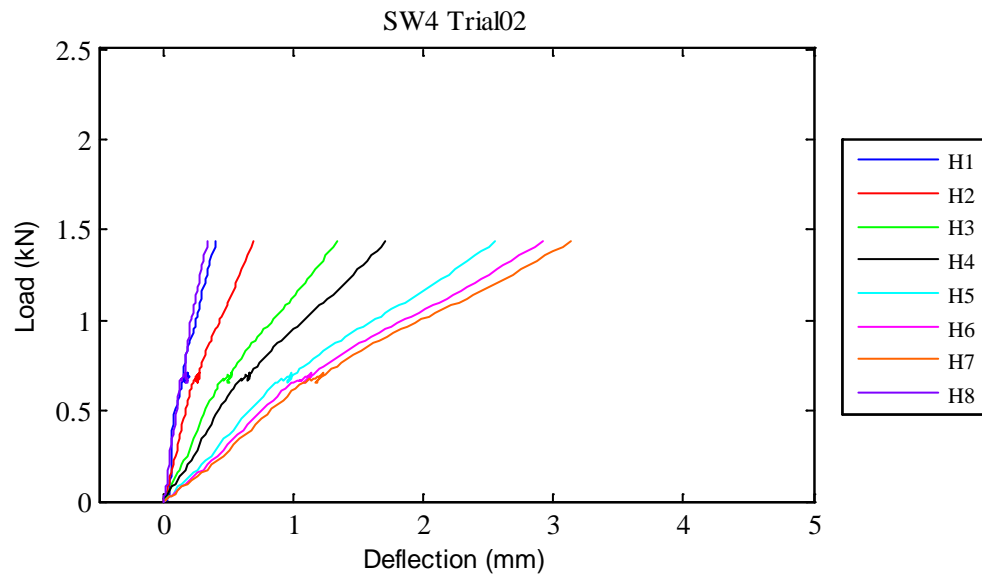
Fig. D.33: SW4 Trial02 load vs. deflection curves
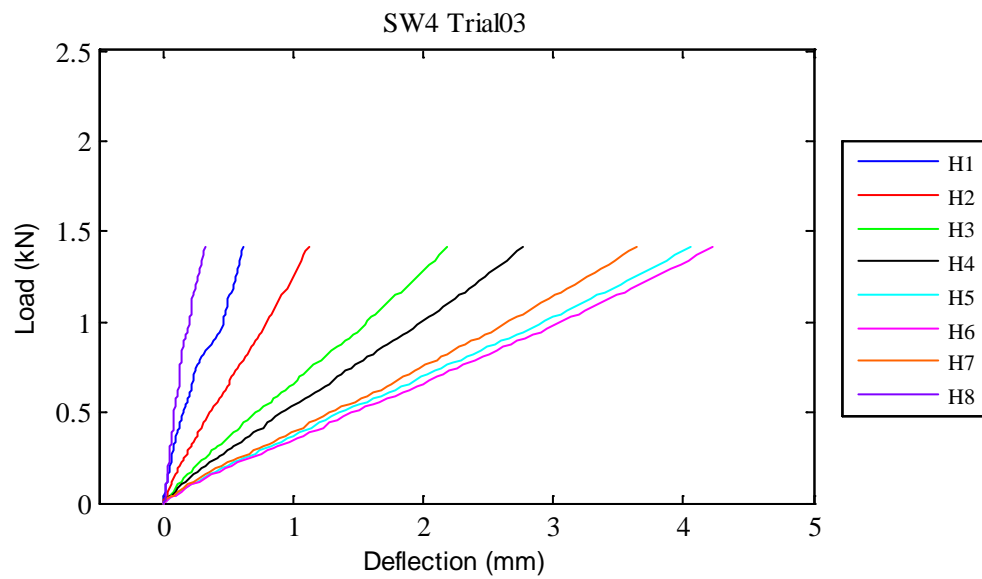
Fig. D.34: SW4 Trial03 load vs. deflection curves
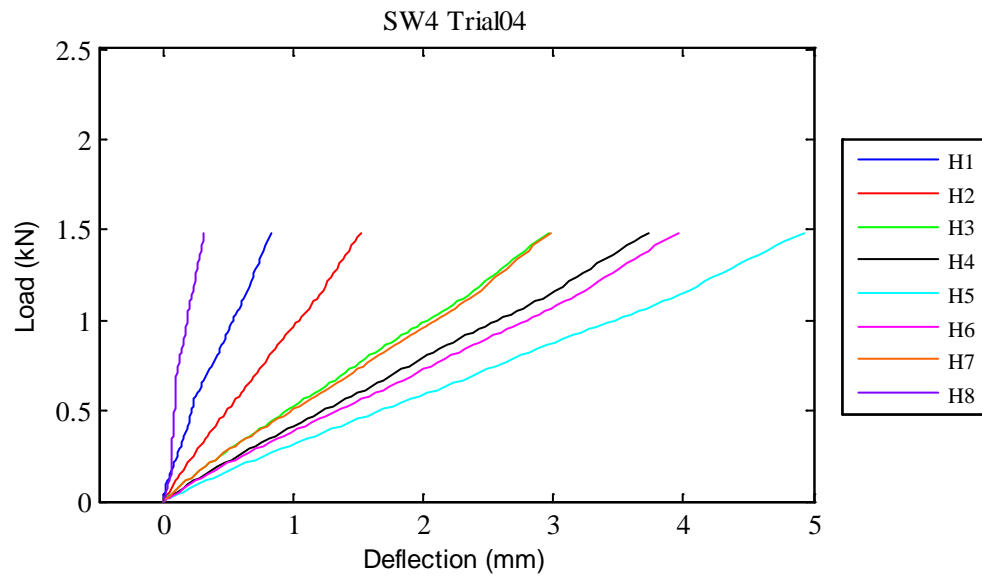
Fig. D.35: SW4 Trial04 load vs. deflection curves
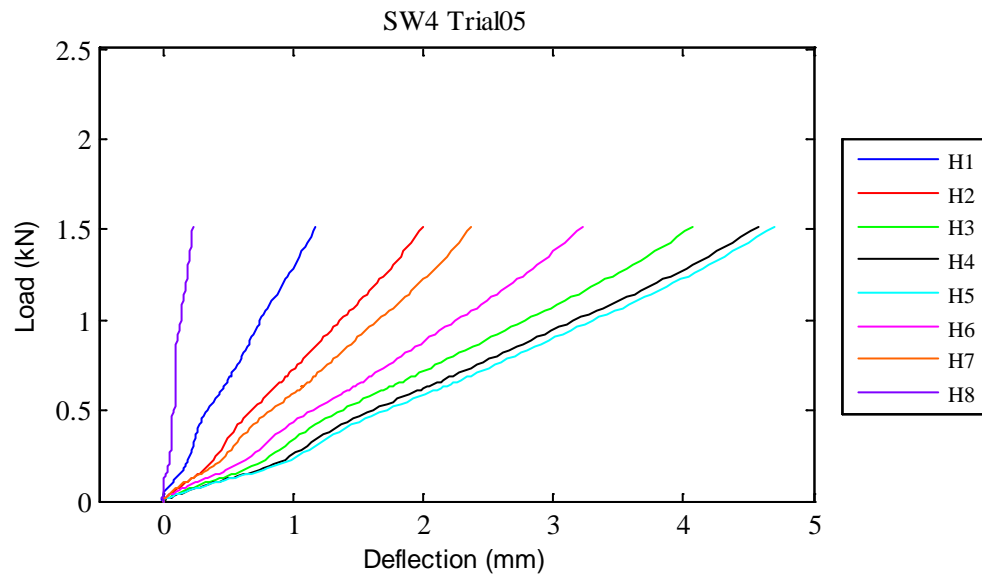
Fig. D.36: SW4 Trial05 load vs. deflection curves
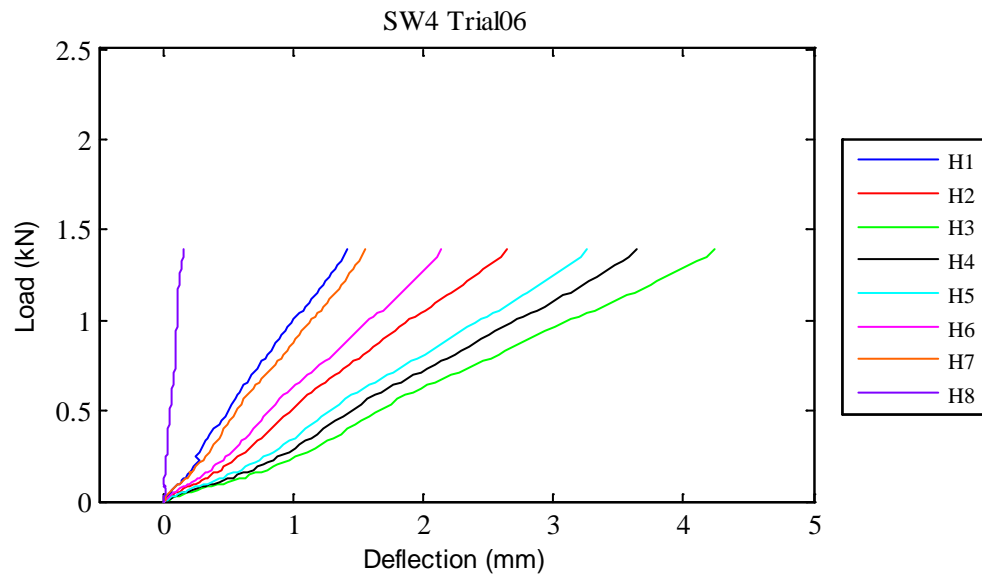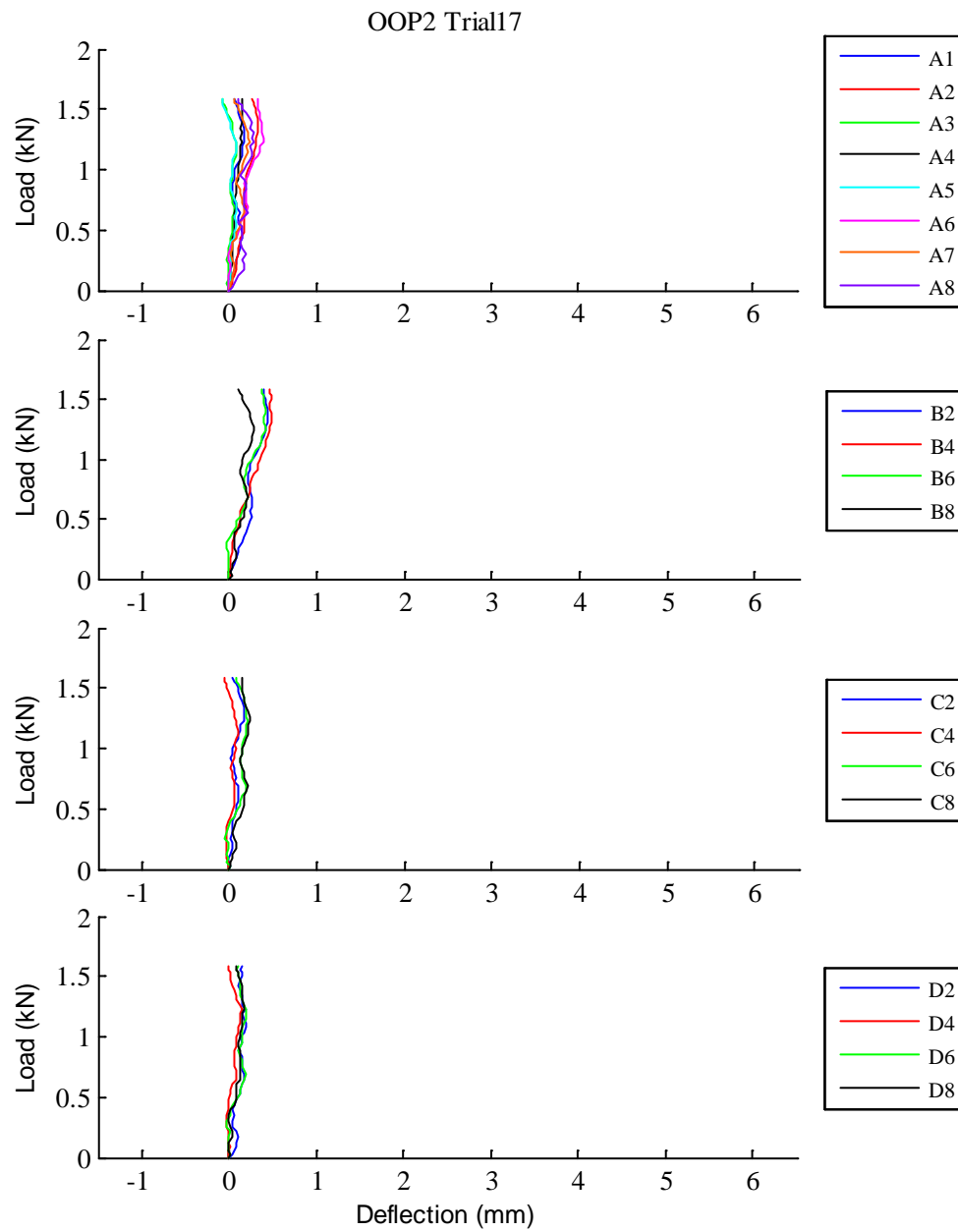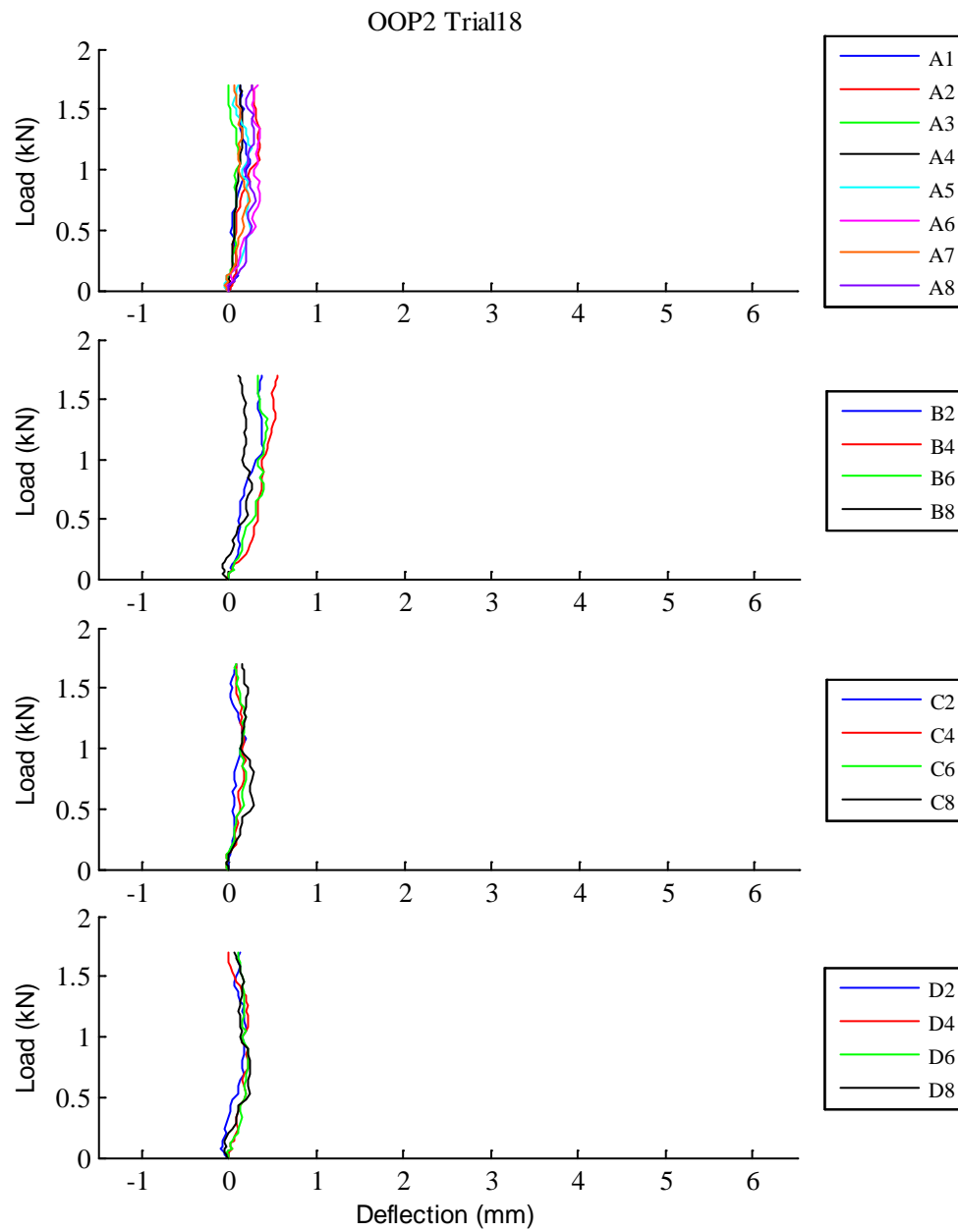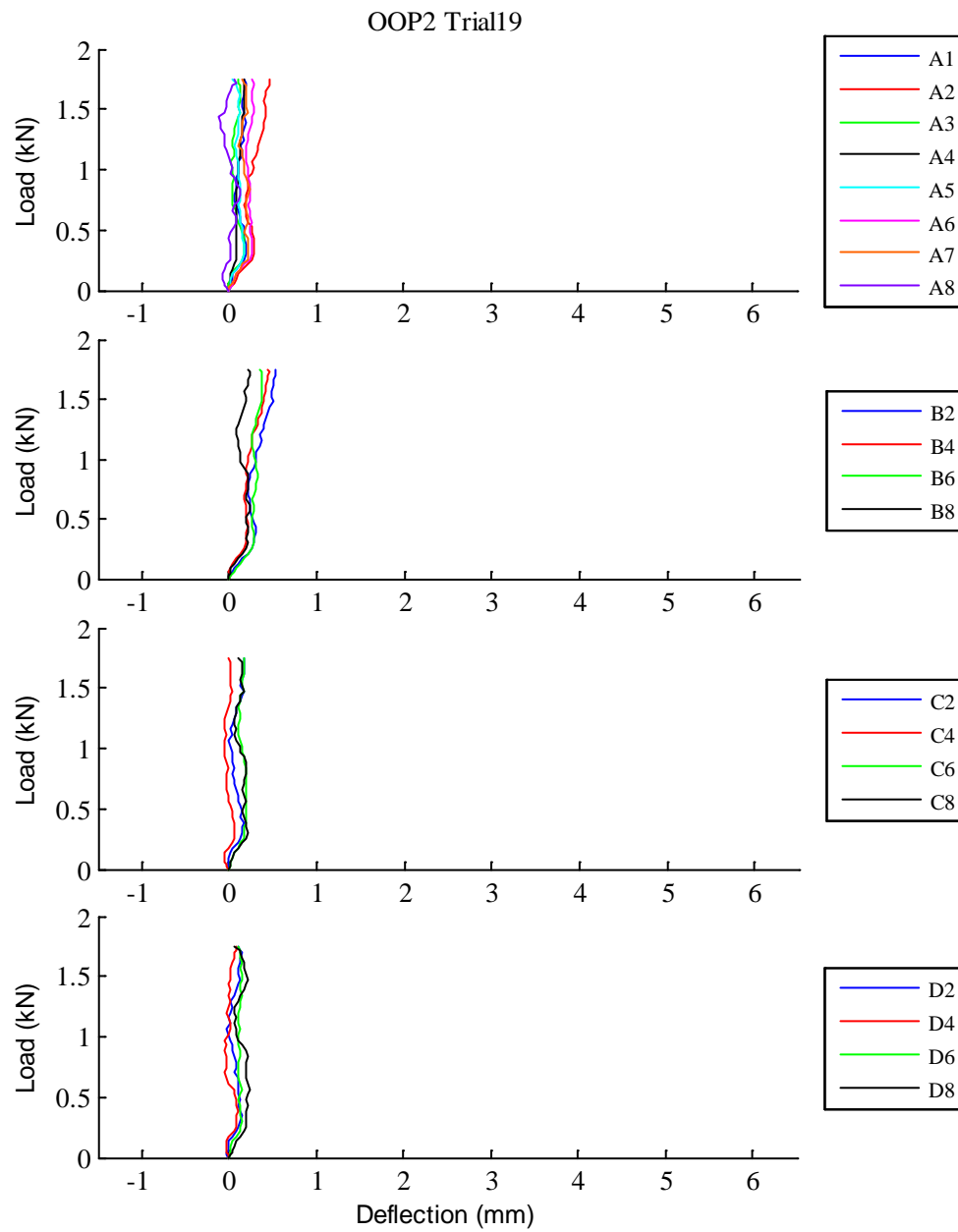
Fig. D.37: SW4 Trial06 load vs. deflection curves
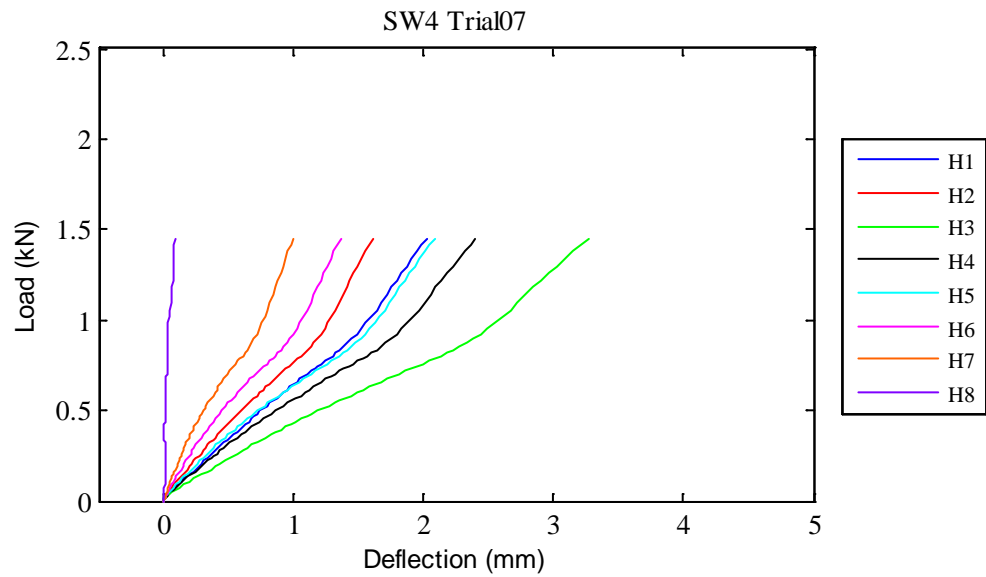
Fig. D.38: SW4 Trial07 load vs. deflection curves
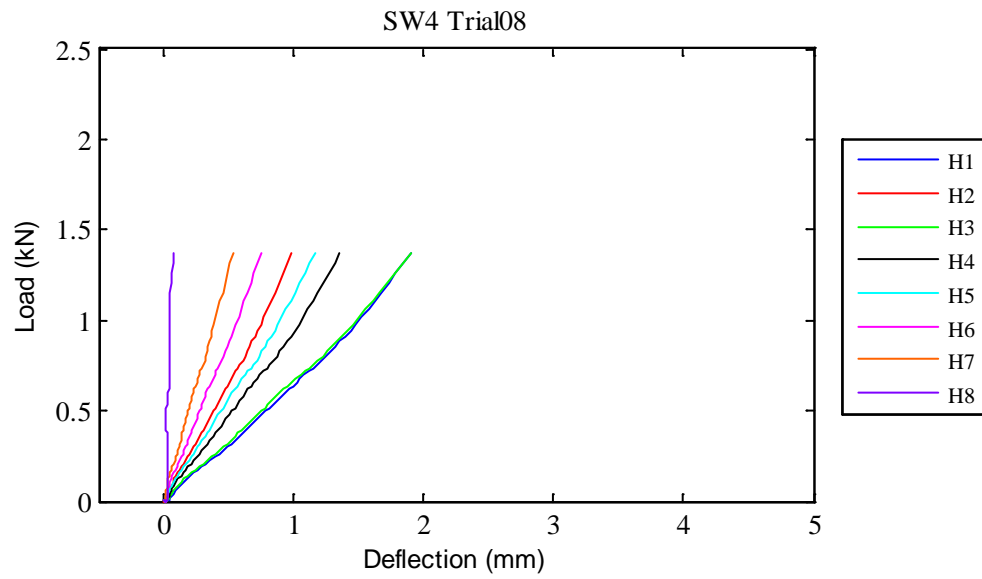
Fig. D.39: SW4 Trial08 load vs. deflection curves
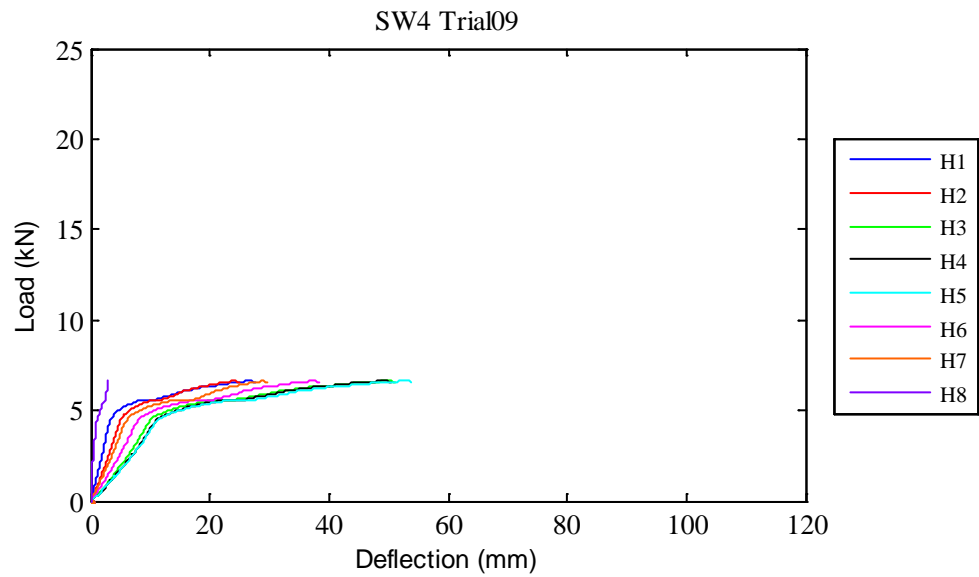
Fig. D.40: SW4 Trial09 load vs. deflection curves
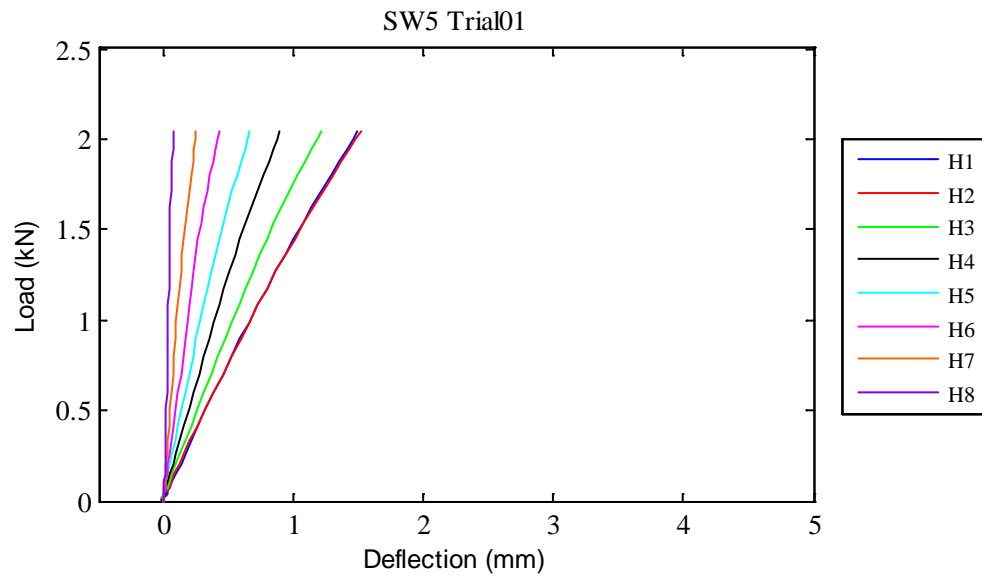
Fig. D.41: SW5 Trial01 load vs. deflection curves
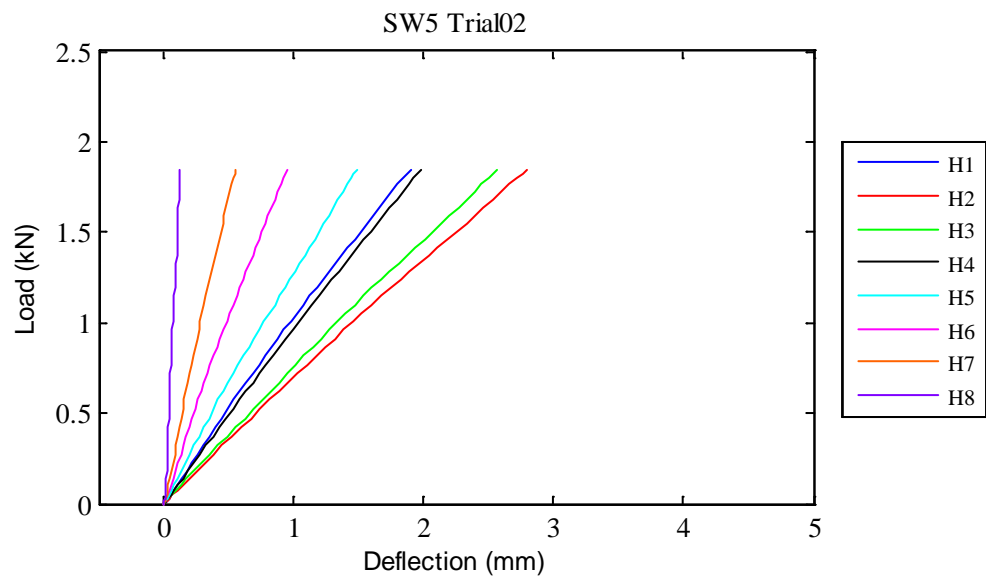
Fig. D.42: SW5 Trial02 load vs. deflection curves
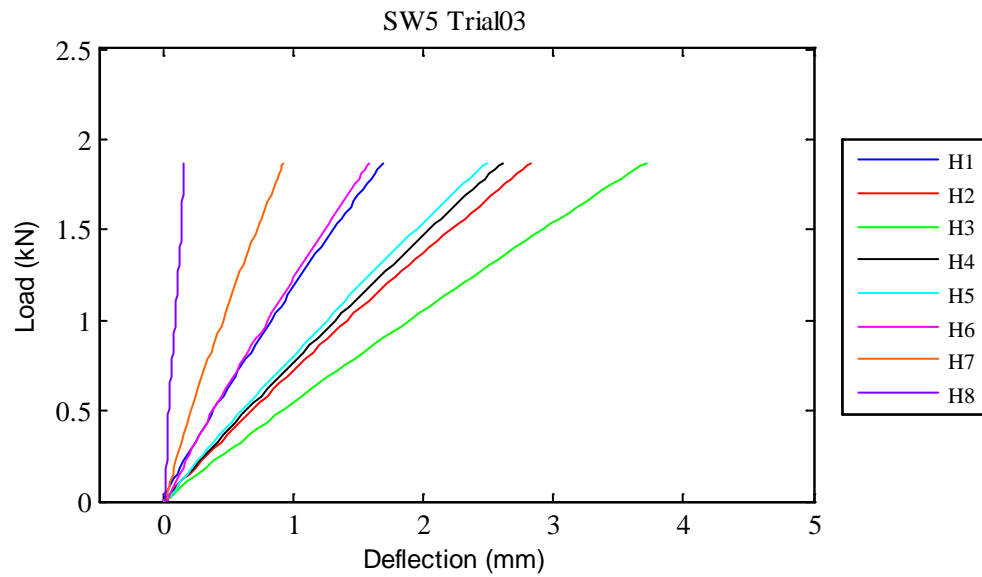
Fig. D.43: SW5 Trial03 load vs. deflection curves
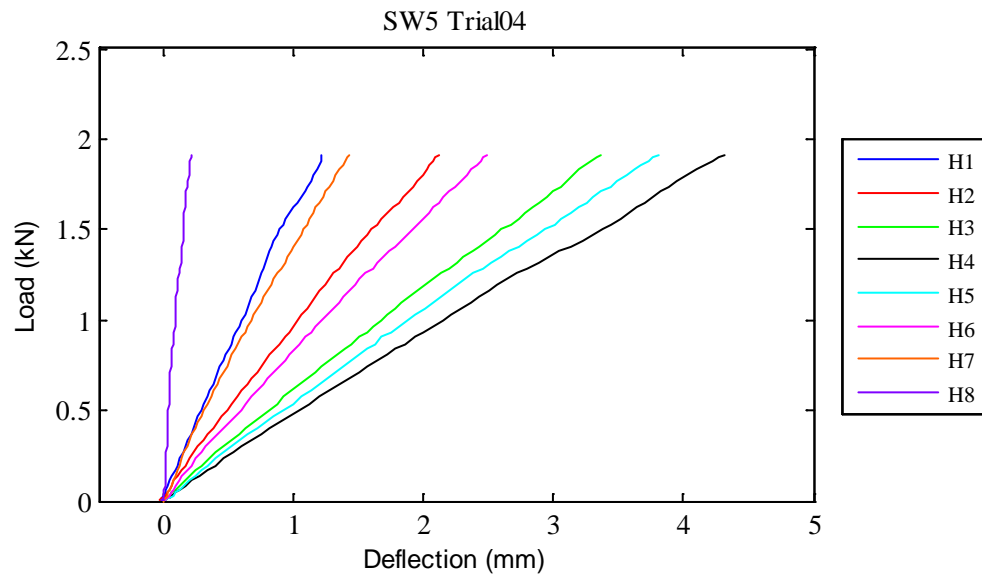
Fig. D.44: SW5 Trial04 load vs. deflection curves
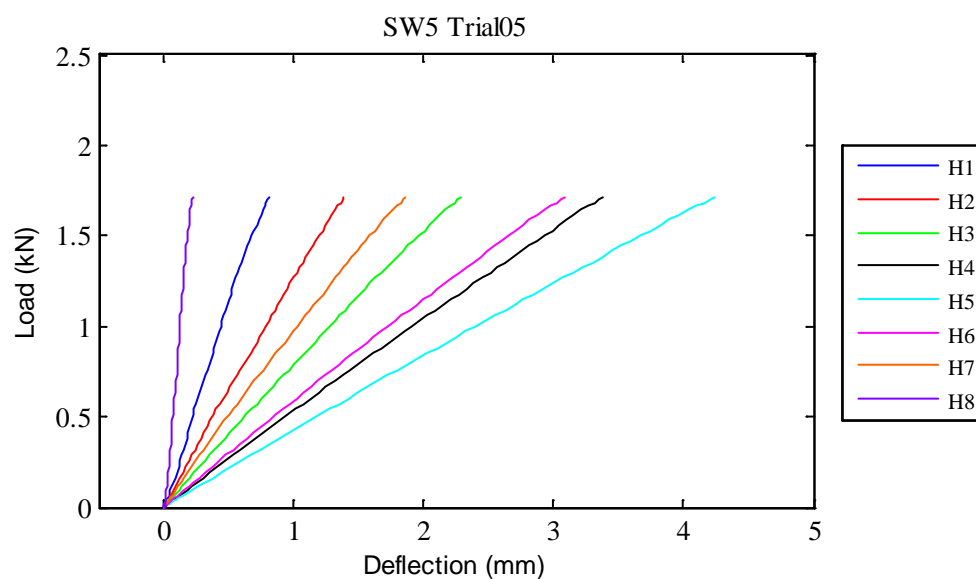
Fig. D.45: SW5 Trial05 load vs. deflection curves
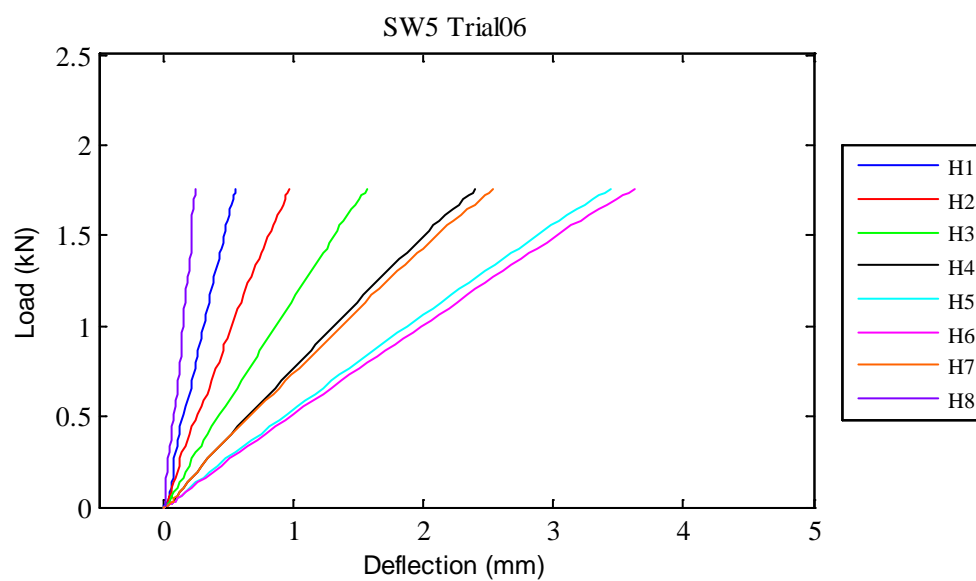
Fig. D.46: SW5 Trial06 load vs. deflection curves
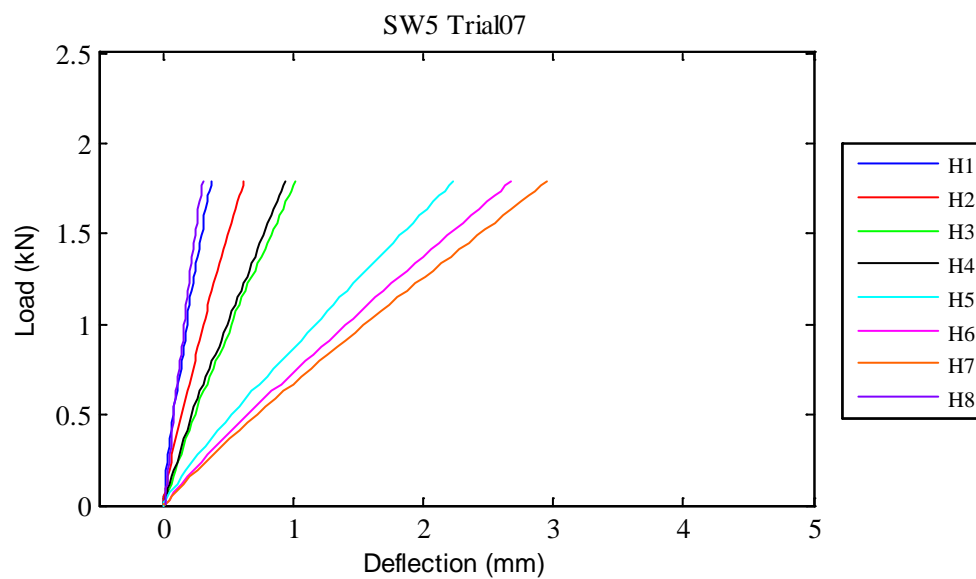
Fig. D.47: SW5 Trial07 load vs. deflection curves
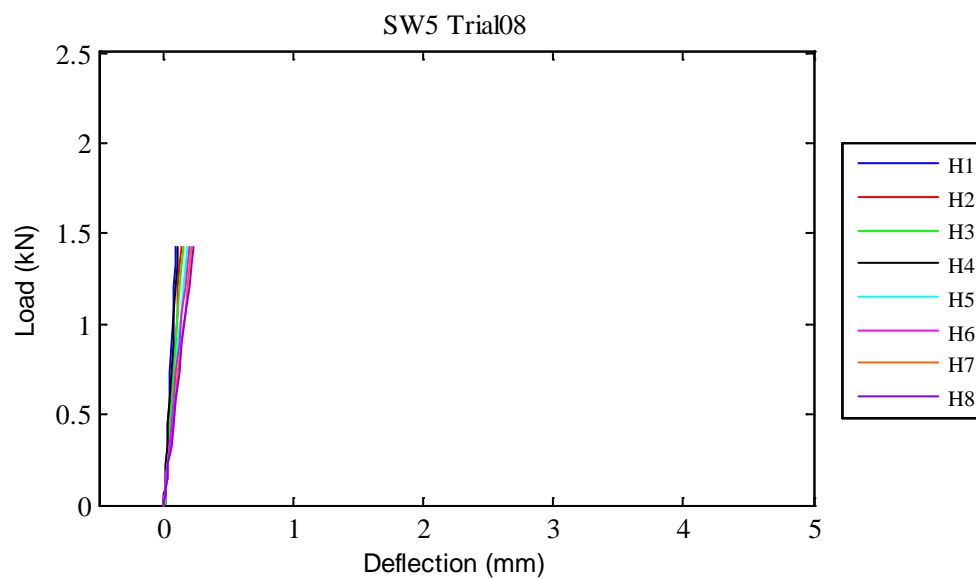
Fig. D.48: SW5 Trial08 load vs. deflection curves
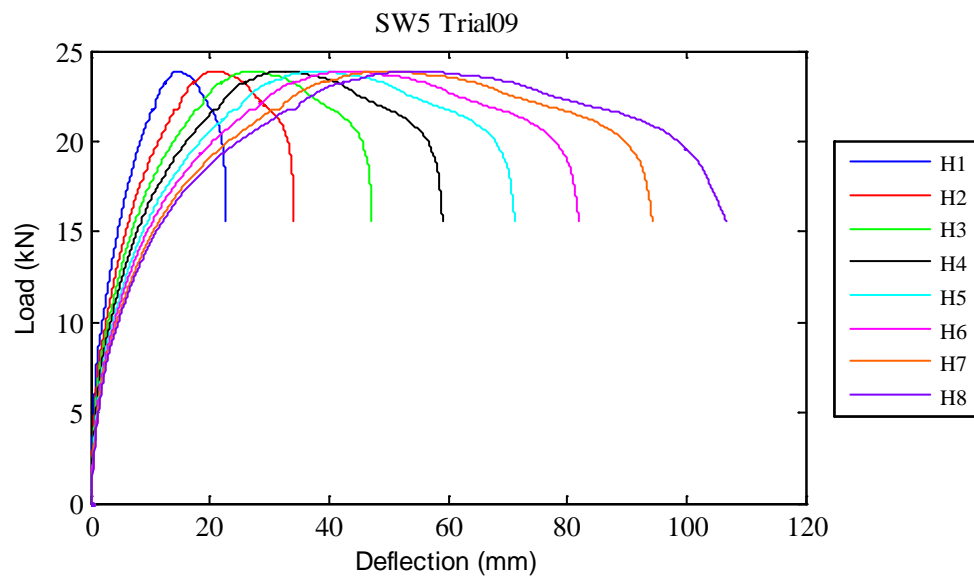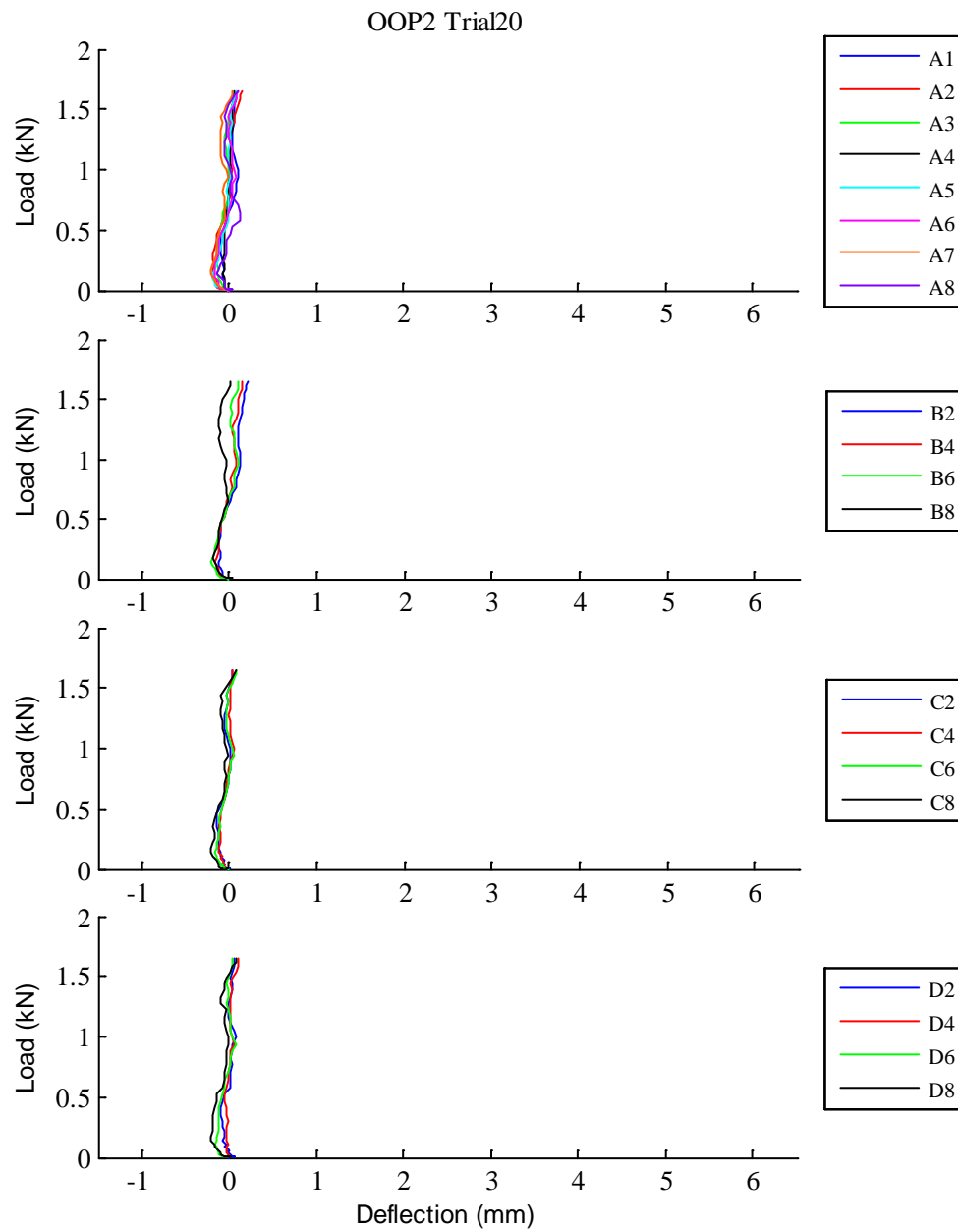
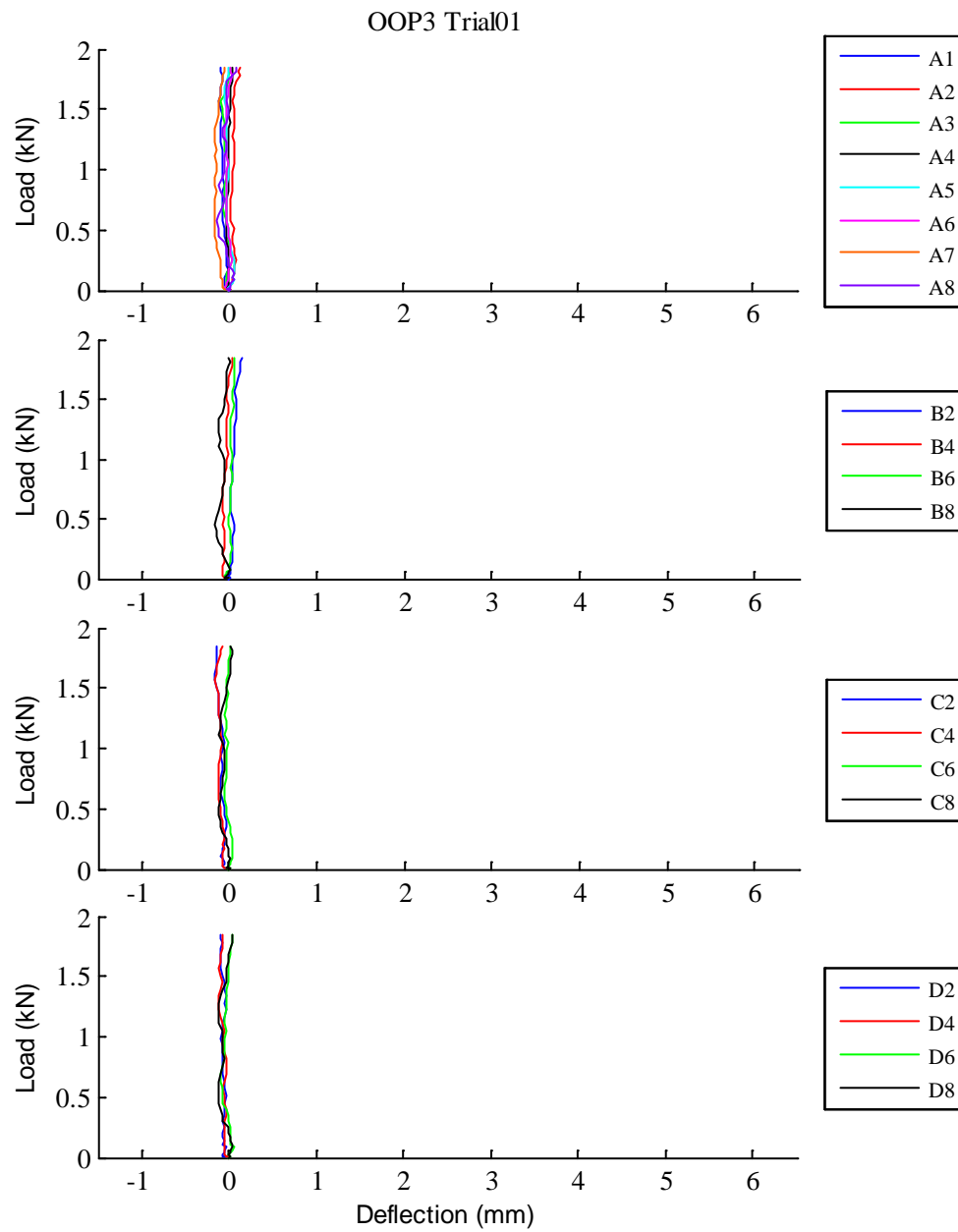Fig. D.49: SW5 Trial09 load vs. deflection curves
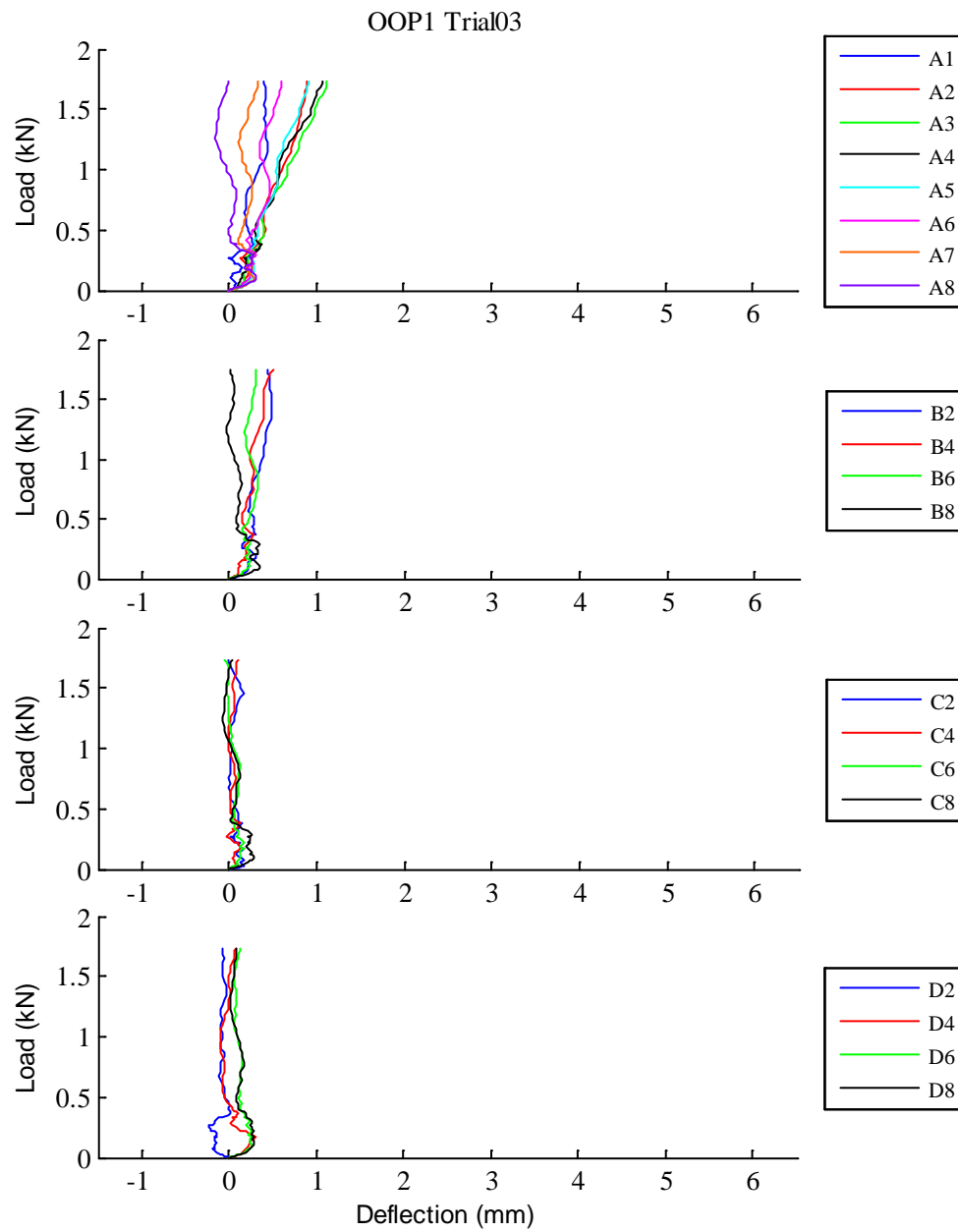
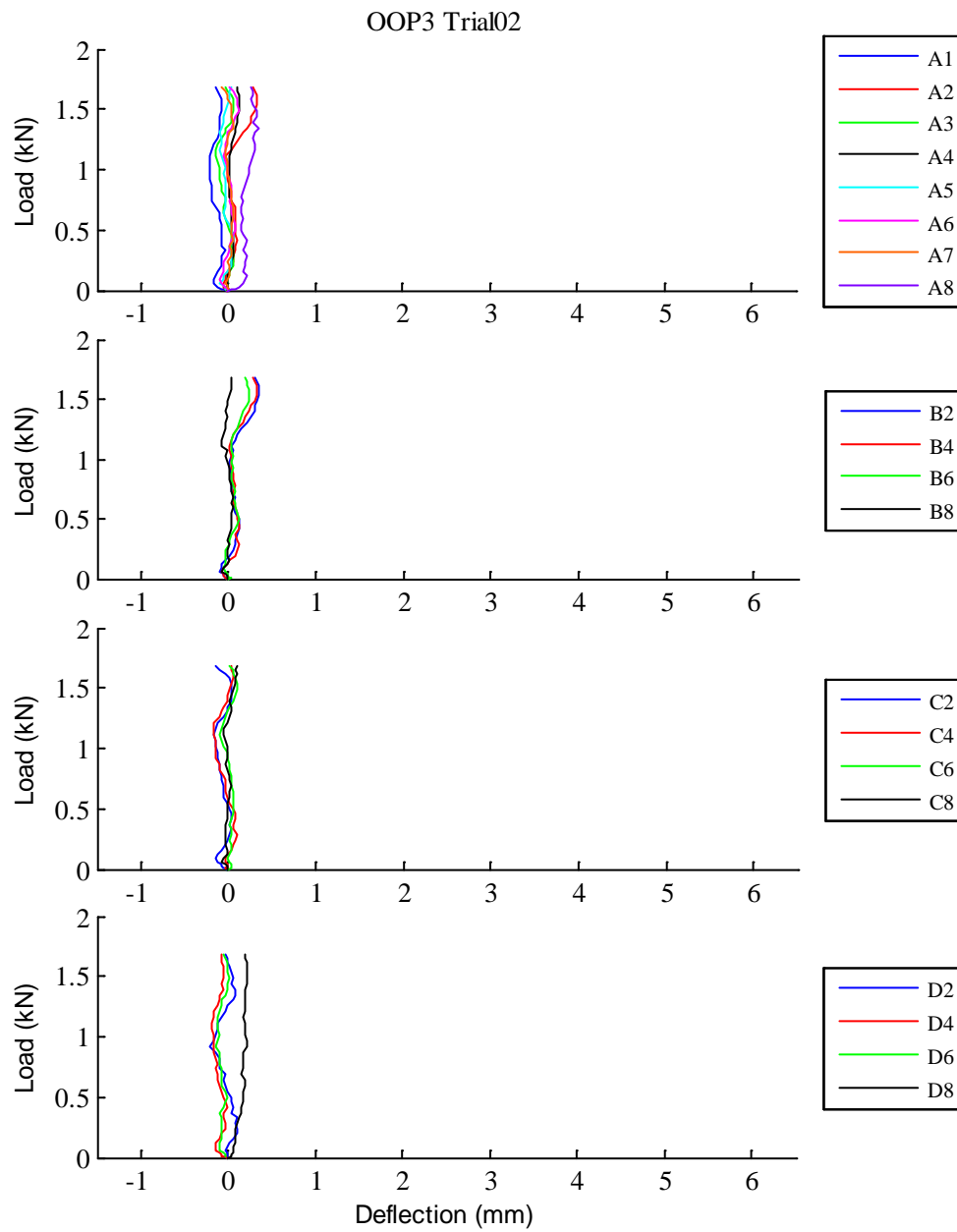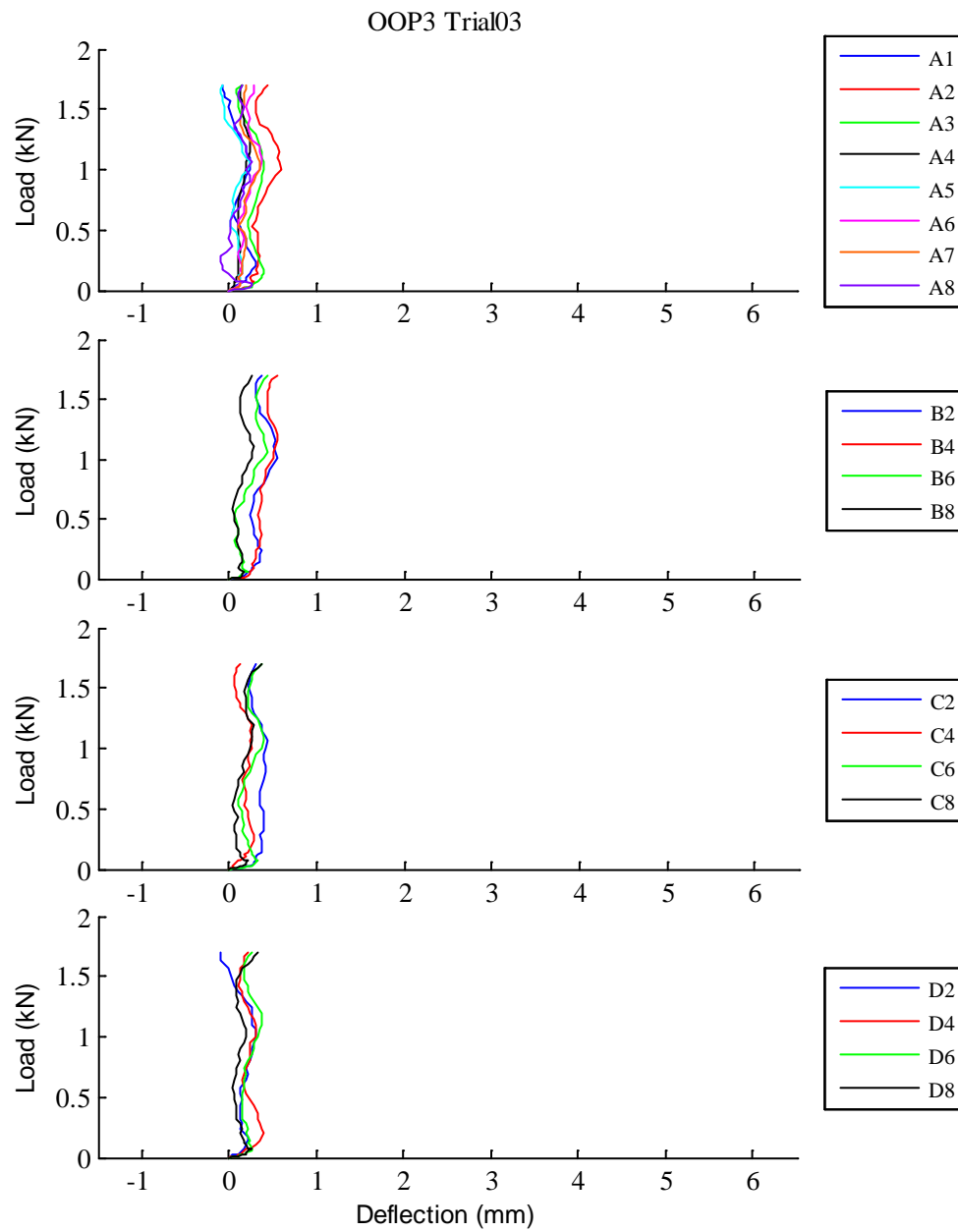Fig. D.50: OOP1 Trial03 load vs. deflection curves
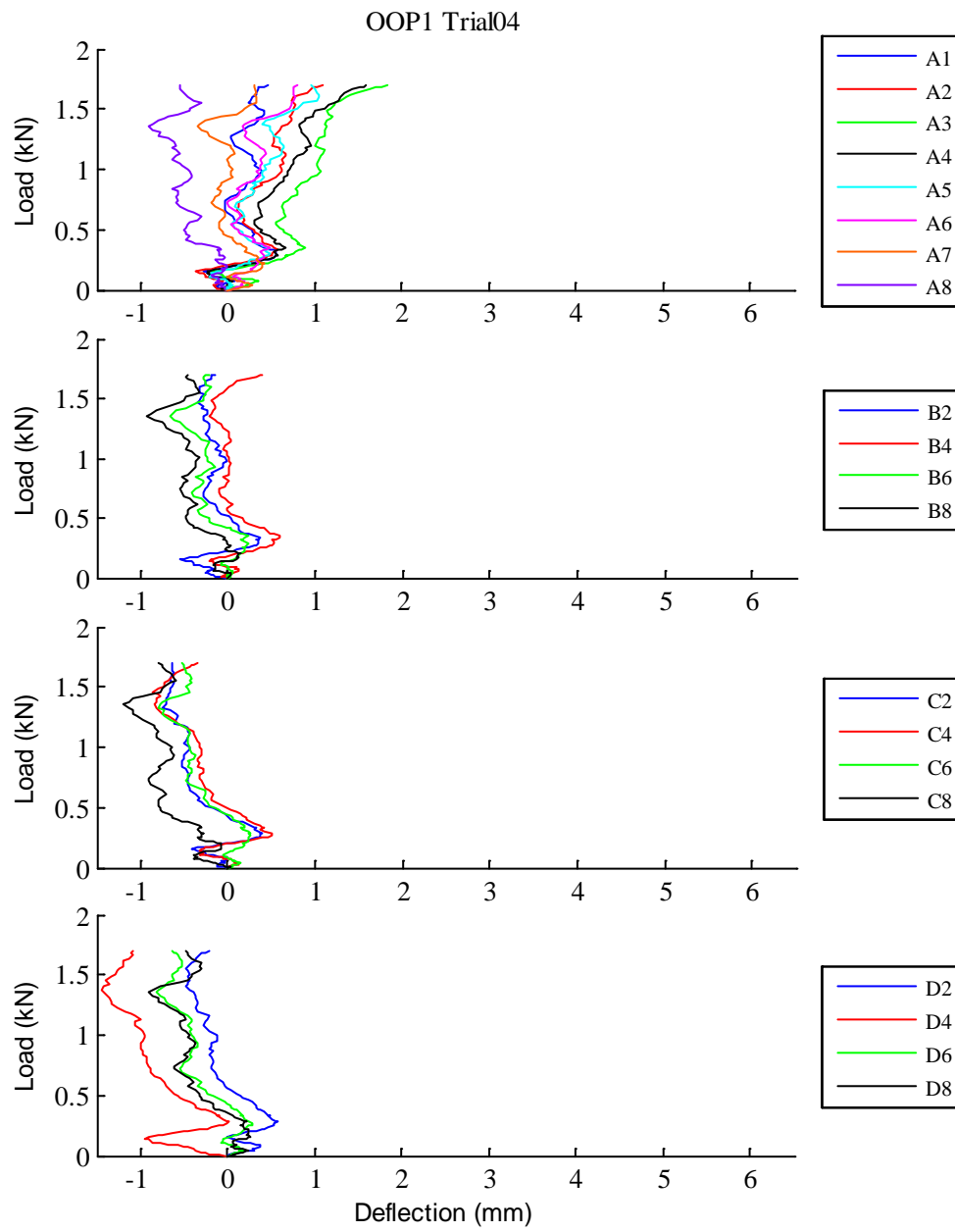
Fig. D.51: OOP1 Trial04 load vs. deflection curves
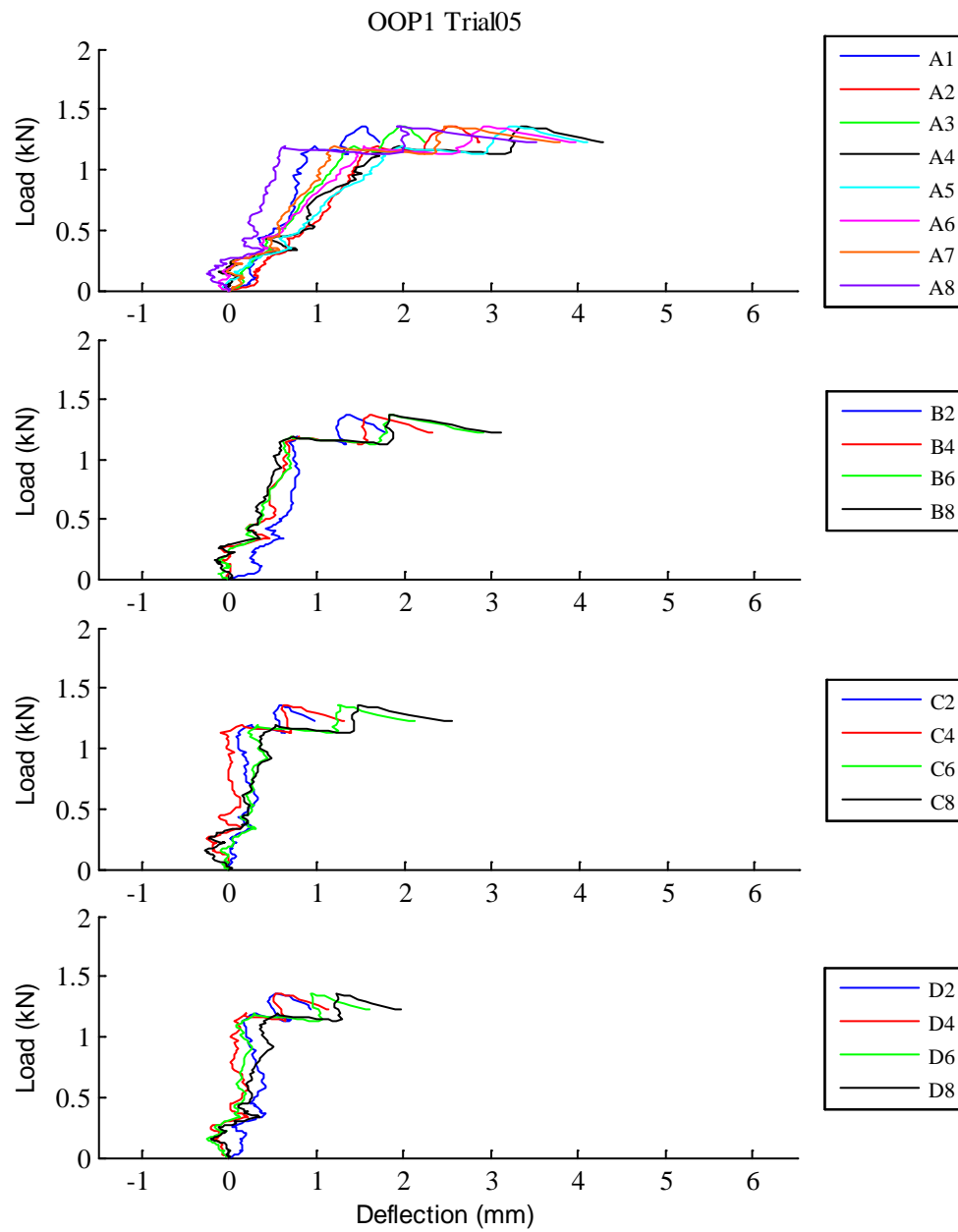
Fig. D.52: OOP1 Trial05 load vs. deflection curves
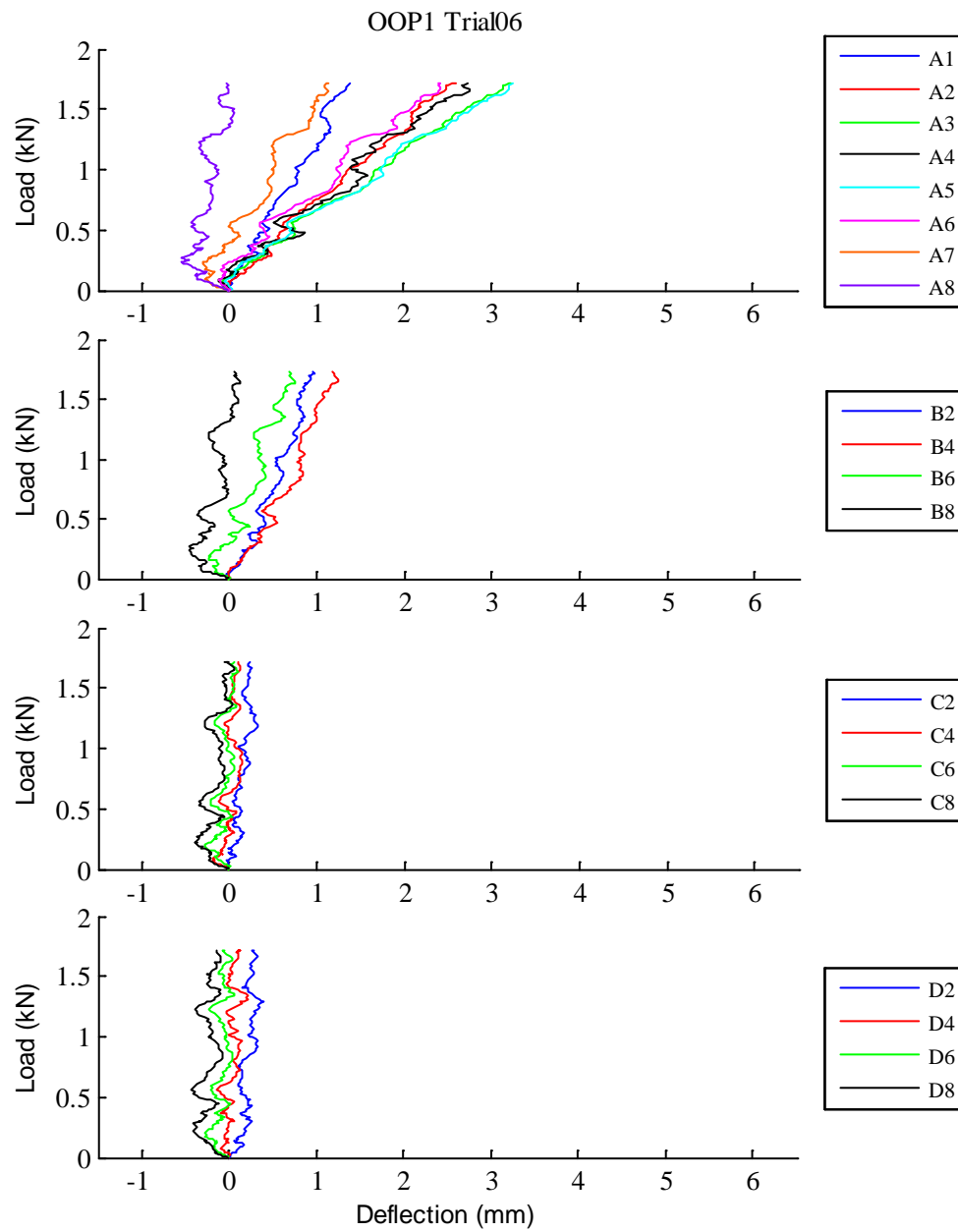
Fig. D.53: OOP1 Trial06 load vs. deflection curves
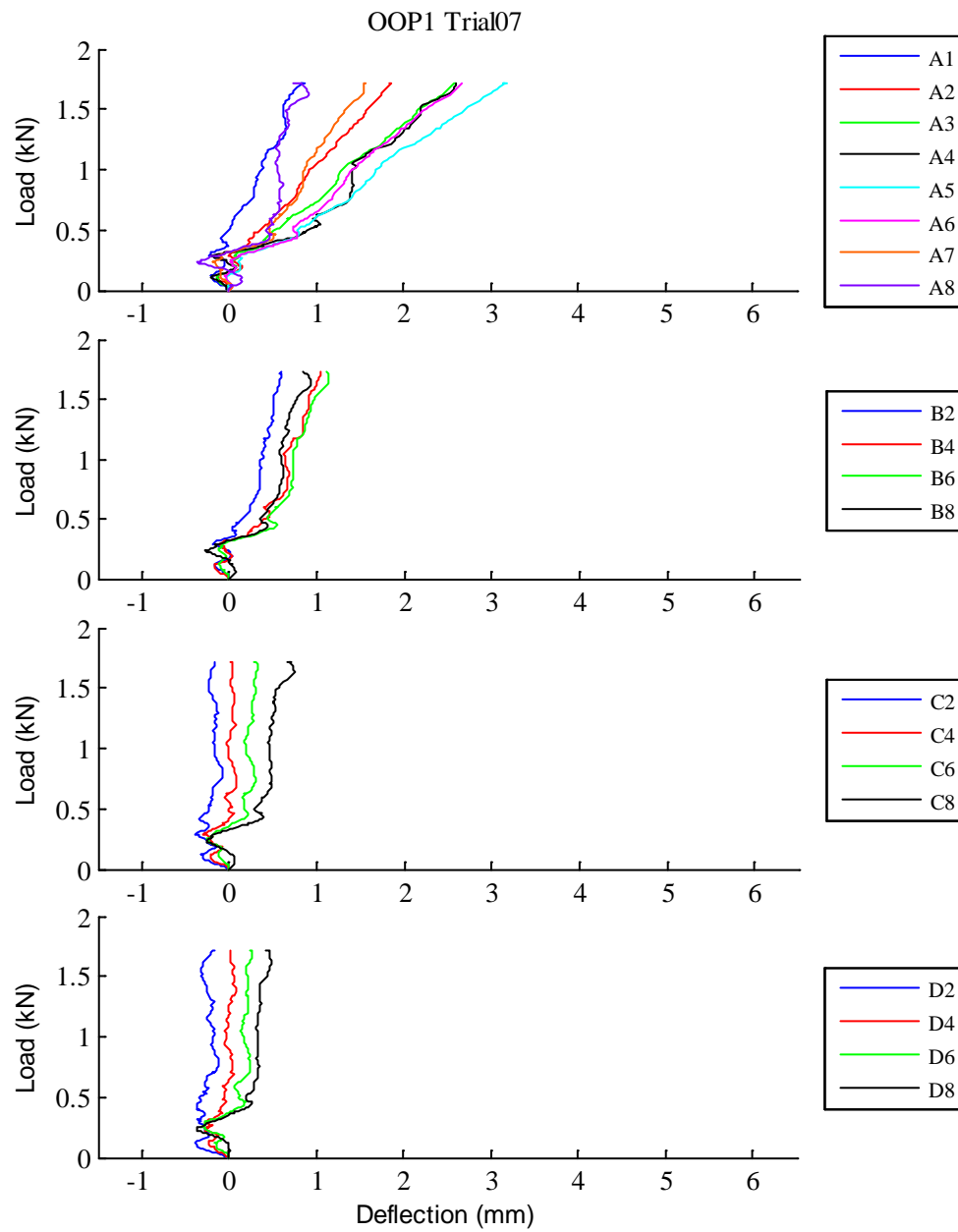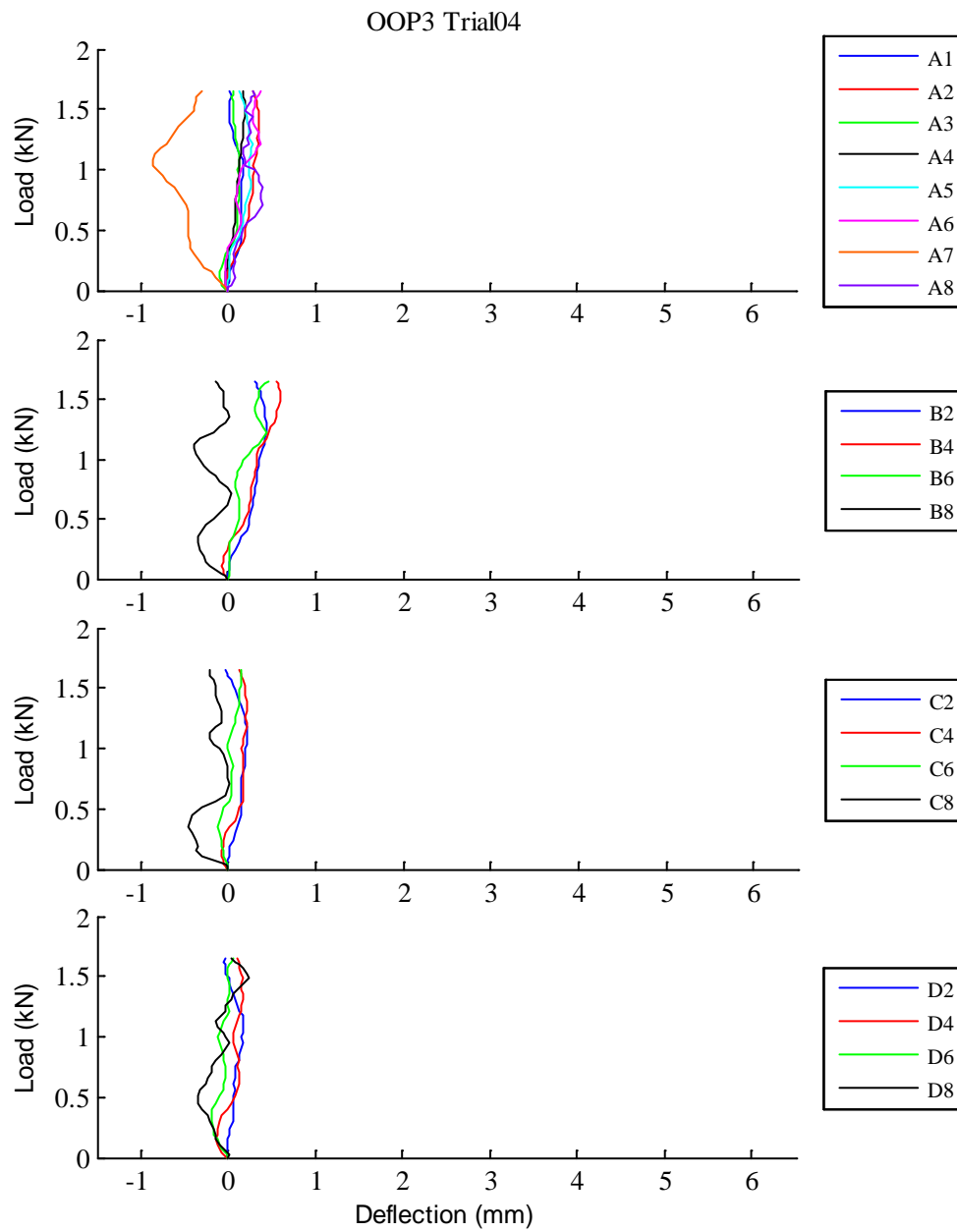
Fig. D.54: OOP1 Trial07 load vs. deflection curves
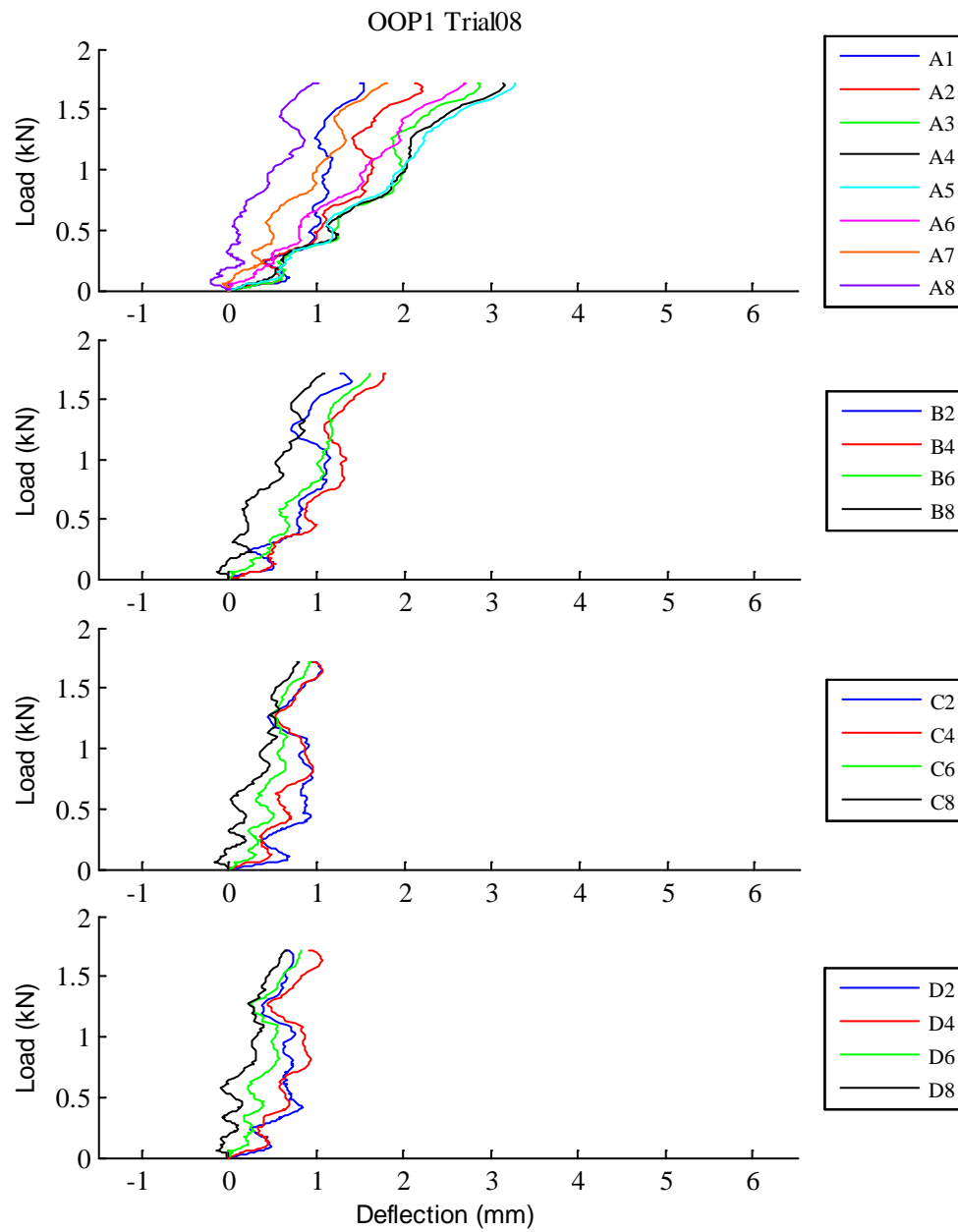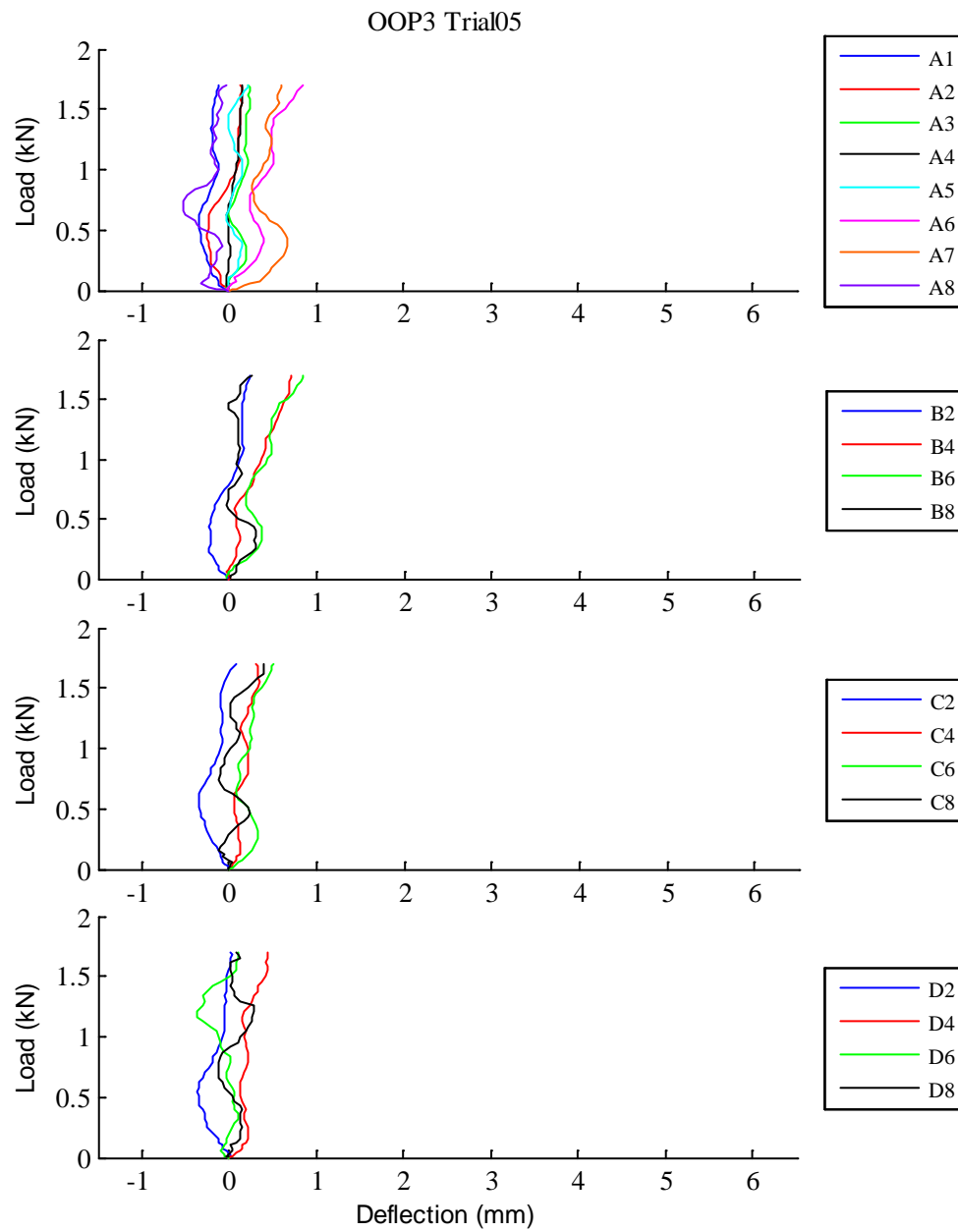
Fig. D.55: OOP1 Trial08 load vs. deflection curves
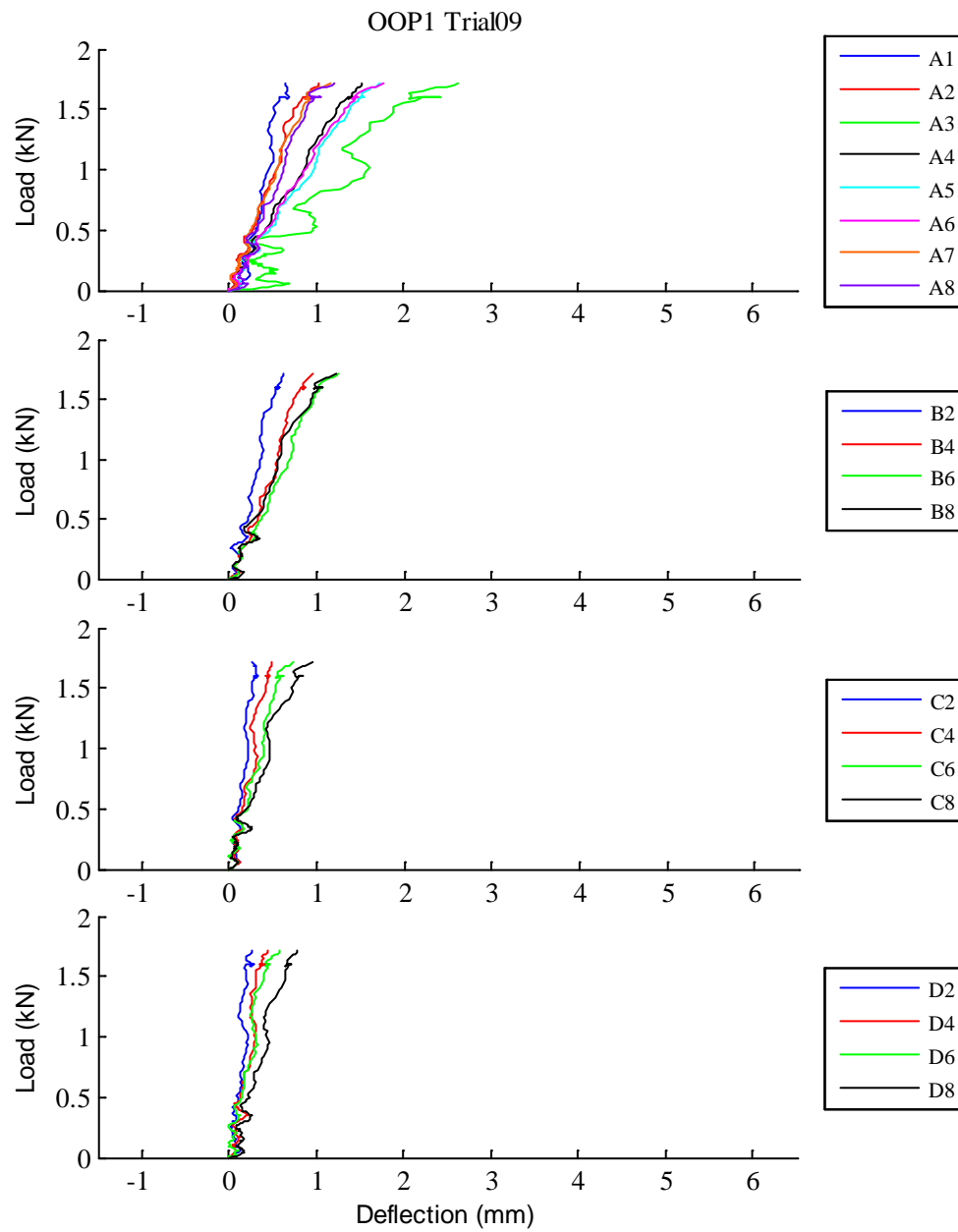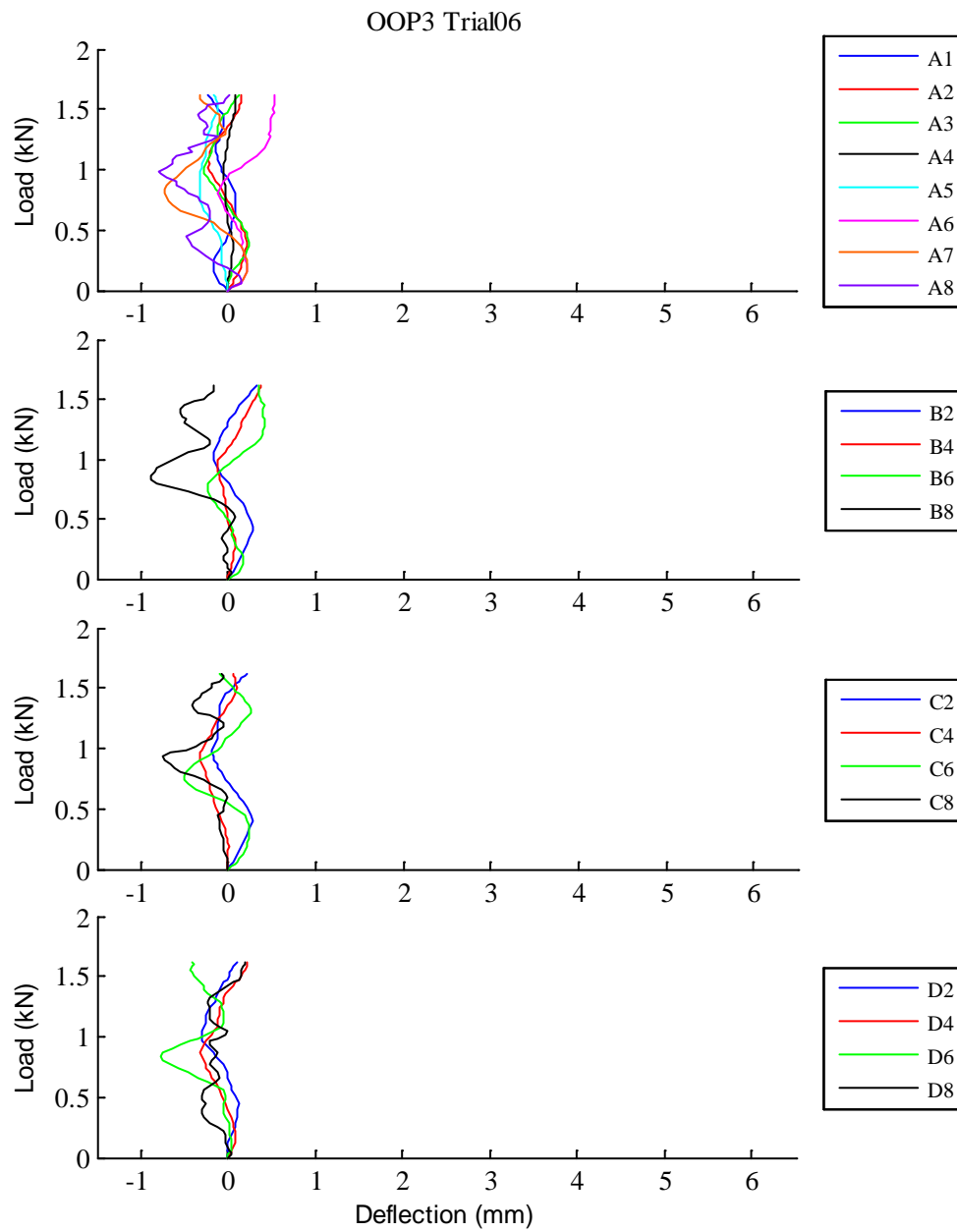
Fig. D.56: OOP1 Trial09 load vs. deflection curves
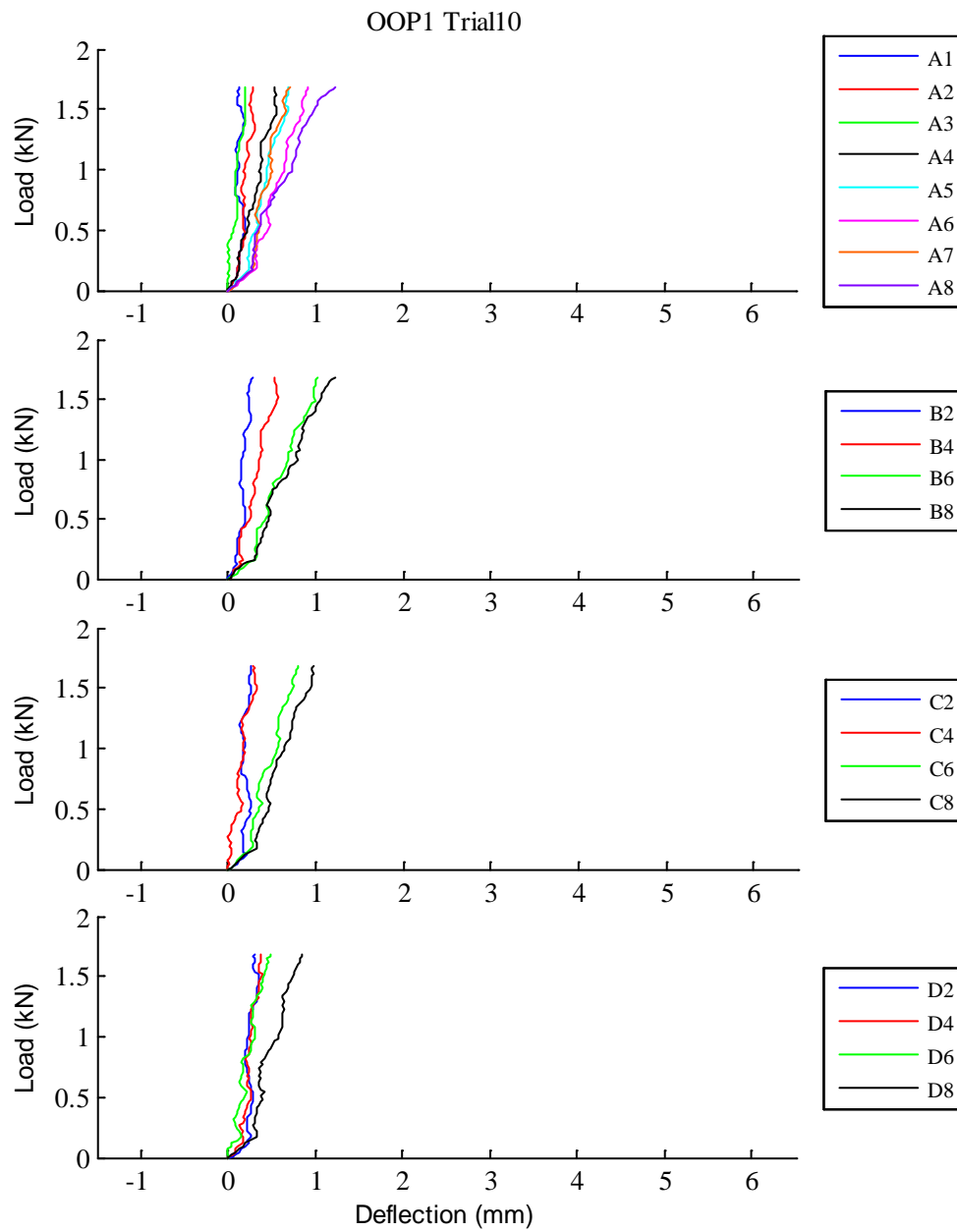
Fig. D.57: OOP1 Trial10 load vs. deflection curves
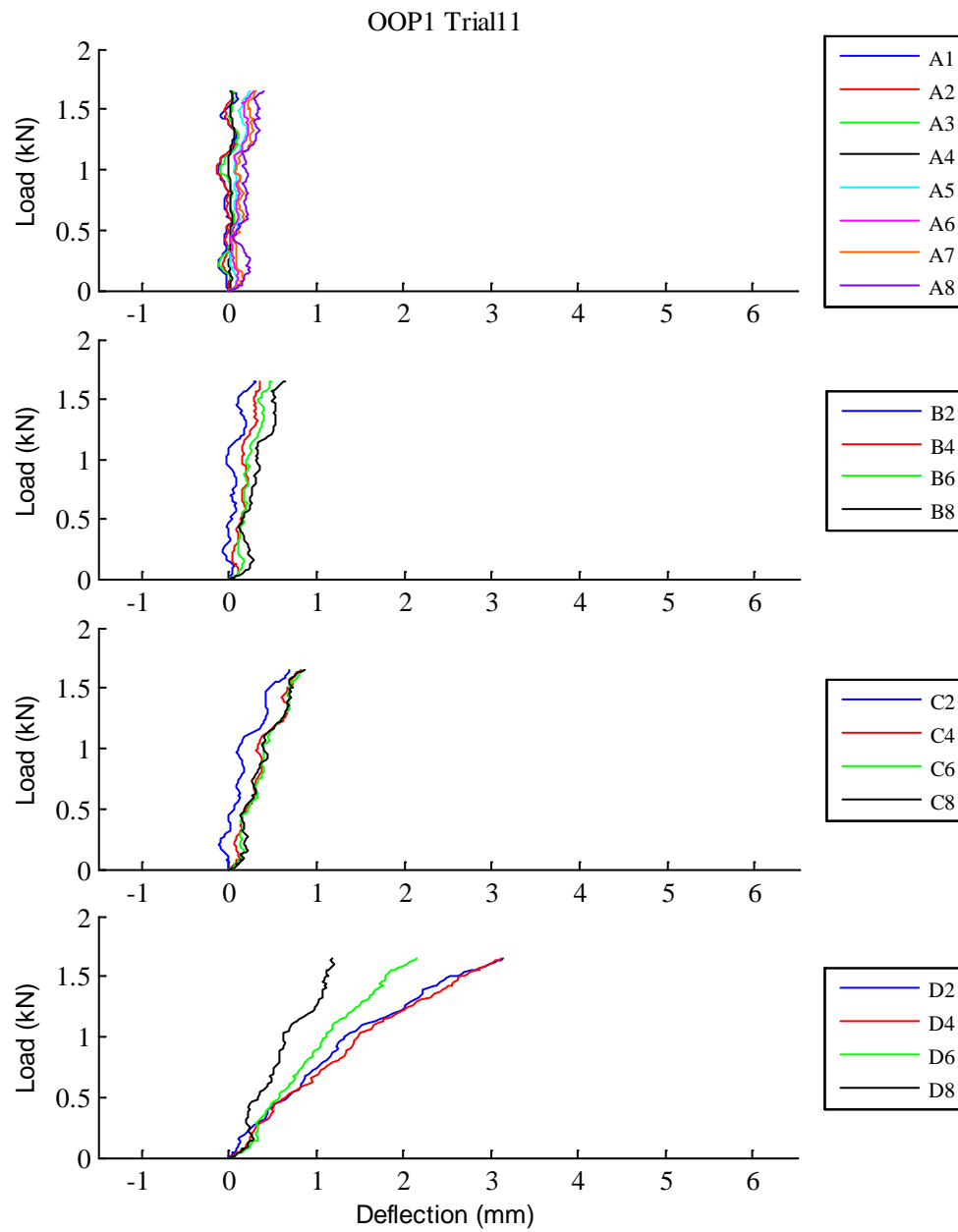
Fig. D.58: OOP1 Trial11 load vs. deflection curves
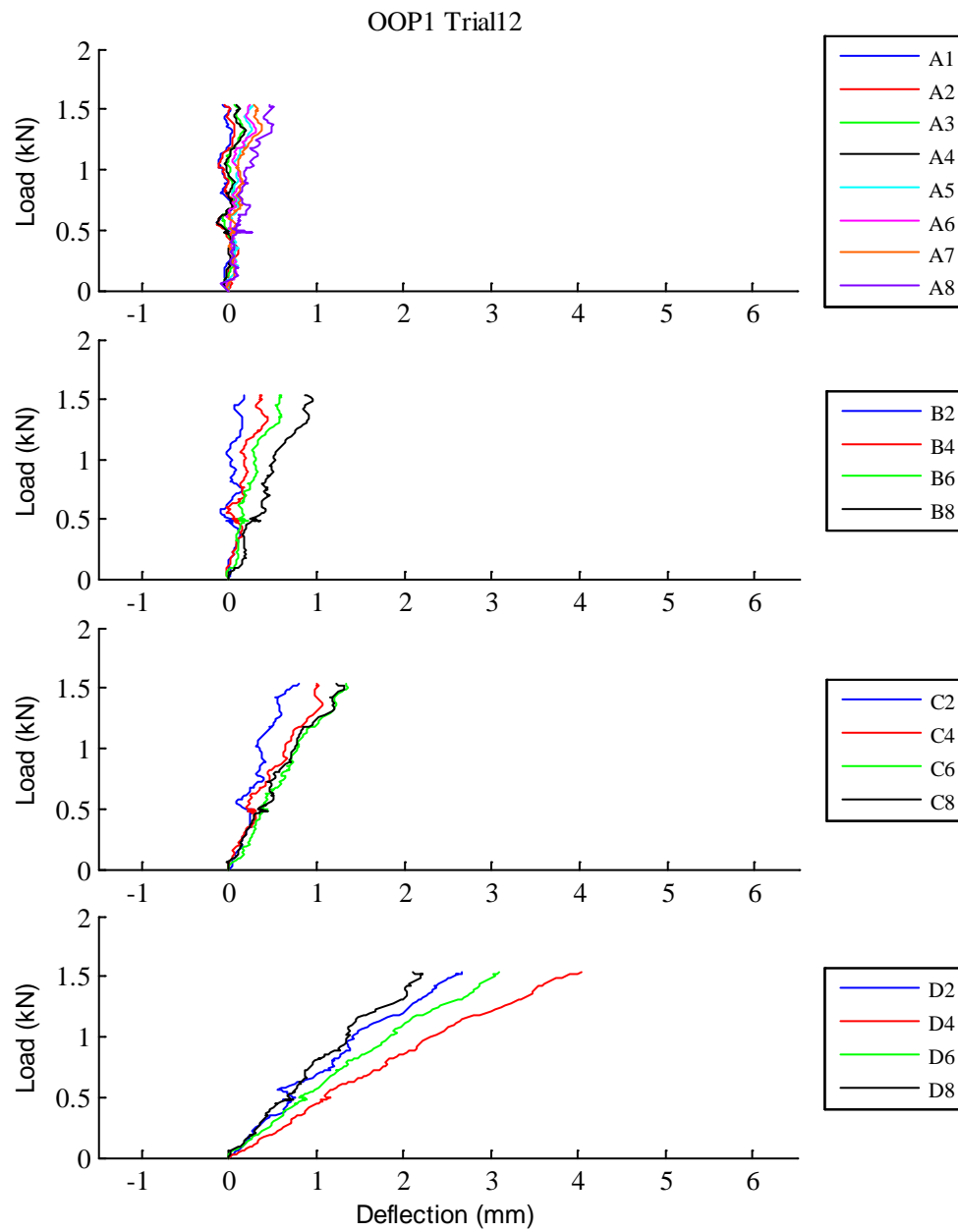
Fig. D.59: OOP1 Trial12 load vs. deflection curves
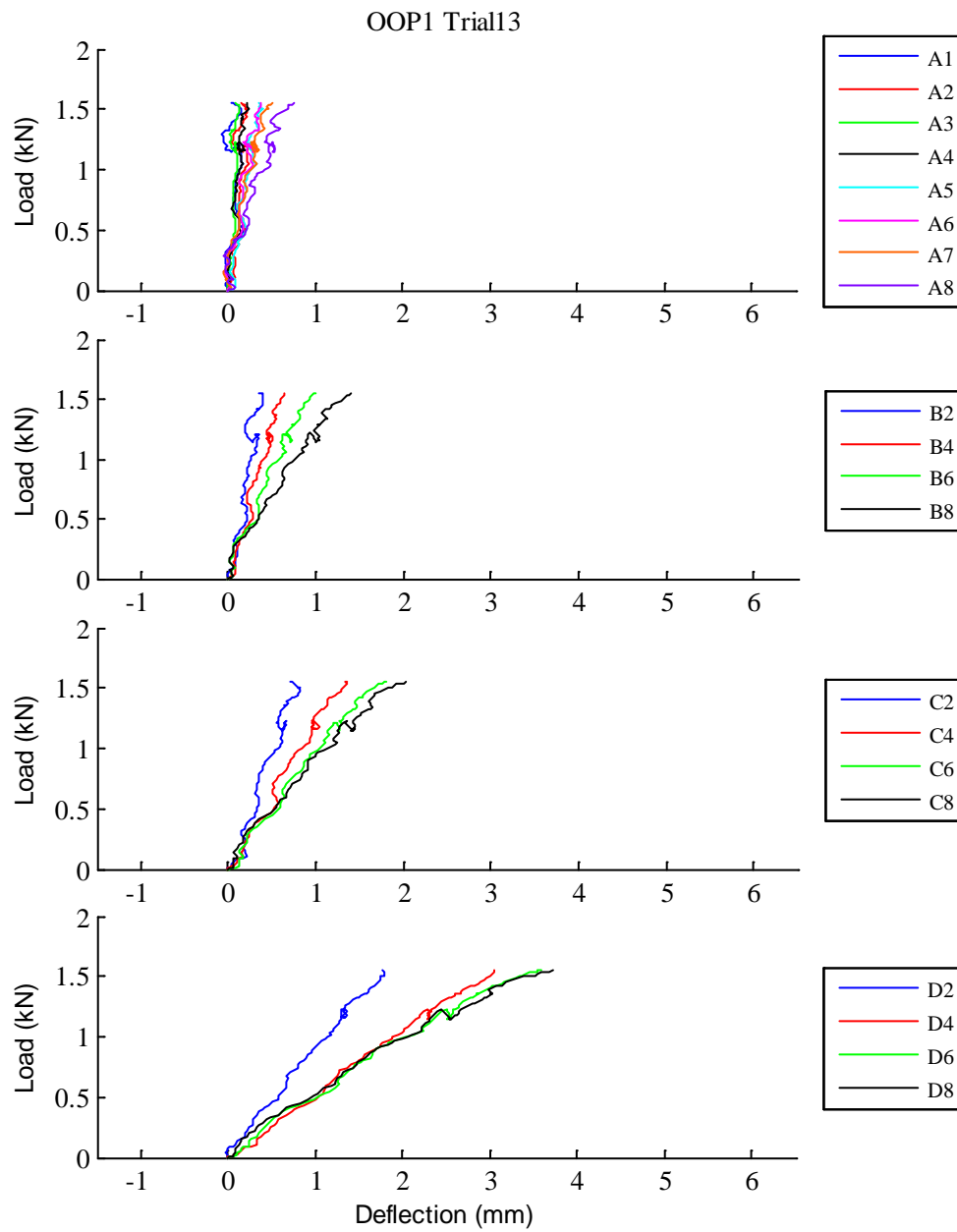
Fig. D.60: OOP1 Trial13 load vs. deflection curves
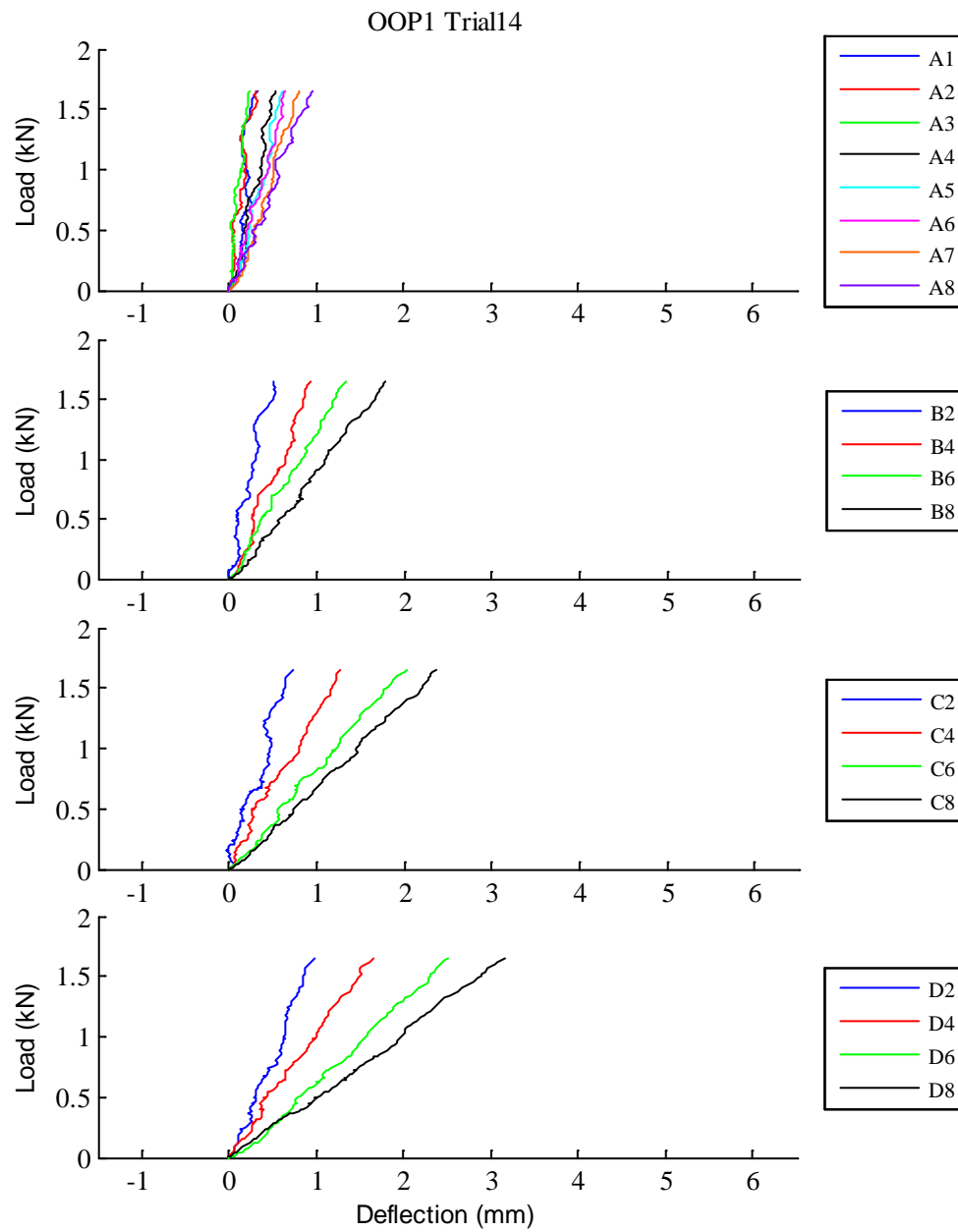
Fig. D.61: OOP1 Trial14 load vs. deflection curves
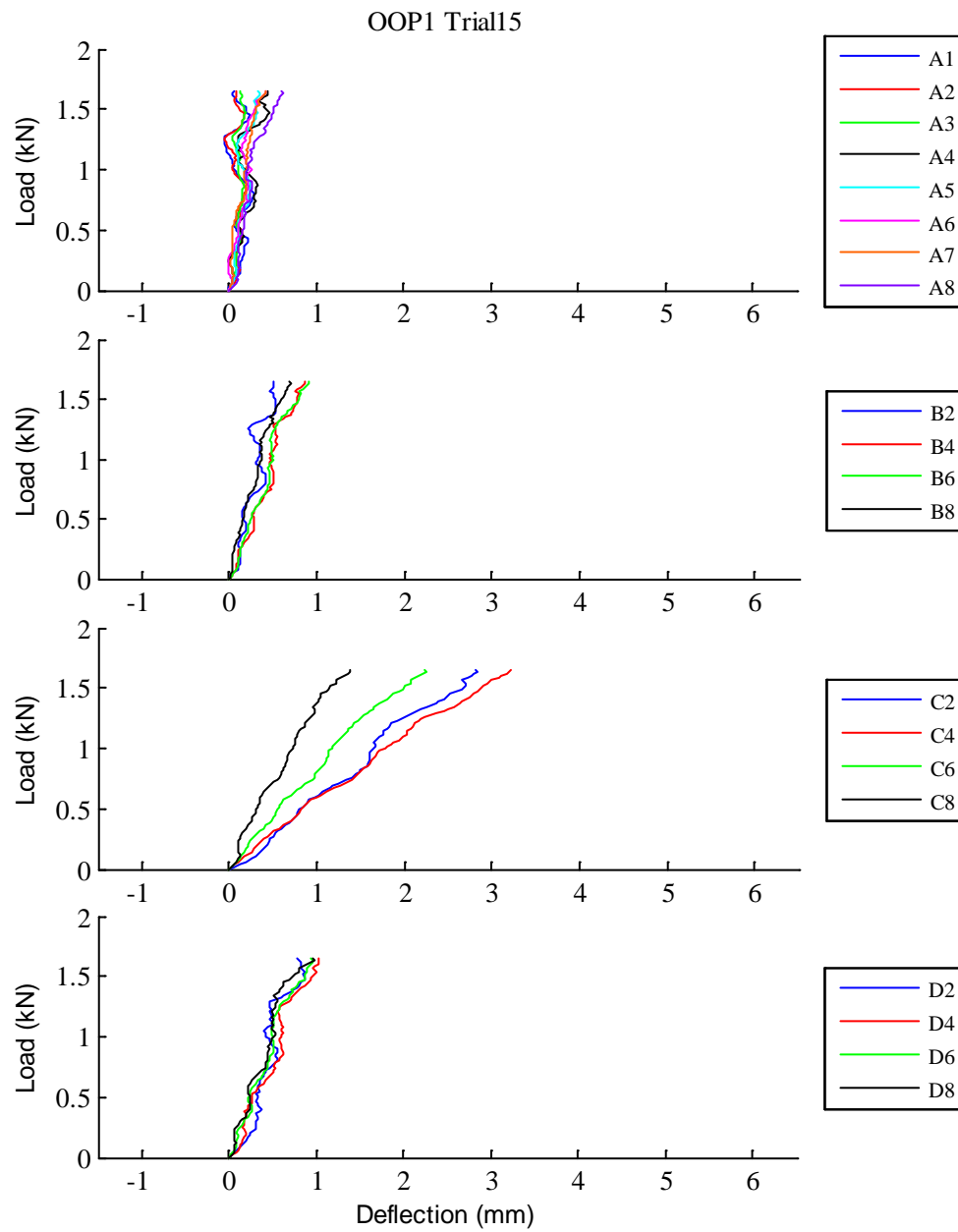
Fig. D.62: OOP1 Trial15 load vs. deflection curves
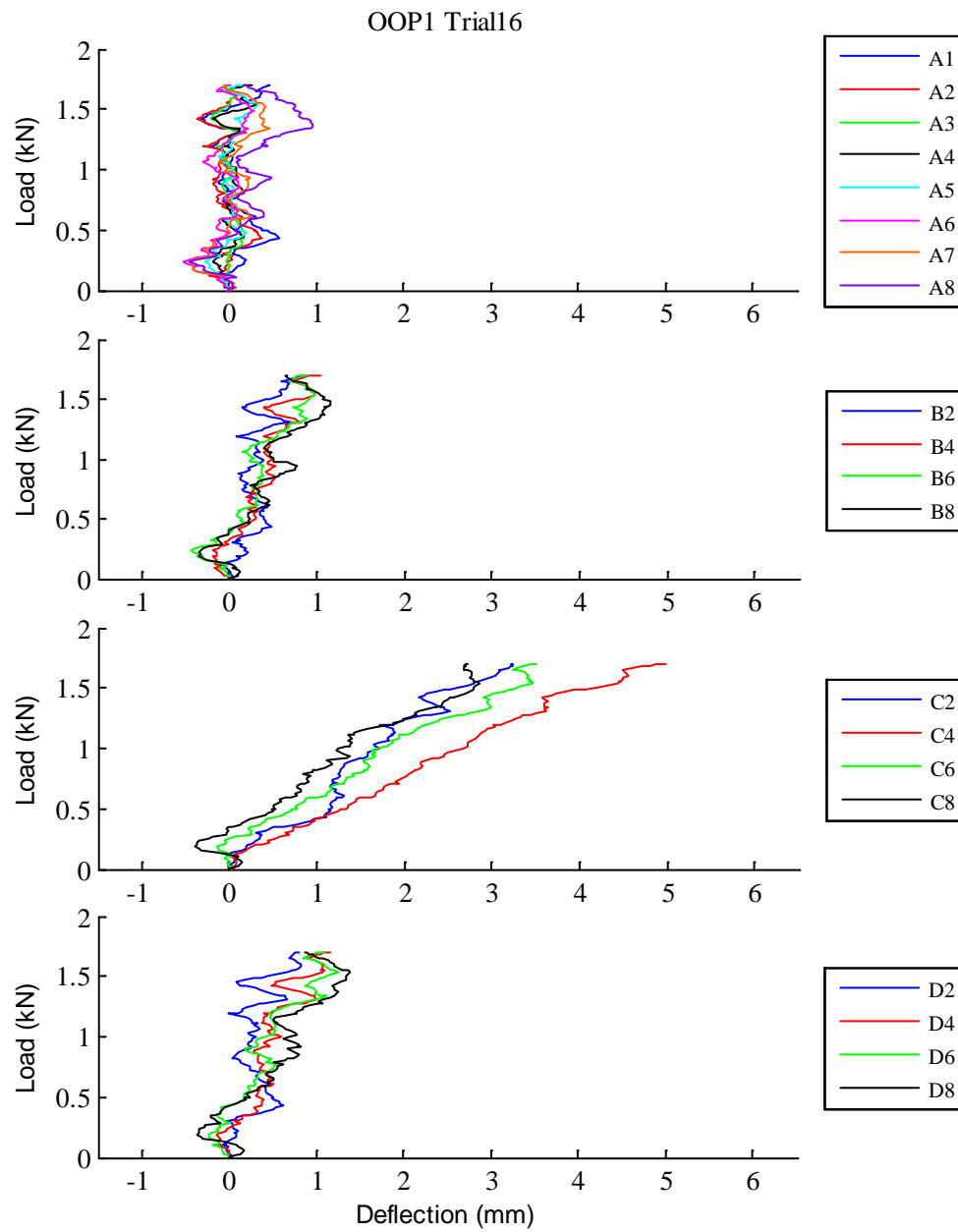
Fig. D.63: OOP1 Trial16 load vs. deflection curves
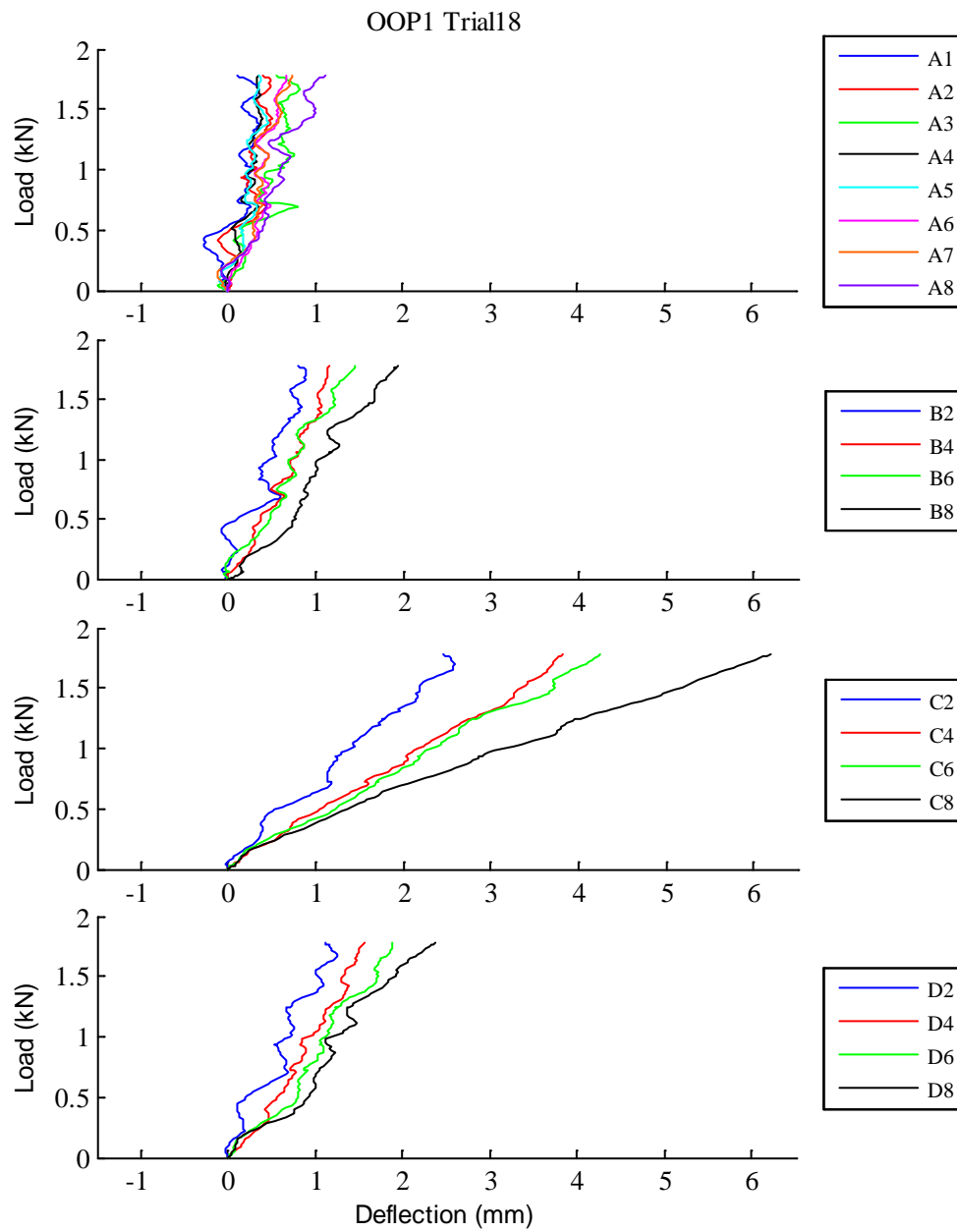
Fig. D.64: OOP1 Trial18 load vs. deflection curves
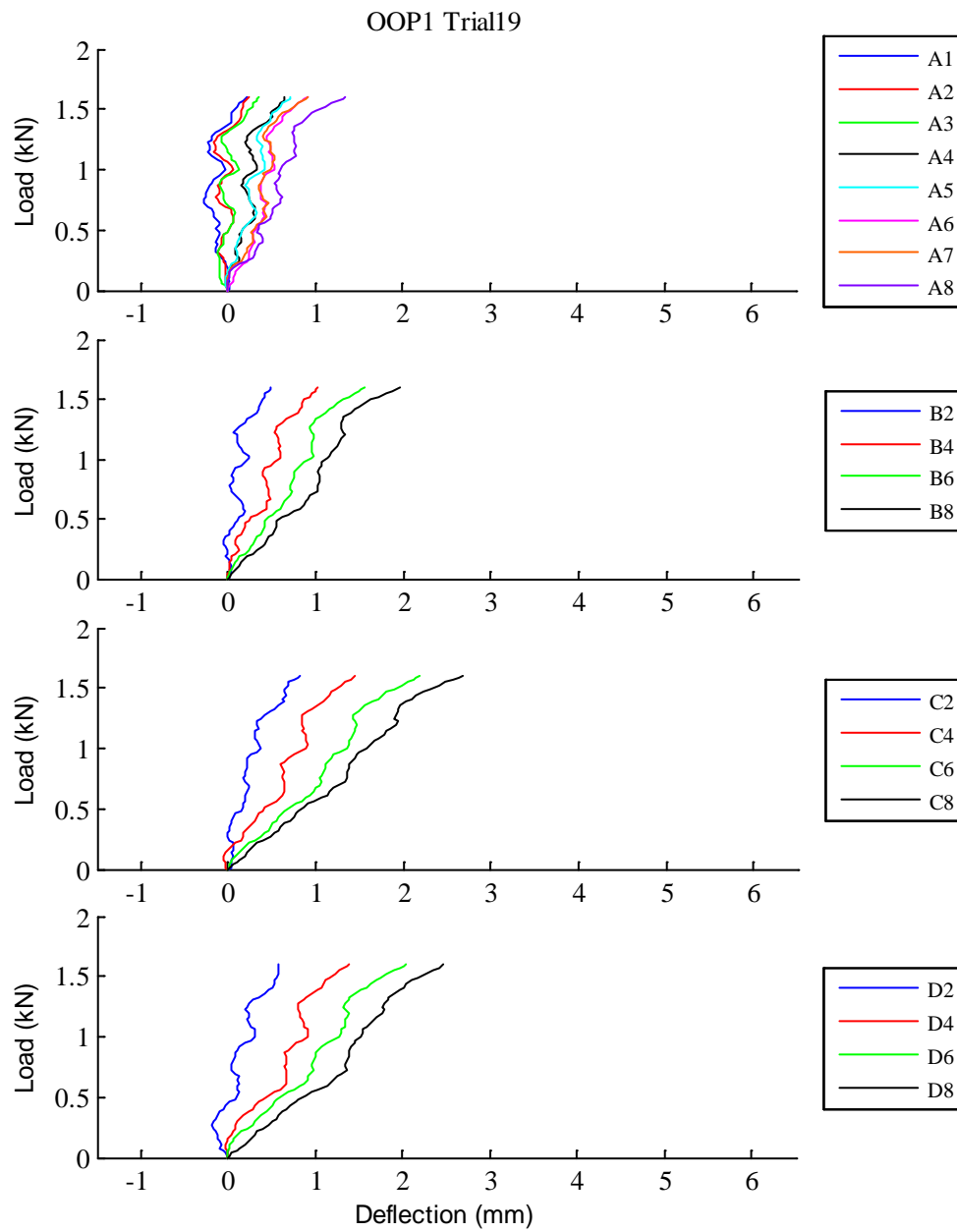
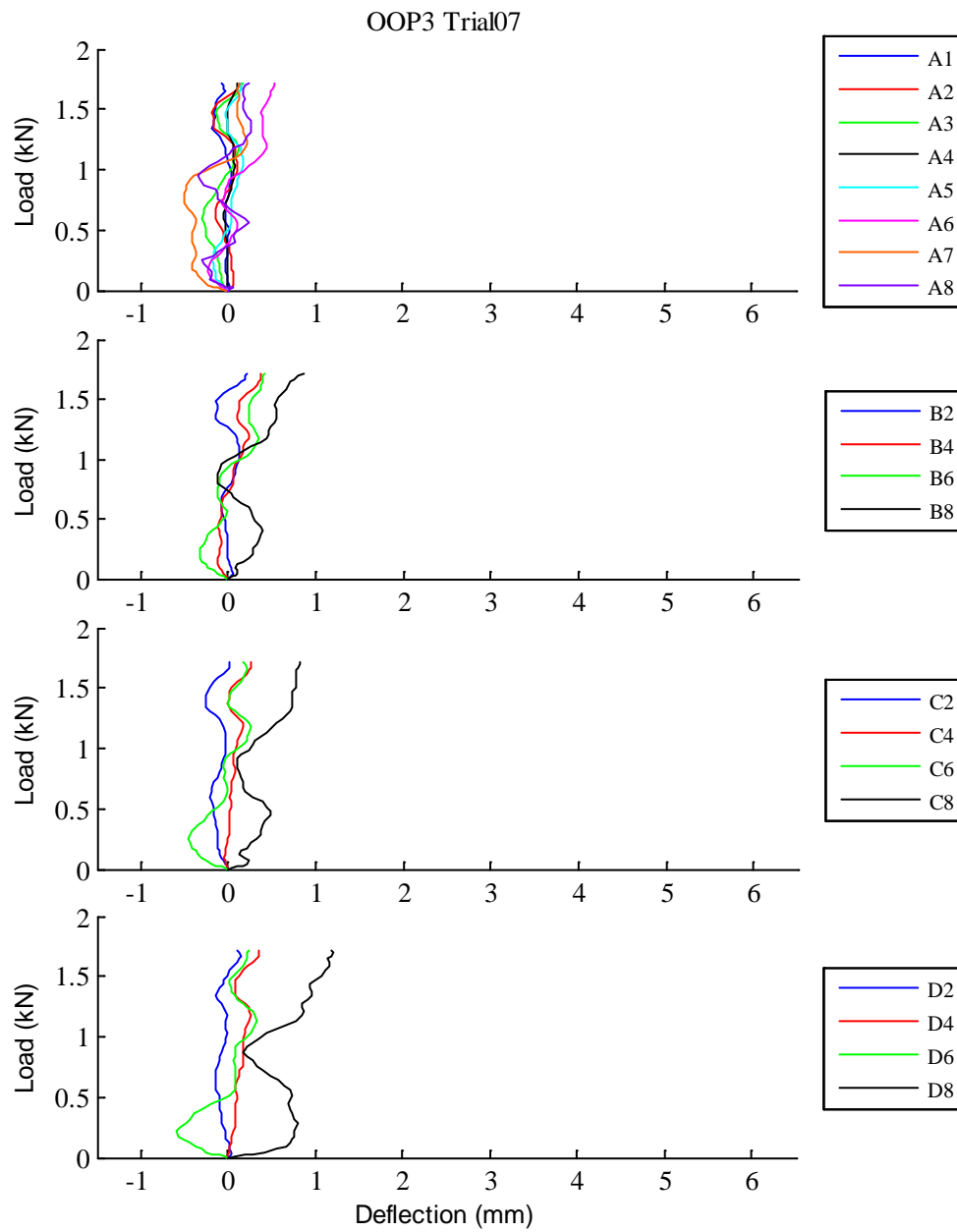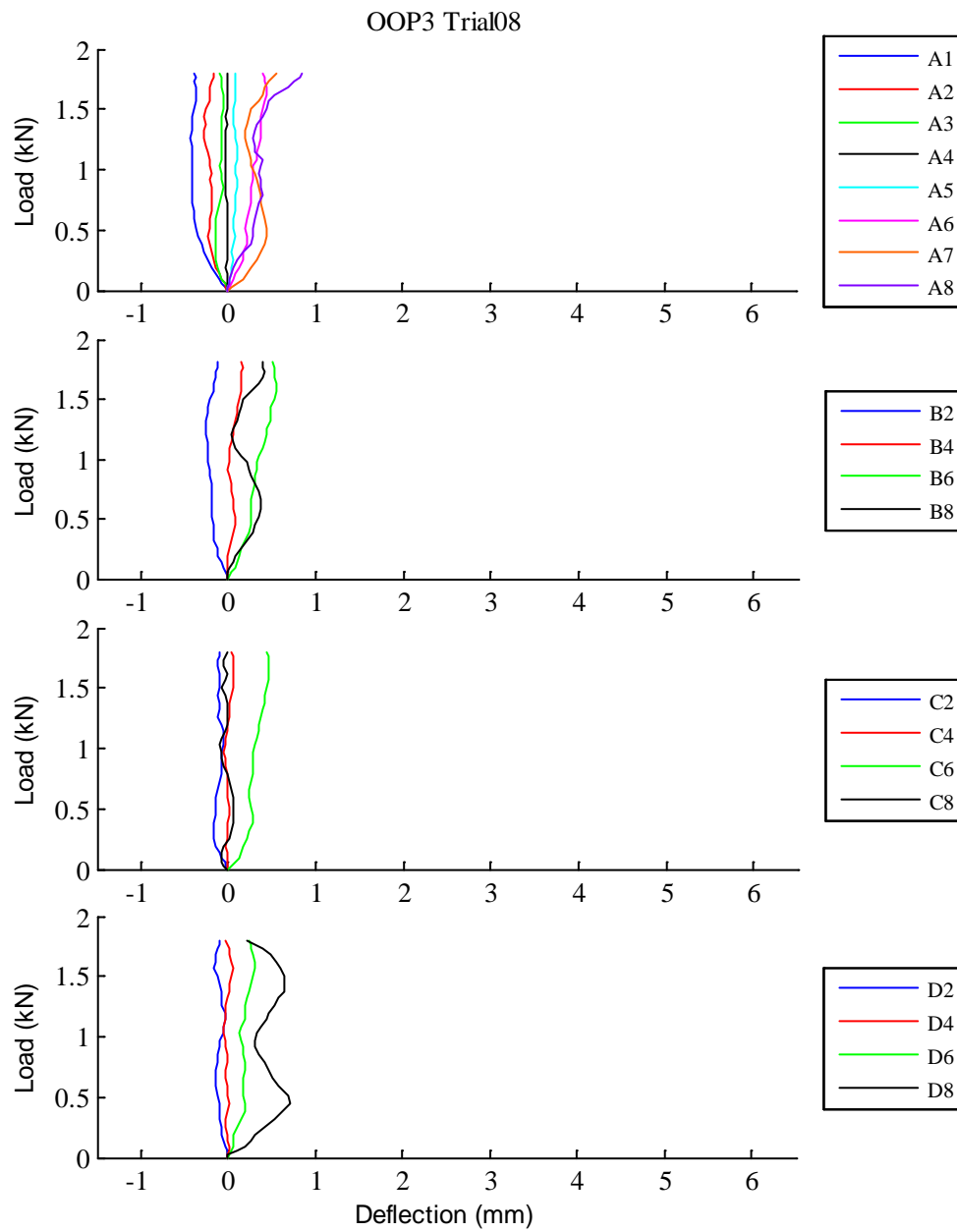Fig. D.65: OOP1 Trial19 load vs. deflection curves
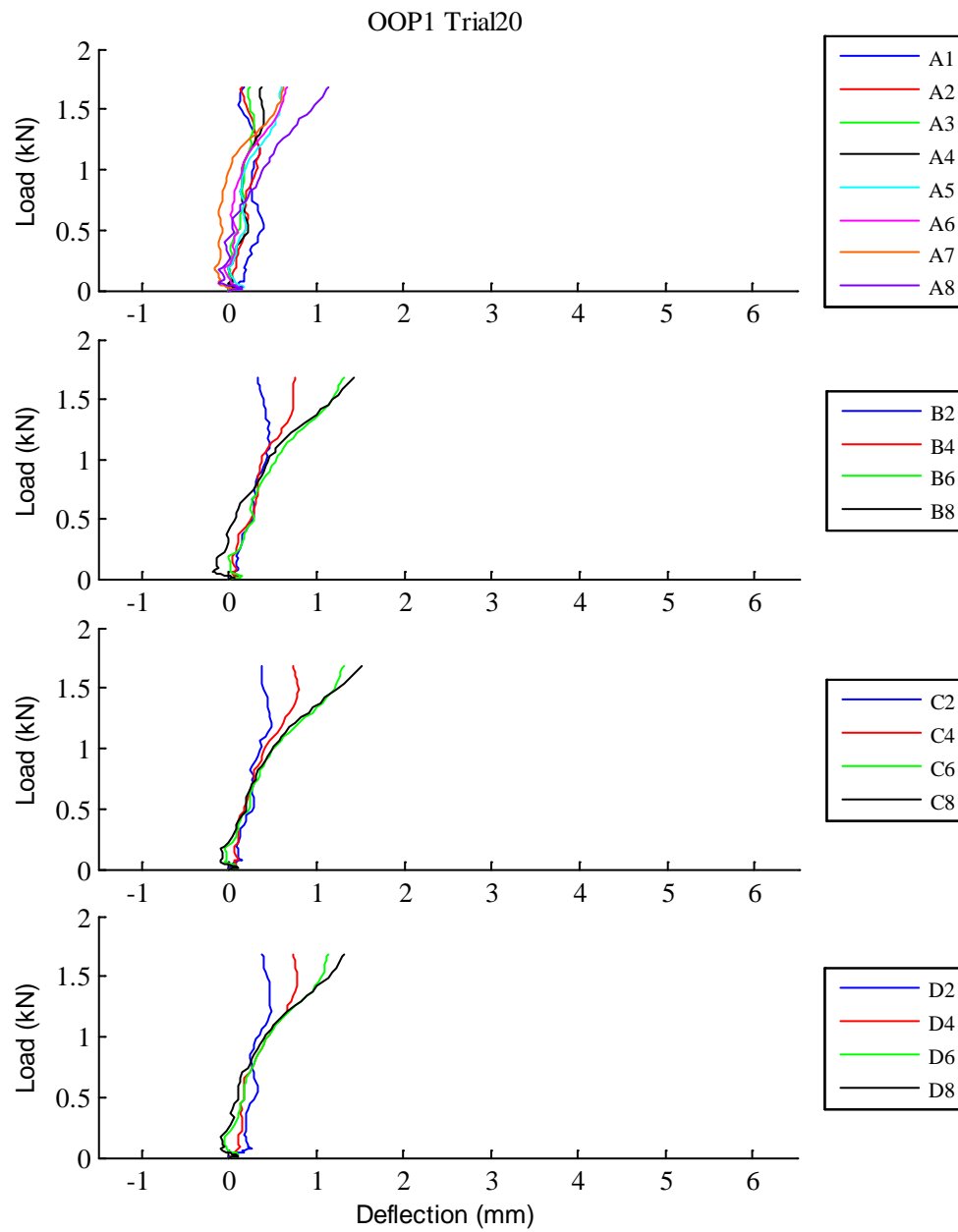
Fig. D.66: OOP1 Trial20 load vs. deflection curves

Fig. D.67: OOP1 Trial21 load vs. deflection curves

Fig. D.68: OOP1 Trial22 load vs. deflection curves

Fig. D.69: OOP1 Trial23 load vs. deflection curves

Fig. D.70: OOP2 Trial01 load vs. deflection curves

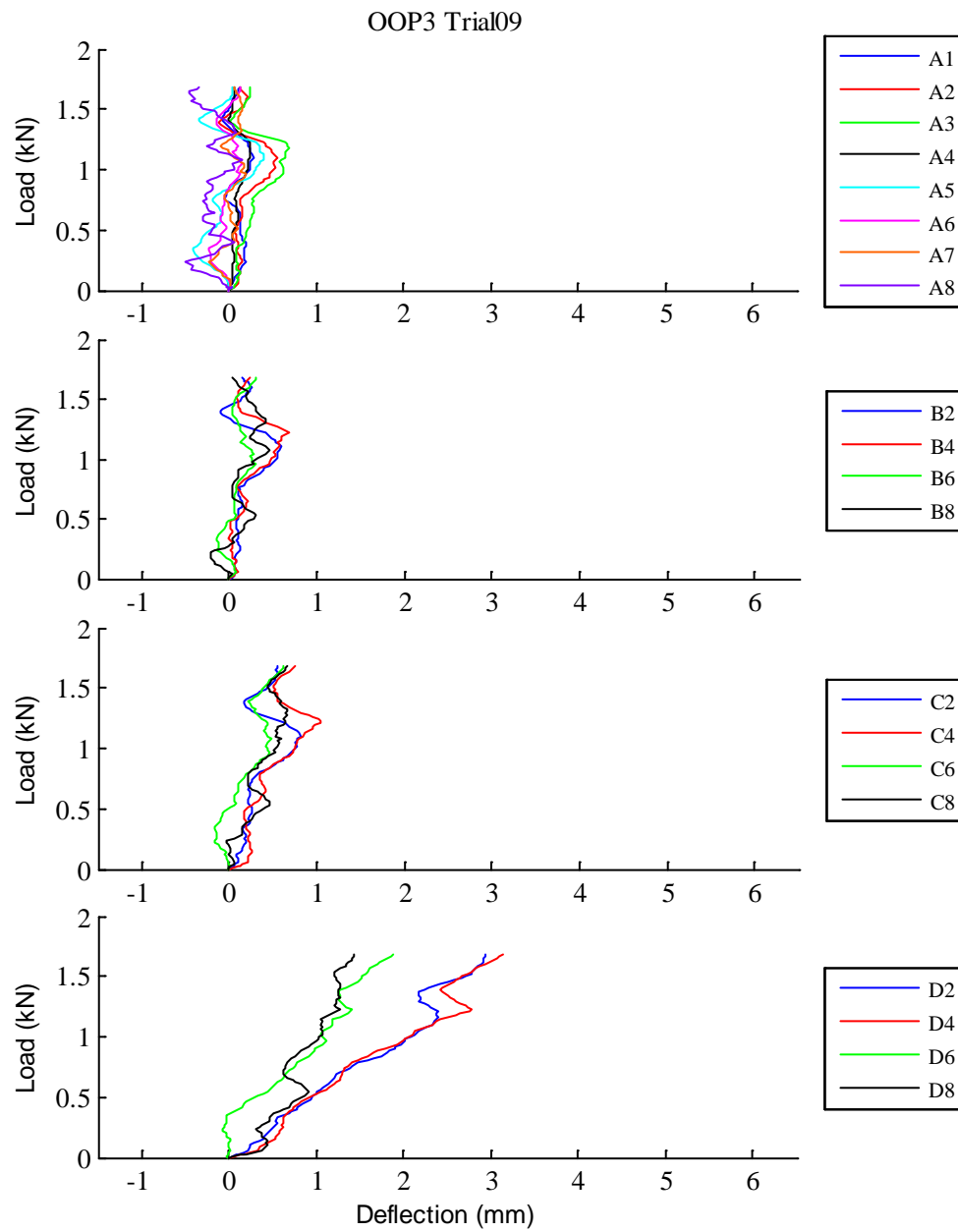Fig. D.71: OOP2 Trial02 load vs. deflection curves
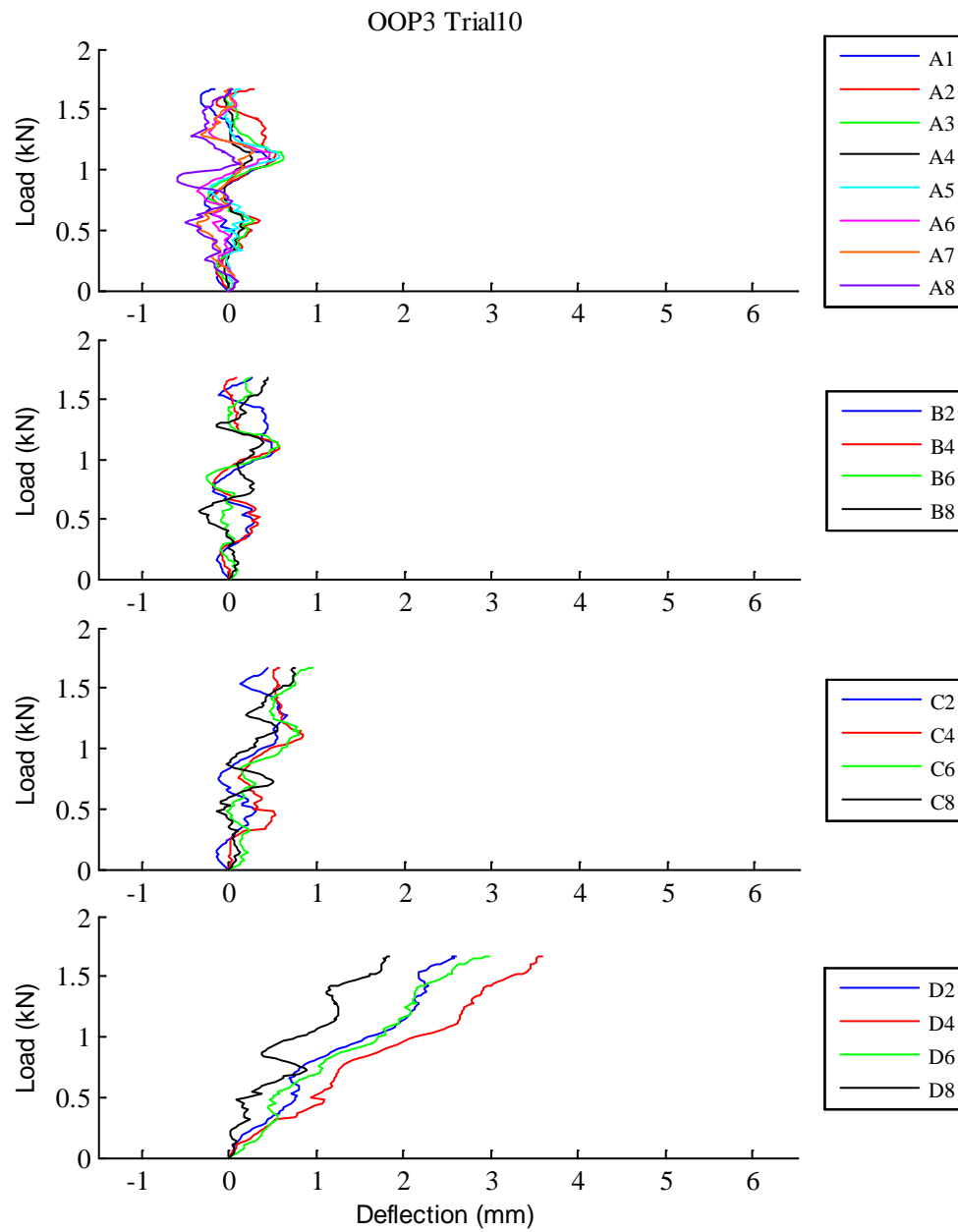
Fig. D.72: OOP2 Trial03 load vs. deflection curves

Fig. D.73: OOP2 Trial04 load vs. deflection curves

Fig. D.74: OOP2 Trial05 load vs. deflection curves

Fig. D.75: OOP2 Trial06 load vs. deflection curves

Fig. D.76: OOP2 Trial07 load vs. deflection curves

Fig. D.77: OOP2 Trial08 load vs. deflection curves

Fig. D.78: OOP2 Trial09 load vs. deflection curves

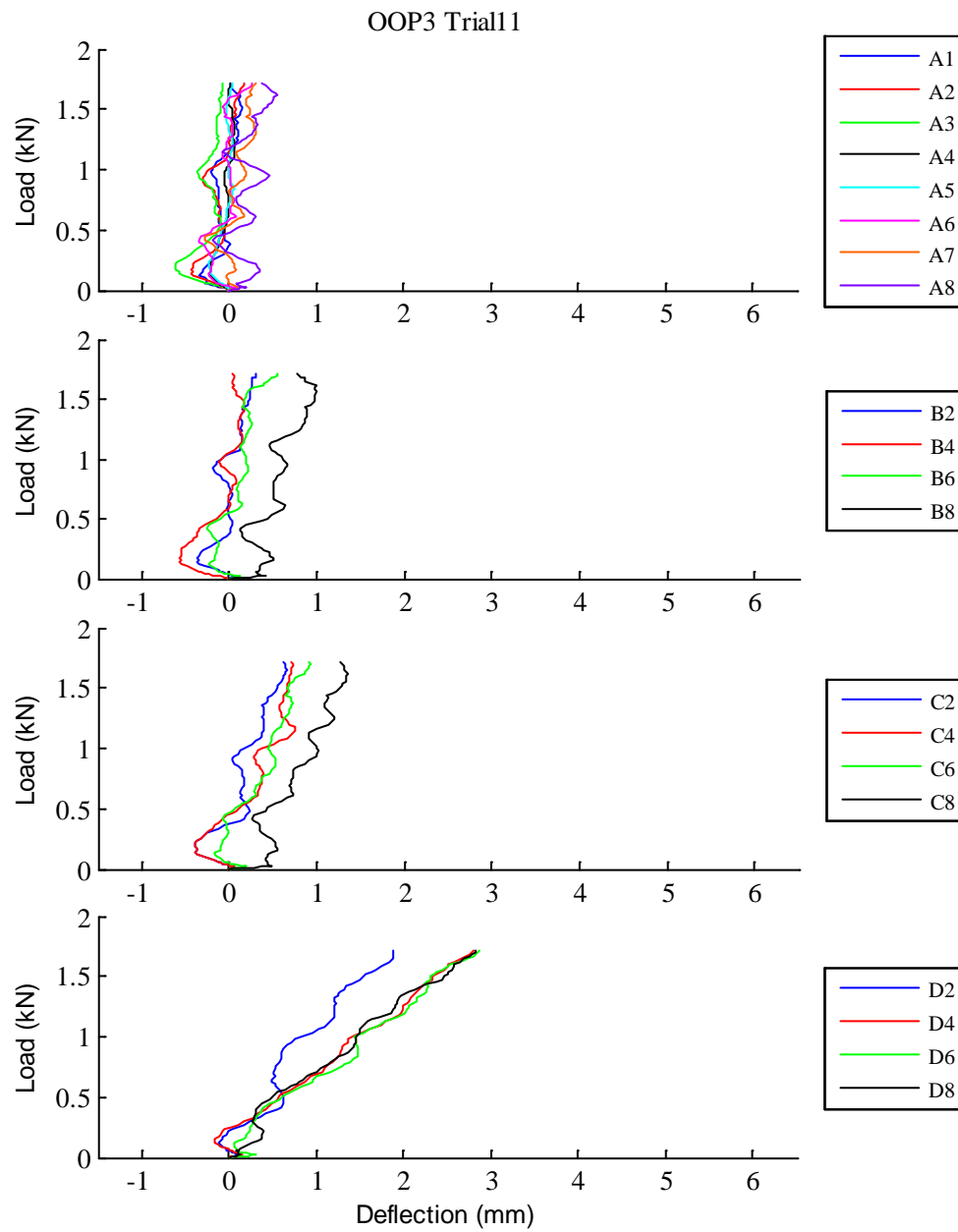Fig. D.79: OOP2 Trial10 load vs. deflection curves
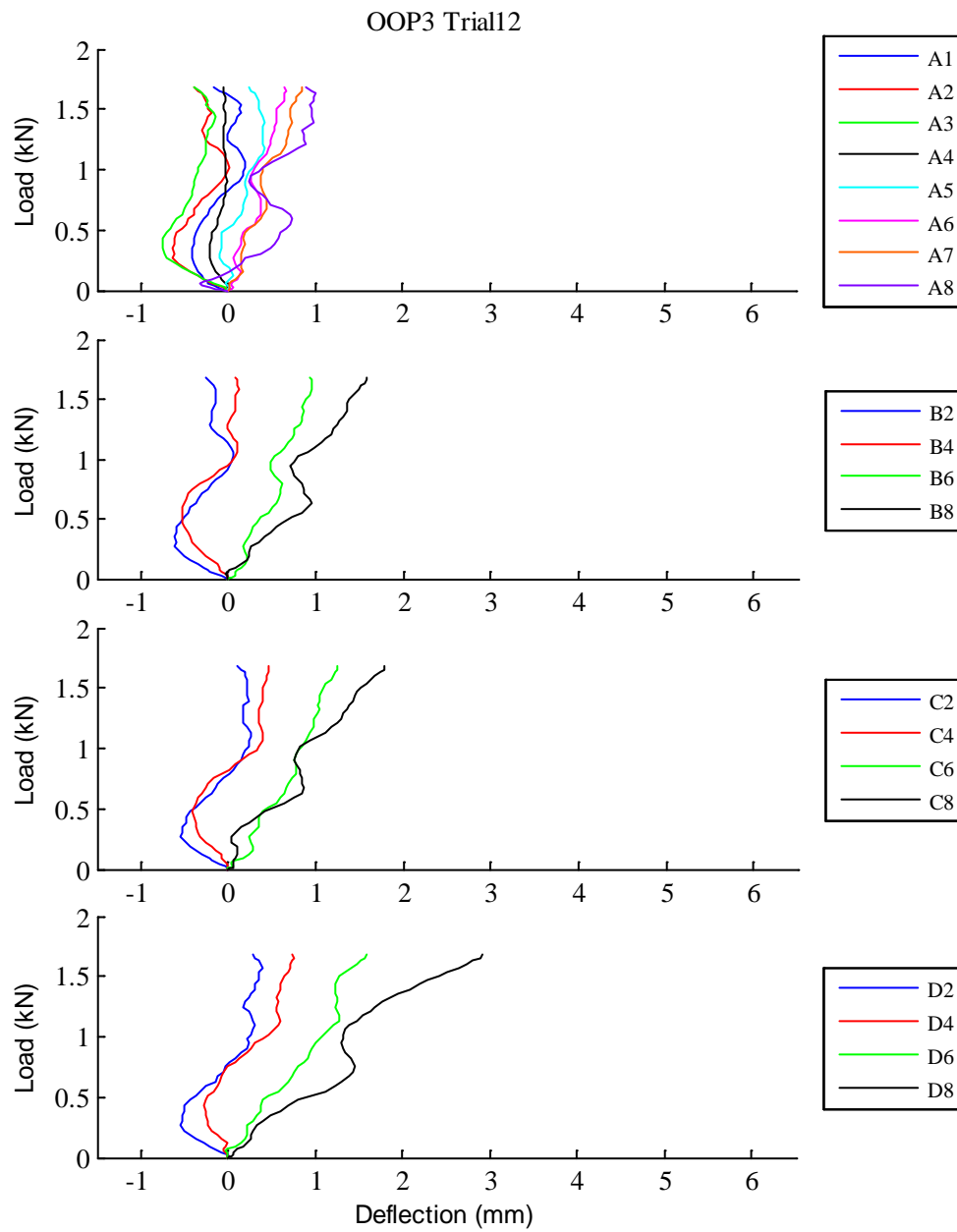
Fig. D.80: OOP2 Trial11 load vs. deflection curves
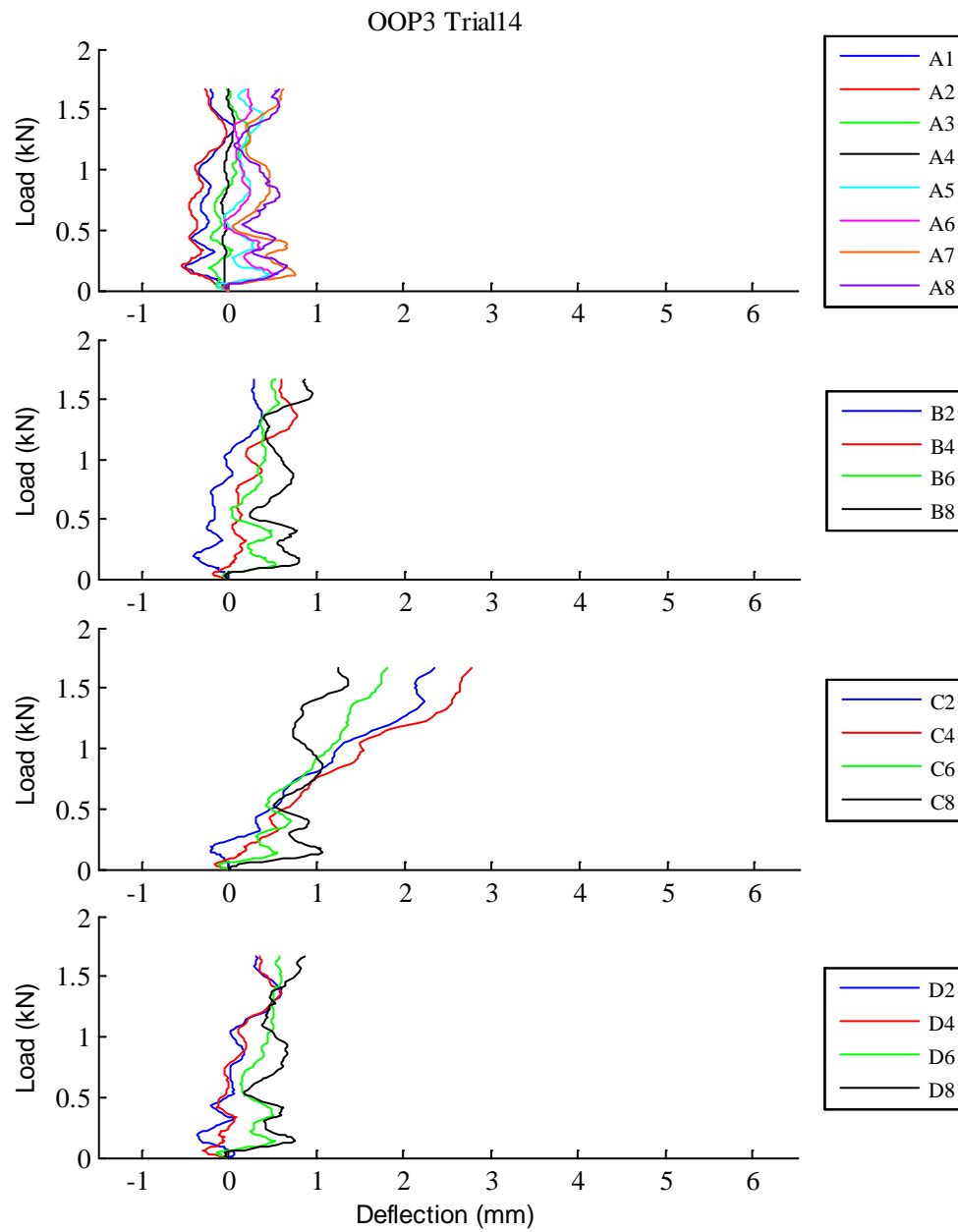
Fig. D.81: OOP2 Trial12 load vs. deflection curves

Fig. D.82: OOP2 Trial13 load vs. deflection curves

Fig. D.83: OOP2 Trial14 load vs. deflection curves
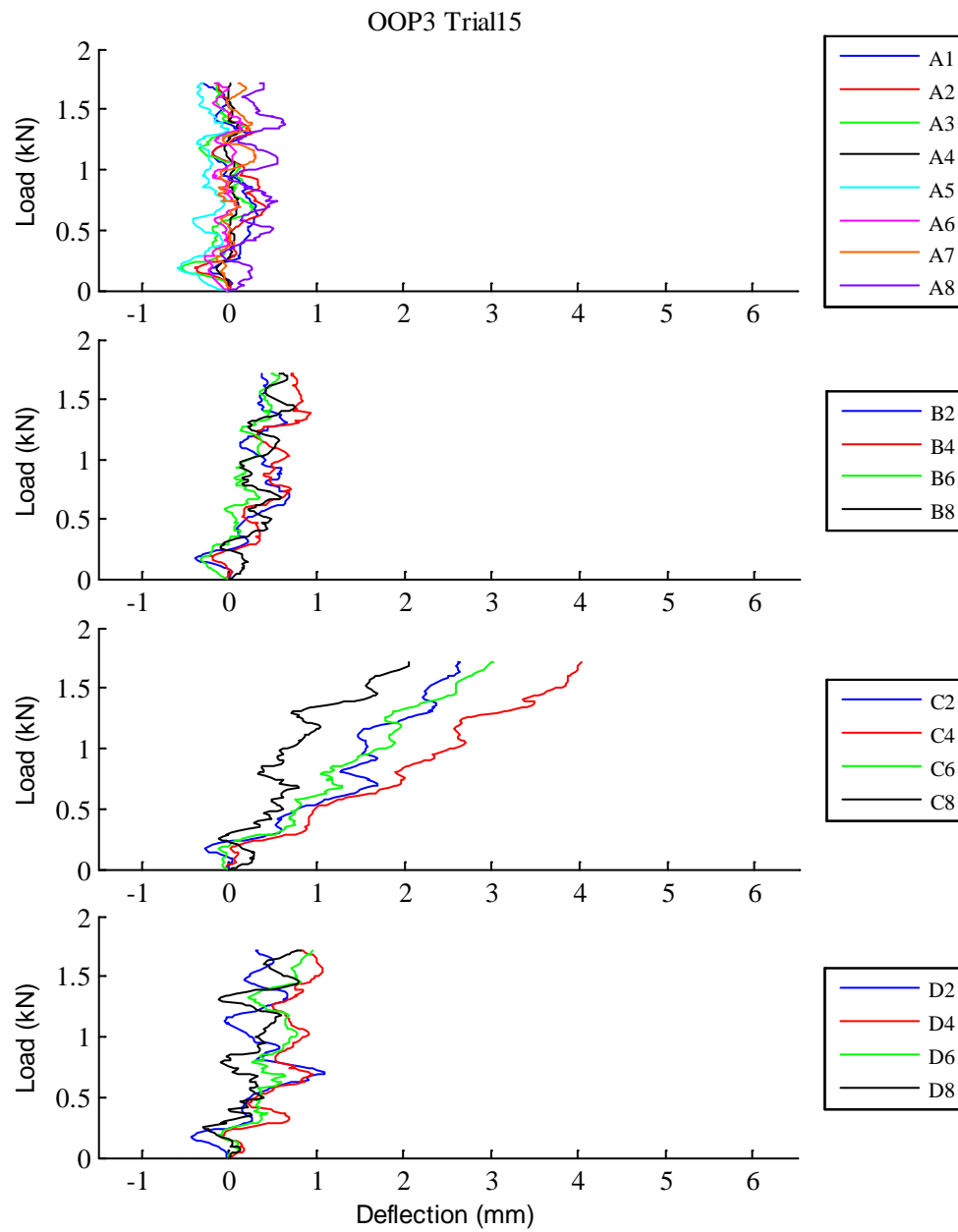
Fig. D.84: OOP2 Trial15 load vs. deflection curves

Fig. D.85: OOP2 Trial16 load vs. deflection curves

Fig. D.86: OOP2 Trial17 load vs. deflection curves

Fig. D.87: OOP2 Trial18 load vs. deflection curves

Fig. D.88: OOP2 Trial19 load vs. deflection curves

Fig. D.89: OOP2 Trial20 load vs. deflection curves

Fig. D.90: OOP3 Trial01 load vs. deflection curves

Fig. D.91: OOP3 Trial02 load vs. deflection curves

Fig. D.92: OOP3 Trial03 load vs. deflection curves
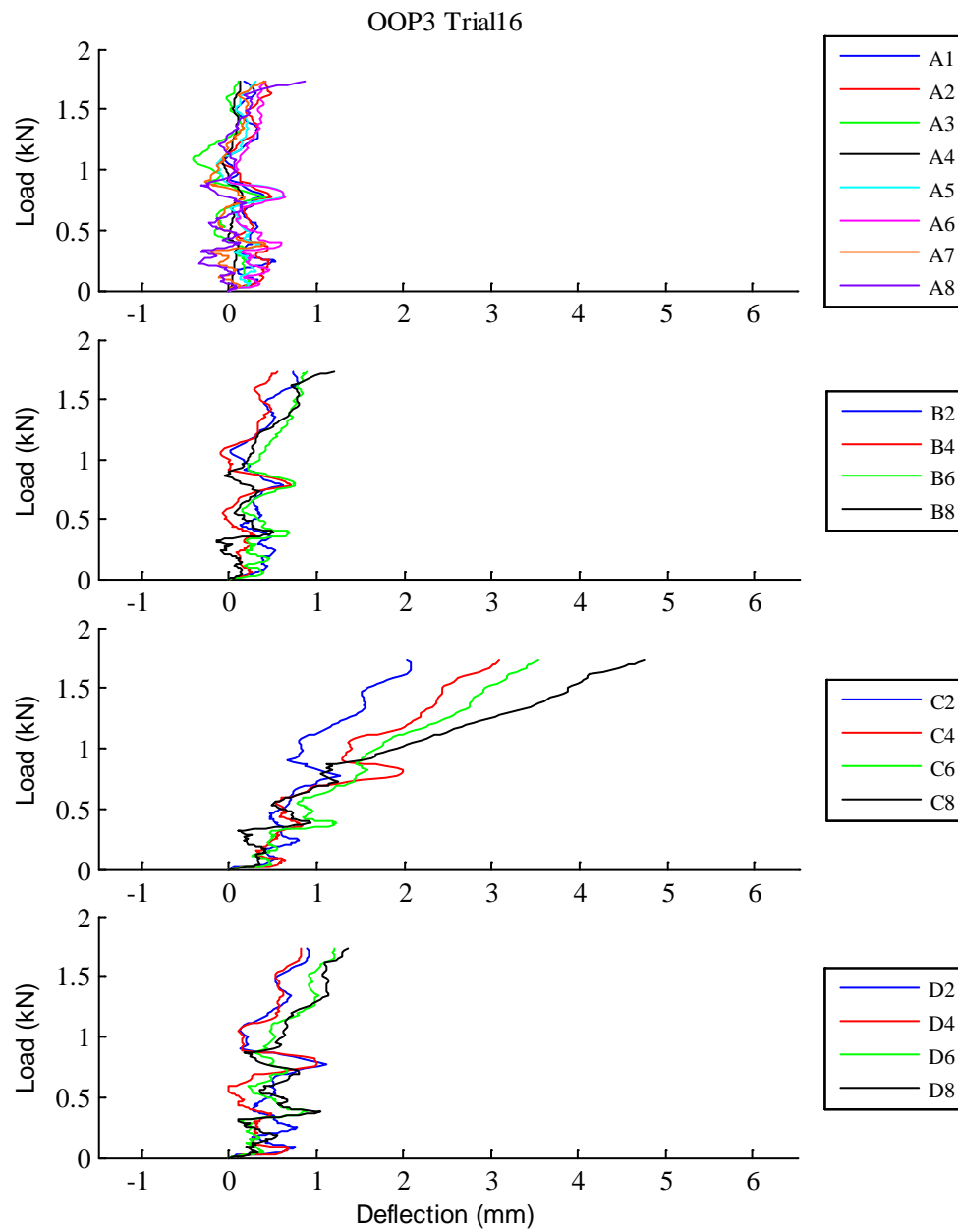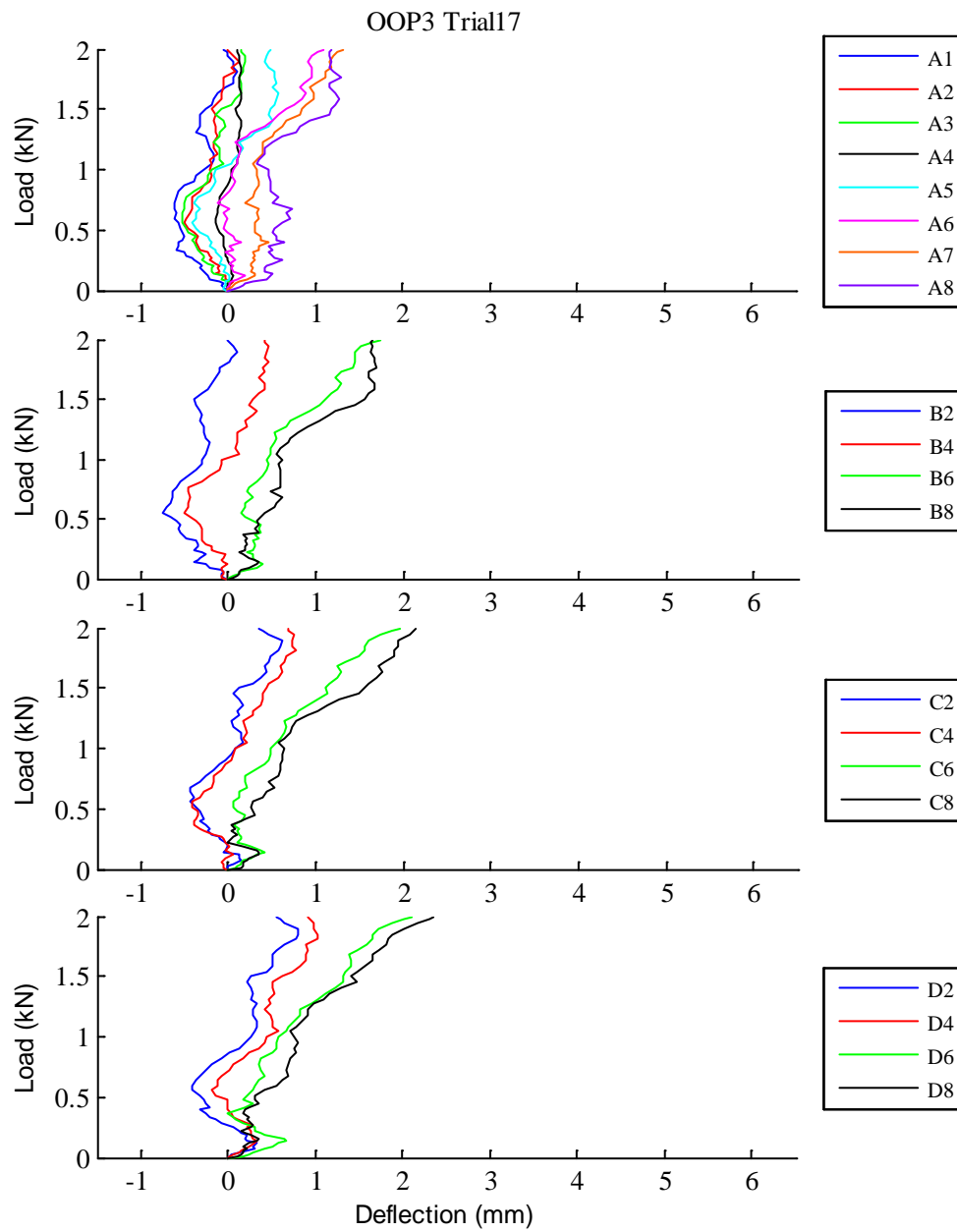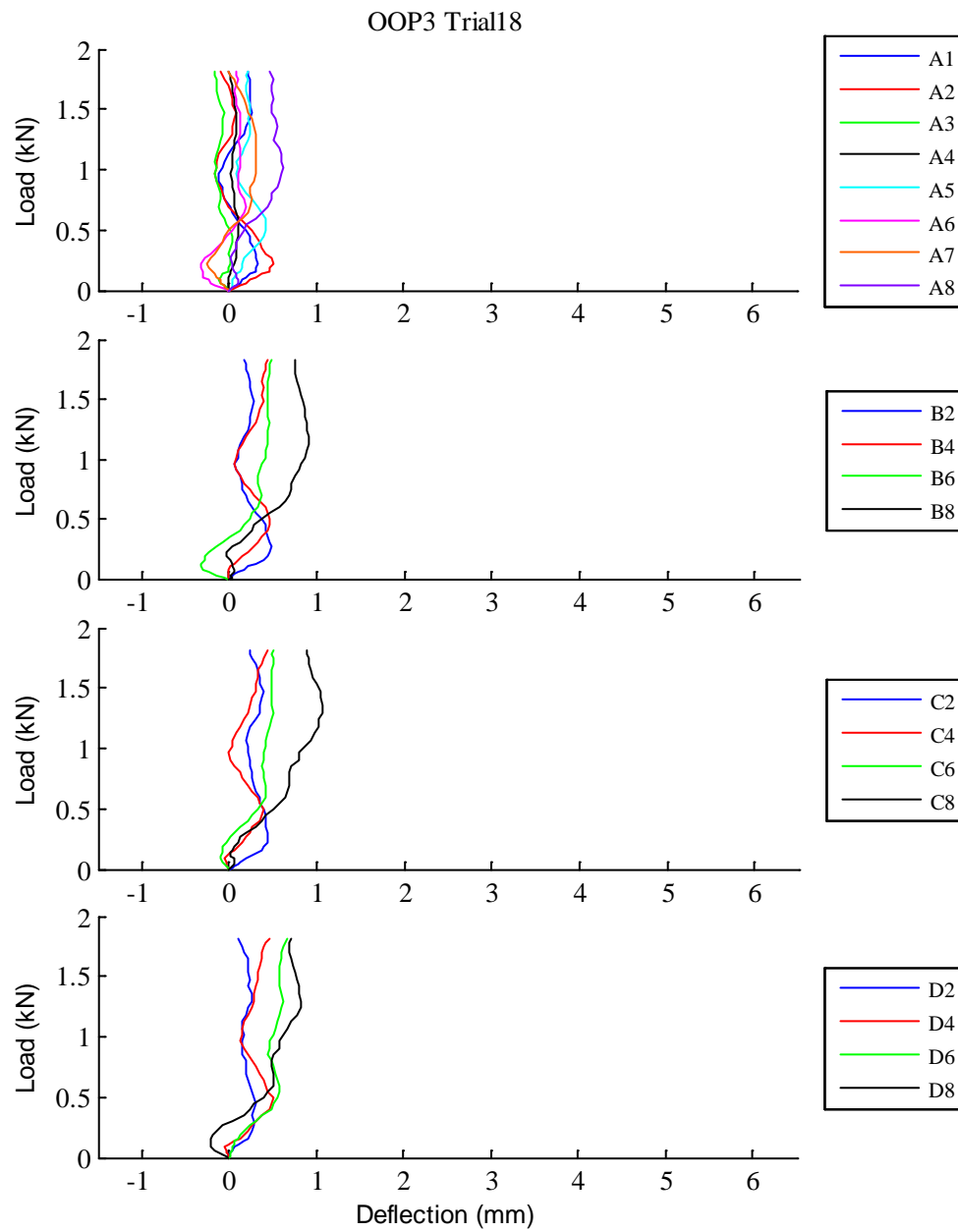
Fig. D.93: OOP3 Trial04 load vs. deflection curves

Fig. D.94: OOP3 Trial05 load vs. deflection curves

Fig. D.95: OOP3 Trial06 load vs. deflection curves

Fig. D.96: OOP3 Trial07 load vs. deflection curves

Fig. D.97: OOP3 Trial08 load vs. deflection curves

Fig. D.98: OOP3 Trial09 load vs. deflection curves

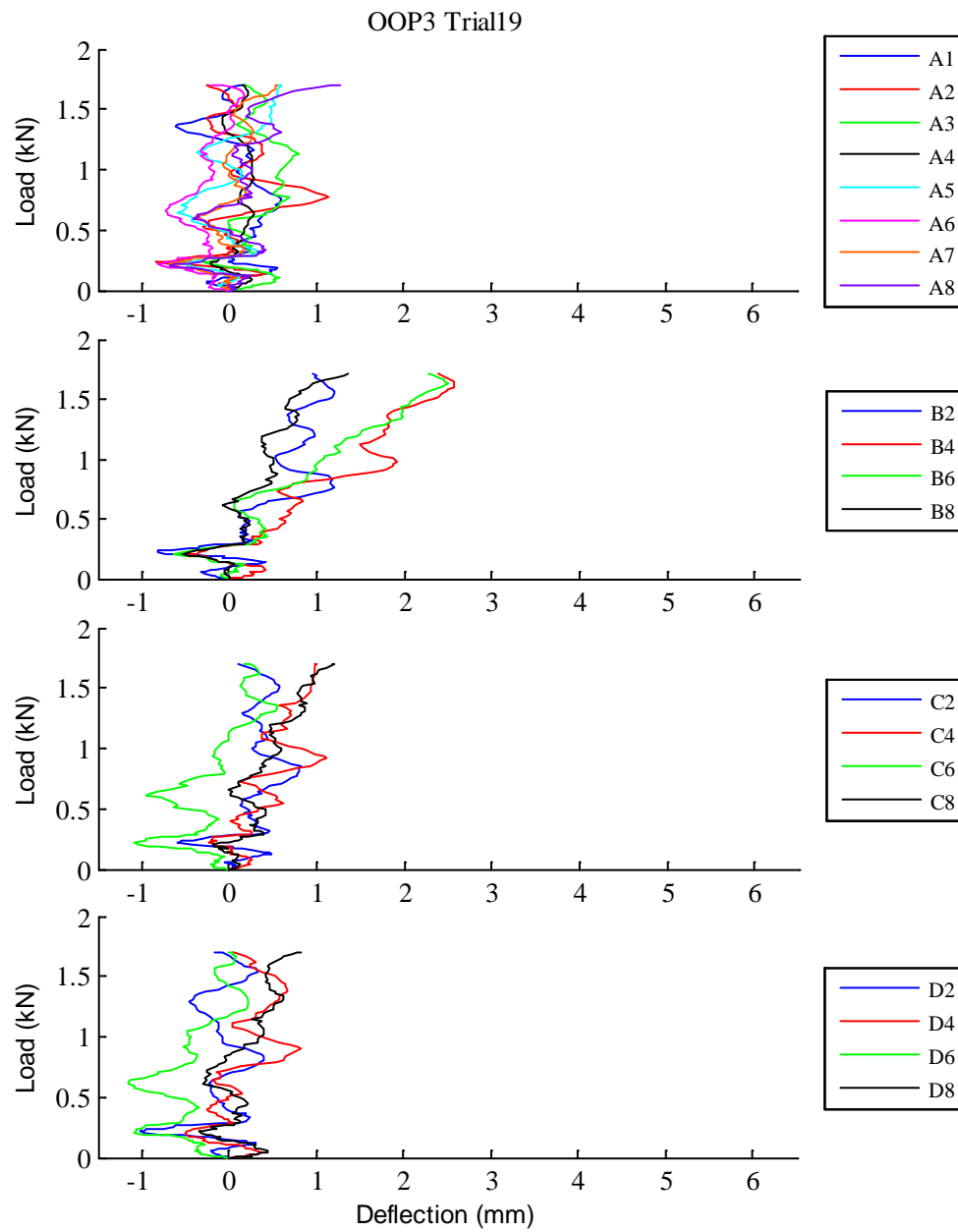Fig. D.99: OOP3 Trial10 load vs. deflection curves

Fig. D.100: OOP3 Trial11 load vs. deflection curves

Fig. D.101: OOP3 Trial12 load vs. deflection curves

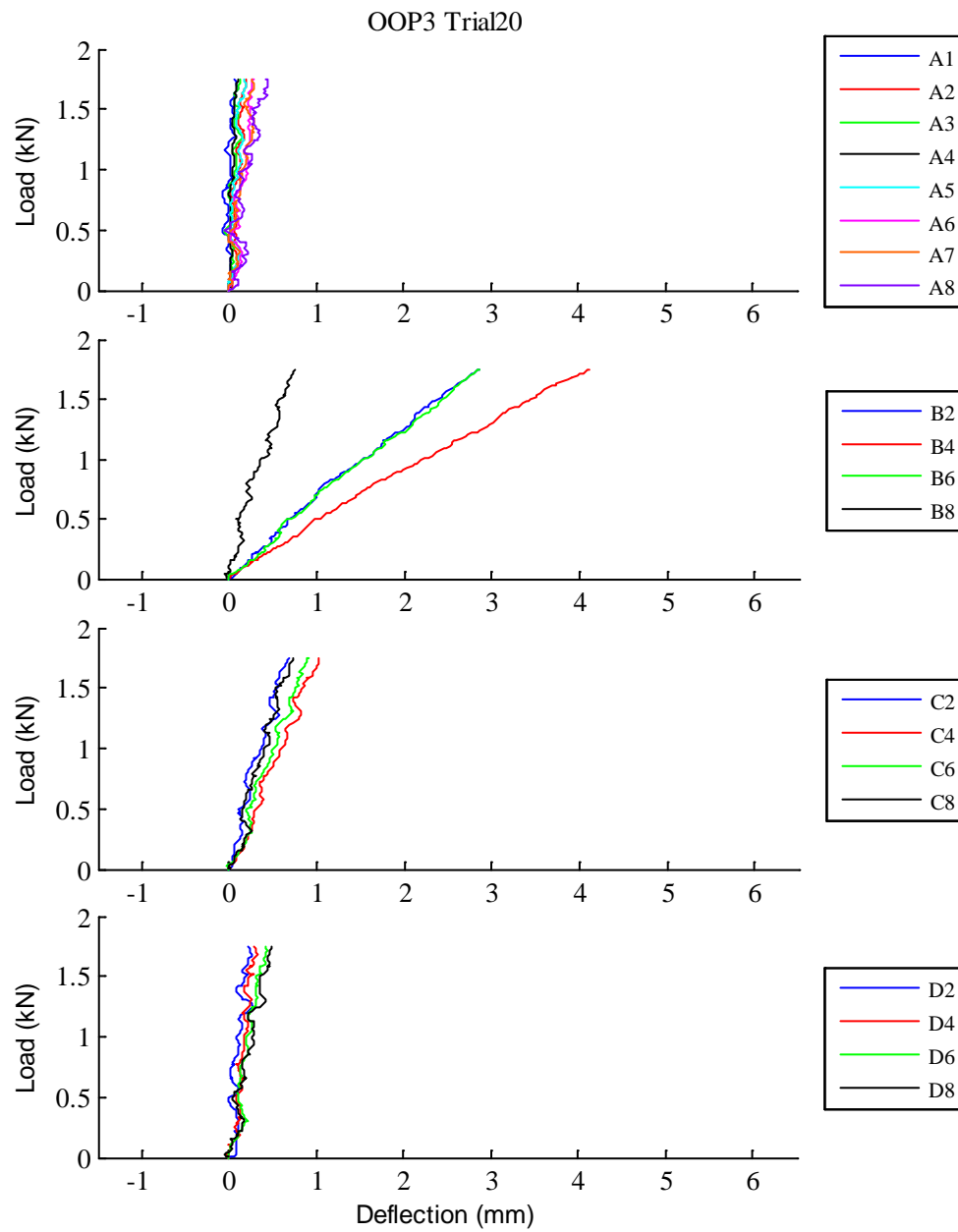Fig. D.102: OOP3 Trial14 load vs. deflection curves

Fig. D.103: OOP3 Trial15 load vs. deflection curves

Fig. D.104: OOP3 Trial16 load vs. deflection curves

Fig. D.105: OOP3 Trial17 load vs. deflection curves

Fig. D.106: OOP3 Trial18 load vs. deflection curves

Fig. D.107: OOP3 Trial19 load vs. deflection curves

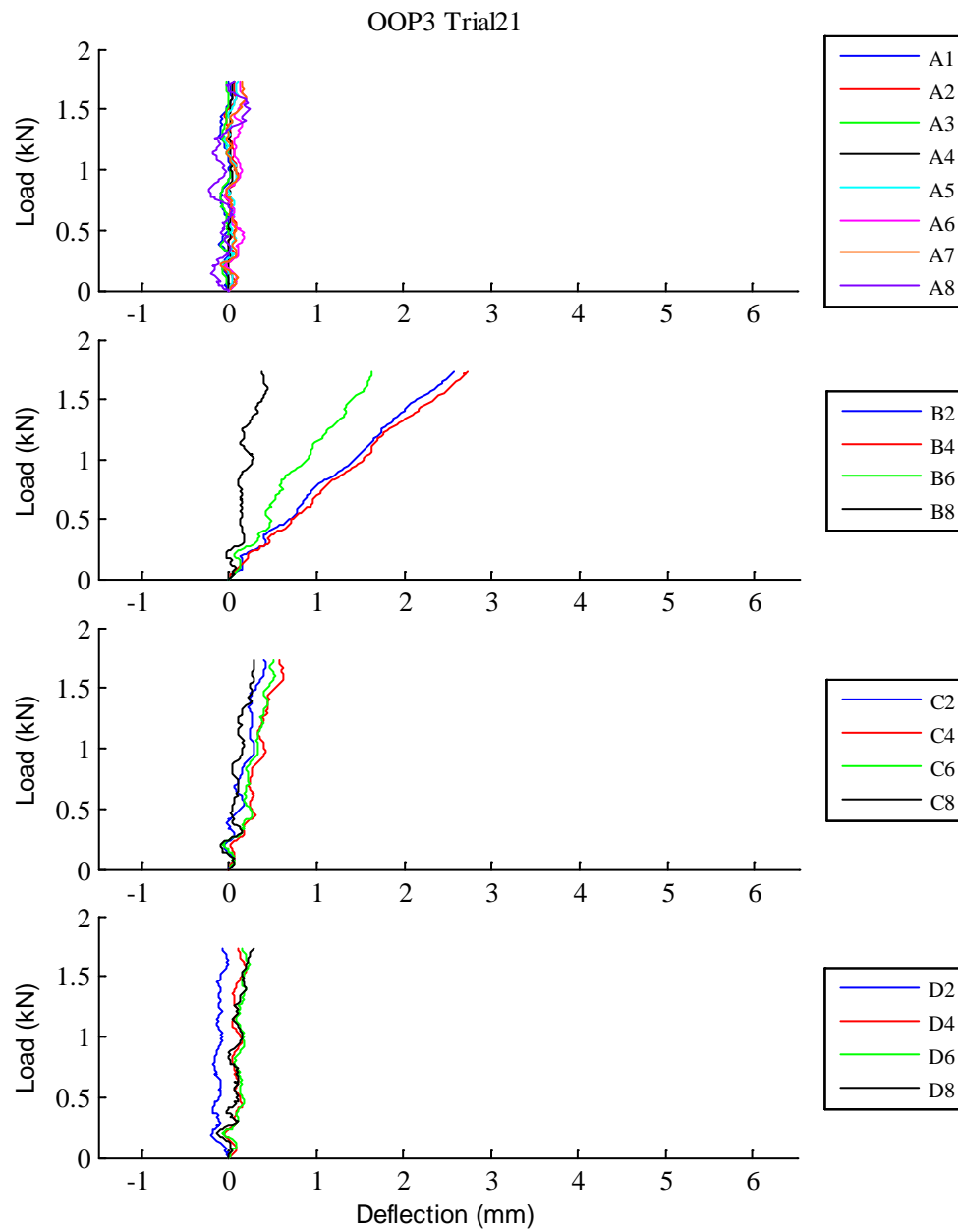Fig. D.108: OOP3 Trial20 load vs. deflection curves
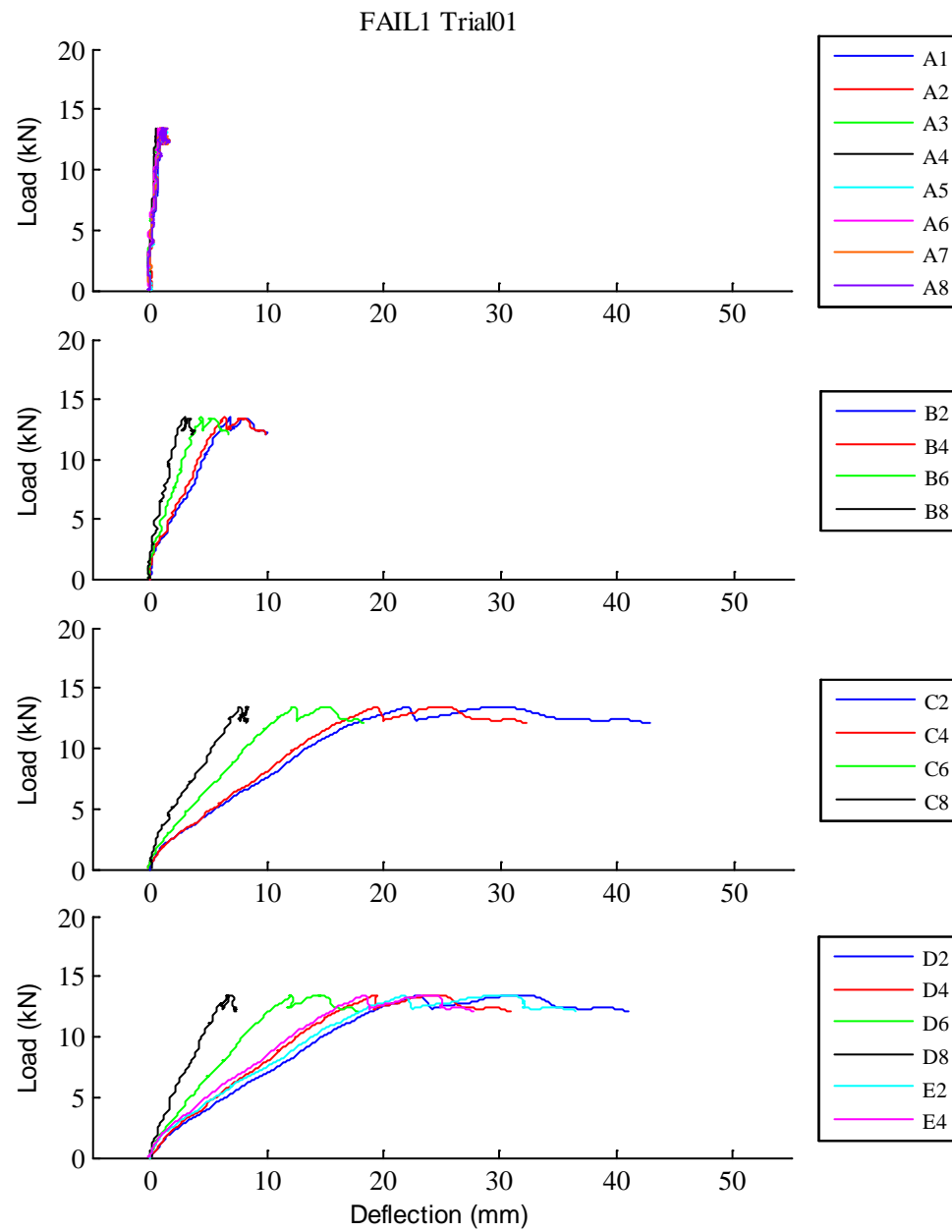
Fig. D.109: OOP3 Trial21 load vs. deflection curves

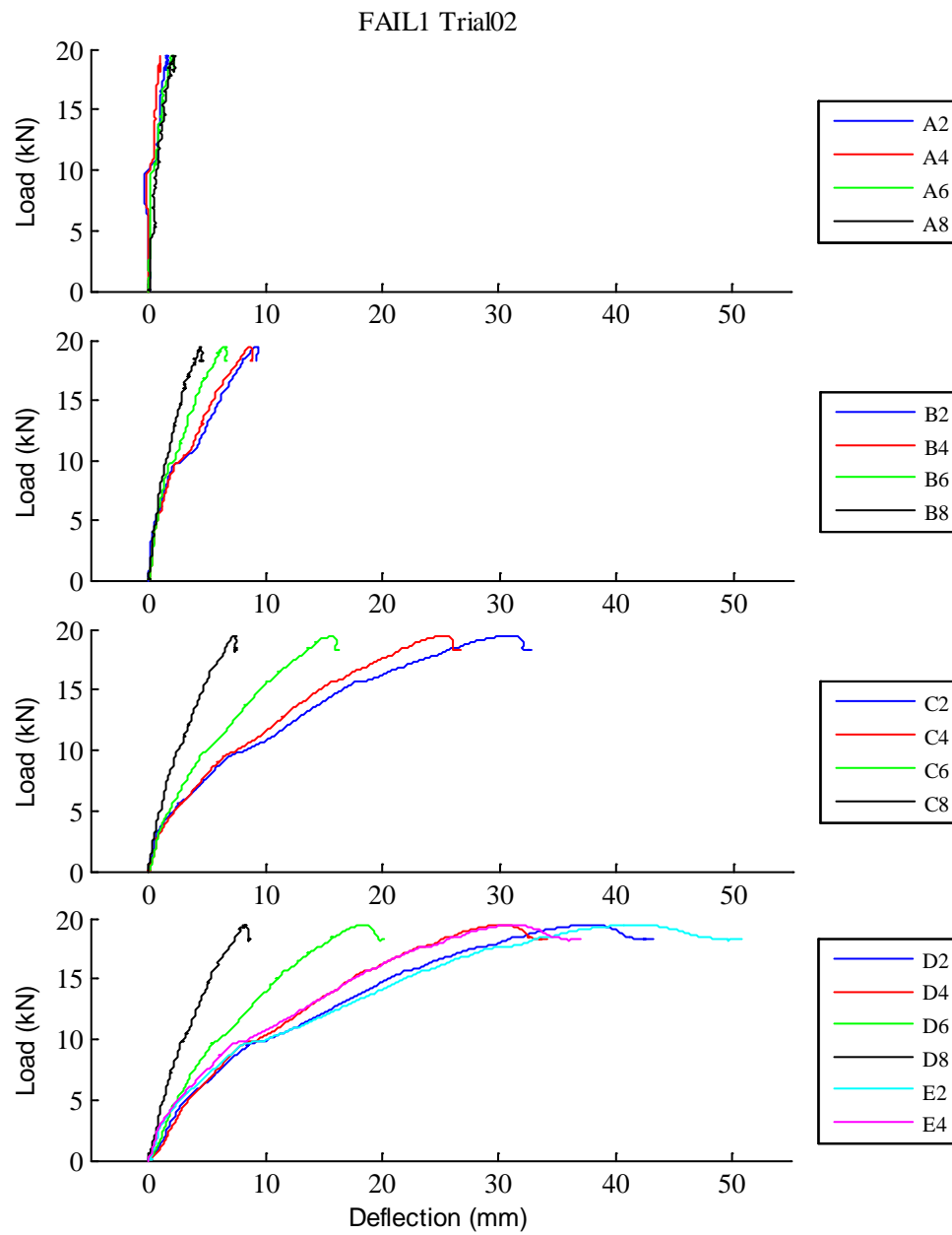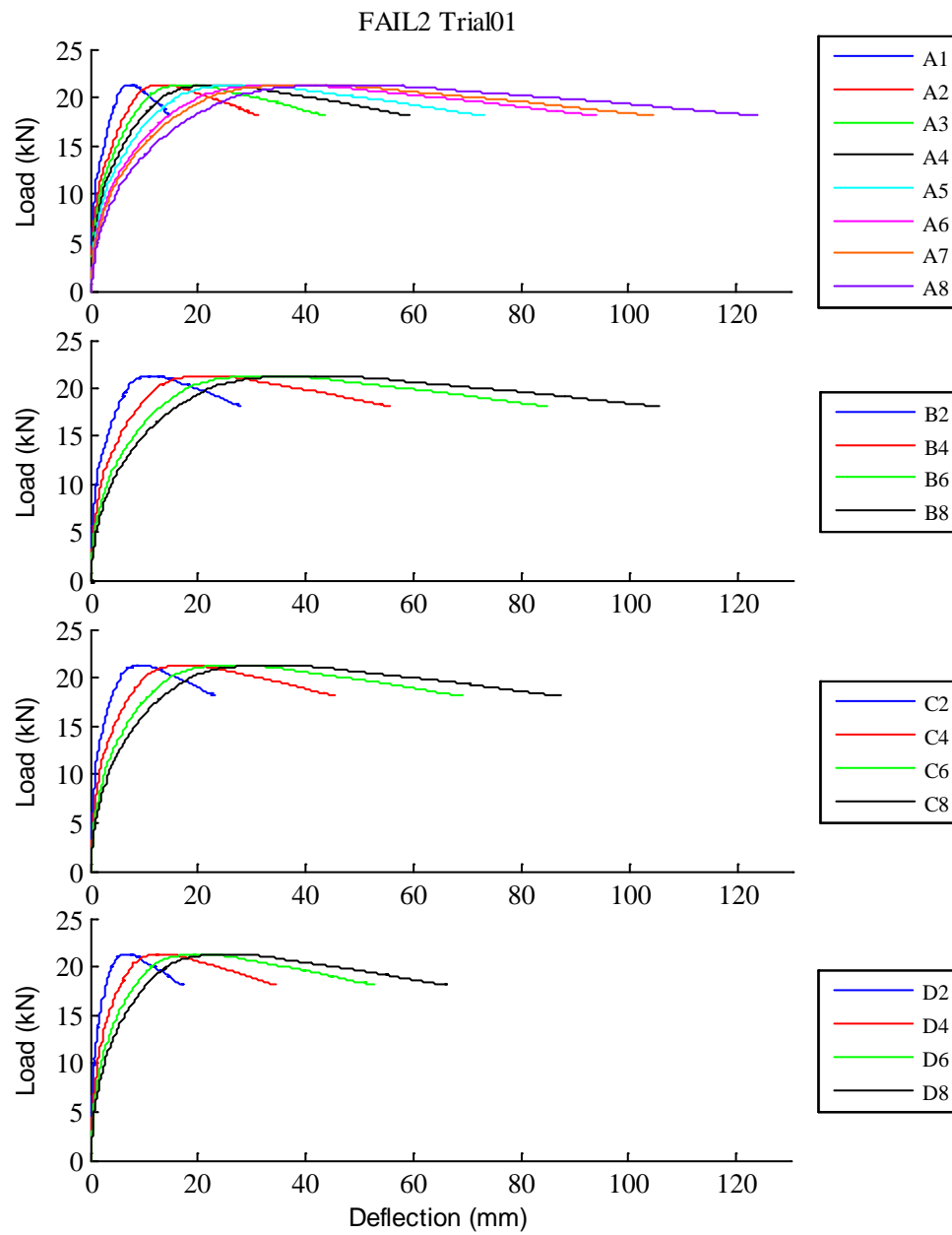Fig. D.110: FAIL1 Trial01 load vs. deflection curves

Fig. D.111: FAIL1 Trial02 load vs. deflection curves

Fig. D.112: FAIL2 Trial01 load vs. deflection curves